NASA TECHNICAL NOTE

NASA TN D-8455 c.1

NASA TN D-8455

BEHAVIOR OF AIRCRAFT ANTISKID BRAKING SYSTEMS ON DRY AND WET RUNWAY SURFACES

A Slip-Ratio-Controlled System With Ground Speed Reference From Unbraked Nose Wheel

John A. Tanner and Sandy M. Stubbs

Langley Research Center
Hampton, Va. 23665

NATIONAL AERONAUTICS AND SPACE ADMINISTRATION · WASHINGTON, D. C. · OCTOBER 1977

1. Report No.	2. Government Accession No.
NASA TN D-8455	

4. Title and Subtitle
BEHAVIOR OF AIRCRAFT ANTISKID BRAKING SYSTEMS ON DRY AND WET RUNWAY SURFACES - A SLIP-RATIO-CONTROLLED SYSTEM WITH GROUND SPEED REFERENCE FROM UNBRAKED NOSE WHEEL

October 1977

6. Performing Organization Code

7. Author(s)
John A. Tanner and Sandy M. Stubbs

8. Performing Organization Report No.
L-11292

10. Work Unit No.
505-08-31-01

9. Performing Organization Name and Address
NASA Langley Research Center
Hampton, VA 23665

11. Contract or Grant No.

13. Type of Report and Period Covered
Technical Note

12. Sponsoring Agency Name and Address
National Aeronautics and Space Administration
Washington, DC 20546

14. Sponsoring Agency Code

15. Supplementary Notes

16. Abstract

An experimental investigation was conducted at the Langley aircraft landing loads and traction facility to study the braking and cornering response of a slip-ratio-controlled aircraft antiskid braking system with ground speed reference derived from an unbraked nose wheel. This investigation, conducted on dry and wet runway surfaces, utilized one main gear wheel, brake, and tire assembly of a McDonnell Douglas DC-9 series 10 airplane. During maximum braking, the average ratio of the drag-force friction coefficient developed by the antiskid system to the maximum drag-force friction coefficient available was higher on the dry surface than on damp and flooded surfaces and was reduced with lighter vertical loads, higher yaw angles, and when new tire treads were replaced by worn treads. Similarly, the average ratio of side-force friction coefficient developed by the tire under antiskid control to the maximum side-force friction coefficient available to a freely rolling yawed tire decreased with increasing yaw angle, generally increased with ground speed, and decreased when tires with new treads were replaced by those with worn treads. The interaction between braking and cornering indicated that, during antiskid cycling on a dry surface, the side-force friction coefficient was typically reduced by more than 40 percent; on a flooded surface, this coefficient was reduced to negligible values. During the transition from a dry to a flooded surface under heavy braking, the wheel entered into a deep skid but the antiskid system reacted quickly and permitted the wheel to regain ground speed and to resume braking on the flooded surface while preventing subsequent deep skids. Brake pressure recovery was rapid following the transition from a flooded to a dry surface.

17. Key Words (Suggested by Author(s))	18. Distribution Statement
Cornering Aircraft tires Antiskid braking system	Unclassified - Unlimited Subject Category 05

19. Security Classif. (of this report)	20. Security Classif. (of this page)	21. No. of Pages	22. Price*
Unclassified	Unclassified	166	$6.75

*For sale by the National Technical Information Service, Springfield, Virginia 22161

CONTENTS

BEHAVIOR OF AIRCRAFT ANTISKID BRAKING SYSTEMS ON DRY AND WET RUNWAY SURFACES

A SLIP-RATIO-CONTROLLED SYSTEM WITH GROUND SPEED REFERENCE FROM UNBRAKED NOSE WHEEL

John A. Tanner and Sandy M. Stubbs
Langley Research Center

SUMMARY

An experimental investigation was conducted at the Langley aircraft landing loads and traction facility to study the braking and cornering response of a slip-ratio-controlled aircraft antiskid braking system with ground speed reference derived from an unbraked nose wheel. This investigation, conducted on dry and wet runway surfaces, utilized one main gear wheel, brake, and tire assembly of a McDonnell Douglas DC-9 series 10 airplane.

During maximum braking, the average ratio of the drag-force friction coefficient developed by the antiskid system to the maximum drag-force friction coefficient available was higher on the dry surface than on damp and flooded surfaces and was reduced with lighter vertical loads, higher yaw angles, and when new tire treads were replaced by worn treads. Similarly, the average ratio of side-force friction coefficient developed by the tire under antiskid control to the maximum side-force friction coefficient available to a freely rolling yawed tire decreased with increasing yaw angle, generally increased with ground speed, and decreased when tires with new treads were replaced by those with worn treads. The interaction between braking and cornering indicated that, during antiskid cycling on a dry surface, the side-force friction coefficient was typically reduced by more than 40 percent; on a flooded surface, this coefficient was reduced to negligible values. During the transition from a dry to a flooded surface under heavy braking, the wheel entered into a deep skid but the antiskid system reacted quickly and permitted the wheel to regain ground speed and to resume braking on the flooded surface while preventing subsequent deep skids. Brake pressure recovery was rapid following the transition from a flooded to a dry surface.

INTRODUCTION

Over the years the number and variety of airplanes using antiskid braking systems have steadily increased, with most current commercial and military jet airplanes being equipped with various skid control devices. The earliest antiskid systems were generally designed to prevent wheel lockups and excessive tire wear on dry pavements. Modern skid control devices, however, are more sophisticated and are designed to provide maximum braking effort while maintaining

full antiskid protection under all weather conditions. Operating statistics of modern jet airplanes indicate that these antiskid systems are both effective and dependable; the several million landings that are made each year in routine fashion with no serious operating problems attest to this fact. However, it has also been well established, both from flight tests and from field experience, that the performance of these systems is subject to degradation when the runway becomes slippery; consequently, dangerously long roll-out distances and reduced steering capability can result during some airplane landing operations (refs. 1 to 5). There is a need to study different types of antiskid braking systems to find the sources of the degraded performance that occur under adverse runway conditions; there is also a need to obtain data for the development of more advanced systems that will insure safe ground handling operations under all weather conditions.

In an effort to meet these needs, an experimental research program has been undertaken to study the performance of several different airplane antiskid braking systems under the controlled conditions afforded by the Langley aircraft landing loads and traction facility (formerly called the Langley landing loads track). The types of skid control devices undergoing study in this program include a velocity-rate-controlled system (ref. 6), a slip-ratio-controlled system with ground speed reference from an unbraked nose wheel, a slip-ratio-controlled system with ground speed reference from a braked wheel, a slip-velocity-controlled system, and a system which relies upon differential pump control. The investigation of these systems is being conducted with one main wheel, brake, and tire assembly of a McDonnell Douglas DC-9 series 10 airplane.

The purpose of this paper is to present the results from a study of the performance of a slip-ratio-controlled antiskid braking system with unbraked nose-wheel input under maximum braking effort. The parameters varied in the study included ground speed, tire loading, yaw angle, tire tread condition, system operating pressure, and runway wetness conditions. A discussion of the effects of each of these parameters on the performance of the skid control system is presented. In addition, comparisons are made between data obtained with the skid control system and data obtained from braking tests without antiskid protection.

Messier-Hispano provided the antiskid system hardware for this investigation and Jean Guichard provided technical assistance.

SYMBOLS

Values are given in both SI and U.S. Customary Units. The measurements and calculations were made in U.S. Customary Units. Factors relating the two systems are given in reference 7.

F_V tire vertical force

F_X drag force parallel to plane of wheel

F_Y side force perpendicular to plane of wheel

P	power
r	tire rolling radius
S	wheel slip ratio
t	time
V	carriage speed
η	performance ratio
μ	friction coefficient
ψ	yaw angle
ω	test wheel angular velocity

Subscripts:

b	braking
c	cornering
d	drag
f	final value
g	gross
max	maximum value
o	initial value
r	free rolling
s	side
t	tire

A bar over a symbol denotes an average value.

APPARATUS AND TEST PROCEDURE

Test Tires

The tires used in this investigation were 40 × 14, type VII, bias-ply aircraft tires of 22 ply rating with a rated maximum speed of 200 knots (1 knot = 0.5144 m/s). The tires were stock retreads with a six-groove pattern and the study included both new and worn tread configurations. A photograph of two tires having new and worn treads is presented in figure 1. The new tread

had a groove depth of 0.71 cm (0.28 in.) and was considered new until the groove depth decreased to 0.36 cm (0.14 in.). A commercially available tire grinding machine was employed to remove tread rubber uniformly from the retreaded tire until only a groove depth of 0.05 cm (0.02 in.) remained. This simulated worn tire was probably in a worse wear condition than is normally experienced in airplane operations. Throughout this investigation the tire inflation pressure was maintained at the normal airline operational pressure of 0.97 MPa (140 psi).

Test Facility

The investigation was performed on a test carriage at the Langley aircraft landing loads and traction facility described in reference 8. Figure 2 is a photograph of the carriage with the test wheel assembly installed; figure 3 is a close-up view of the wheel and tire and shows details of the instrumented dynamometer which was used instead of a landing gear strut to support the wheel and brake assembly because it provided an accurate measurement of the ground forces.

For the tests described in this paper, approximately 244 m (800 ft) of the available 366 m (1200 ft) of the flat concrete test runway were used to provide braking and cornering data on a dry surface, on an artificially damp surface, on an artificially flooded surface, and on a random dry/damp surface. With the exception of transient runway friction tests, the entire runway had a uniform surface wetness condition, and antiskid cycling occurred for the entire 244 m (800 ft). The 61 m (200 ft) of runway preceding the test section were used for the initial wheel spin-up and brake actuation, and the 61 m (200 ft) beyond the test section were retained for brake release. In order to obtain a damp condition, the test surface was lightly wetted with no standing water. For the flooded runway condition, the test section was surrounded by a flexible dam and flooded to a depth of approximately 1.0 cm (0.4 in.). The random dry/damp surface condition was attained by wetting the test section at random. No water depth measurements were made for this condition.

The concrete surface in the test area had a light broom finish in a transverse direction, and the surface texture was somewhat smoother than that for most operational concrete runways. The runway surface roughness for the 244-m (800-ft) test section was not uniform, as shown by the texture depth measurements in the following table:

Station		Average texture depth	
m	ft	μm	in.
61	200	115	0.00453
122	400	245	.00965
183	600	145	.00571
244	800	137	.00539
305	1000	155	.00610

Details of the texture depth measurement technique are presented in reference 9. The average texture depth of the test runway was 154 μm (0.00606 in.), which is slightly less than that of a typical operational runway. (See ref. 10, for example.) The test runway was quite level compared with airport runways and had no crown for drainage purposes. During the course of testing on the dry surface, particularly with a yawed tire, rubber was deposited on the runway and it was necessary to clean the surface periodically.

Skid Control System

A slip-ratio-controlled skid control system with ground speed reference from an unbraked nose wheel, typical of that used on several European commercial and military jet airplanes, was used in this investigation. The system was configured to simulate a braking system that had electronic and hydraulic components, including correct line lengths and sizes, for a single main wheel of a DC-9 series 10 airplane. Figure 4 is a photograph of the major hydraulic components of the simulated braking system installed on the test carriage; figure 5 is a schematic of the system. The brake system is activated by opening the pilot metering valve (fig. 5) which allows the brake fluid to flow from a high pressure reservoir and brake selector valve, through the normally open antiskid control valve and hydraulic fuse, to the brake. A pneumatic piston was used to open the pilot metering valve to its full stroke; thus maximum braking for all tests was provided. The bicycle-type, lightweight trailing wheel shown in figure 6 was used to simulate the airplane nose wheel and to provide a ground speed reference for the antiskid logic electronics. During antiskid braking, dc voltages (developed by generators driven by the braked test wheel and the simulated unbraked nose wheel) proportional to the wheel speeds are input to the electronic antiskid control box which computes the slip ratio of the braked wheel. (Slip ratio is the instantaneous ratio of slip speed of the braked wheel ($V - \omega r$) to the carriage speed (V)). This ratio is then compared with a preset slip ratio threshold value of approximately 0.15 (0.13 on dry surfaces to 0.18 on flooded surfaces), and a skid signal (dc current) is generated and transmitted to the antiskid control valve to reduce the brake pressure when the slip ratio is higher than the assigned threshold value and to increase brake pressure when the slip ratio is lower than the assigned value.

Typical time histories of wheel speed, slip ratio, skid signal, brake pressure, and the resulting drag-force friction coefficient are presented in figure 7 to help describe the system operation. Figure 7(a) presents time histories for the entire run and figure 7(b) presents an expanded segment of the run from 1.2 to 3.2 sec to illustrate more clearly the antiskid cycling action. Figure 7 shows that, as brake pressure is applied, the wheel speed decreases; this decrease increases the slip ratio until it exceeds the threshold value and thus generates a skid signal. For example, in figure 7(b), during the time between approximately 1.4 and 2.1 sec, the slip ratio has several spikes above the threshold value which, in turn, generate a skid signal. The skid signal seems to have an oscillating characteristic that is especially noticeable at 2.1 sec. Here the slip ratio drops substantially below the threshold level and the skid signal continues with four or five additional decaying oscillations. The antiskid system cycling frequency is approximately 10 to 12 Hz and the skid

signal modulates the brake pressure quite well; thus, any deep skids are prevented and a relatively stable friction-coefficient trace is produced.

Instrumentation

The tire friction forces were measured by means of the dynamometer which is shown in figure 3 and illustrated schematically in figure 8. Strain gages were mounted on the five dynamometer support beams: two of the beams were used for measuring vertical forces, two were used for measuring drag forces parallel to the wheel plane, and a single beam was used for measuring side force perpendicular to the wheel plane. Three accelerometers on the test wheel axle provided information for inertia corrections to the force data. The brake torque was measured with torque links which were independent of the drag-force beams. Transducers were installed in the hydraulic system to measure pressures at the pilot metering valve, at the hydraulic fuse, at the brake, and in the return line between the brake and the hydraulic reservoir. A steel-reinforced, cogged, rubber timing belt was driven by the test wheel to turn an auxiliary axle which drove the pulse (ac) alternators and dc generators that were used to obtain a measure of the test wheel angular velocity. Signals from one of the dc generators supplied wheel-speed information to the antiskid system. The skid signal produced by the antiskid system was recorded for an examination of its characteristics. A lightweight trailing wheel simulating the nose wheel on an airplane was mounted to the side of the test carriage (as shown in fig. 6), and the output from a dc generator mounted on its axle was recorded and was also routed to the antiskid control box to provide a measure of carriage speed. All data outputs were fed into appropriate signal conditioning equipment and then into two frequency-modulated tape recorders. A time code was fed into the two recorders simultaneously to provide synchronization of the two sets of data.

Test Procedure

The technique for the braking tests with and without antiskid protection consisted of setting the dynamometer and tire assembly to the preselected yaw angle, propelling the test carriage to the desired speed, applying a preselected vertical load on the tire, and monitoring the outputs from the onboard instrumentation. For antiskid tests, the brake was actuated by a pneumatic piston at the pilot metering valve, which gave full pedal deflection or maximum braking, and the antiskid system modulated the braking effort. The runway surface condition was essentially uniform over the entire length; the brake was applied the full distance and was released just prior to carriage arrestment. In addition to antiskid braking tests, single-cycle braking tests were made without antiskid protection. These single brake cycles consisted of applying sufficient brake pressure to bring the tire from a free-rolling condition to a locked-wheel skid and then releasing the brake to allow full tire spin-up prior to the next cycle. For single-cycle braking, the runway surface was divided into three sections (dry, damp, and flooded) and brake pressure was applied by triggering devices at each section along the test track. The nominal carriage speeds for both types of tests ranged from 40 to 100 knots, as measured approximately midway along the runway. After initial acceleration, the carriage was in a coast mode and there was a slow speed decay through the test section due to air drag,

friction, and the antiskid braking of the test tire itself. Tire vertical loading was varied from approximately 58 kN (13 000 lbf) to 120 kN (27 000 lbf), which represented a nominal landing weight and refused take-off weight, respectively, for a single wheel of the DC-9. Tests were run at tire yaw angles of 0°, 3°, and 6° and at a nominal brake system pressure of 21 MPa (3000 psi). In addition, several tests were run at a nominal brake-system pressure of 14 MPa (2000 psi).

Data Reduction

Except for the ac alternator signals, all data recorded on magnetic tape were filtered to 60 Hz, digitized at 250 samples/sec, and stored on tape. From these digitized data, direct measurements were obtained of the carriage speed, the braked-wheel angular velocity, the skid signal generated by the antiskid system, the brake pressure and torque, the drag force F_x, the side force F_y, the vertical force applied to the tire F_v, and the accelerations of the dynamometer. The instantaneous force data that were corrected for acceleration effects were combined to compute the instantaneous drag-force friction coefficient μ_d parallel to the direction of motion and the side-force friction coefficient μ_s perpendicular to the direction of motion. The load transfer between the two drag-force beams (fig. 8) provided a measure of the alining torque about the vertical or steering axis of the wheel. The braked-wheel alternator signal was converted to wheel speed, which was combined with carriage speed to yield wheel slip speed and slip ratio. Time histories of some of the measured parameters for a typical antiskid braking test are presented in figure 9(a). The vertical and drag forces are each a summation of two data channels with corrections made for acceleration effects. The time histories of figure 9(b) are the parameters calculated from the data of figure 9(a). Although brake pressure is a measured parameter, it is included in figure 9(b) to serve as a reference.

DEFINITIONS

An adequate assessment of the performance and behavior of the antiskid braking system, which was subjected to a wide variety of operational conditions during these tests, requires careful consideration of many variables. Two methods developed in reference 6 are used to analyze the performance of the antiskid braking system - one based upon tire friction coefficients and the other based upon generated stoppping and cornering power. The various friction and power parameters used to describe the antiskid-system performance are discussed in the following paragraphs.

Tire Friction Terms

Time histories of wheel speed, skid signal, drag-force friction coefficient μ_d, and side-force friction coefficient μ_s for a typical antiskid braking test are presented in figure 10 to help define those parameters which describe the tire frictional behavior under antiskid control. For the test

illustrated, the brakes were applied at approximately 2 sec on the time scale and many skid cycles were generated over the test-section length.

Drag-force friction coefficients.- The drag-force friction coefficient that is observed before the brakes are applied results from the tire rolling resistance and is labeled μ_r in figure 10. For those tests on flooded surfaces, μ_r also includes the resistance attributed to fluid drag. The drag-force friction coefficient measured at the incipient wheel skid point normally represents the maximum value of μ_d which the tire can develop at that instant. For this antiskid system, however, with its high cycling frequency, a maximum available friction coefficient for each run is difficult to obtain. In order to assign a single value of the maximum available drag-force friction coefficient for a given run, a number of $\mu_{d,max}$ values were read at fixed time increments (10 points shown in fig. 10) and averaged to produce $\bar{\mu}_{d,max}$. Values of $\bar{\mu}_{d,max}$ are not available for the torque-limited braking tests because, in those cases, the maximum friction level was not reached. (Torque limited in this investigation refers to a situation where, for a given supply pressure, the brake torque is insufficient to cause a complete spin-down of the tire.) It is apparent that no antiskid cycling occurs when the brake is torque limited.

The average drag-force friction coefficient $\bar{\mu}_d$ developed by the antiskid system during a given test is defined by the expression

$$\bar{\mu}_d = \frac{1}{t_f - t_o} \int_{t_o}^{t_f} \mu_d \, dt \tag{1}$$

where t_o and t_f, identified in figure 10, enclose the time interval over which $\bar{\mu}_d$ is measured. The time t_o represented the point at which the pressure at the brake neared the maximum system pressure or when the first skid occurred; the time t_f was taken just prior to brake release at the end of the test section. The average drag-force friction coefficient was computed for each braking test with the use of numerical integration techniques.

Side-force friction coefficients.- The maximum side-force friction coefficient $\mu_{s,max}$ is observed in figure 10 to occur when the yawed wheel is freely rolling prior to brake application. The average side-force friction coefficient $\bar{\mu}_s$ developed by the antiskid system during braking is defined by an expression similar to that for $\bar{\mu}_d$. This expression

$$\bar{\mu}_s = \frac{1}{t_f - t_o} \int_{t_o}^{t_f} \mu_s \, dt \tag{2}$$

was also computed by numerical integration techniques for each yawed-wheel braking test.

Antiskid-System Effectiveness

It is a formidable task to evaluate an antiskid system in terms of efficiency or effectiveness. The ideal evaluation would assign a single performance number to the system; however, this is impossible because of the number of variables which must be considered. In an attempt to provide a rational and unbiased method of evaluating the performance of the antiskid braking system, the following performance ratios and power terms are used.

Performance ratios.- In order to obtain a measure of the braking performance of the antiskid system, the average friction coefficient developed by the system during a run was divided by the average maximum friction coefficient developed by the system during that run. This braking performance ratio η_b is defined by the expression

$$\eta_b = \frac{\bar{\mu}_d - \mu_r}{\bar{\mu}_{d,max} - \mu_r} \tag{3}$$

and provides an indication of how well the antiskid system is using the available friction coefficient during maximum braking. For equation (3), the tire rolling resistance friction coefficient μ_r is subtracted from both the available $\bar{\mu}_{d,max}$ and the developed $\bar{\mu}_d$ friction coefficients in order to isolate the braking portion of the drag force. A similar ratio η_c is used to define the cornering performance

$$\eta_c = \frac{\bar{\mu}_s}{\mu_{s,max}} \tag{4}$$

Power terms.- As defined in reference 6, the performance of an antiskid system can also be expressed in terms of the gross stopping power developed by the braking system and by the stopping and cornering power developed by the tire. These various power terms are defined in reference 6 in terms of the wheel speed V (equivalent to carriage speed), the drag force F_x parallel to the wheel plane, the side force F_y perpendicular to the wheel plane, the yaw angle ψ, and the slip ratio S. Slip ratio is the instantaneous ratio of slip speed of the braked wheel $(V - \omega r)$ to the carriage speed V and is given by the following equation:

$$S = \frac{V - \omega r}{V} \tag{5}$$

where r for the test tire equals 0.492 m (1.613 ft), as determined by averaging the rolling radii from the number of free-rolling tests. Time histories of some of these variables during a typical antiskid braking test are presented in figure 11. The following power expressions are defined over the interval between t_o and t_f.

The gross stopping power $P_{d,g}$ developed by the antiskid system during a braking test is

$$P_{d,g} = \frac{1}{t_f - t_o} \int_{t_o}^{t_f} (F_x \cos \psi + F_y \sin \psi) V \, dt \qquad (6)$$

where $F_x \cos \psi + F_y \sin \psi$ converts the measured drag and side forces noted in figure 11 to a single drag force opposing carriage motion. The product of velocity and time yields the distance through which the force acts and completes the work equation. Dividing the work by the duration provides a measure of the power being generated.

A measure of the stopping power dissipated by the tire $P_{d,t}$ is given by

$$P_{d,t} = \frac{1}{t_f - t_o} \int_{t_o}^{t_f} \left[(F_x \cos \psi + F_y \sin \psi) VS + F_y \sin \psi \, (1 - S)V \right] dt \qquad (7)$$

where the carriage speed is multiplied by the slip ratio to obtain the slip speed (relative speed between tire and pavement). The last term in equation (7), $\int_{t_o}^{t_f} F_y \sin \psi \, (1 - S)V \, dt$, is an estimate of the work dissipated by the rolling resistance, which is attributed to a yawed rolling tire.

The cornering power dissipated by the tire $P_{c,t}$ can be closely approximated by the expression

$$P_{c,t} = \frac{1}{t_f - t_o} \int_{t_o}^{t_f} (F_y \cos \psi - F_x \sin \psi)(1 - S)V \sin \psi \, dt \qquad (8)$$

where $F_y \cos \psi - F_x \sin \psi$ converts the measured side and drag forces to a single side force perpendicular to the direction of motion and where $(1 - S)V$ is the braked wheel speed which, when multiplied by $\sin \psi$, gives a measure of the tire lateral slip speed.

If F_x, F_y, and V are measured in U.S. Customary Units, then the values determined from equations (6), (7), and (8) must be divided by 550 to express the power terms in units of horsepower.

RESULTS AND DISCUSSION

Pertinent data obtained from all the antiskid braking tests are presented in table I, together with parameters which describe each test condition. In addition, time histories of key parameters from all the tests are presented in the appendix. The tabular data and the appendix time histories are given for the convenience of the user in plotting the data in ways other than those presented in this report. The following sections describe the braking system behavior, the tire frictional behavior under skid control, and the antiskid-system performance under a variety of operating conditions.

Braking System Behavior

In order to adequately study the performance of the antiskid system, it is first necessary to establish the response characteristics of the braking system and its components. The following paragraphs describe the pressure-torque response, the brake hydraulic response, the antiskid-system electronic response, and the braking-system response to transient runway friction conditions.

Pressure-torque response.- The relationship between brake pressure and brake torque is illustrated by the time histories in figure 12. The data presented in the figure are for a run that was torque limited during approximately 40 percent of the test, and was so chosen to minimize the effects of cyclic braking on the pressure-torque response. For the test condition illustrated, braking was initiated at about 1 sec and the brake pressure rapidly increased to the nominal system operating pressure of 21 MPa (3000 psi). The figure shows that when braking is initiated, the torque developed by the brake increases rapidly from 0 to approximately 21.7 kN-m (16 000 ft-lbf) and gradually increases with continued braking until the antiskid system is called upon to modulate the brake pressure in an effort to maintain the desired slip ratio and to prevent a wheel lockup. Figure 12 also shows that continued heavy braking causes the brake torque to dimish until the antiskid system is no longer modulating the brake pressure. The gradual torque rise which occurred during initial braking and the loss in torque (brake fade) which was noted near the end of the test are most likely due to the heating of surfaces within the brake. Another illustration of brake heating effects is found in figure 9(a). For that particular test the antiskid system was forced to gradually reduce the average brake pressure from approximately 18 MPa (2600 psi) at the start of the run to about 10 MPa (1450 psi) at the end of the run to maintain a uniform brake torque of approximately 18 kN-m (1300 ft-lb) throughout the braking test.

Hydraulic and electronic response.- Time histories of the pressure response at the antiskid control valve and at the brake during a typical antiskid braking test are presented in figure 13. In this example, the brake is not torque limited and the antiskid system is actively modulating the brake pressure. Although approximately 3 m (10 ft) of the hydraulic line and a line fuse separate the two transducers, no measurable hydraulic lags can be detected between them as the pressure response spikes of each occur at approximately the same time, as shown by the dashed lines in the figure. However, approximately 50 msec is required for a complete pressure dump due to the lags caused by line flow restrictions; this duration closely corresponds to the approximate time noted in figure 14 for the tire to lock up following a transition from a dry section to a flooded section of the runway.

The electronic response characteristics of the antiskid system can be described by examining the test wheel speed signal, the skid signal generated by the antiskid system, and the brake pressure. Typical time histories of these signals are presented in figure 14 for a transition from a dry section to a flooded section of the runway. As the dashed vertical line in the figure indicates, there is essentially no time lag between the wheel incipient skid point, the initiation of the skid signal, and subsequent brake pressure dump.

Response to runway friction transition.- The adaptive characteristics of the antiskid system are illustrated by time histories of the wheel speed, the skid signal, the brake pressure, and the drag-force friction coefficient as presented in figure 15 for two transient runway friction conditions. The response of the braking system to a single transition from a dry to a flooded runway surface is presented in figures 15(a) and 15(b) for nominal carriage speeds of 41 knots and 100 knots, respectively. At both test speeds, the brake pressure reached a nominal system operating pressure of 21 MPa (3000 psi) and was modulated by the antiskid system on the dry surface. Upon entering the flooded section, the wheel in both tests rapidly decelerated to a deep skid, as noted by the immediate reduction in wheel speed. At a carriage speed of 41 knots, the antiskid system reacted quickly to permit the wheel to recover from the skid, and the remainder of the braking test was conducted with proper antiskid protection. At a carriage speed of 100 knots the wheel did not recover but continued to skid even though the antiskid system responded properly and released all brake pressure. The predicted spin-up hydroplaning speed for the tire, based upon a tire inflation pressure of 0.97 MPa (140 psi), was 91 knots (equivalent to a wheel speed of 15.16 rps); thus, once the tire had spun down, insufficient torque was being developed between the tire and the pavement to spin the tire up. (See ref. 5.)

Time histories of test runs that were selected to illustrate the response of the braking system during the transition from a flooded to a dry runway surface are presented in figures 15(c) and 15(d), for nominal carriage speeds of 43 knots and 102 knots, respectively. In both tests, the wheel was spun up to carriage speed on a dry surface prior to entering the flooded test section and the brakes were applied at or near the flooded section. Figure 15(c) shows that, at 43 knots, the antiskid system properly controlled the braking action on the flooded portion of the runway and maintained a mean brake pressure of approximately 6 to 8 MPa (900 to 1200 psi). Note that at 3.3 sec, changes in the developed drag-force friction coefficient resulted in corresponding changes in brake pressure. Upon reaching the dry runway, the brake pressure rapidly increased to a mean value of approximately 14 MPa (2000 psi). In figure 15(d), however, upon entering the flooded test section at 110 knots, the wheel commenced to spin down due to dynamic tire hydroplaning, which caused the skid signal to become saturated. The predicted tire spin-down hydroplaning speed, based upon an inflation pressure of 0.97 MPa (140 psi), was 106 knots (equivalent to a wheel speed of 17.66 rps). (See ref. 5.) Upon reaching the dry section, the wheel rapidly spun up to carriage speed and the brake pressure increased to a maximum pressure of nearly 21 MPa (3000 psi) in approximately 0.7 sec. Subsequent braking on the dry runway was with normal antiskid protection.

Tire Frictional Behavior Under Skid Control

Effect of test parameters on maximum drag-force friction coefficient.- The average maximum drag-force friction coefficient $\bar{\mu}_{d,max}$ as developed by the unyawed tire under dry, damp, and flooded conditions is presented as a function of carriage speed in figure 16. The fairings in the figure are linear least-squares curve fits of the data. As expected, values of $\bar{\mu}_{d,max}$ for the wet runways are substantially lower than those for the dry runway and the difference becomes greater with increasing water depth, particularly at the higher

speeds; also, they approach negligible values on the flooded runway near the predicted tire spin-down hydroplaning speed of 106 knots. Noted in the figure is the maximum value of the drag-force friction coefficient, 0.78, which was predicted from the empirical expression developed in reference 11 for the test tire operating at very low speeds. It is apparent from the fairings that the dry data for $\bar{\mu}_{d,max}$ would fall below this prediction if extrapolated to zero speed. The reason for this apparent difference can be explained by examining the data of figure 17 where values of $\mu_{d,max}$ that were obtained solely during the first wheel spin-down at the initial brake application for each test are presented as a function of carriage test speed. These values represent the maximum friction coefficients available from an unheated tire and are faired by a straight line that corresponds to a least-squares fit of the data and which, when extended to very low ground speeds, agrees very closely with the value of $\bar{\mu}_{d,max}$ that was empirically determined from reference 11 for cold tires during a single braking cycle. For comparison purposes, the fairing of the average values of $\bar{\mu}_{d,max}$ obtained over the entire duration of each of the eight test runs (fig. 16) is also presented in the figure. The maximum friction developed during the initial brake cycle is shown to exceed the average maximum developed throughout each of the tests, particularly those conducted at speeds below approximately 80 knots. The lower average maximum values are attributed to the high tire temperatures generated as the antiskid system maintains the tire at a relatively constant slip ratio.

The data of figure 16 were obtained at a yaw angle of 0°. The fairings of these data for the three surface conditions are reconstructed in figure 18, together with corresponding data obtained at yaw angles of 3° and 6°, to show the effect of yaw angle on $\bar{\mu}_{d,max}$. The figure shows that the effect of yaw angle is dependent upon the surface condition. With the introduction of yaw, $\bar{\mu}_{d,max}$ is shown to be reduced on the dry surface but to be relatively unaffected when the surface was damp or flooded.

The effect of tire tread wear on $\bar{\mu}_{d,max}$ is presented in figure 19 where the values of $\bar{\mu}_{d,max}$ for tires having new and worn treads are plotted as a function of carriage speed under the three test surface conditions. The new tread data were obtained from the faired curves of figure 16. The data indicate that when the new tread is replaced by a worn tread, $\bar{\mu}_{d,max}$ is increased on the dry surface and is reduced on the damp and flooded runway surfaces. These trends are in reasonable agreement with similar trends noted in references 2 and 6.

Effect of test parameters on maximum side-force friction coefficient.- The maximum side-force friction coefficients available to the free-rolling tire under dry, damp, and flooded conditions are plotted as a function of carriage speed in figure 20. The fairings in the figure are linear least-squares curve fits of the data. The values of $\mu_{s,max}$ always occur during the free-rolling portion of the run and, for the wet runway surfaces, are lower than those for the dry runway surface with the difference becoming greater with increasing water depth and speed. As expected, the values of $\mu_{s,max}$ at a yaw angle of 6° are substantially higher than those at a yaw angle of 3° on the dry and damp runway surfaces. On the flooded surface, however, this trend was not as clearly defined as the values of $\mu_{s,max}$ at both yaw angles are shown to approach 0 in the region of the predicted tire spin-down hydroplaning speed of 106 knots.

The effect of tread wear on $\mu_{s,max}$ is shown in figure 21 where the values of $\mu_{s,max}$ at a yaw angle of 6° on dry, damp, and flooded runway surfaces are plotted as a function of carriage speed. The new-tread data were obtained from the faired curves in figure 20 for a yaw angle of 6°. The data show insignificant differences between the values of $\mu_{s,max}$ that are developed with new and worn treads on the dry surface, but there is a definite friction loss on the wet surfaces when the new tire tread is replaced by a worn one. Further, the friction loss appears to become more pronounced with increasing water depth.

Interaction between braking and cornering.- Typical tire friction response to antiskid braking on dry and flooded runway surfaces (interaction between braking and cornering) is presented in figure 22. The drag- and side-force friction coefficients, μ_d and μ_s, respectively, for the tire yawed to 3° and operating at a nominal carriage speed of 72 knots are plotted as a function of wheel slip ratio. The data presented in the figure illustrate the irregular nature of the friction coefficient to which the antiskid braking system must respond. The random perturbations can be attributed to a combination of such factors as small fluctuations in the tire vertical load due to runway unevenness, flexibility in the wheel support which would be reflected in the measured drag and side forces, variations in the runway surface friction characteristics, tire and brake temperatures, and the spring coupling provided by the tire between the wheel and the pavement. Reference 12 discusses some of these factors in detail.

The data presented in figure 22 also illustrate the traction losses associated with flooded runway operations. For example, on the dry runway, the maximum value of μ_d is 0.55, but it never exceeds 0.25 on the flooded runway. A somewhat smaller loss is noted in the maximum side-force friction coefficients. The figure also demonstrates the deterioration in tire cornering capability with increased braking effort (slip ratio). The value of μ_s is reduced approximately 44 percent on the dry runway at a slip ratio of only 0.15, which is the maximum value reached in the test illustrated, and μ_s is reduced to a negligible value at a slip ratio of 0.2 on the flooded surface. These trends are consistent with those noted for similar antiskid braking tests in references 1 and 6 and further illustrate the cornering/braking dilemma faced by antiskid manufacturers.

Effect of cyclic braking on maximum drag-force friction coefficient.- A comparison between the values of $\mu_{d,max}$ measured during single-cycle braking tests made without antiskid protection and the average of corresponding values measured under the same test conditions with the antiskid system operational is presented in figure 23. The data are presented separately for dry, damp, and flooded test conditions and for all the test conditions combined. These data include coefficients for tests at various speeds, yaw angles, vertical loads, and for worn as well as new tread configurations. The data for each test condition are faired by a least-squares fit through the plot origins. The data indicate that the maximum drag-force friction coefficients obtained from single-cycle braking tests tend to be higher than the average maximum coefficients developed by the antiskid system on the dry and flooded surfaces and tend to underestimate those on a damp surface. When the data for all three surface wetness conditions are compared simultaneously, the tendency is for the single-cycle data to be higher than the maximum drag-force friction coefficient available to the antiskid system. These results, which are in close agreement with

the results reported in reference 6, imply that braking performance calculations that are based upon the values of $\bar{\mu}_{d,max}$ obtained from a number of antiskid cycles would be more representative than those based on $\mu_{d,max}$ from a single braking cycle because the latter neglects, among other things, runway surface variations and tire heating effects.

Antiskid-System Performance

Braking performance.- In this section, two terms are used to present a measure of antiskid performance: (1) the performance ratio which assesses the ability of the antiskid system to use the friction that is available at the tire/runway interface; and (2) the total stopping power which essentially describes the extent of the braking effort that is developed by the antiskid system.

Antiskid braking performance ratios η_b were computed and listed in table I for all braking tests except those which were torque limited throughout the entire run, those involving tire hydroplaning, and those performed to examine the effects of a runway friction transition. Figure 24 is a plot of η_b presented as a function of the average maximum available drag-force friction coefficient $\bar{\mu}_{d,max}$. With the exceptions mentioned, all the data are plotted in the figure and the wide range of test variables (surface condition, yaw angle, carriage speed, tire wear, etc.) resulted in the scatter shown. The braking performance ratio for all damp and flooded tests varied from 0.47 to 0.94 with an average value of 0.80. The magnitude of $\bar{\mu}_{d,max}$ on these wetted surfaces never exceeded 0.4. The braking performance ratios for the dry surface tests varied from 0.79 to 1.00 with an average value of 0.94 where the range of $\bar{\mu}_{d,max}$ extended from 0.43 to 0.65. For the four runs on random dry/damp surfaces where $\mu_{d,max}$ ranged from 0.37 to 0.54, the average braking performance ratio was 0.76. Thus the antiskid braking system is shown to suffer a loss in performance on wet surfaces - the surfaces that have the greatest need for good performance since they have lower friction coefficients.

In order to illustrate the effect that various test parameters have on the braking performance ratios of the antiskid system, the data are presented in bar-graph form. Figure 25 presents these data in terms of $\bar{\eta}_b$, a numerical average of all data from a given test condition. For example, the dry, 50-knot bar graph is the average of all dry runs conducted at 50 knots, including the various yaw angles, vertical forces, and tread configurations. The trends observed for some of these test conditions may be influenced by a small sample size. On the dry surface, $\bar{\eta}_b$ increases slightly with tire vertical loadings, decreases when the new tread is replaced with a worn tread, and suggests no discernible trend for variations in the carriage speed and wheel yaw angle. The average performance ratio on the wet surfaces is shown to decrease with increasing carriage speed, increasing yaw angle, and when the new tread is replaced by a worn tread and to increase with increasing vertical force on the tire. The trends described here on both wet and dry surfaces are in agreement with trends observed from another antiskid system and reported in reference 6 for variations in carriage speed, tire vertical loading, and tread condition. However, some differences do exist between these data and those of reference 6 as to the effect that yaw angle changes have on the performance ratio. The data presented

in figure 25 suggest that the braking performance of this antiskid system may be degraded as the aircraft yaw angle approaches 6°, as might occur during cross-wind operations, may be reduced by excessive wing lift during the landing roll-out, and may be reduced by excessive tire wear, particularly under wet runway conditions.

The gross stopping power $P_{d,g}$ (eq. (6)) developed by the antiskid system, which is a measure of the overall antiskid braking effort, is listed in table I for each test condition. Bar graphs which are the average of these data are presented in figure 26 to describe the effects of test-parameter variations. Data from torque-limited tests and from tests involving tire hydroplaning are included in the figure but not data from tests performed under transient runway friction conditions. As expected, because of higher available friction coefficients, the gross stopping power on the dry surface is much higher than that on the wet runway surfaces. On the dry surface, $\bar{P}_{d,g}$ increases with carriage speed and tire vertical force, and decreases with yaw angle. The tire tread condition appeared to have little effect. On the wet surfaces, $\bar{P}_{d,g}$ increases with tire vertical force, decreases with tread wear, is lower at a yaw angle of 6° than at angles of either 0° or 3°, and there is no discernible trend for variations in carriage speed.

The stopping power dissipated by the tire alone $P_{d,t}$ (eq.(7)) is only a small fraction of the gross stopping power but it does provide an indication of the tread wear associated with braking effort; thus, the ideal antiskid system would maximize $P_{d,g}$ and minimize $P_{d,t}$. Values of $P_{d,t}$ are listed in table I for each test condition. These data are averaged and plotted as bar graphs in figure 27 to show the effects attributed to test-parameter variations. Data from all tests except those performed to study the effect of a runway friction transition are included in the figure. The figure shows that for corresponding conditions, $\bar{P}_{d,t}$ is higher on the dry surface than on the wet surfaces, as would be expected since higher forces are generated on the dry surface. On a dry surface, $\bar{P}_{d,t}$ increases with yaw angle and when a new tread is replaced by a worn tread, decreases with tire vertical force, and there is no discernible trend for changes in carriage speed. On the wet runway surfaces, $\bar{P}_{d,t}$ increases with carriage speed, increases with tire vertical force, decreases when a worn tread is used, and there is no discernible trend for variations in the yaw angle. The data in figure 27 indicate that the most severe tread wear occurs during combined braking and cornering operations on a dry surface.

The ratio of tire stopping power to gross stopping power for each test is plotted as a function of $\bar{\mu}_{d,max}$ in figure 28. Data are not included for torque-limited tests, for tests performed under transient runway friction conditions, or for tests involving tire hydroplaning. The curves which fair the data represent a least-squares fit and indicate that the ratio increases as the surface friction level decreases, perhaps due to hydroplaning effects and to an increasing slip ratio threshold on lower friction surfaces. The figure also shows that the general effect of increasing the wheel yaw angle is to increase the percentage of the total stopping power dissipated by the tire; thus an increase in tire wear, which was suggested by the amount of rubber deposited on the runway during yawed rolling tests is indicated.

Cornering performance.- Antiskid systems are not designed to maximize cornering performance since good cornering is not compatible with heavy braking, but cornering is important for directional control, especially when cross winds are present.

The antiskid system cornering performance ratio η_c for the individual braking tests at yaw angles of 3° and 6° is listed in table I and is presented in figure 29 as a bar graph for the average values for each set of test conditions. The data indicate that $\bar{\eta}_c$ was higher on the dry surface than on the wet surfaces. In addition, the average cornering performance ratio is shown to decrease for both surface conditions with increasing yaw angle and when the new tire was replaced by a worn one. The effect of increasing carriage speed was generally to improve $\bar{\eta}_c$ on both the dry and wet surfaces.

The cornering power dissipated by the tire $P_{c,t}$ (eq. (8)) not only is indicative of the overall cornering capability of the tire during the antiskid controlled braking, but also provides an indication of the increased tread wear associated with the steering effort. The effects of test-parameter variations on $\bar{P}_{c,t}$ are presented in figure 30 as bar graphs. The data indicate that the values of $\bar{P}_{c,t}$ are, as expected, considerably higher on the dry surface than on the wet surfaces and increase with yaw angle and speed on both surfaces. The value of $\bar{P}_{c,t}$ was higher for the worn tread condition on the dry surface and was higher for the new tread condition on the wet surfaces. Although $\bar{\eta}_c$ decreased with increasing yaw angle (fig. 29), the values of $P_{c,t}$ increased substantially when the yaw angle was increased from 3° to 6° (fig. 30); thus the need for both power terms and performance ratio terms when studying the characteristics of antiskid systems is illustrated.

CONCLUDING REMARKS

An experimental investigation was conducted at the Langley aircraft landing loads and traction facility to study the braking and cornering response of a slip-ratio-controlled aircraft antiskid braking system with ground speed reference derived from an unbraked nose wheel. The investigation, conducted on dry and wet runway surfaces, utilized one main gear wheel, brake, and tire assembly of a McDonnell Douglas DC-9 series 10 airplane.

During maximum braking, the average ratio of the drag-force friction coefficient developed by the antiskid system to the maximum drag-force friction coefficient available was higher on the dry surface than on damp and flooded surfaces and was reduced with lighter vertical loads, higher yaw angles, and when new tire treads were replaced by worn treads. Similarly, the average ratio of side-force friction coefficient developed by the tire under antiskid control to the maximum side-force friction coefficient available to a freely rolling yawed tire decreased with increasing yaw angle, generally increased with ground speed, and decreased when tires with new treads were replaced by those with worn treads.

The average gross stopping power generated by the brake system was considerably higher on the dry surface than on the wet surfaces. That portion of the

stopping power which was dissipated by the tire and which provided an indication of the tire wear was observed to be greatest during combined braking and cornering on a dry surface.

The interaction between braking and cornering indicated that, during antiskid cycling on a dry surface, the side-force friction coefficient was typically reduced by more than 40 percent; on a flooded surface, this coefficient was reduced to negligible values.

During the transition from a dry to a flooded surface under heavy braking, the wheel entered into a deep skid but the antiskid system reacted quickly and permitted the wheel to regain ground speed and to resume braking on the flooded surface while preventing subsequent deep skids. Brake pressure recovery was rapid following the transition from a flooded to a dry surface.

Langley Research Center
National Aeronautics and Space Administration
Hampton, VA 23665
June 30, 1977

REFERENCES

1. Tanner, John A.: Performance of an Aircraft Tire Under Cycle Braking and of a Currently Operational Antiskid Braking System. NASA TN D-6755, 1972.

2. Horne, Walter B.; and Leland, Trafford J. W.: Influence of Tire Tread Pattern and Runway Surface Condition on Braking Friction and Rolling Resistance of a Modern Aircraft Tire. NASA TN D-1376, 1962.

3. Tracy, William V., Jr.: Wet Runway Aircraft Control Project (F-4 Rain Tire Project). ASD-TR-74-37, U.S. Air Force, Oct. 1974. (Availble from DDC as AD A004 768.)

4. Danhof, Richard H.; and Gentry, Jerauld R.: RF-4C Wet Runway Performance Evaluation. FTC-TR-66-6, U.S. Air Force, May 1966. (Available from DDC as AD 486 049.)

5. Horne, Walter B.; McCarty, John L.; and Tanner, John A.: Some Effects of Adverse Weather Conditions on Performance of Airplane Antiskid Braking Systems. NASA TN D-8202, 1976.

6. Stubbs, Sandy M.; and Tanner, John A.: Behavior of Aircraft Antiskid Braking Systems on Dry and Wet Runway Surfaces - A Velocity-Rate-Controlled, Pressure-Bias-Modulated System. NASA TN D-8332, 1976.

7. Metric Practice Guide. E 380-72, American Soc. Testing & Mater., June 1972.

8. Tanner, John A.: Fore-and-Aft Elastic Response Characteristics of 34 × 9.9, Type VII, 14 Ply-Rating Aircraft Tires of Bias-Ply, Bias-Belted, and Radial-Belted Design. NASA TN D-7449, 1974.

9. Leland, Trafford J. W.; Yager, Thomas J.; and Joyner, Upshur T.: Effects of Pavement Texture on Wet-Runway Braking Performance. NASA TN D-4323, 1968.

10. Yager, Thomas J.; Phillips, W. Pelham; Horne, Walter B.; and Sparks, Howard C. (appendix D by R. W. Sugg): A Comparison of Aircraft and Ground Vehicle Stopping Performance on Dry, Wet, Flooded, Slush-, Snow-, and Ice-Covered Runways. NASA TN D-6098, 1970.

11. Smiley, Robert F.; and Horne, Walter B.: Mechanical Properties of Pneumatic Tires With Special Reference to Modern Aircraft Tires. NASA TR R-64, 1960. (Supersedes NACA TN 4110.)

12. Batterson, Sidney A.: A Study of the Dynamics of Airplane Braking Systems as Affected by Tire Elasticity and Brake Response. NASA TN D-3081, 1965.

TABLE I.- SUMMARY OF TEST

Run	Tire tread condition	Brake supply pressure		Yaw angle, deg	Surface condition	Vertical load		Nominal carriage speed, knots	$\bar{\mu}_d$	$\bar{\mu}_{d,max}$	μ_r	Brake performance ratio
		MPa	psi			kN	lbf					
1	New	19	2700	0	Dry	63.6	14 300	97	0.58	0.59	0.03	0.98
2	New	21	3000	0	Dry	81.8	18 400	44	.54	.57	.02	.95
3	New	21	3000	0	Dry	80.1	18 000	68	.58	.59	.04	.98
4	New	20	2890	0	Dry	81.8	18 400	95	.57	.57	.03	1.00
5	New	20	2940	0	Dry	81.4	18 300	98	.52	.54	.03	.96
6	New	21	3000	0	Dry	98.3	22 100	39	.53	.54	.02	.98
7	New	21	2950	0	Dry	98.3	22 100	68	.51	.51	.02	1.00
8	New	21	2950	0	Dry	97.4	21 900	98	.50	.53	.04	.94
9	New	21	3000	0	Damp	62.3	14 000	47	.32	.36	.05	.87
10	New	21	3000	0	Damp	63.2	14 200	71	.26	.33	.02	.77
11	New	21	3000	0	Damp	61.8	13 900	103	.16	.19	.03	.81
12	New	21	3000	0	Damp	81.0	18 200	46	.31	.35	.03	.88
13	New	21	3000	0	Damp	80.5	18 100	73	.29	.35	.03	.81
14	New	21	3000	0	Damp	81.0	18 200	99	.21	.25	.03	.82
15	New	21	3000	0	Damp	97.9	22 000	46	.30	.33	.03	.90
16	New	21	3000	0	Damp	97.4	21 900	72	.28	.31	.02	.90
17	New	21	3000	0	Damp	97.4	21 900	101	.26	.29	.04	.88
18	New	21	3000	0	Damp	117.9	26 500	45	.33	.35	.04	.94
19	New	21	3000	0	Damp	118.3	26 600	41	.33	.35	.02	.94
20	New	20	2900	0	Damp	118.3	26 600	72	.28	.32	.03	.86
21	New	21	3000	0	Damp	118.8	26 700	99	.28	.26	.05	.91
22	New	21	3000	0	Flooded	61.8	13 900	74	.18	.19	.06	.92
23	New	20	2930	0	Flooded	61.8	13 900	101	.06		.04	
24	New	20	2880	0	Flooded	61.4	13 800	102	.07		.07	
25	New	21	3000	0	Flooded	81.4	18 300	50	.26	.29	.03	.88
26	New	21	3000	0	Flooded	81.0	18 200	74	.17	.19	.05	.86
27	New	20	2900	0	Flooded	80.5	18 100	75	.16	.17	.04	.92
28	New	20	2910	0	Flooded	80.1	18 000	100	.06		.03	
29	New	21	3000	0	Flooded	97.9	22 000	46	.27	.30	.03	.89
30	New	21	3000	0	Flooded	97.0	21 800	72	.19	.21	.04	.88
31	New	21	3000	0	Flooded	98.8	22 200	100	.07		.07	
32	New	19	2820	0	Flooded	122.3	27 500	46	.25	.28	.04	.88
33	New	18	2640	0	Flooded	118.8	26 700	72	.18	.21	.04	.82
34	New	19	2770	0	Flooded	117.9	26 500	103	.06		.05	
35	New	19	2760	0	Dry/Flooded	83.2	18 700	41		.61/.28		
36	New	19	2780	0	Dry/Flooded	84.1	18 900	70		.55/.19		
37	New	19	2820	0	Dry/Flooded	85.0	19 100	100		.46/		
38	New	19	2800	0	Flooded/Dry	83.2	18 700	43		.32/.50		
39	New	19	2840	0	Flooded/Dry	63.6	14 300	73		.18/.57		
40	New	20	2870	0	Flooded/Dry	64.5	14 500	102		/.57		
41	New	21	3000	0	Random Dry/Damp	79.6	17 900	65	.38	.46	.04	.81
42	New	21	3000	3	Dry	80.5	18 100	39	.52	.53	.03	.98
43	New	21	3000	3	Dry	81.8	18 400	72	.49	.50	.03	.98
44	New	21	3000	3	Dry	82.3	18 500	99	.47	.49	.02	.96
45	New	21	3000	3	Damp	81.0	18 200	46	.31	.36	.03	.85
46	New	21	3000	3	Damp	81.0	18 200	70	.24	.30	.04	.74
47	New	21	3000	3	Damp	80.1	18 000	98	.26	.32	.06	.77
48	New	19	2800	3	Flooded	64.5	14 500	48	.24	.28	.04	.83
49	New	19	2820	3	Flooded	82.3	18 500	72	.16	.19	.04	.80
50	New	20	2860	3	Flooded	83.2	18 700	102	.06		.06	
51	New	21	3000	6	Dry	81.4	18 300	40	.46	.48	.06	.95
52	New	21	3000	6	Dry	81.4	18 300	67	.45	.47	.07	.95
53	New	21	3000	6	Dry	82.3	18 500	97	.43	.44	.06	.97
54	New	21	3000	6	Damp	81.0	18 200	44	.28	.31	.04	.89
55	New	21	3000	6	Damp	81.0	18 200	70	.22	.28	.06	.73

CONDITIONS AND RESULTS

Percent of run time brake was torque limited	$\bar{\mu}_s$	$\mu_{s,max}$	Cornering performance ratio	Average slip ratio	Gross stopping power		Tire stopping power		Tire cornering power		Hydro-planing	Run
					kW	hp	kW	hp	kW	hp		
24	0			0.09	1962	2631	172	231		0	No	1
	0			.15	1134	1521	164	220		0		2
14	.01			.09	1764	2366	153	205		0		3
39	.01			.10	2476	3321	235	315		0		4
39	0			.07	2248	3014	148	198		0		5
	0			.15	1187	1592	166	223		0		6
23	0			.09	1929	2587	169	226		0		7
47	0			.06	2619	3512	151	202		0		8
	0			.18	542	727	95	127		0		9
	0			.12	658	882	78	104		0		10
	-.01			.15	538	722	75	101		0		11
	0			.16	664	890	104	140		0		12
	0			.15	953	1278	137	184		0		13
	0			.14	931	1248	124	166		0		14
	.01			.15	772	1035	112	150		0		15
	.01			.14	1111	1490	145	195		0		16
	.01			.12	1429	1916	158	212		0		17
	0			.14	1004	1347	136	183		0		18
	.01			.13	937	1257	113	151		0		19
	.01			.12	1339	1796	146	196		0		20
	.01			.12	1687	2262	189	253		0		21
	.02			.16	439	589	69	92		0		22
	.01			.88	213	285	188	252		0	Yes	23
	.01			.64	236	317	146	196		0	Yes	24
	0			.16	594	796	92	123		0	No	25
	.01			.16	570	764	89	120		0		26
	.01			.18	529	710	89	120		0		27
	0			.87	283	380	251	336		0	Yes	28
	.01			.16	702	941	108	145		0	No	29
	.01			.16	735	985	113	151		0	No	30
	.02			.82	303	406	251	337		0	Yes	31
	0			.14	928	1244	125	168		0	No	32
	.01			.18	856	1148	150	201		0	No	33
	.02			.81	358	480	250	335		0	Yes	34
	0				905	1213	156	209		0	No	35
	0				1251	1677	151	202		0	No	36
	0				1209	1621	114	153		0	No/Yes	37
	0				701	940	95	128		0	No	38
	0				825	1107	92	123		0		39
	.01				923	1238	221	296		0		40
	0			.13	1136	1524	128	172		0		41
	.14	.26	0.54	.16	952	1277	163	219	13	17		42
	.17	.24	.71	.10	1590	2132	190	255	26	35		43
	.19	.26	.73	.08	2089	2801	217	291	41	55		44
	.10	.18	.56	.15	662	888	112	150	10	14		45
	.10	.20	.50	.14	773	1037	124	166	16	21		46
	.10	.16	.63	.13	1150	1542	168	225	21	28		47
	.07	.21	.33	.20	431	578	85	114	5	7		48
	.05	.14	.36	.14	538	721	84	112	7	10		49
	.01			.91	312	419	259	347	1	2	Yes	50
	.22	.43	.51	.15	849	1139	173	232	37	49	No	51
	.28	.43	.65	.10	1376	1845	241	323	8	11		52
	.30	.43	.70	.09	1851	2482	303	406	124	166		53
	.16	.24	.67	.16	580	778	127	171	29	39		54
	.15	.22	.68	.14	696	933	148	198	44	59		55

TABLE I.-

Run	Tire tread condition	Brake supply pressure		Yaw angle, deg	Surface condition	Vertical load		Nominal carriage speed, knots	$\bar{\mu}_d$	$\bar{\mu}_{d,max}$	μ_r	Brake performance ratio
		MPa	psi			kN	lbf					
56	New	21	3000	6	Damp	81.0	18 200	98	0.19	0.26	0.05	0.67
57	New	19	2840	6	Flooded	84.1	18 900	45	.24	.28	.06	.82
58	New	19	2740	6	Flooded	84.1	18 900	72	.14	.17	.06	.73
59	New	20	2870	6	Flooded	83.6	18 800	92	.09		.07	
60	New	21	3000	6	Random Dry/Damp	80.1	18 000	70	.31	.37	.06	.81
61	Worn	20	2880	0	Dry	79.6	17 900	42	.60	.63	.02	.95
62	Worn	21	3000	0	Dry	80.5	18 100	43	.54	.64	.02	.84
63	Worn	20	2920	0	Dry	81.4	18 300	40	.62	.64	.02	.97
64	Worn	20	2860	0	Dry	84.1	18 900	66	.54	.59	.03	.91
65	Worn	20	2910	0	Dry	81.0	18 200	67	.59	.65	.03	.90
66	Worn	20	2910	0	Dry	81.0	18 200	100	.57			
67	Worn	20	2880	0	Dry	81.4	18 300	97	.56			
68	Worn	18	2640	0	Damp	83.6	18 800	43	.30	.37	.03	.79
69	Worn	18	2640	0	Damp	83.6	18 800	44	.28	.35	.03	.78
70	Worn	21	3000	0	Damp	79.2	17 800	48	.19	.21	.02	.89
71	Worn	21	3000	0	Damp	79.6	17 900	48	.18	.22	.02	.80
72	Worn	21	3000	0	Damp	79.2	17 800	47	.22	.26	.02	.83
73	Worn	18	2600	0	Damp	83.2	18 700	72	.22	.32	.03	.66
74	Worn	21	3000	0	Damp	79.2	17 800	74	.14	.18	.03	.73
75	Worn	21	3000	0	Damp	79.2	17 800	72	.18	.25	.04	.67
76	Worn	21	3000	0	Damp	80.1	18 000	100	.21	.27	.04	.74
77	Worn	21	3000	0	Damp	80.5	18 100	99	.14	.21	.03	.60
78	Worn	18	2620	0	Flooded	84.1	18 900	49	.21	.24	.04	.85
79	Worn	21	3000	0	Flooded	78.3	17 600	45	.22	.24	.03	.90
80	Worn	21	3000	0	Flooded	78.3	17 600	73	.12	.14	.06	.75
81	Worn	20	2930	0	Flooded	78.7	17 700	100	.08			
82	Worn	19	2830	0	Flooded	81.4	18 300	93	.07			
83	Worn	21	3000	6	Dry	81.4	18 300	45	.40	.49	.06	.79
84	Worn	21	3000	6	Dry	83.2	18 700	70	.46	.48	.06	.95
85	Worn	19	2690	6	Dry	86.7	19 500	68	.40	.43	.06	.92
86	Worn	21	3000	6	Dry	82.7	18 600	99	.42	.45	.06	.92
87	Worn	19	2750	6	Dry	87.2	19 600	95	.42	.47	.06	.88
88	Worn	19	2750	6	Damp	84.5	19 000	46	.25	.30	.05	.80
89	Worn	21	3000	6	Damp	80.5	18 100	50	.16	.20	.03	.76
90	Worn	21	3000	6	Damp	79.6	17 900	76	.13	.18	.03	.67
91	Worn	18	2620	6	Damp	85.0	19 100	72	.16	.23	.05	.61
92	Worn	21	3000	6	Damp	80.5	18 100	101	.12	.20	.05	.47
93	Worn	17	2470	6	Flooded	85.0	19 100	49	.14	.18	.06	.67
94	Worn	21	3000	6	Flooded	77.0	17 300	46	.23	.26	.08	.83
95	Worn	21	3000	6	Flooded	79.2	17 800	72	.09	.10	.05	.80
96	Worn	19	2660	6	Flooded	83.6	18 800	73	.08	.09	.05	.75
97	Worn	20	2900	6	Flooded	78.3	17 600	85	.07			
98	Worn	19	2690	6	Flooded	82.7	18 600	91	.07		.07	
99	New	14	2000	0	Random Dry/Damp	80.5	18 100	72	.40	.54	.02	.73
100	New	14	2000	0	Dry/Wet	79.2	17 800	100				
101	New	14	2000	0	Wet/Dry	63.6	14 300	45		.39/.58		
102	New	13	1940	0	Wet/Dry	63.6	14 300	100		/.23		
103	New	13	1940	6	Dry	81.0	18 200	70	.50	.51	.09	.98
104	New	14	2000	6	Damp	80.5	18 100	75	.21	.27	.04	.74
105	New	14	2000	6	Random Dry/Damp	78.7	17 700	71	.32	.44	.05	.69

Concluded

Percent of run time brake was torque limited	$\bar{\mu}_s$	$\mu_{s,max}$	Cornering performance ratio	Average slip ratio	Gross stopping power		Tire stopping power		Tire cornering power		Hydro-planing	Run
					kW	hp	kW	hp	kW	hp		
	0.14	0.20	0.70	0.12	849	1138	164	220	57	76	No	56
	.08	.27	.30	.17	536	719	108	145	16	22	↓	57
	.02	.14	.14	.15	482	646	84	112	8	11	↓	58
	-.01			.32	391	525	122	164	2	3	Yes	59
	.23			.15	972	1304	212	284	69	93	No	60
82	-.02			.06	1665	2233	571	766		0	↓	61
	0			.15	1079	1447	147	197		0	↓	62
15	-.02			.13	1184	1588	148	199		0	↓	63
70	0			.08	1747	2343	136	183		0	↓	64
93	0			.06	1787	2397	105	141		0	↓	65
100	.01			.06	2483	3330	152	204		0	↓	66
100	0			.06	2461	3300	149	200		0	↓	67
	-.02			.19	692	928	107	143		0	↓	68
	.01			.19	659	884	105	141		0	↓	69
	0			.17	406	545	70	94		0	↓	70
	0			.23	389	522	86	115		0	↓	71
	0			.20	459	616	88	118		0	↓	72
	.01			.16	793	1064	106	142		0	↓	73
	.01			.18	458	614	79	106		0	↓	74
	0			.20	571	766	106	142		0	↓	75
	0			.19	954	1279	171	229		0	↓	76
	0			.17	676	906	103	138		0	↓	77
	.01			.20	491	659	92	124		0	↓	78
	.02			.20	439	589	85	114		0	↓	79
	.01			.25	367	492	93	125		0	↓	80
	.01			.47	265	355	125	168		0	Yes	81
	0			.87	310	416	251	336		0	Yes	82
	.21	.45	.47	.18	779	1044	195	262	31	42	No	83
	.29	.49	.59	.13	1482	1988	289	388	87	117	↓	84
	.12	.34	.40	.13	1404	1883	237	318	41	55	↓	85
	.28	.47	.60	.13	1904	2553	386	518	119	159	↓	86
	.12	.36	.33	.17	2127	2853	426	572	59	79	↓	87
	.05	.21	.24	.17	584	783	108	145	14	19	↓	88
	.04	.19	.21	.19	350	470	77	103	9	12	↓	89
	.08	.18	.44	.18	425	570	101	136	25	33	↓	90
	.02	.13	.15	.17	641	860	114	153	17	23	↓	91
	.07	.18	.39	.17	559	750	136	183	31	42	↓	92
	-.01	.10	0	.18	348	467	65	87	1	2	↓	93
	.10	.18	.56	.20	474	636	116	155	16	22	↓	94
	.03	.08	.38	.19	262	352	63	84	9	12	↓	95
	-.02	0	0	.19	282	378	54	72	0	0	↓	96
	.01			.73	258	346	190	255	1	1	Yes	97
	.02			.91	317	425	286	384	2	3	Yes	98
41	.01			.10	1296	1738	110	147	0	0	No	99
45	.01				1331	1785	107	144	0	0	↓	100
0	0				679	910	89	119	0	0	↓	101
34	0				1293	1734	114	153	0	0	↓	102
37	.31	.44	.70	.09	1521	2040	241	323	9	12	↓	103
	.13	.24	.54	.13	669	897	133	179	39	52	↓	104
	.25			.14	1007	1351	211	283	73	98	↓	105

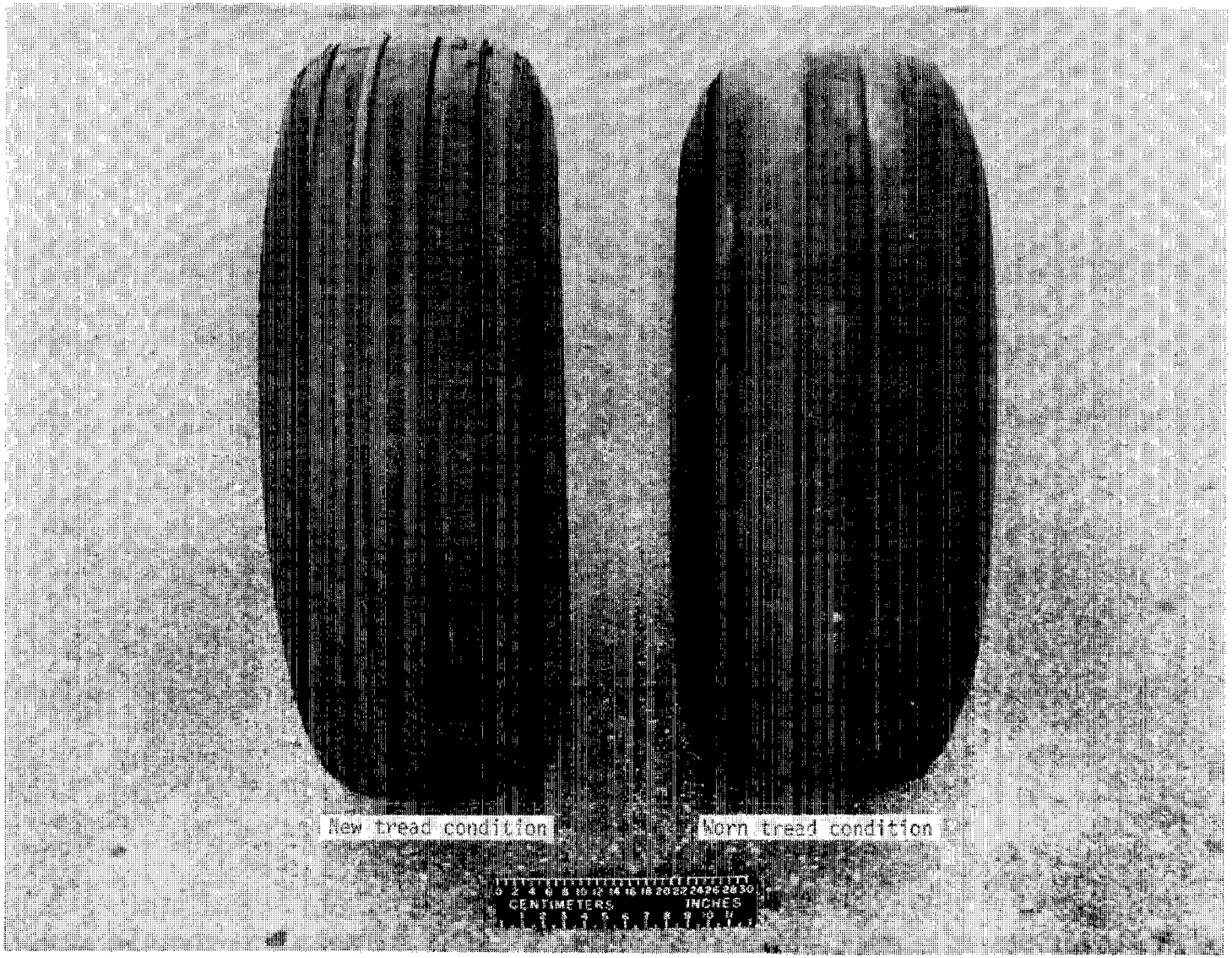

L-76-1704.1

Figure 1.- New and worn tread condition of six-groove, 40 × 14, type VII aircraft test tires.

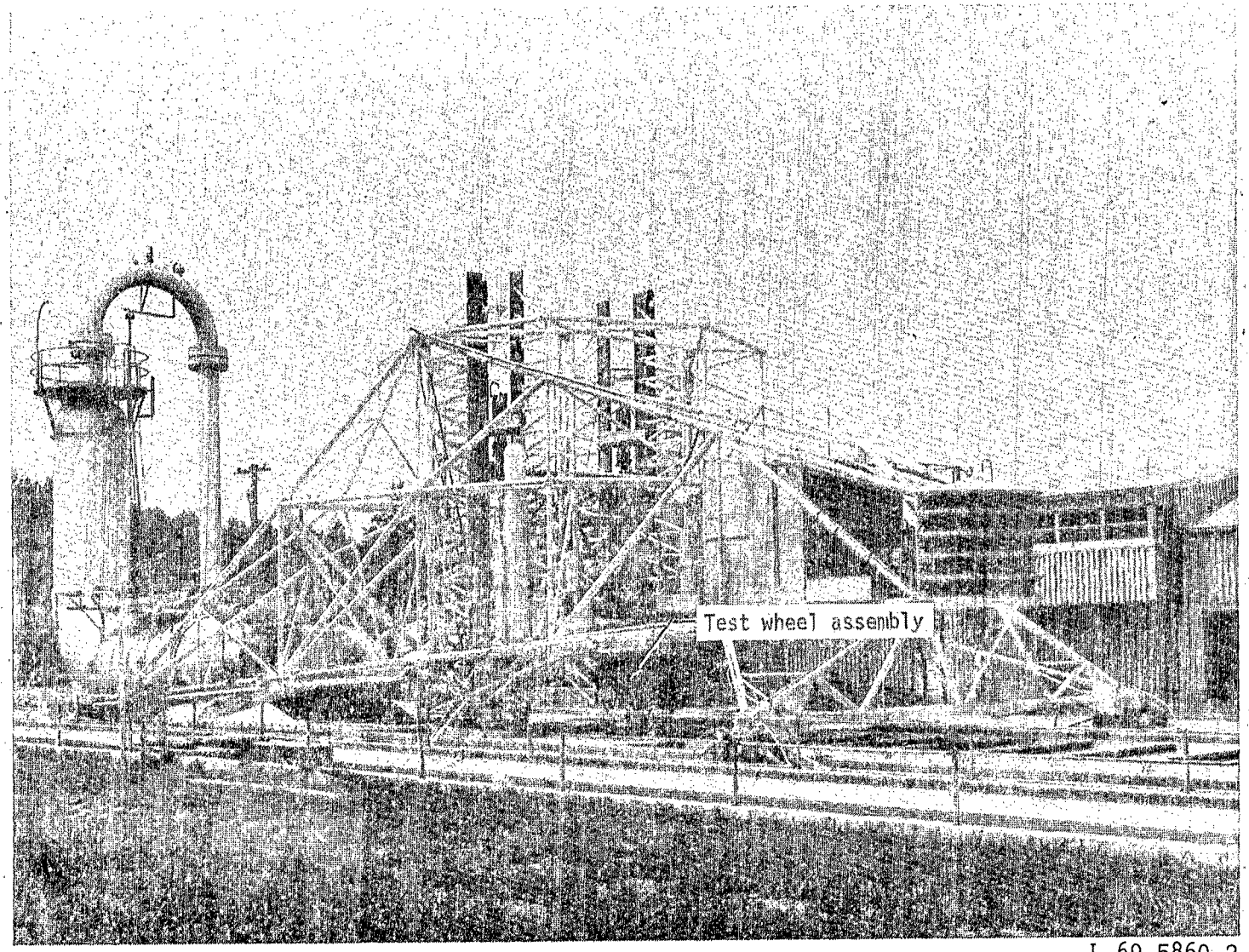

L-69-5860.2

Figure 2.- Test carriage.

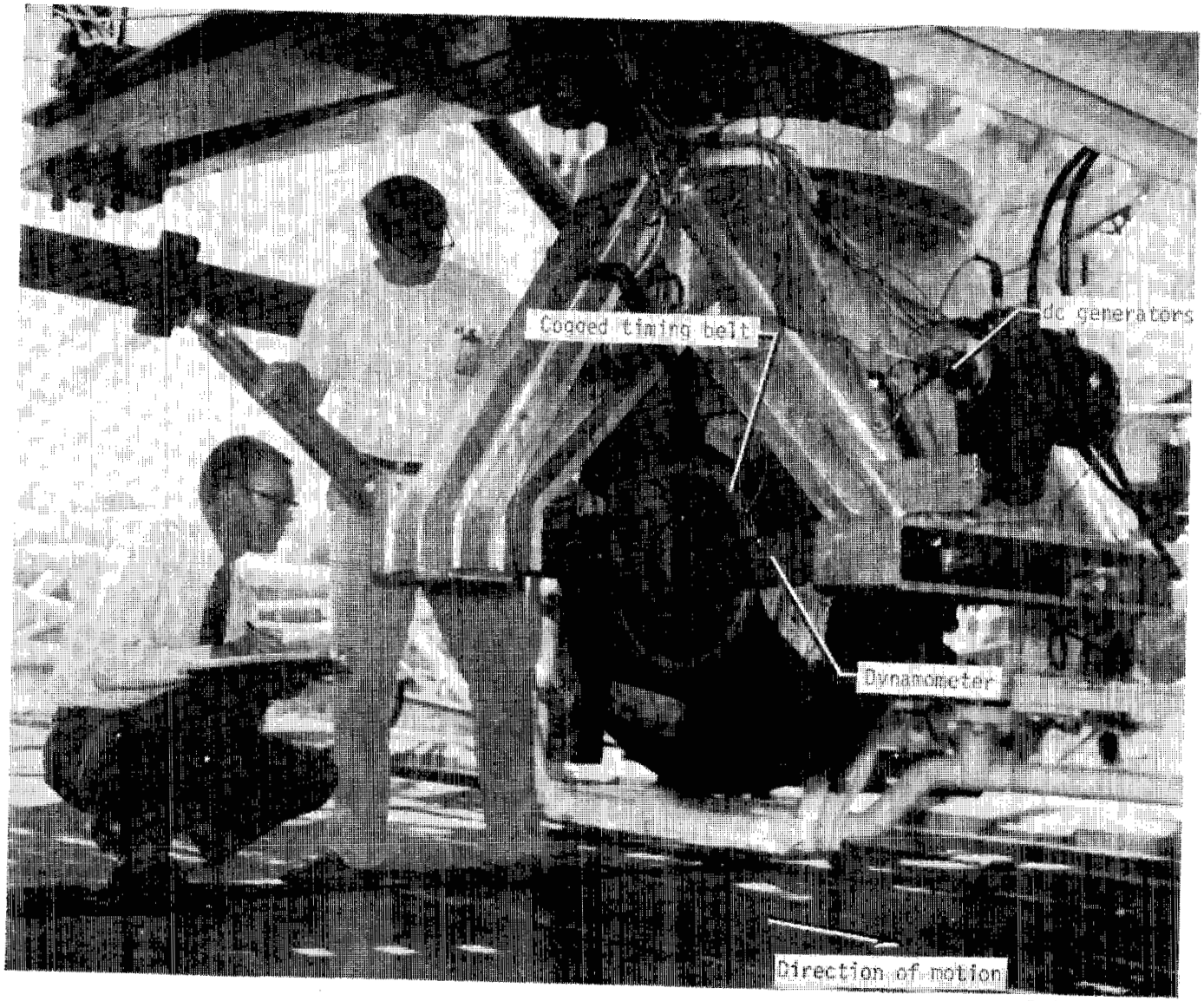

L-75-3427.2

Figure 3.- Close-up view of wheel, tire, and instrumented dynamometer.

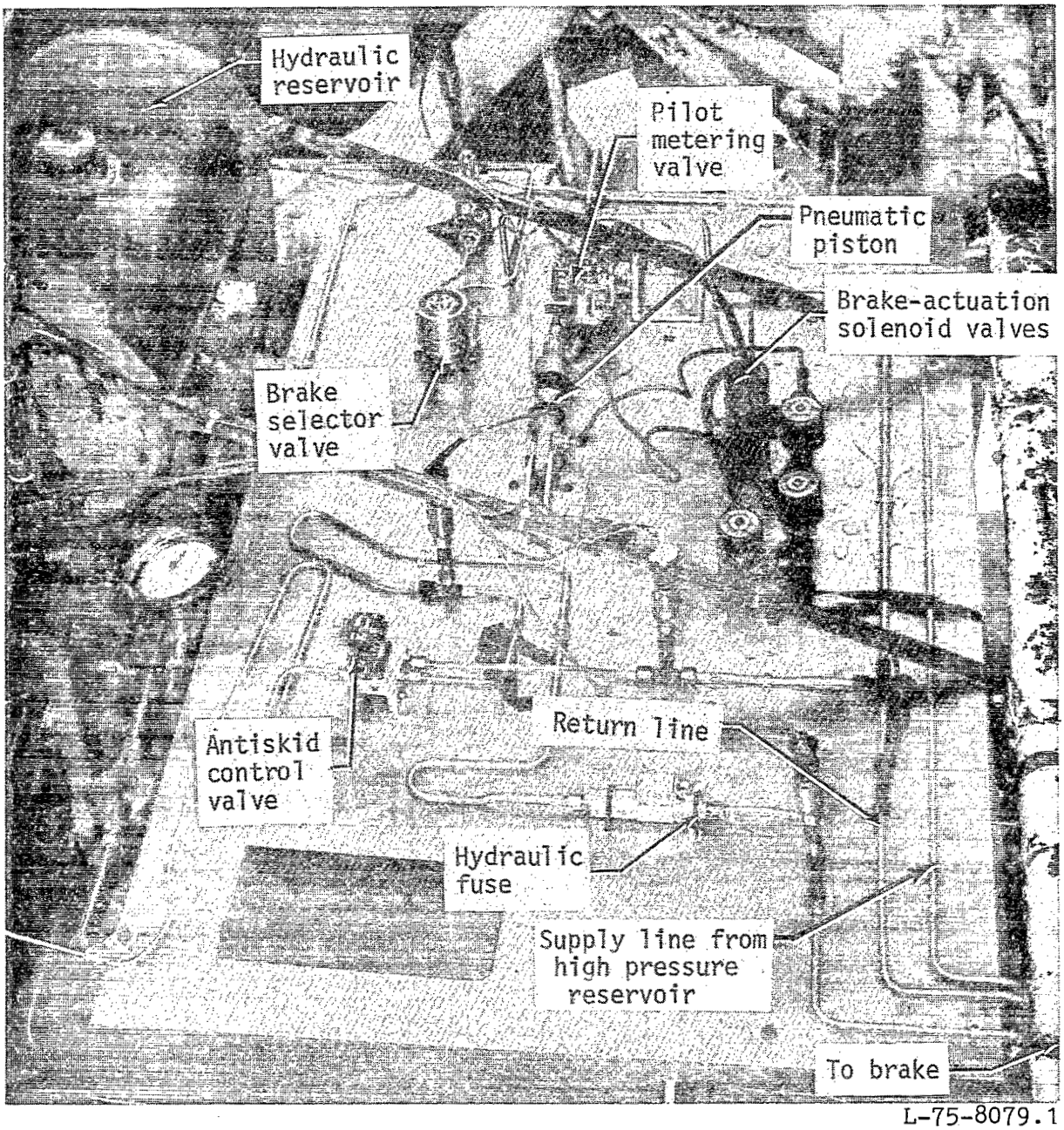

L-75-8079.1

Figure 4.- Layout of simulated braking system on test carriage.

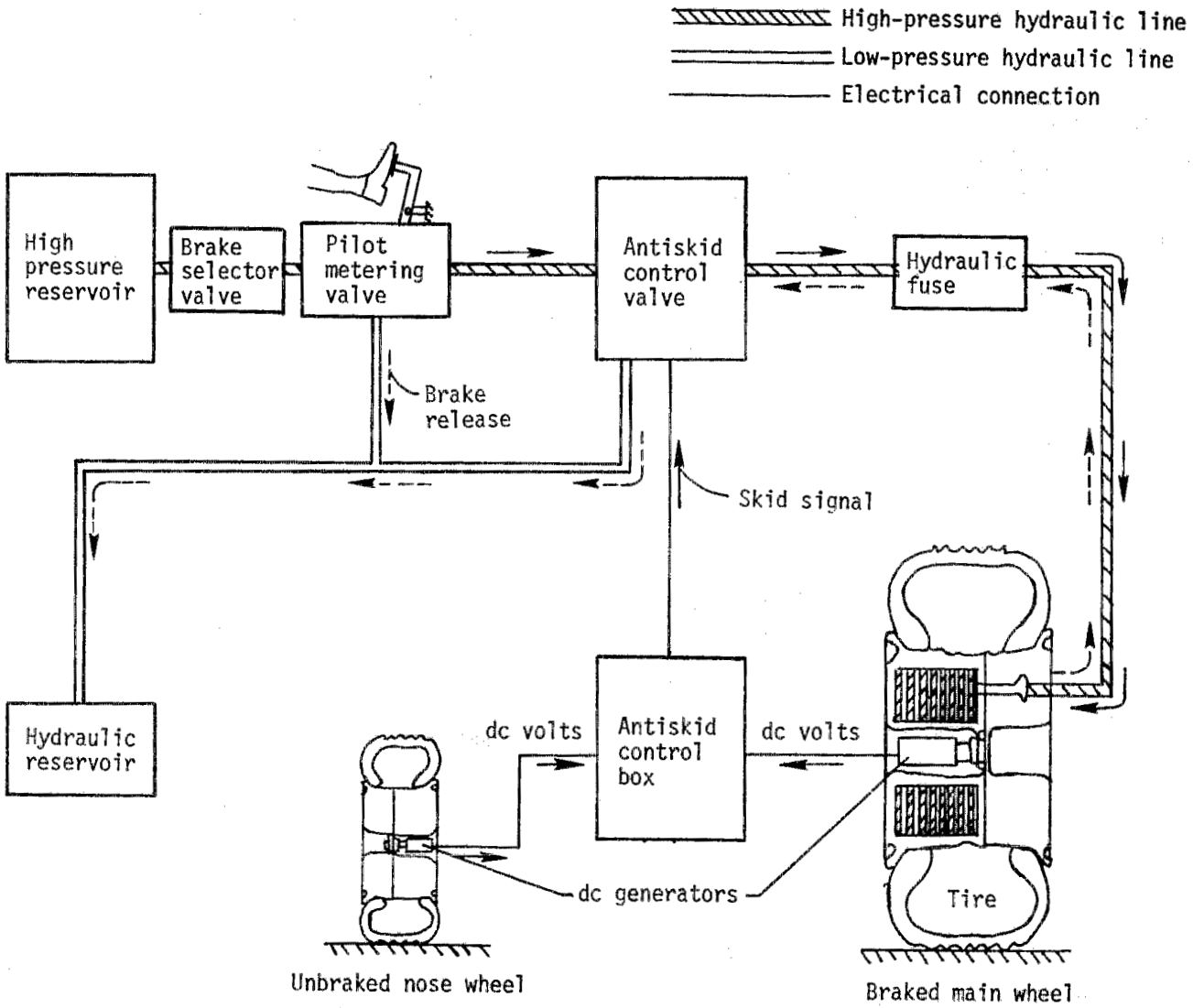

Figure 5.- Schematic diagram of braking system.

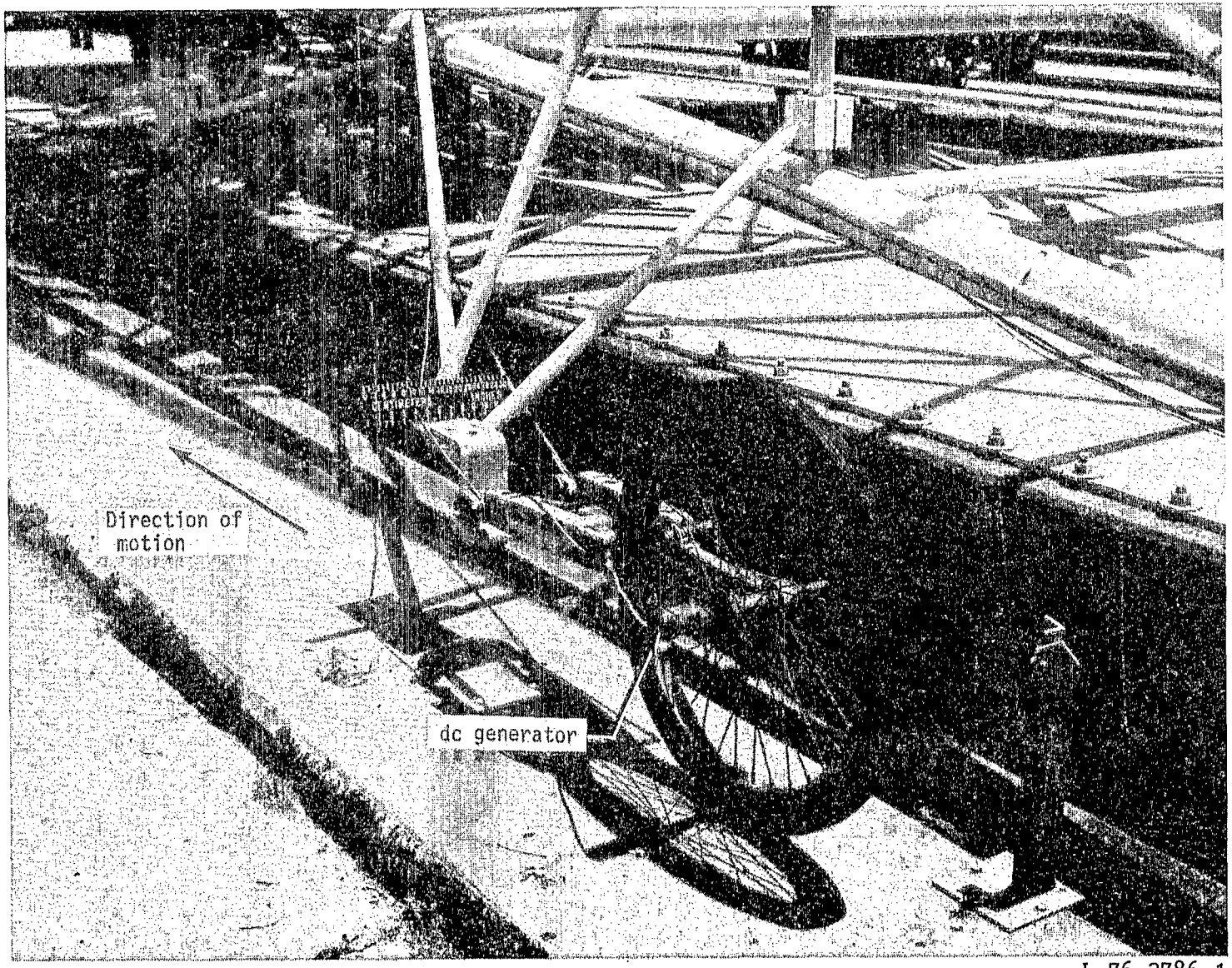

L-76-3786.1

Figure 6.- Lightweight trailing wheel used to simulate airplane nose wheel.

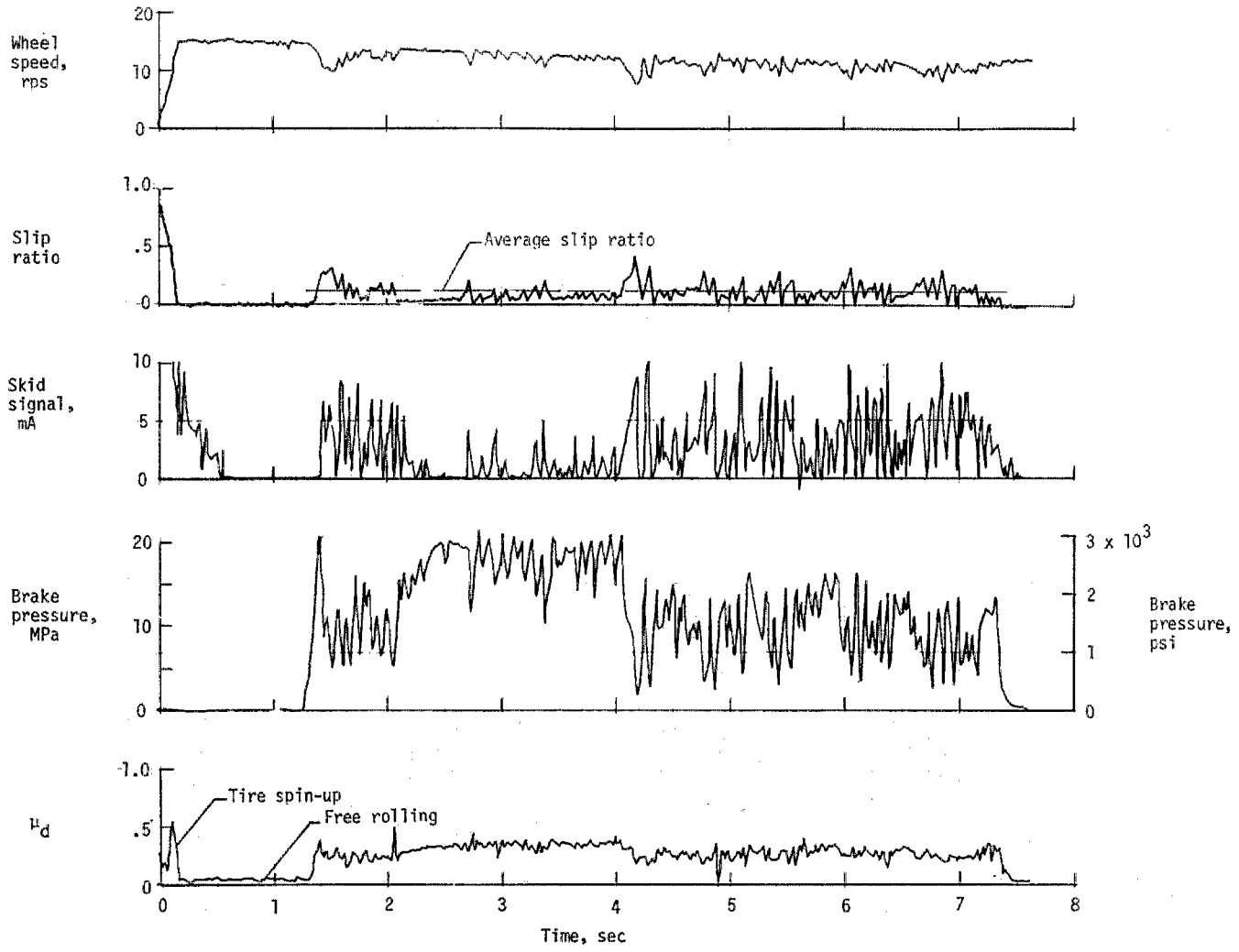

(a) Time histories for an entire run.

Figure 7.- Typical antiskid-system operation. Run 20; yaw angle, 0°; vertical load, 118.3 kN (26 600 lbf); brake supply pressure, 20 MPa (2900 psi); tire condition, new; nominal carriage speed, 72 knots; surface condition, damp.

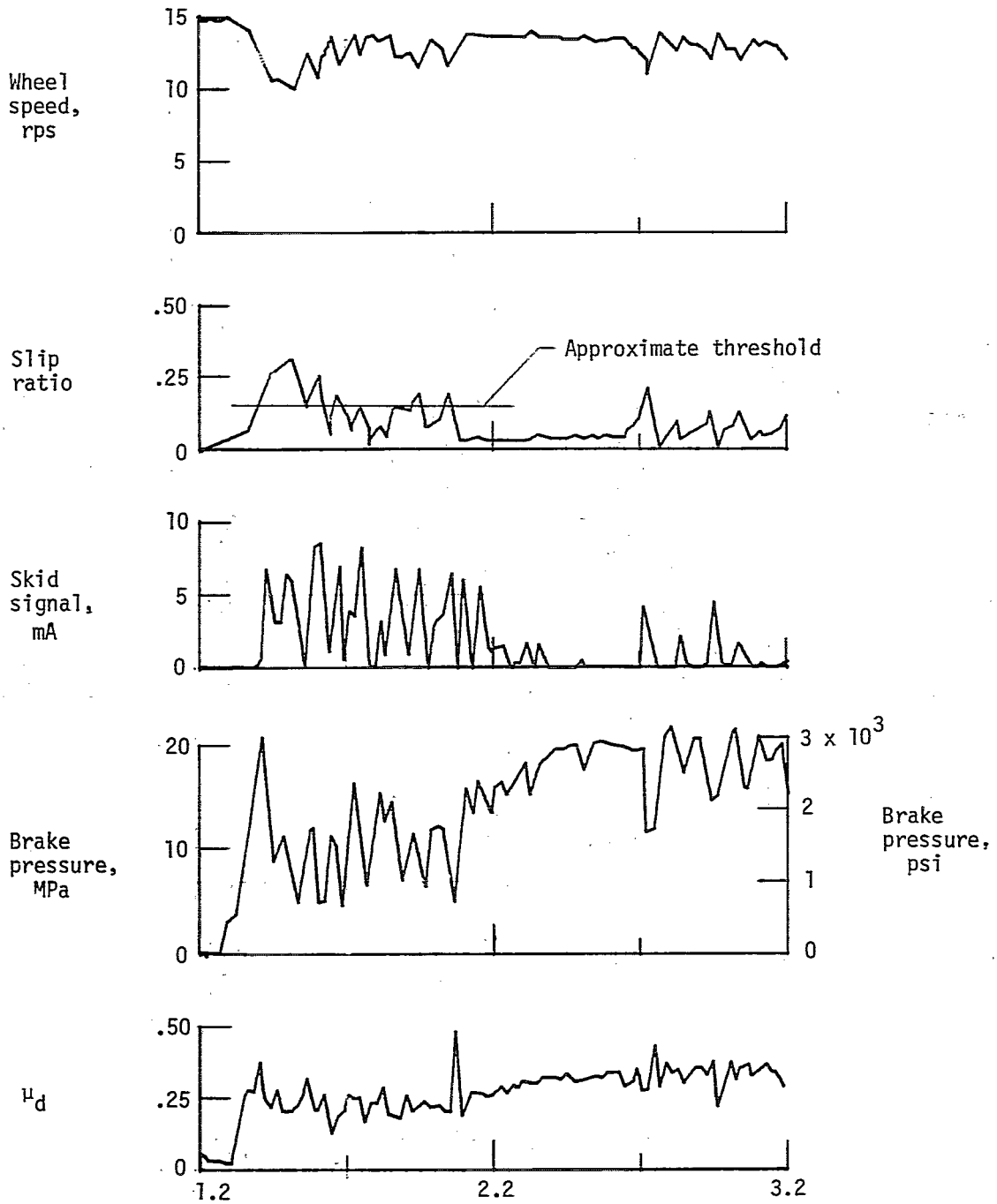

(b) Expanded time histories from 1.2 to 3.2 sec.

Figure 7.- Concluded.

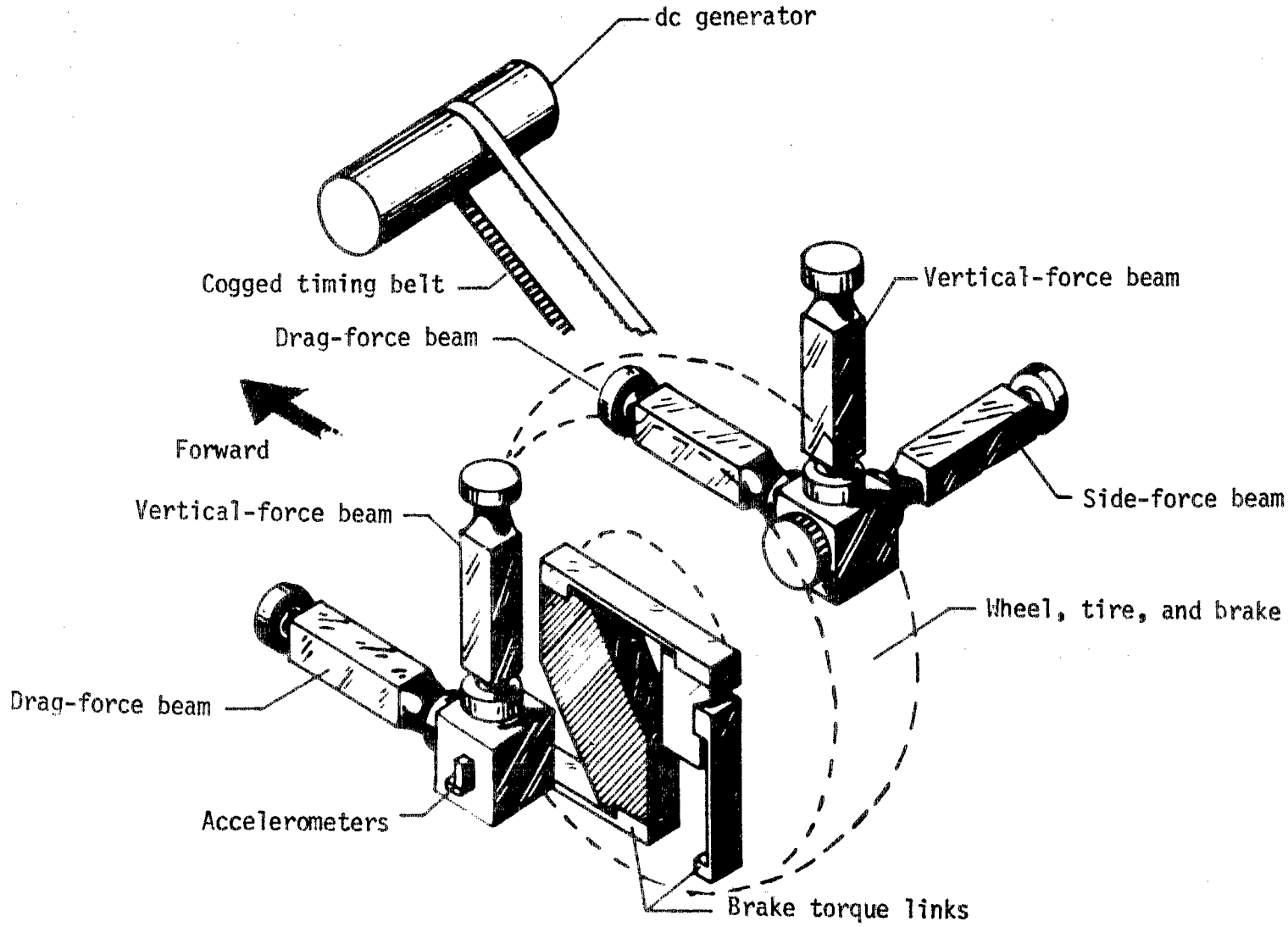

Figure 8.- Dynamometer details.

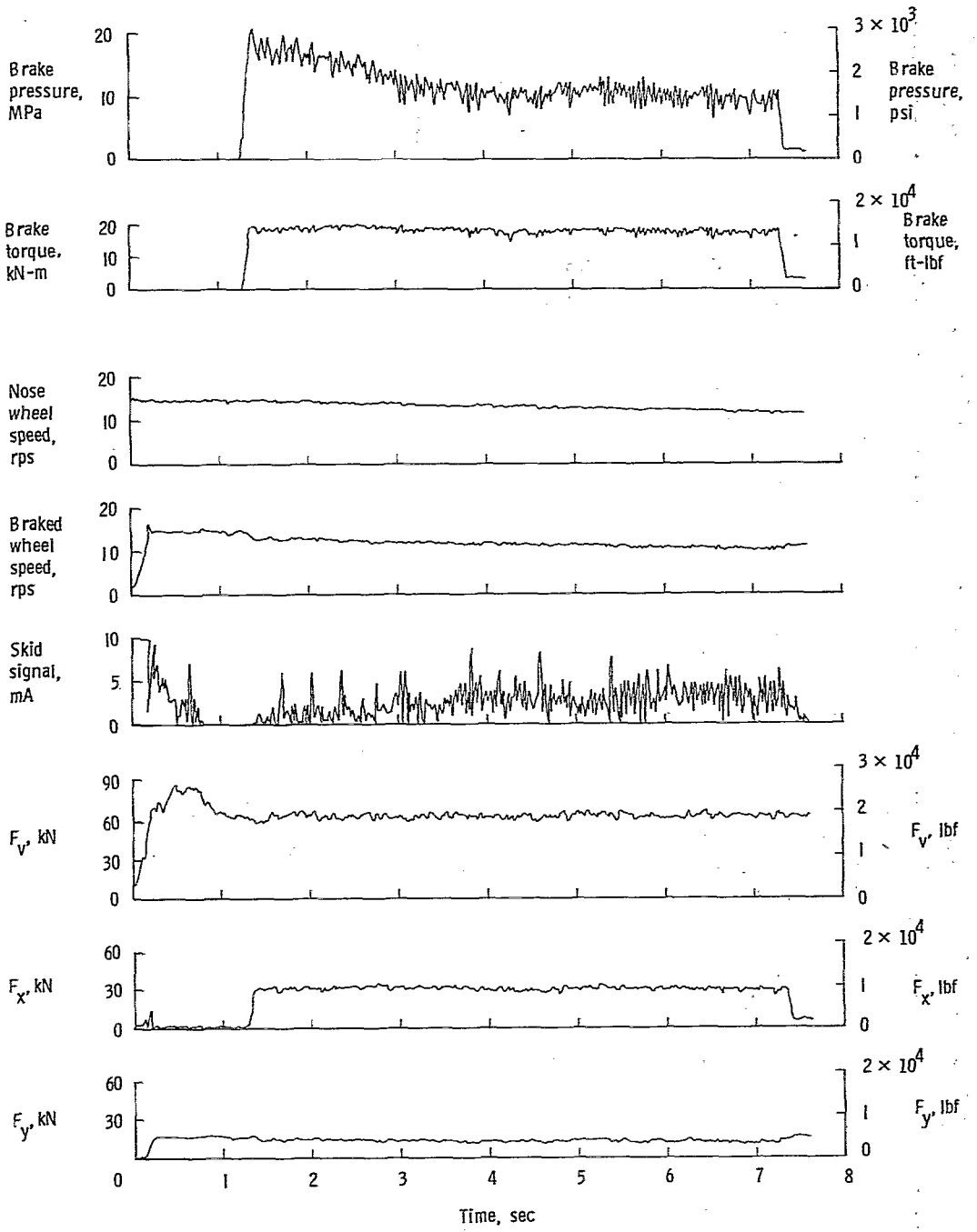

(a) Measured parameters.

Figure 9.- Typical time histories of measured and calculated parameters. Run 43; yaw angle, 3°; vertical load, 81.8 kN (18 400 lbf); brake supply pressure, 21 MPa (3000 psi); tire condition, new; nominal carriage speed, 72 knots; surface condition, dry.

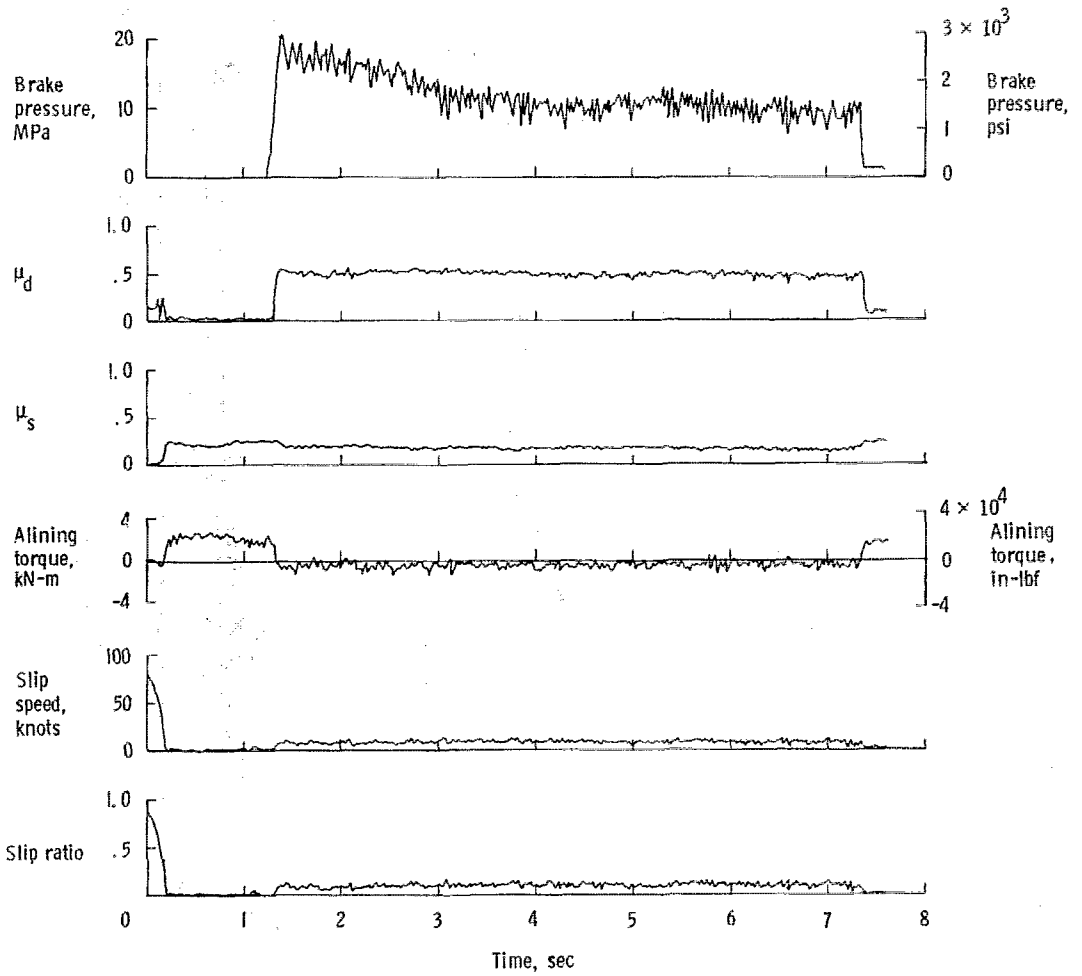

(b) Calculated parameters.

Figure 9.- Concluded.

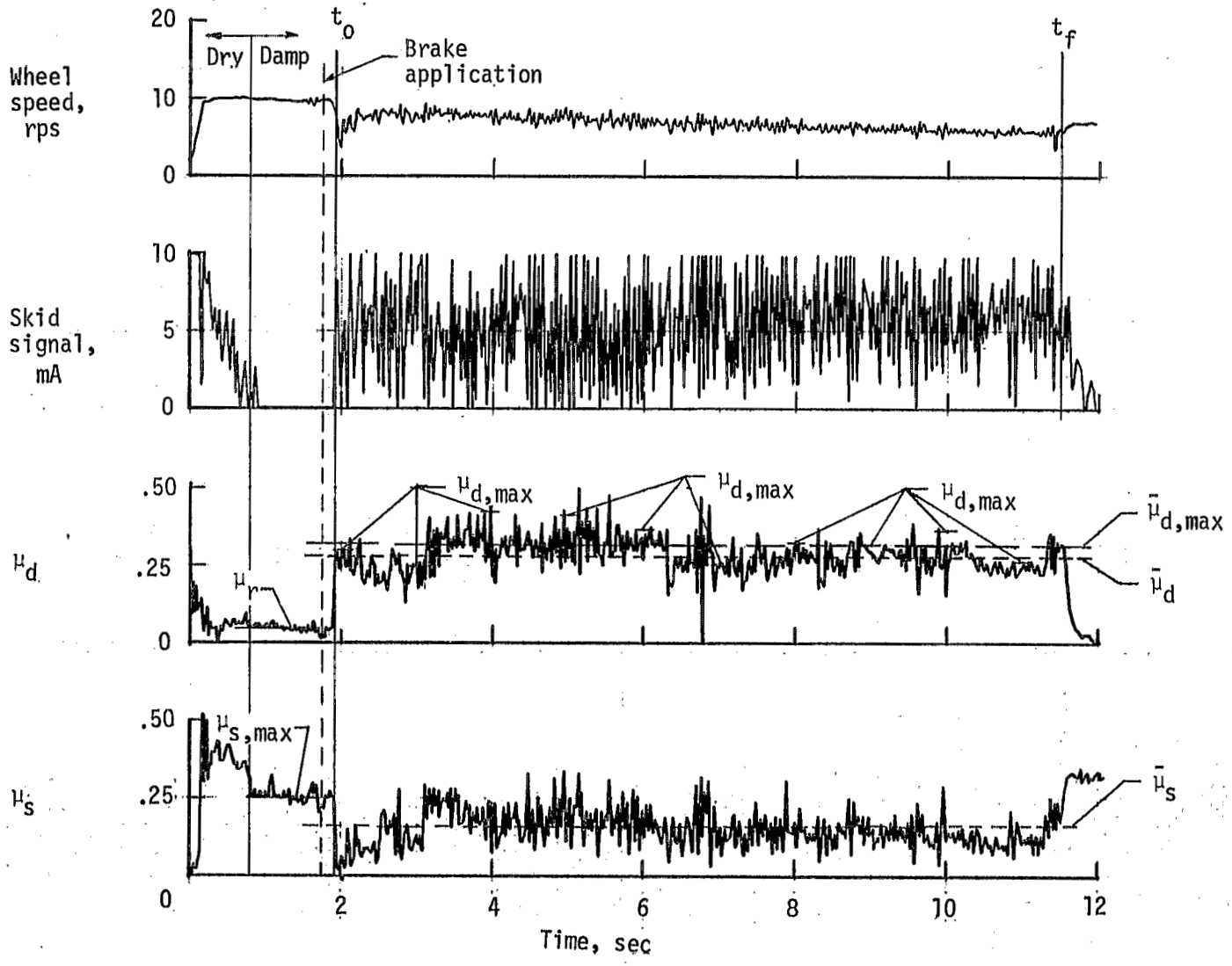

Figure 10.- Definition of various friction terms. Run 54; yaw angle, 6°; vertical load, 81.0 kN (18 200 lbf); brake supply pressure, 21 MPa (3000 psi); tire condition, new; nominal carriage speed, 44 knots; surface condition, damp.

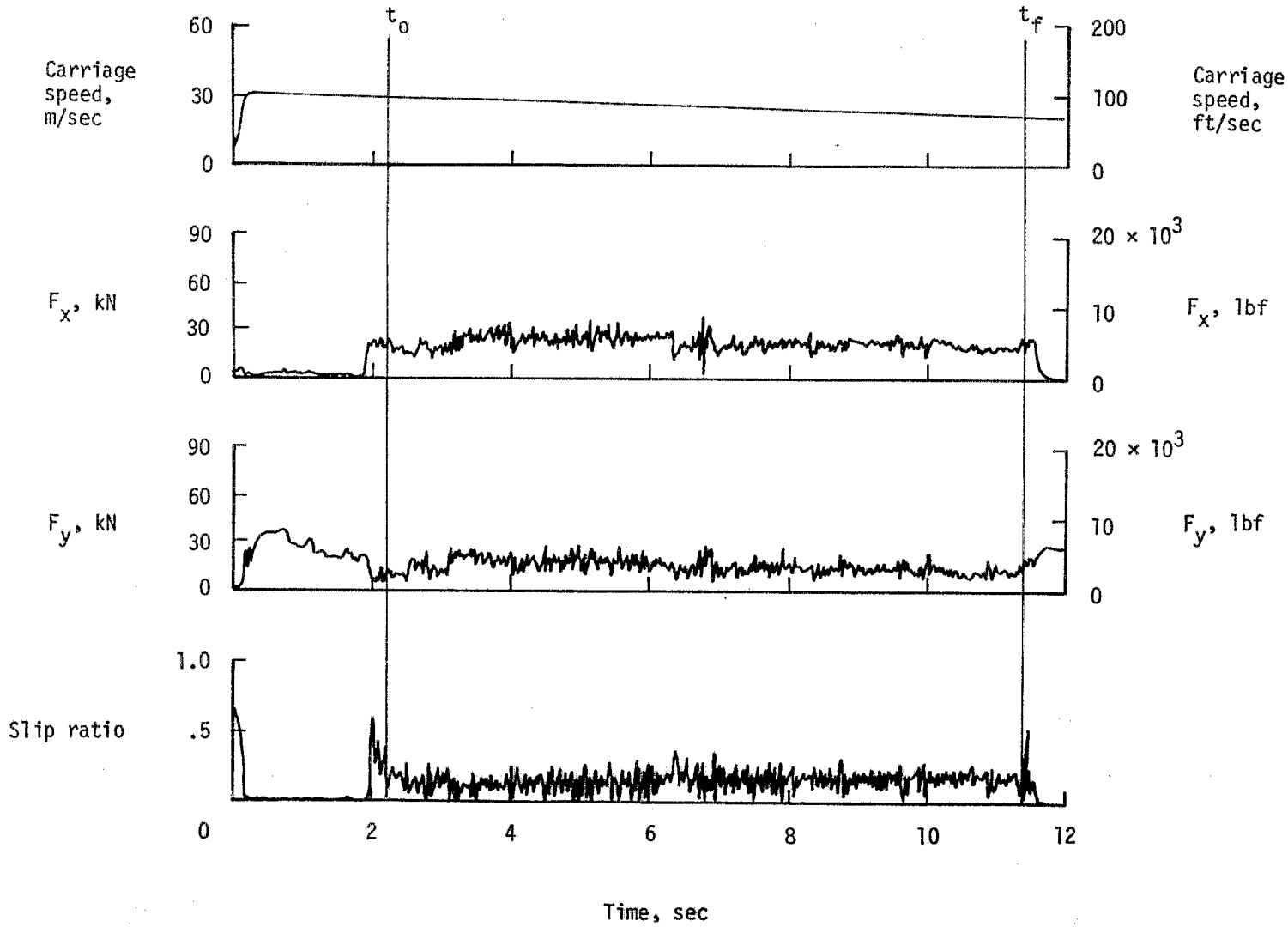

Figure 11.- Typical time histories of variables used to obtain power terms. Run 54; yaw angle, 6°; vertical load, 81.0 kN (18 200 lbf); brake supply pressure, 20 MPa (3000 psi); tire condition, new; nominal carriage speed, 44 knots; surface condition, damp.

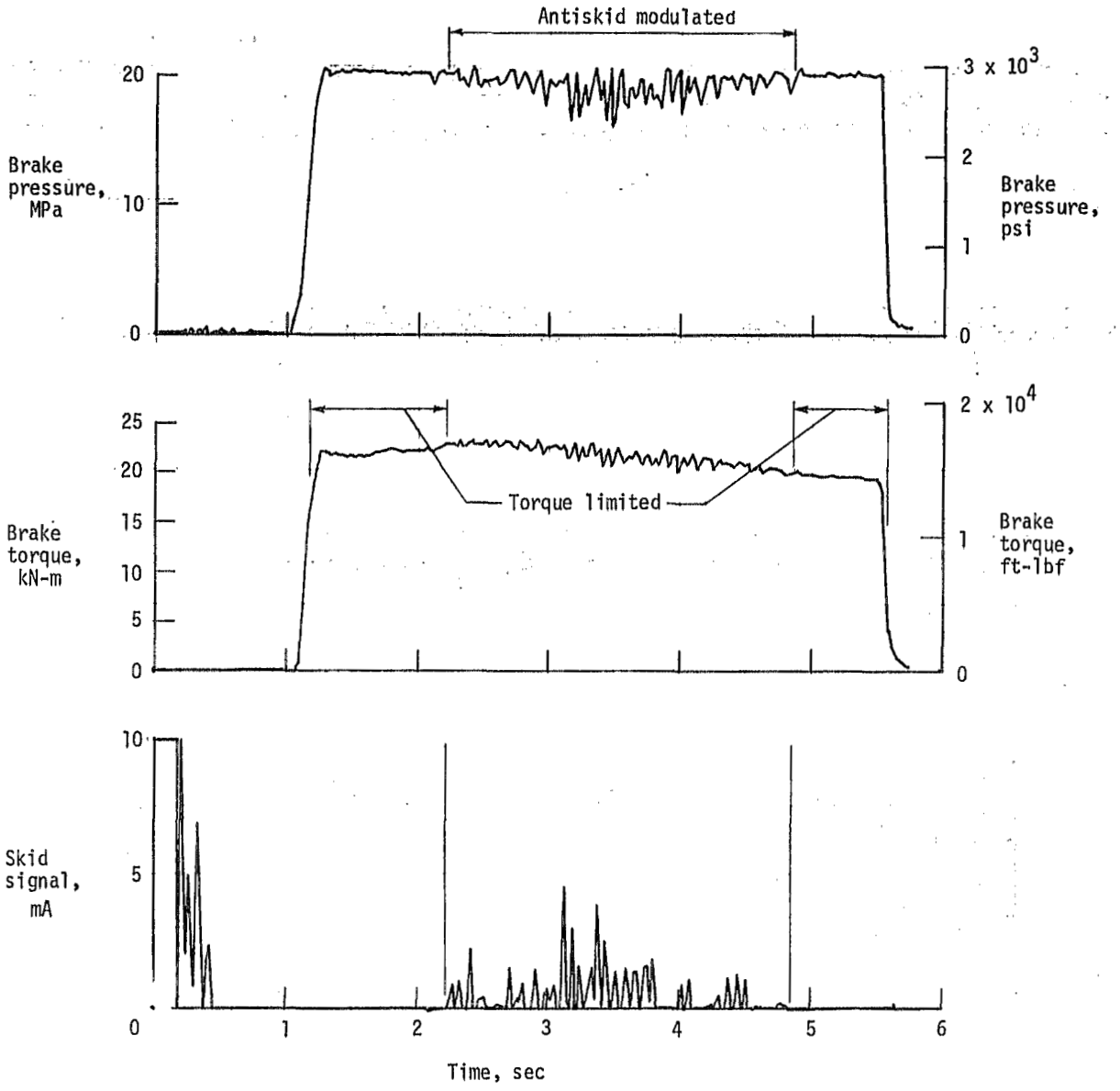

Figure 12.- Typical pressure-torque relationship. Run 4; yaw angle, 0°; vertical load, 81.8 kN (18 400 lbf); brake supply pressure, 20 MPa (2890 psi); tire condition, new; nominal carriage speed, 95 knots; surface condition, dry.

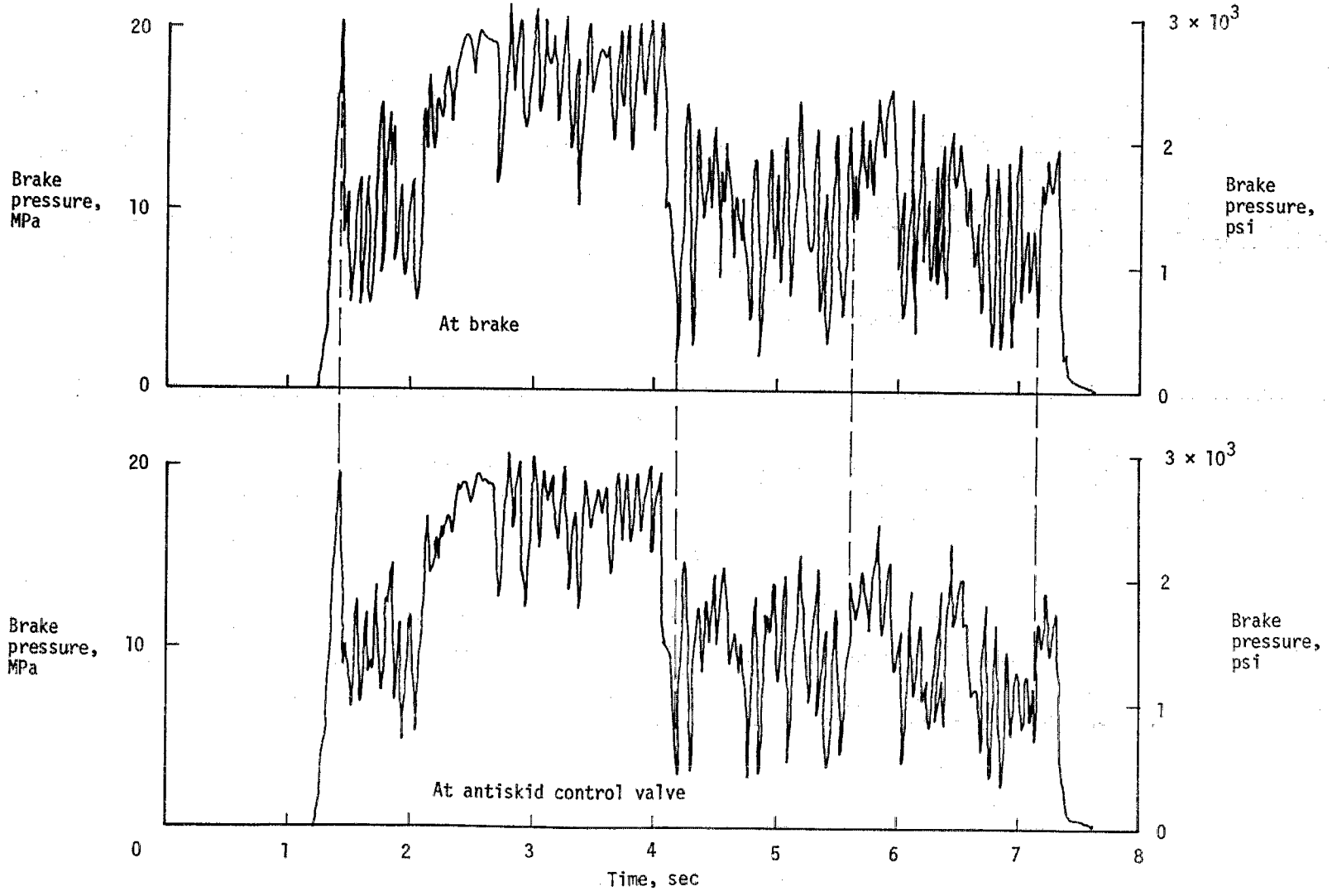

Figure 13.- Typical hydraulic response. Run 20; yaw angle, 0°; vertical load, 118.3 kN (26 600 lbf); brake supply pressure, 20 MPa (2900 psi); tire condition, new; nominal carriage speed, 72 knots; surface condition, damp.

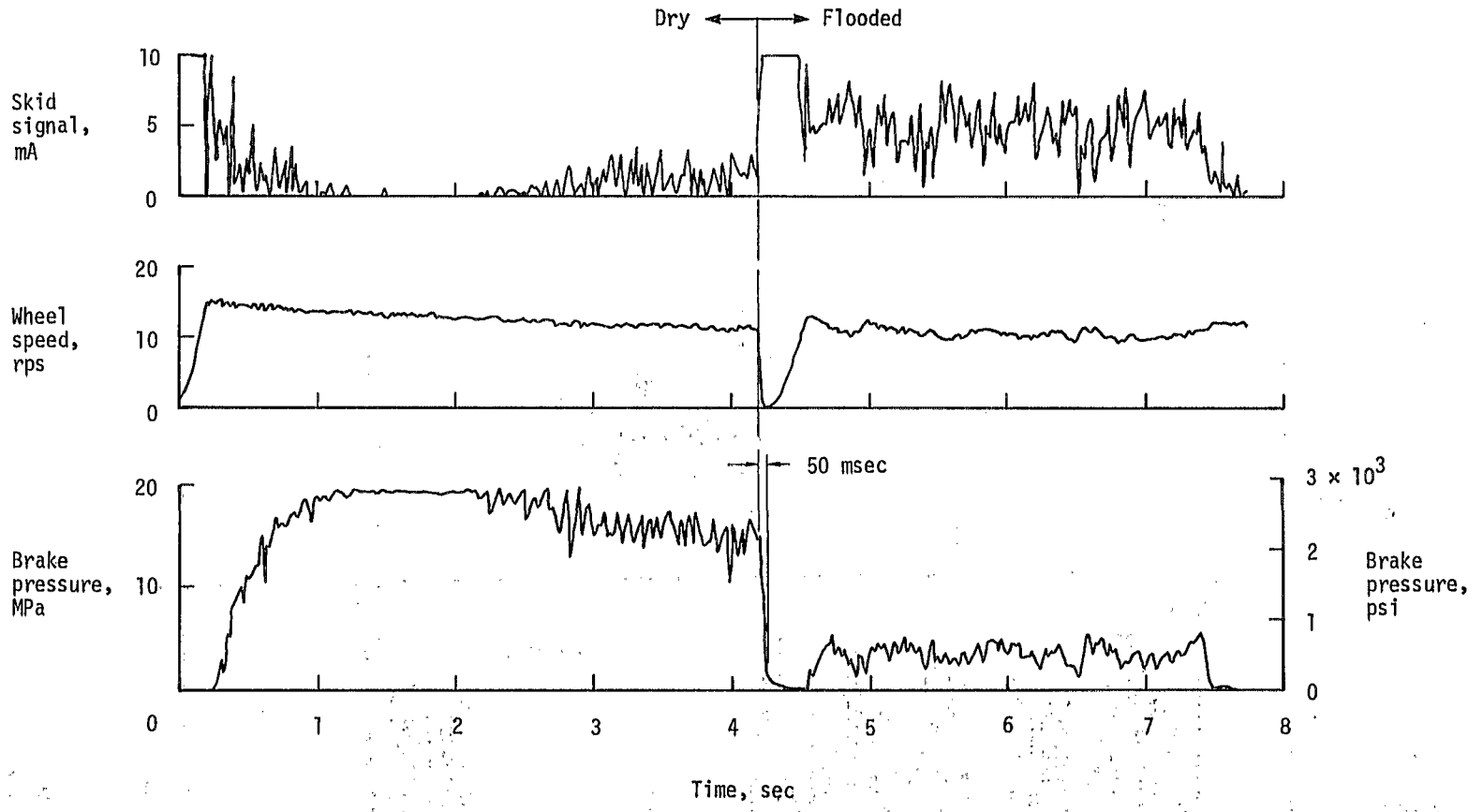

Figure 14.- Typical brake-system electronic response. Run 36; yaw angle, 0°; vertical load, 84.1 kN (18 900 lbf); brake supply pressure, 19 MPa (2780 psi); tire condition, new; nominal carriage speed, 70 knots.

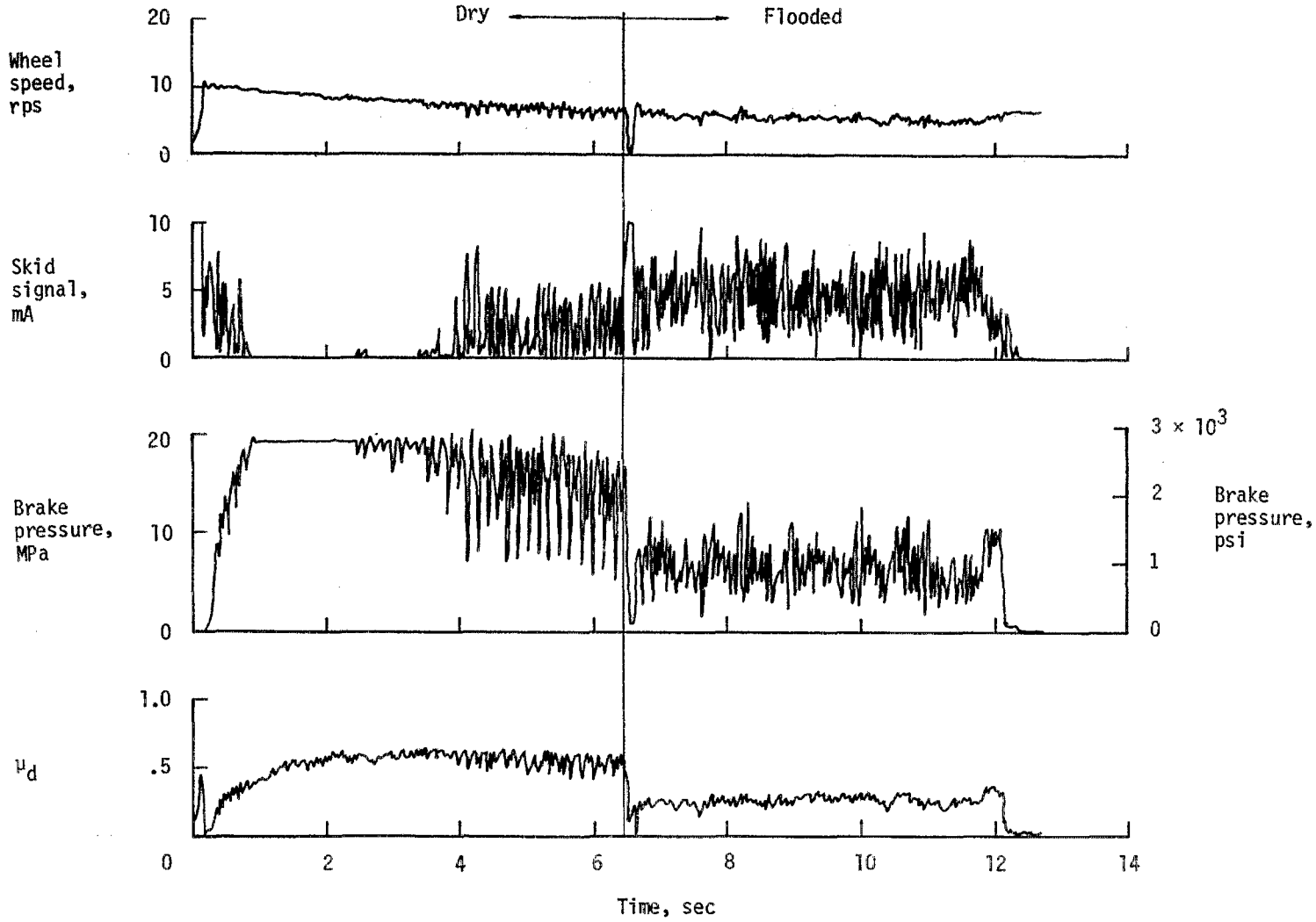

(a) Run 35; nominal carriage speed, 41 knots; yaw angle, 0°; vertical load, 83.2 kN (18 700 lbf); brake supply pressure, 19 MPa (2760 psi); tire condition, new.

Figure 15.- Typical transient runway friction response.

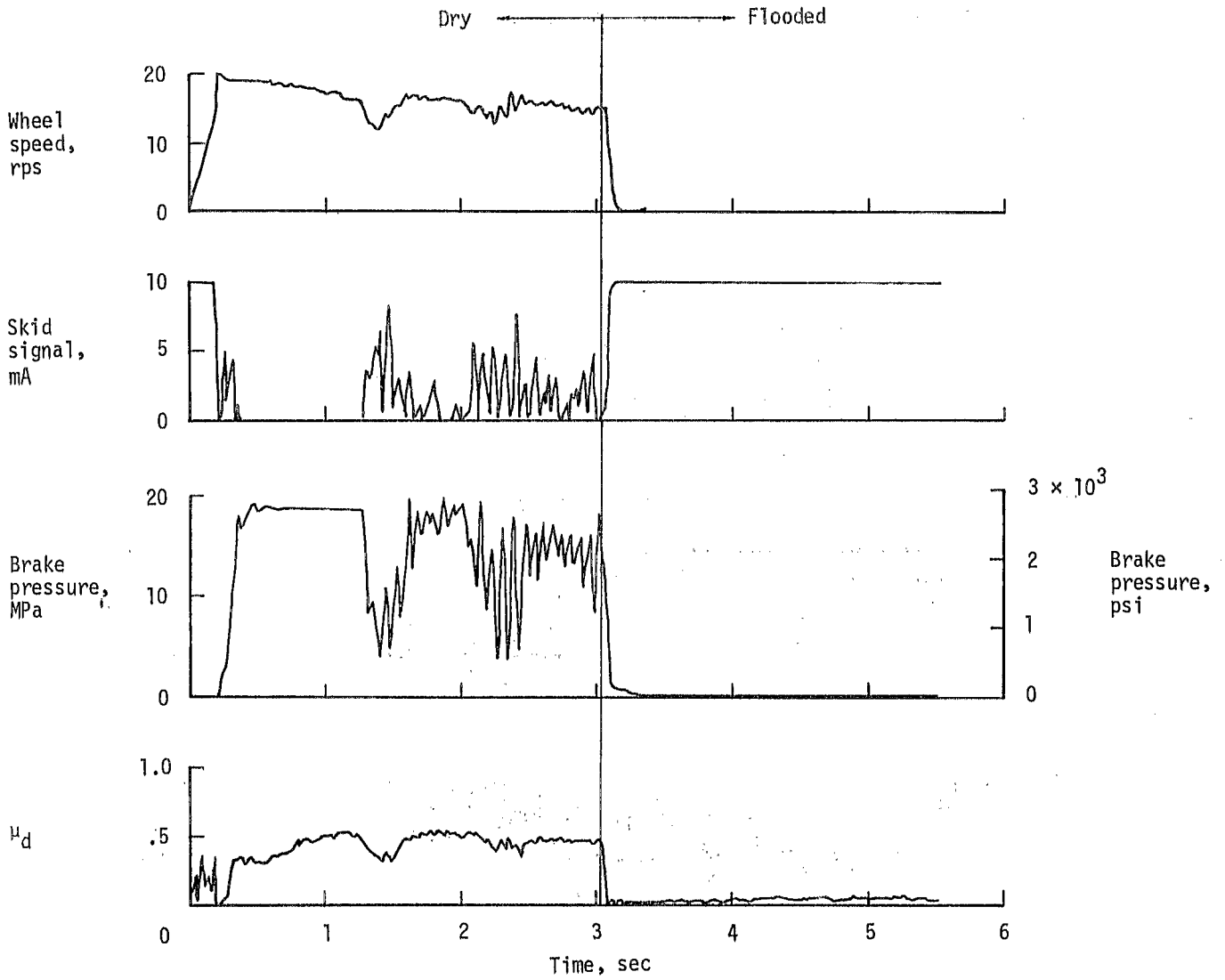

(b) Run 37; nominal carriage speed, 100 knots; yaw angle, 0°; vertical load, 85.0 kN (19 100 lbf); brake supply pressure, 19 MPa (2820 psi); tire condition, new.

Figure 15.- Continued.

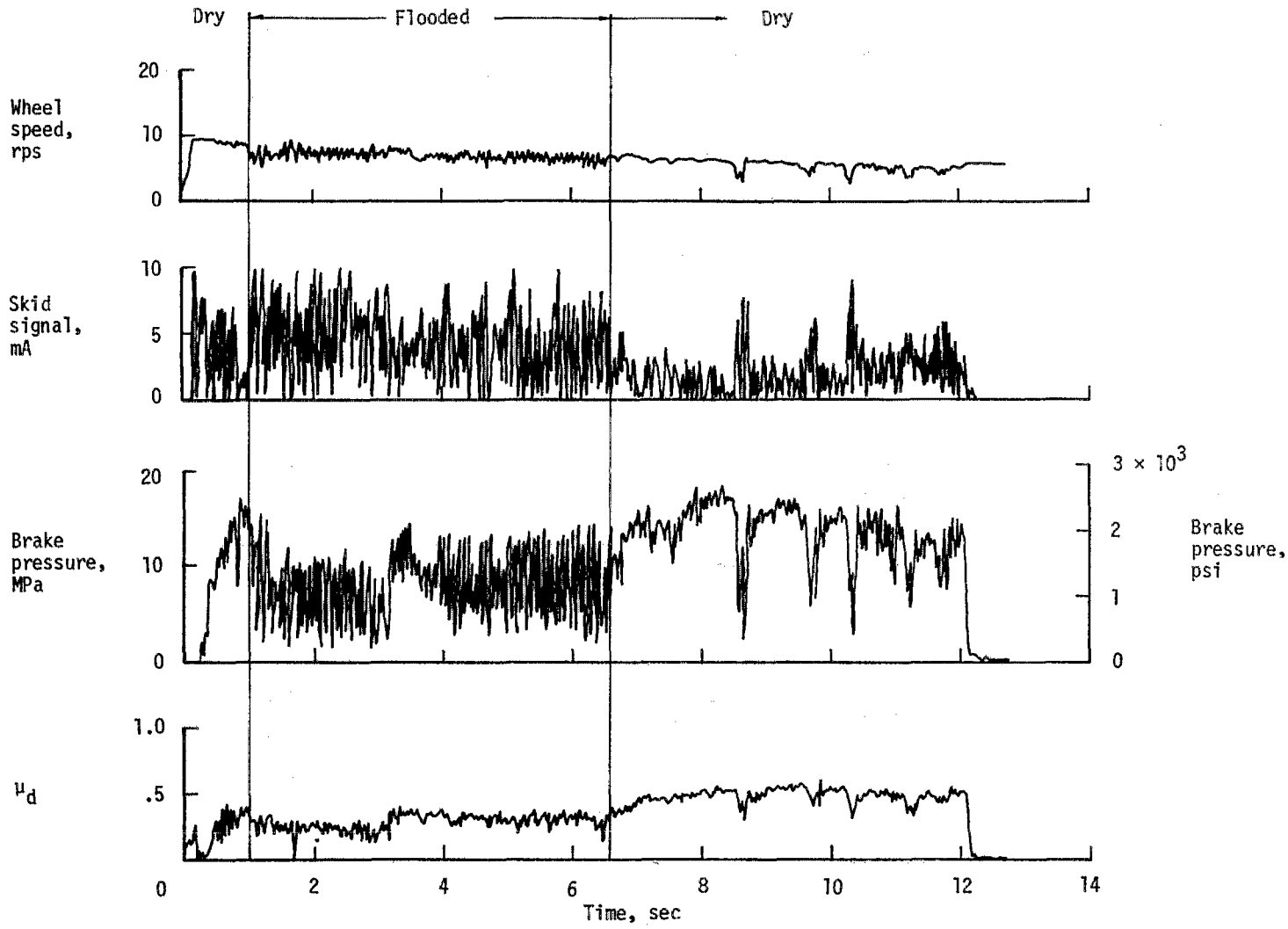

(c) Run 38; nominal carriage speed, 43 knots; yaw angle, 0°; vertical load, 83.2 kN (18 700 lbf); brake supply pressure, 19 MPa (2800 psi); tire condition, new.

Figure 15.- Continued.

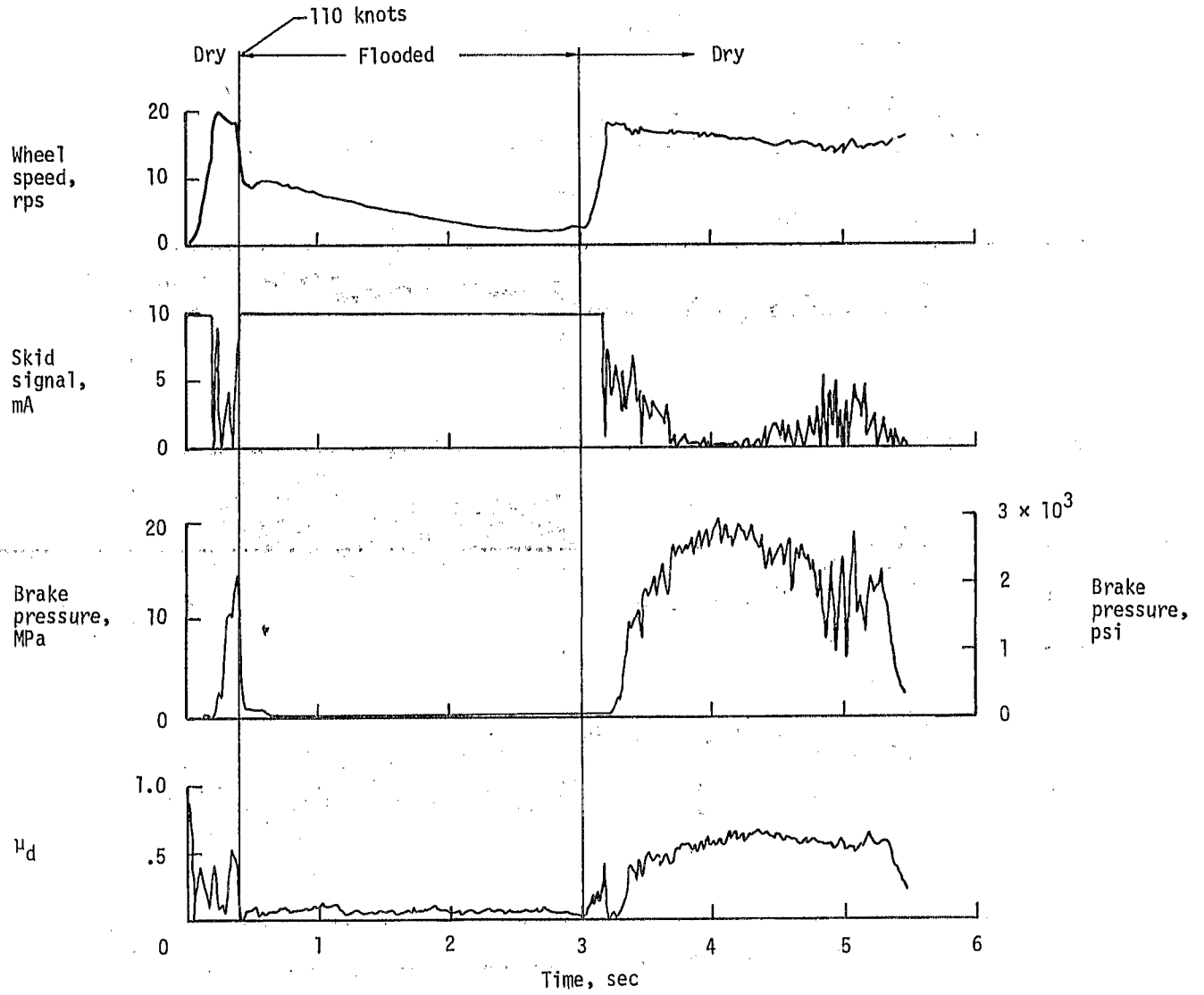

(d) Run 40; nominal carriage speed, 102 knots; yaw angle, 0°; vertical load, 64.5 kN (14 500 lbf); brake supply pressure, 20 MPa (2870 psi); tire condition, new.

Figure 15.- Concluded.

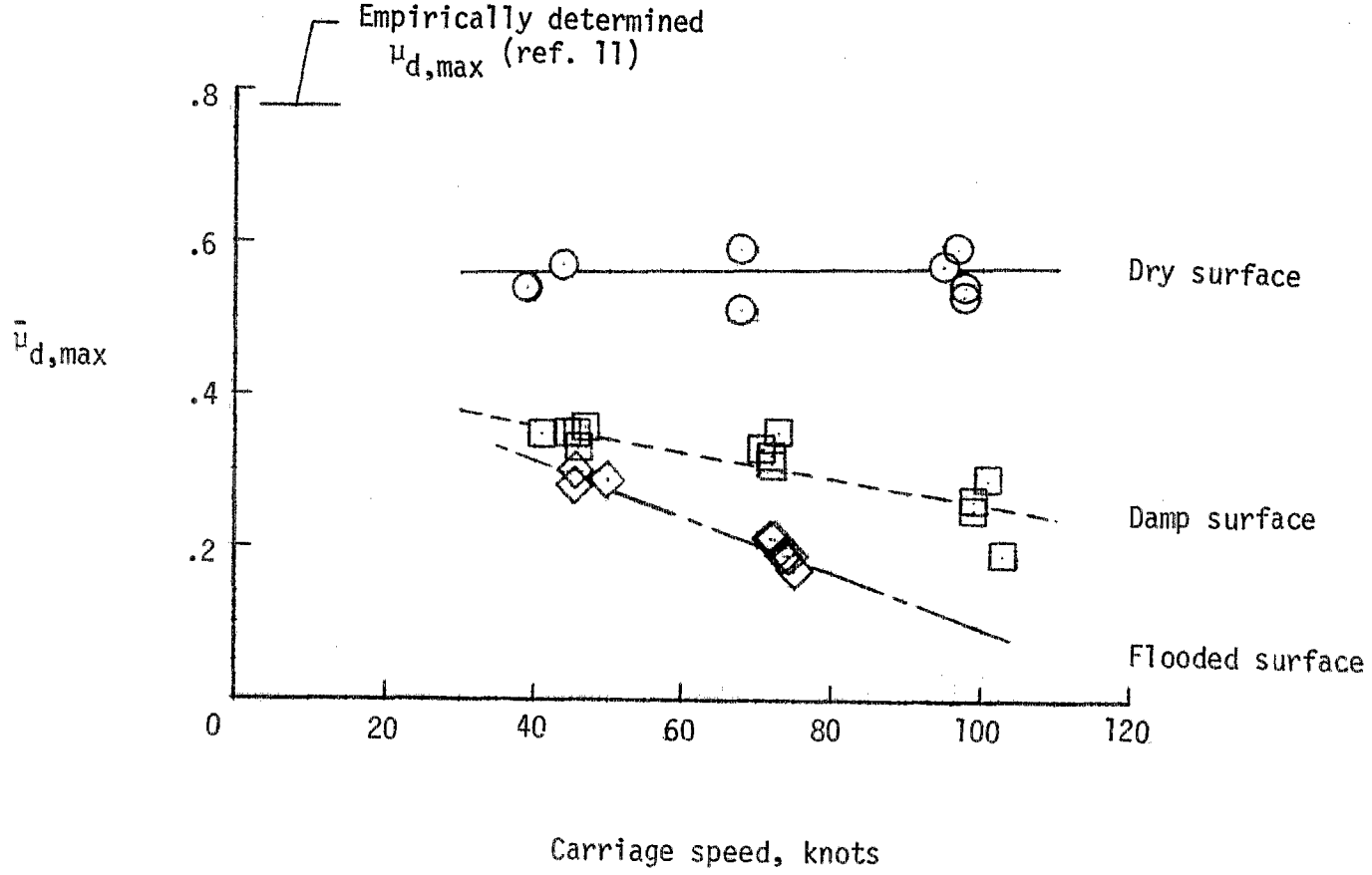

Figure 16.- Effect of carriage speed on maximum drag-force friction coefficient. Yaw angle, 0°; vertical load, 80.1 kN (18 000 lbf); brake supply pressure, 21 MPa (3000 psi); tire condition, new.

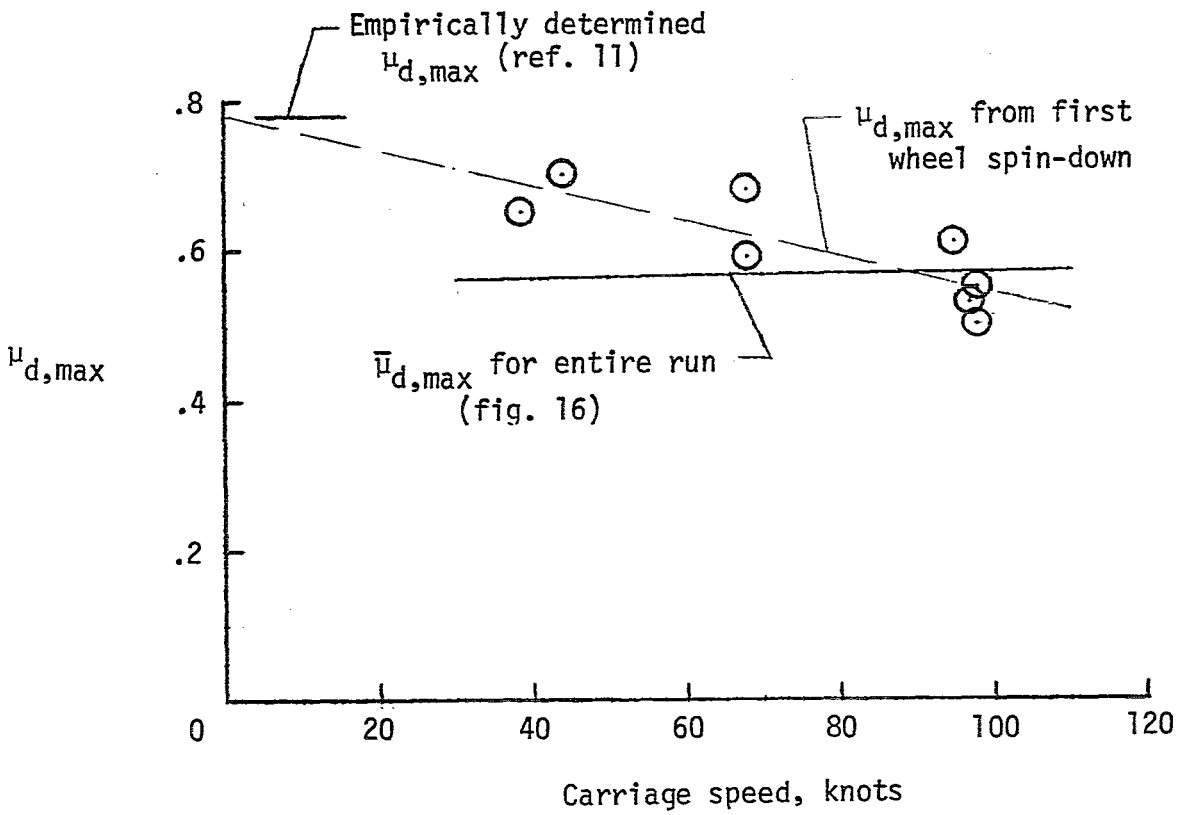

Figure 17.- Dry surface friction coefficients for first wheel spin-down following initial brake application compared with $\bar{\mu}_{d,max}$ obtained during entire run.

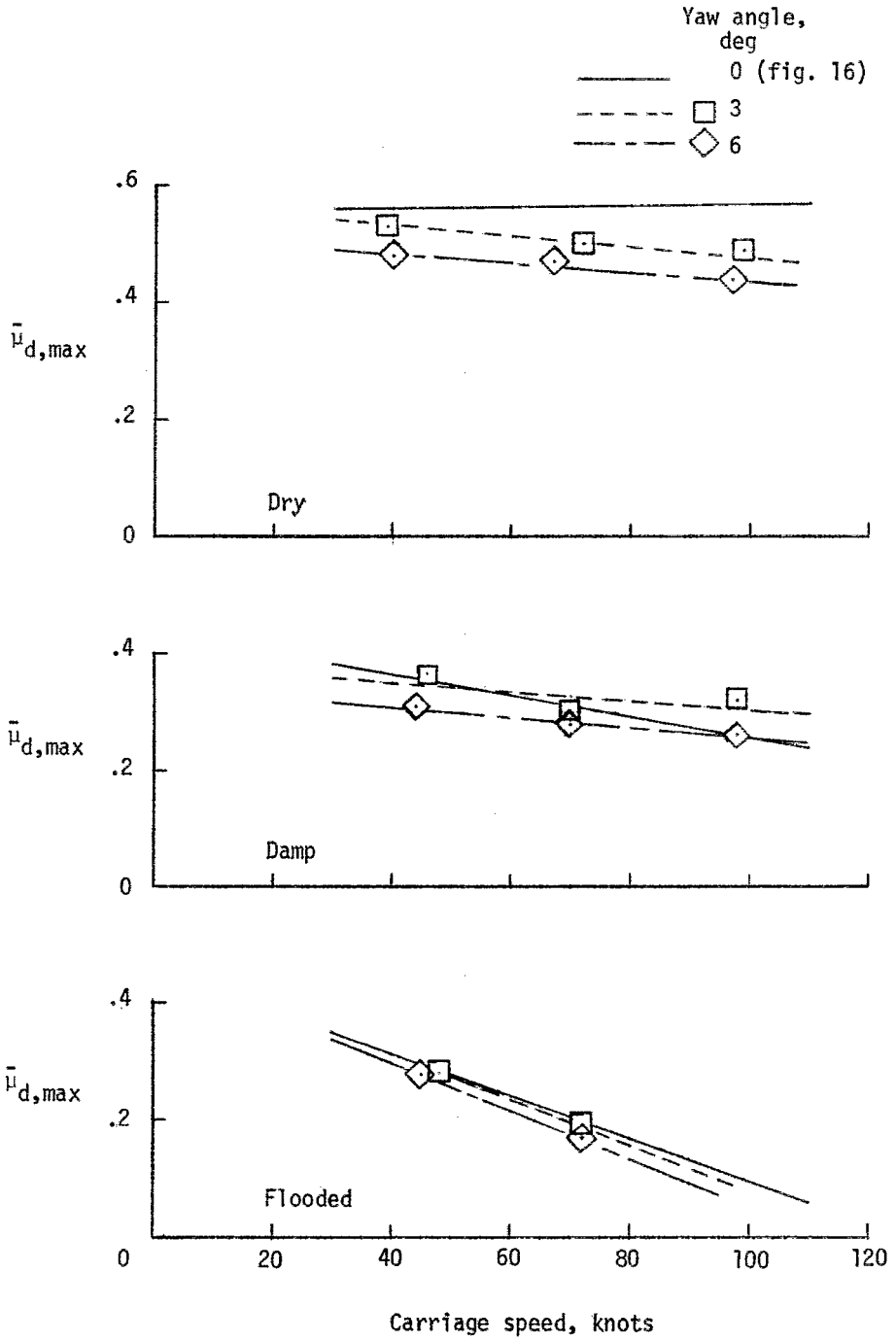

Figure 18.- Effect of yaw angle on maximum drag-force friction coefficient. Vertical load, 80.1 kN (18 000 lbf); brake supply pressure, 21 MPa (3000 psi); tire condition, new.

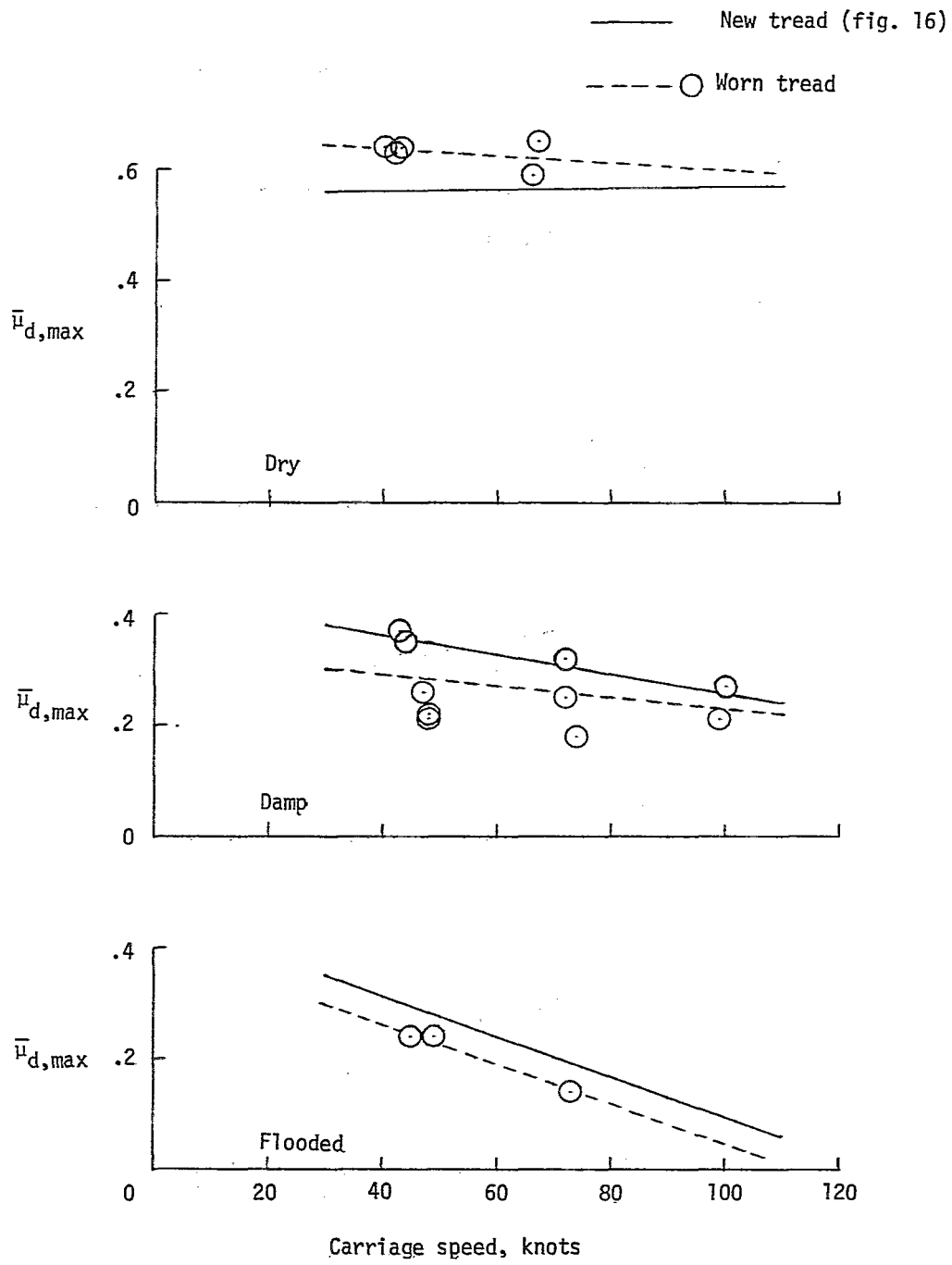

Figure 19.- Effect of tire tread wear on maximum drag-force friction coefficient. Yaw angle, 0°; vertical load, 80.1 kN (18 000 lbf); brake supply pressure, 21 MPa (3000 psi).

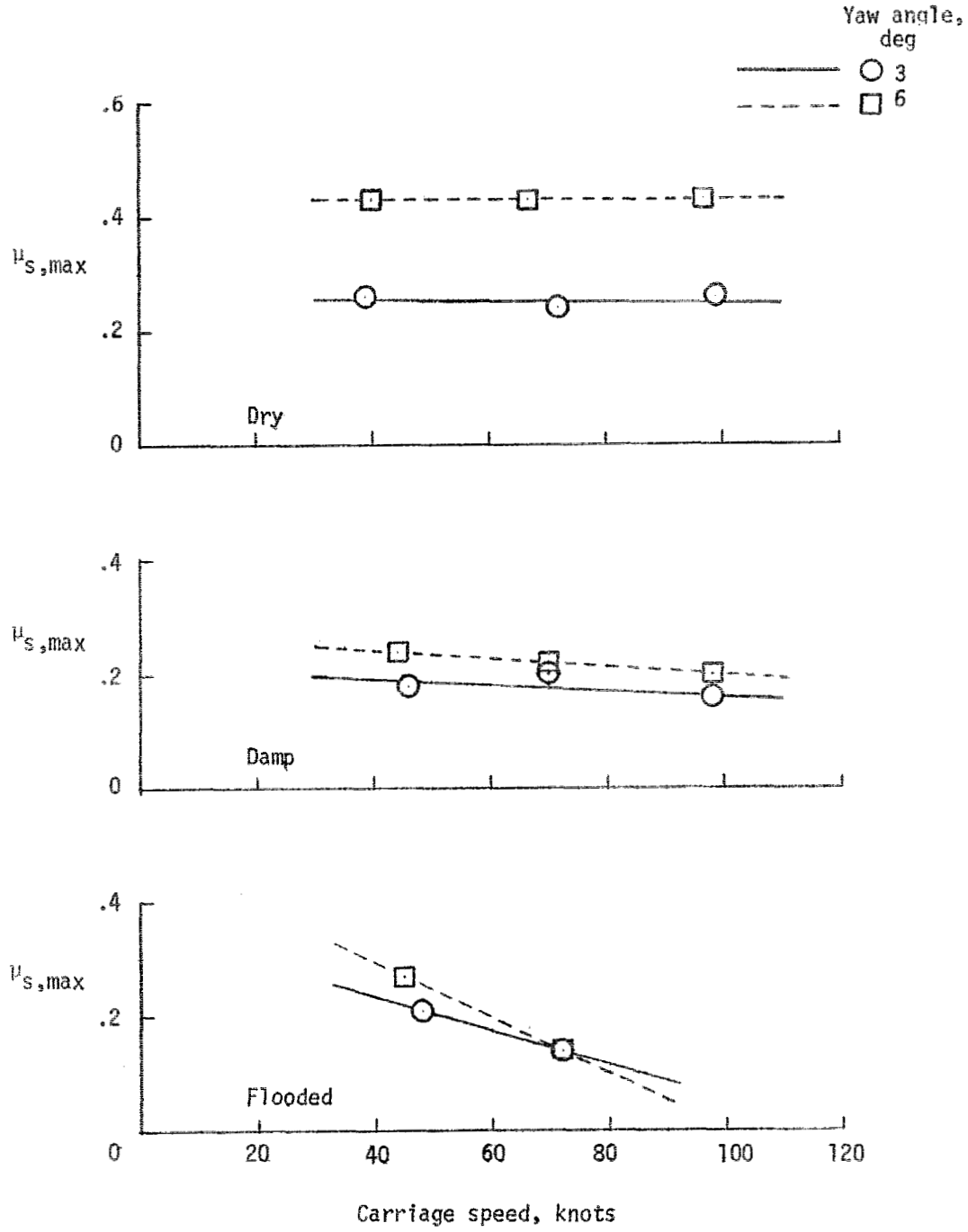

Figure 20.- Effect of carriage speed on maximum side-force friction coefficient. Vertical load, 80.1 kN (18 000 lbf); brake supply pressure, 21 MPa (3000 psi); tire condition, new.

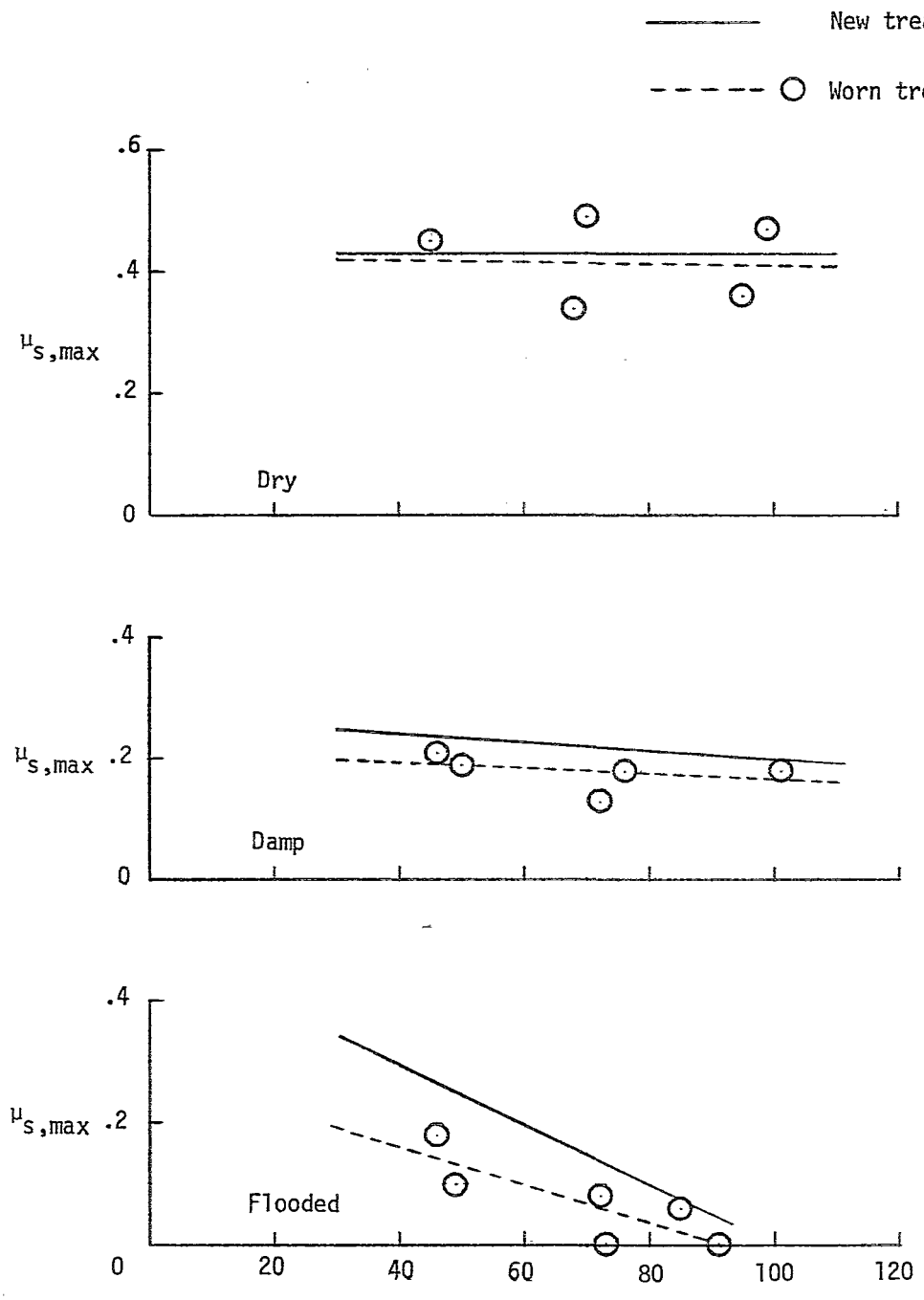

Figure 21.- Effect of tread wear on maximum side-force friction coefficient. Vertical load, 80.1 kN (18 000 lbf); yaw angle, 6°; brake supply pressure, 21 MPa (3000 psi).

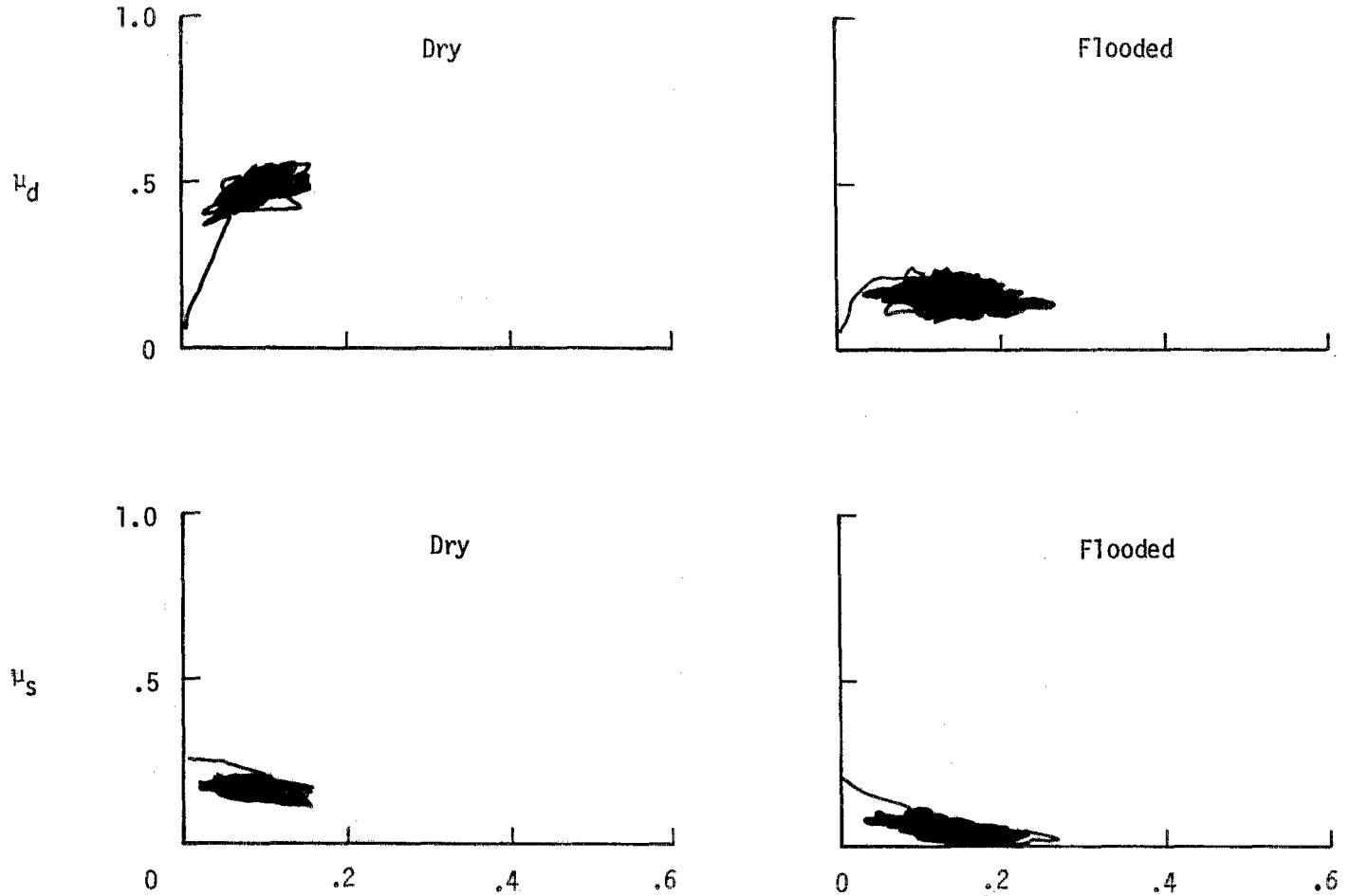

(a) Run no. 43.

(b) Run no. 49.

Figure 22.- Interaction between braking and cornering. Yaw angle, 3°; brake supply pressure 21 MPa (3000 psi); nominal carriage speed, 72 knots.

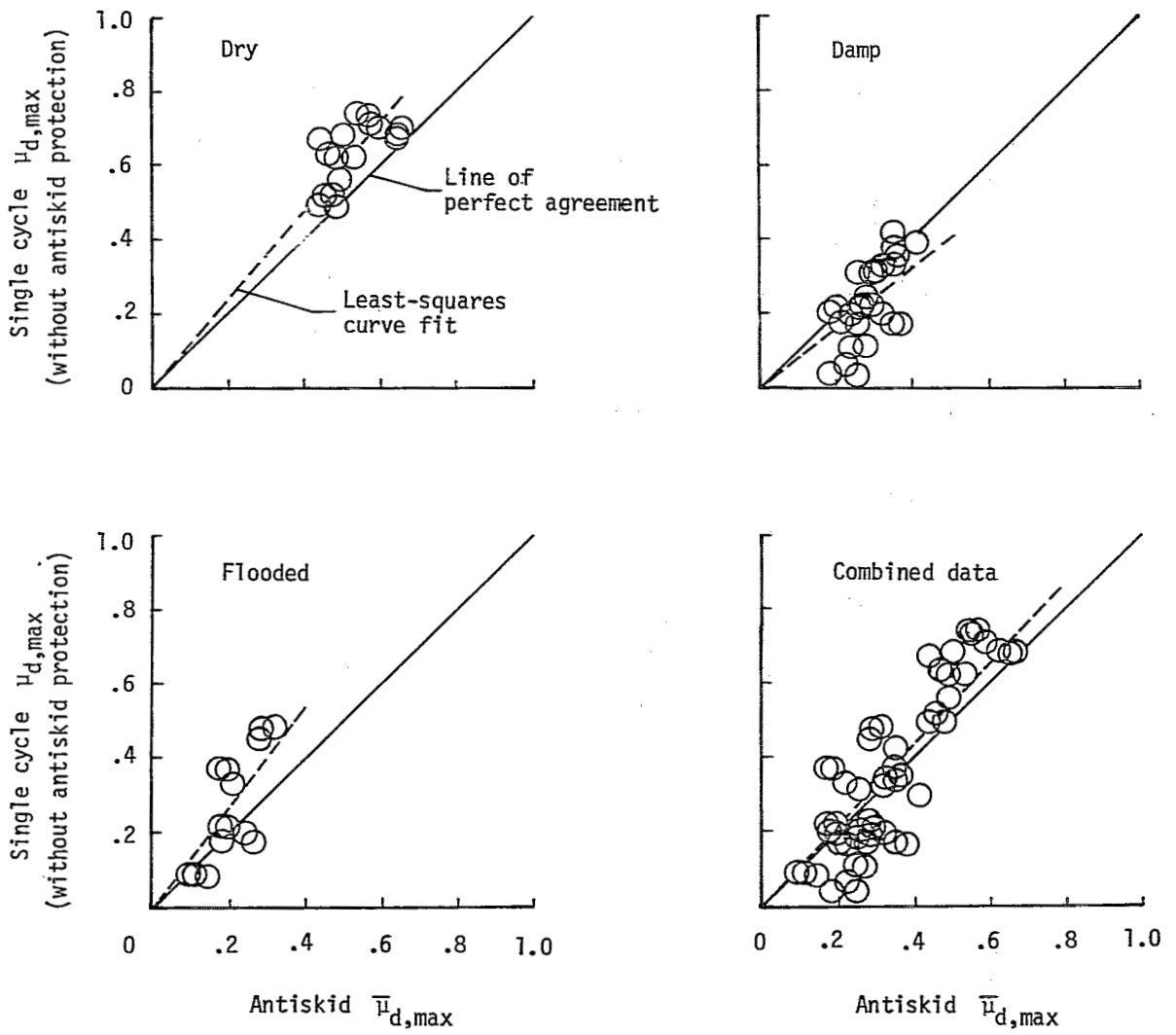

Figure 23.- Effect of cyclic braking on maximum drag-force friction coefficient.

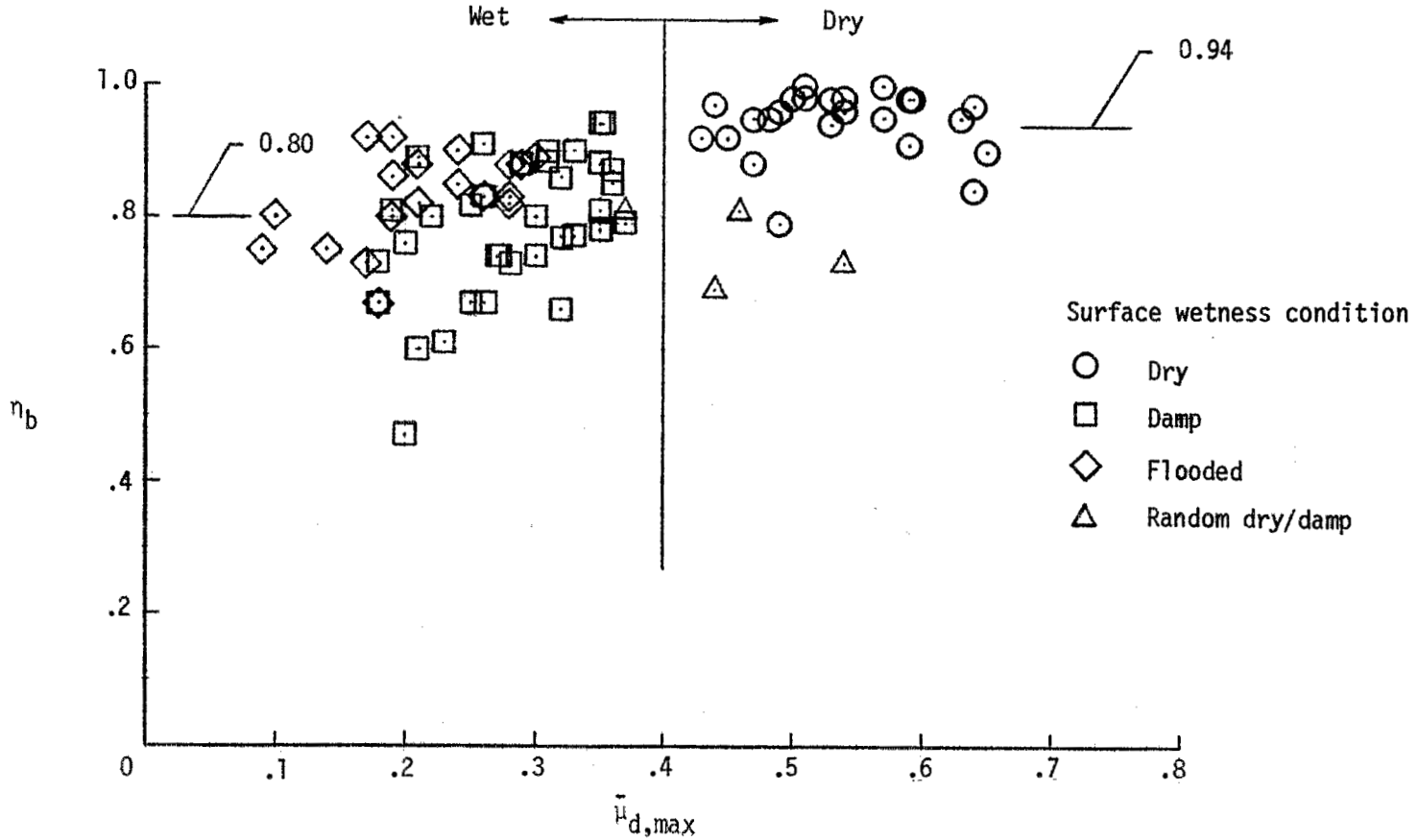

Figure 24.- Effect of maximum drag-force friction coefficient on antiskid braking performance ratio. These data include all runs except those which were torque limited the entire run, those involving tire hydroplaning, and those performed to examine the effects of runway friction transition.

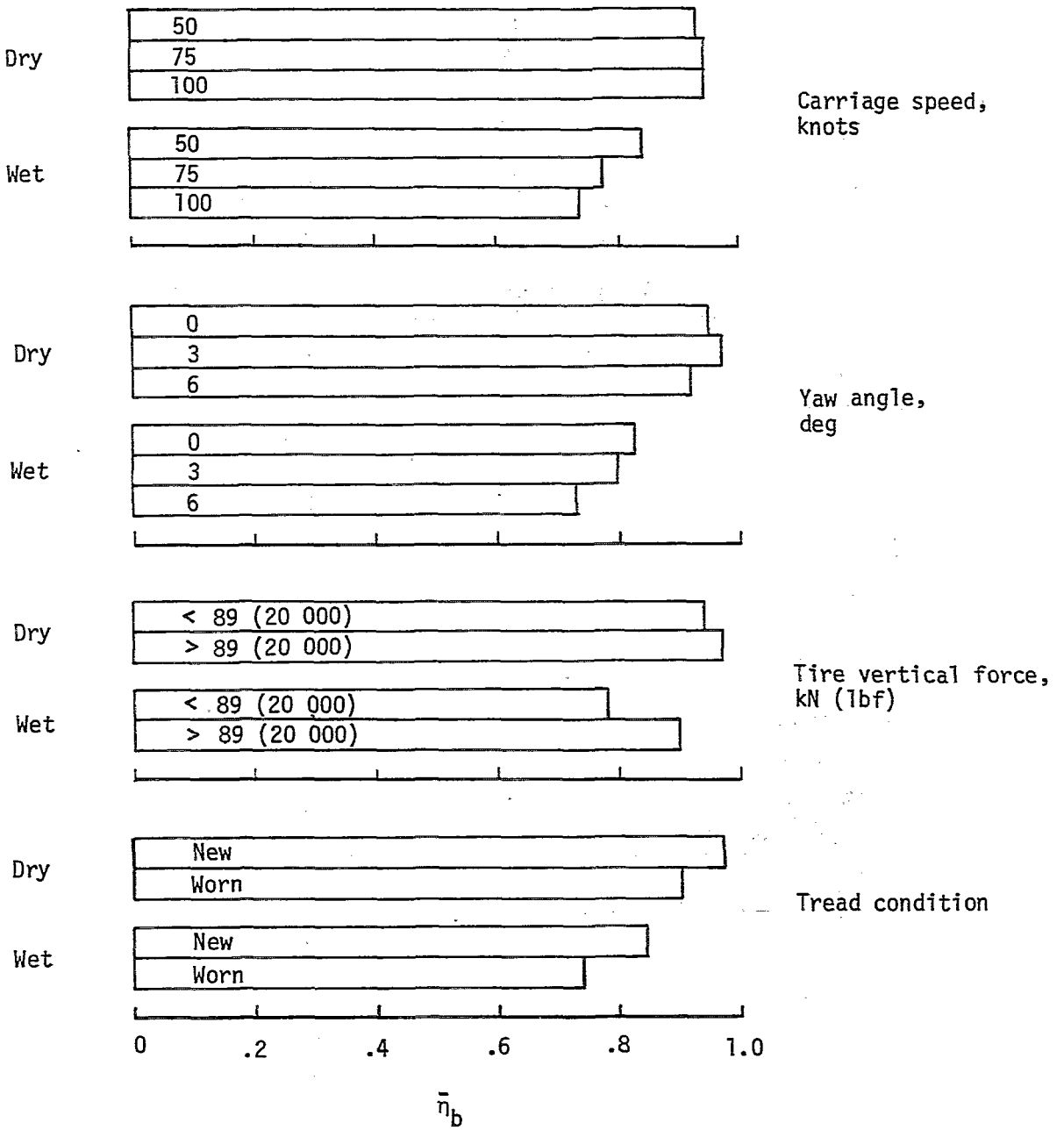

Figure 25.- Effects of test parameters on antiskid braking performance ratios. Each bar graph represents the average of several runs. (See text, p. 15.)

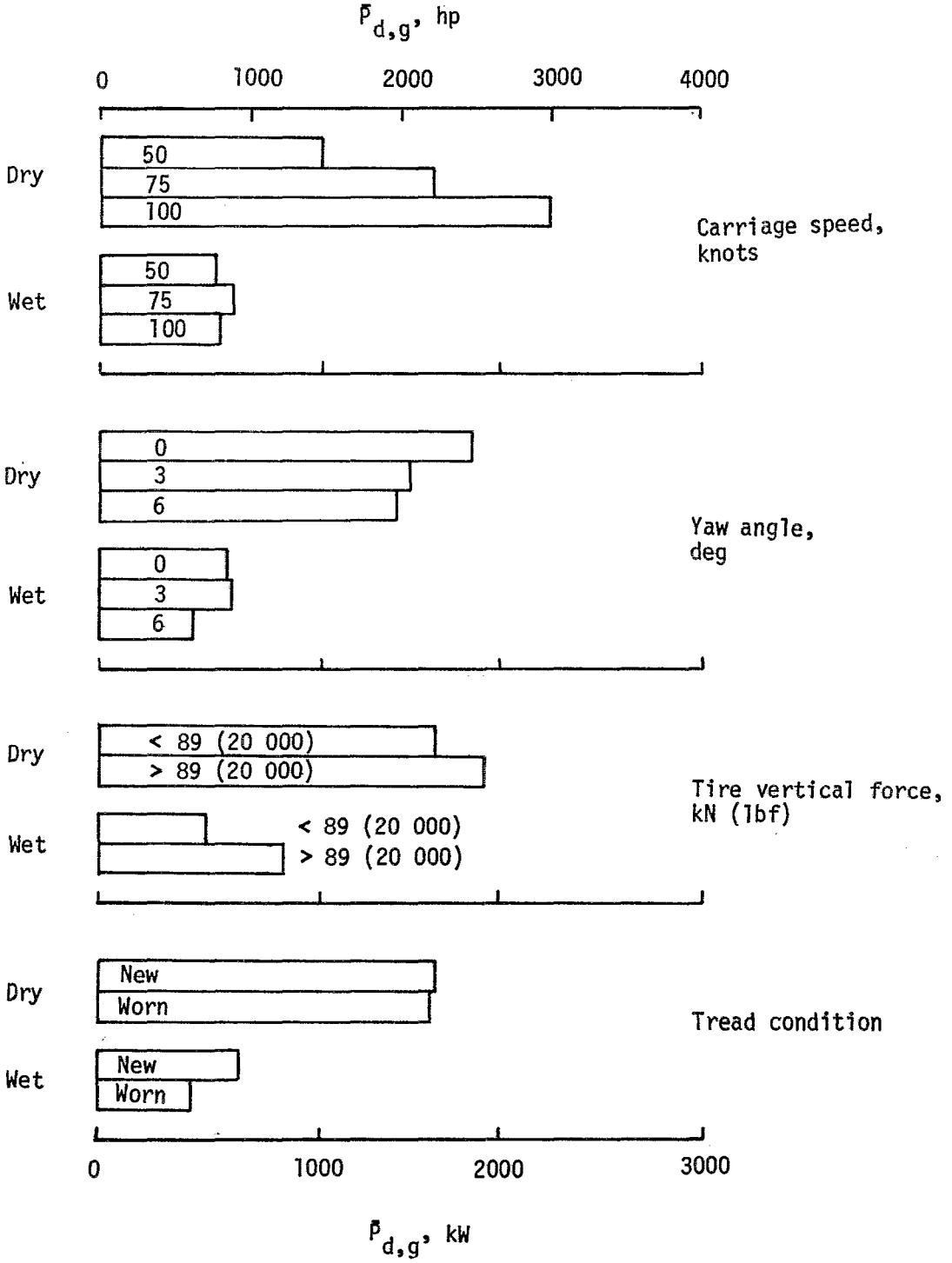

Figure 26.- Effects of test parameters on gross stopping power developed by the antiskid braking system.

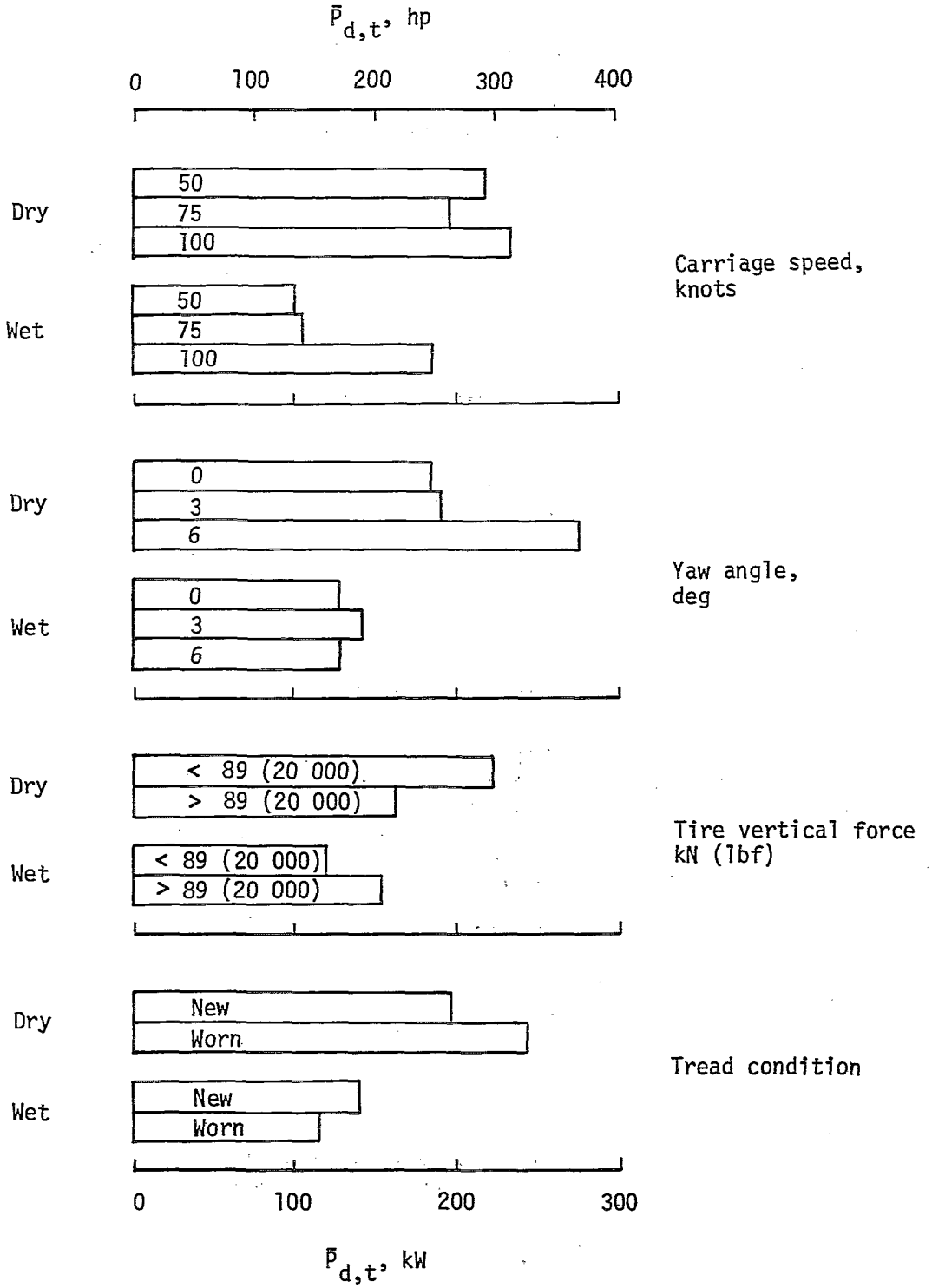

Figure 27.- Effects of test parameters on the stopping power dissipated by the tire.

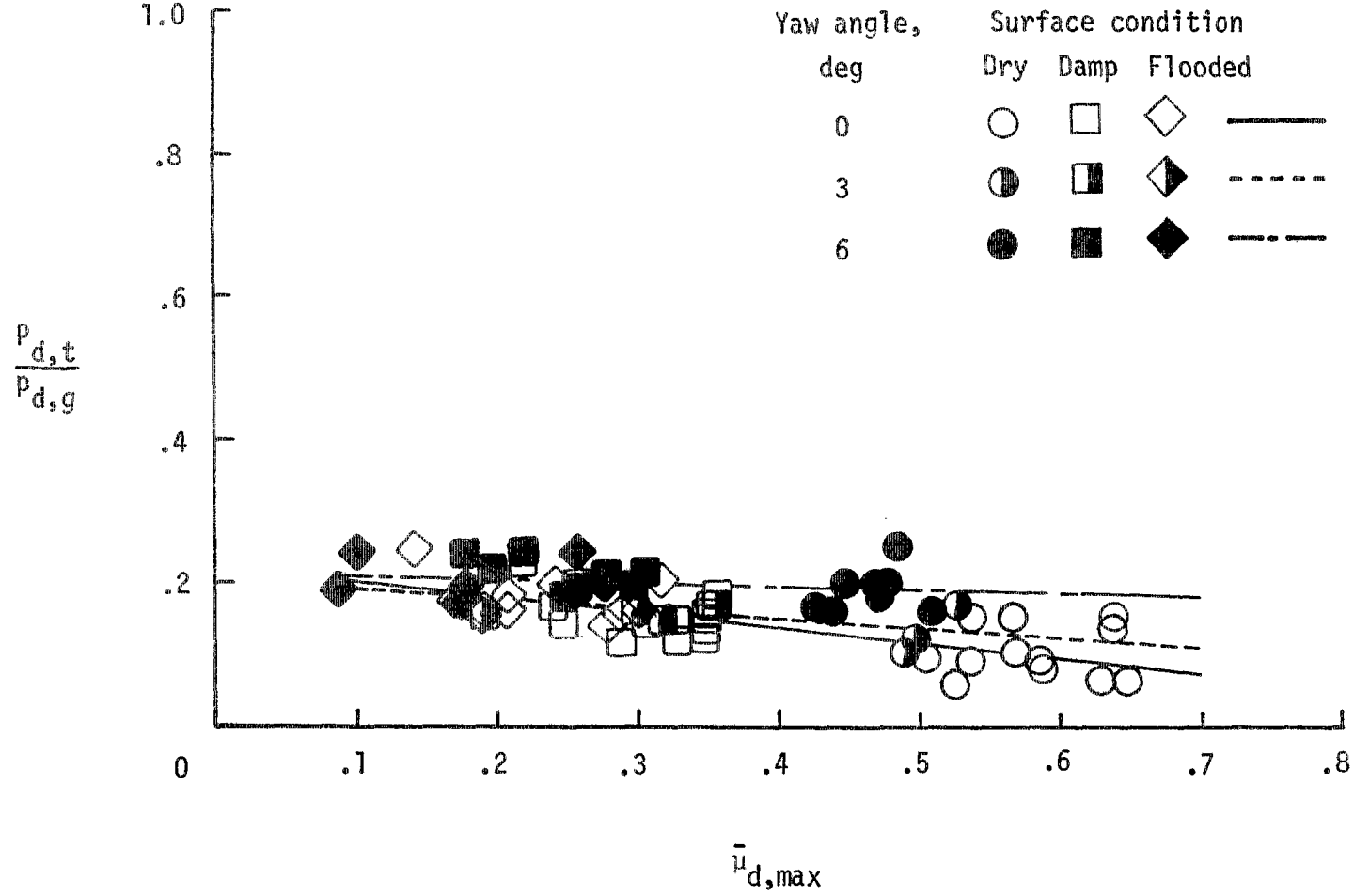

Figure 28.- Effect of maximum drag-force friction coefficient on ratio of tire stopping power to gross stopping power.

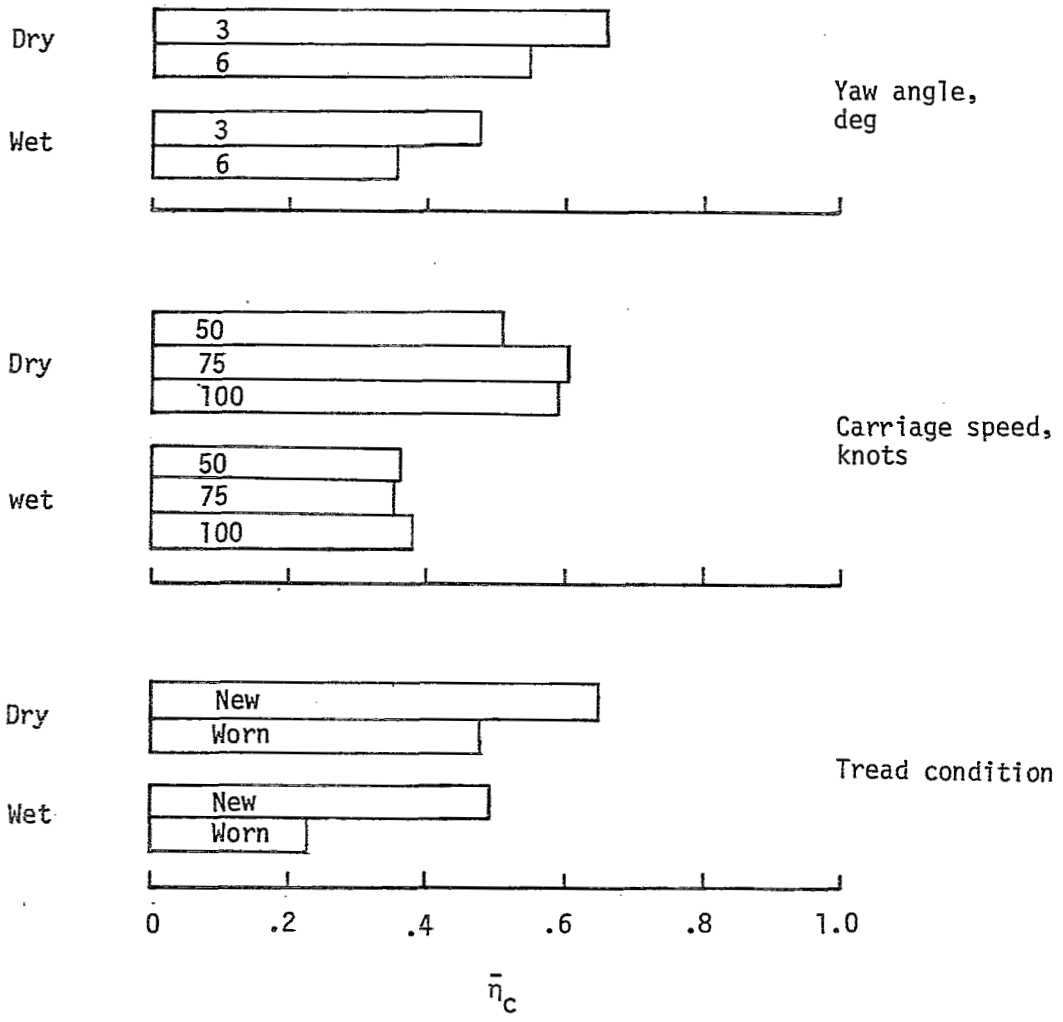

Figure 29.- Effects of test parameters on antiskid cornering performance ratios.

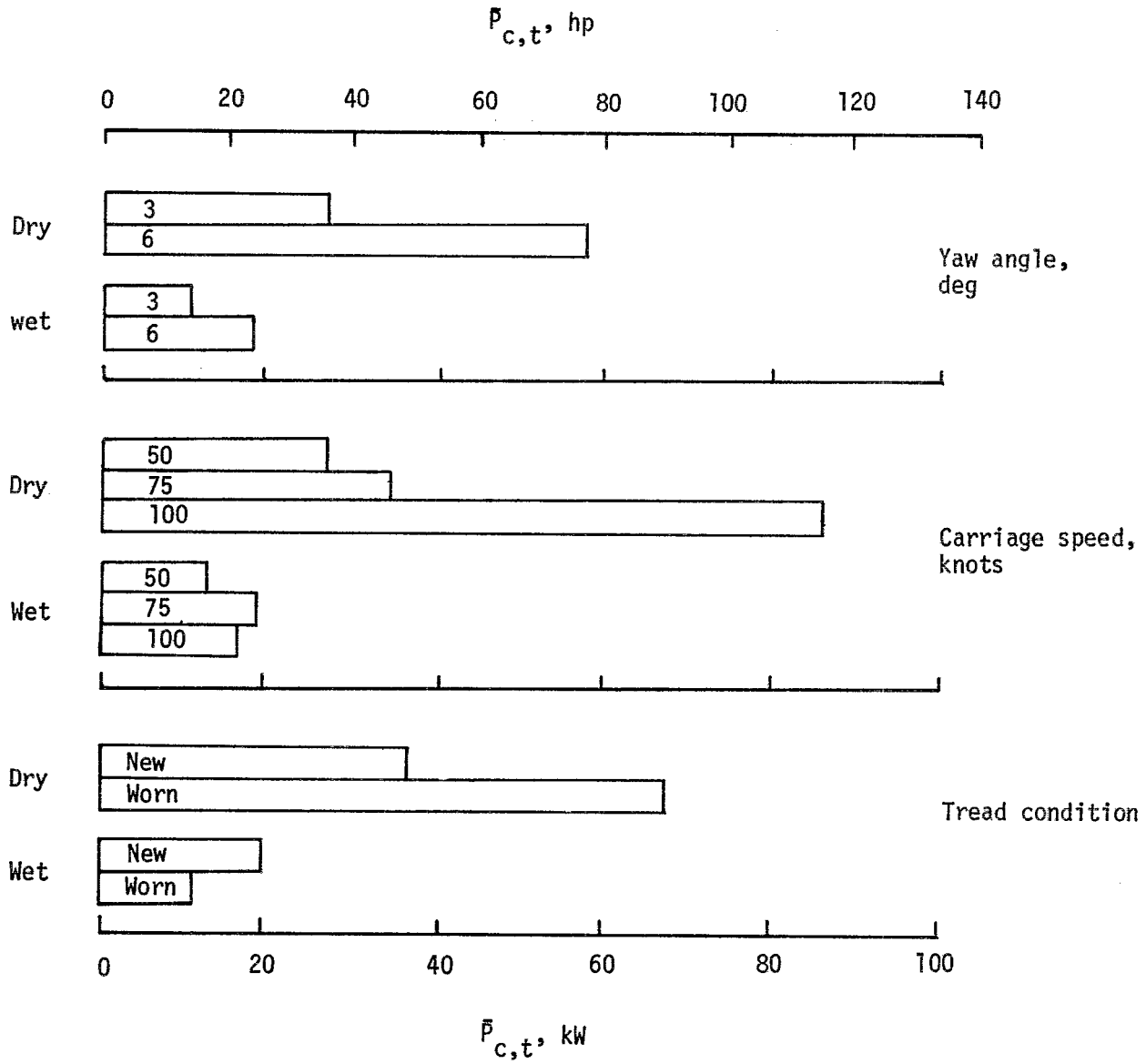

Figure 30.- Effects of test parameters on cornering power dissipated by the tire.

APPENDIX

TIME HISTORIES

This appendix presents time histories in figures A1 to A105 of eight parameters which describe the behavior of the antiskid system during each test condition. These eight parameters, which are wheel speed, skid signal, brake pressure, brake torque, drag-force friction coefficient, side-force friction, alining torque, and slip ratio, are given for the convenience of the user in studying detail characteristics of the antiskid system.

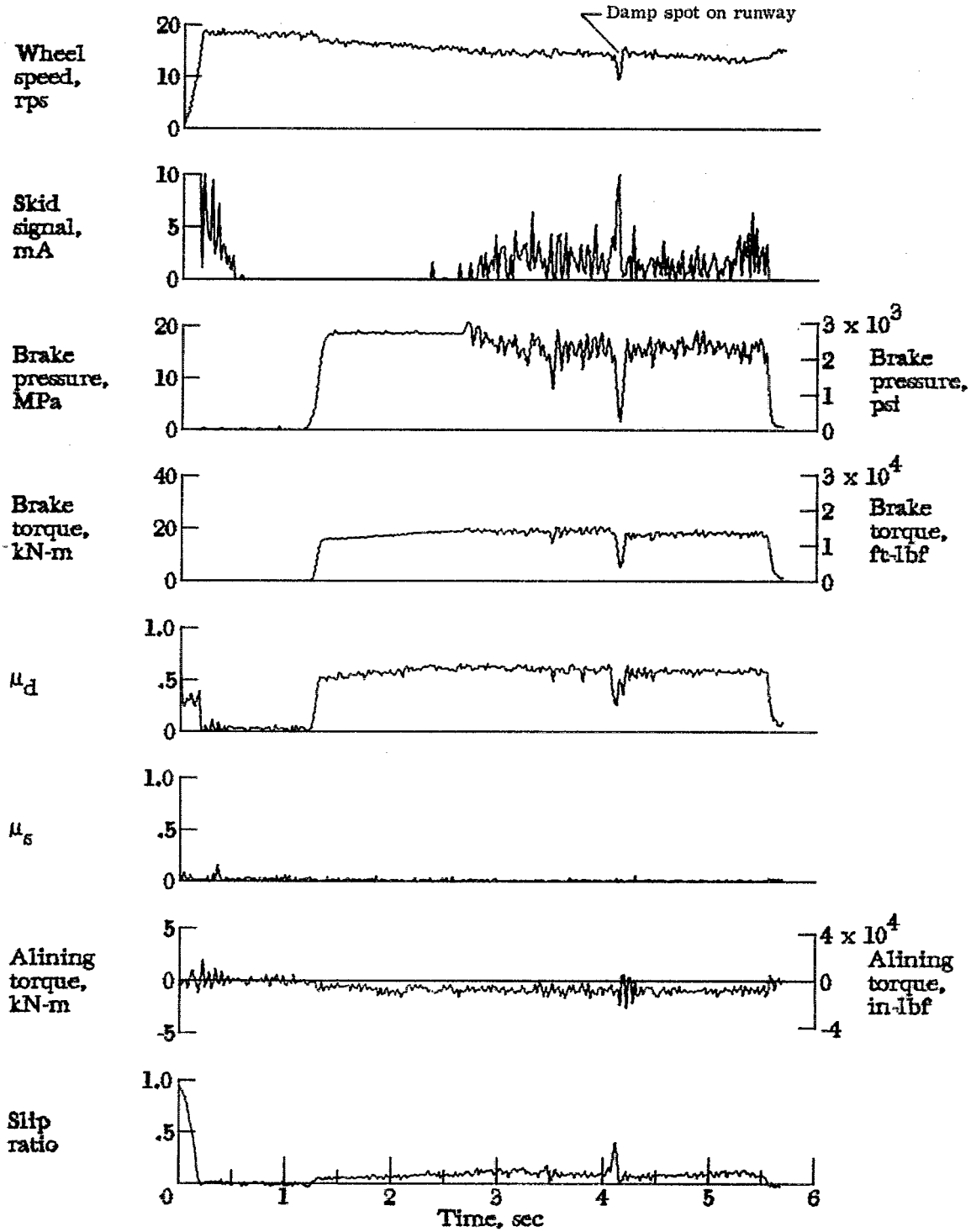

Figure A1.- Time histories for run 1. Nominal carriage speed, 97 knots; vertical load, 63.6 kN (14 300 lbf); yaw angle, 0°; brake pressure, 19 MPa (2700 psi); tire condition, new; surface condition, dry.

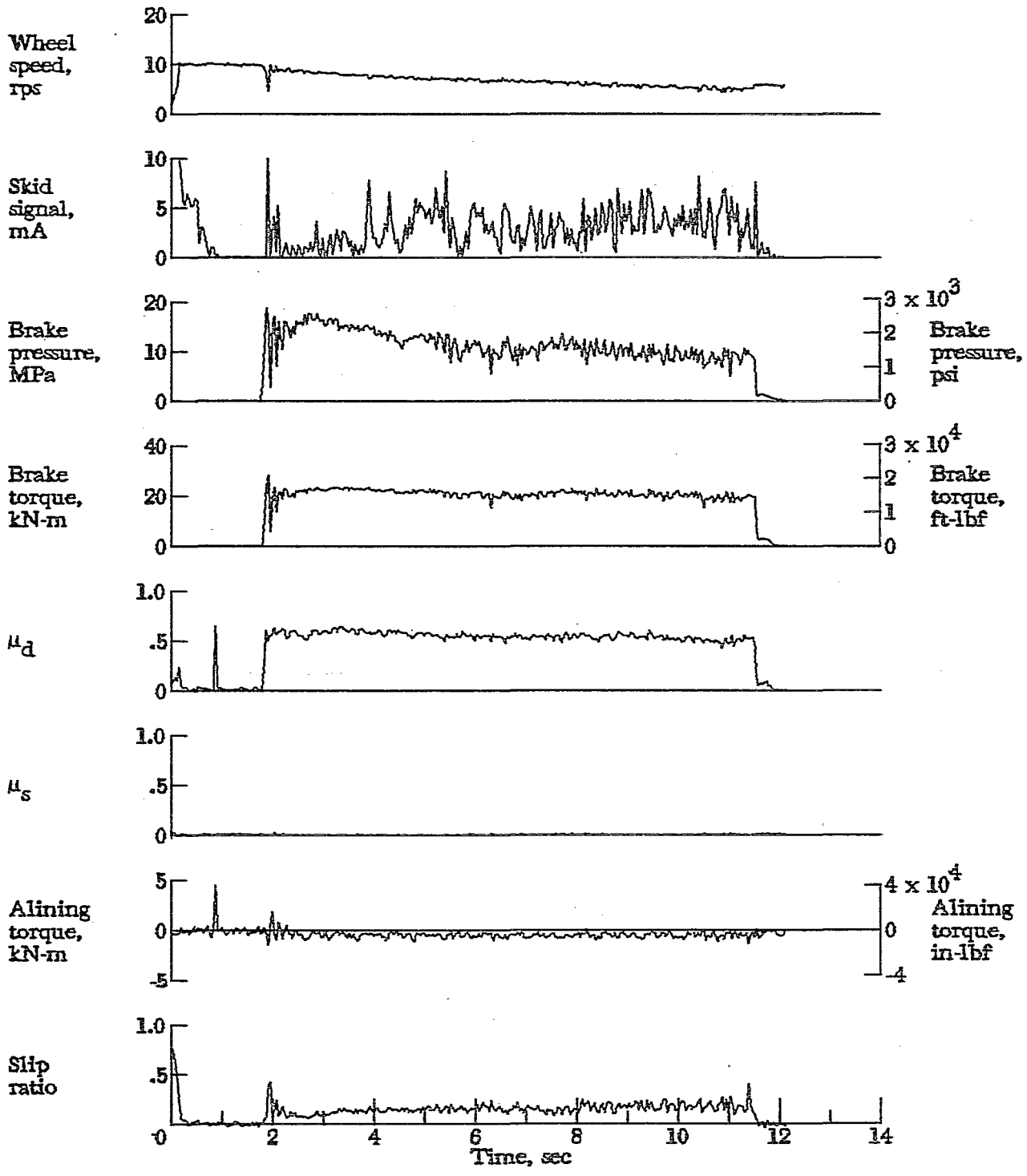

Figure A2.- Time histories for run 2. Nominal carriage speed, 44 knots; vertical load, 81.8 kN (18 400 lbf); yaw angle, 0°; brake pressure, 21 MPa (3000 psi); tire condition, new; surface condition, dry.

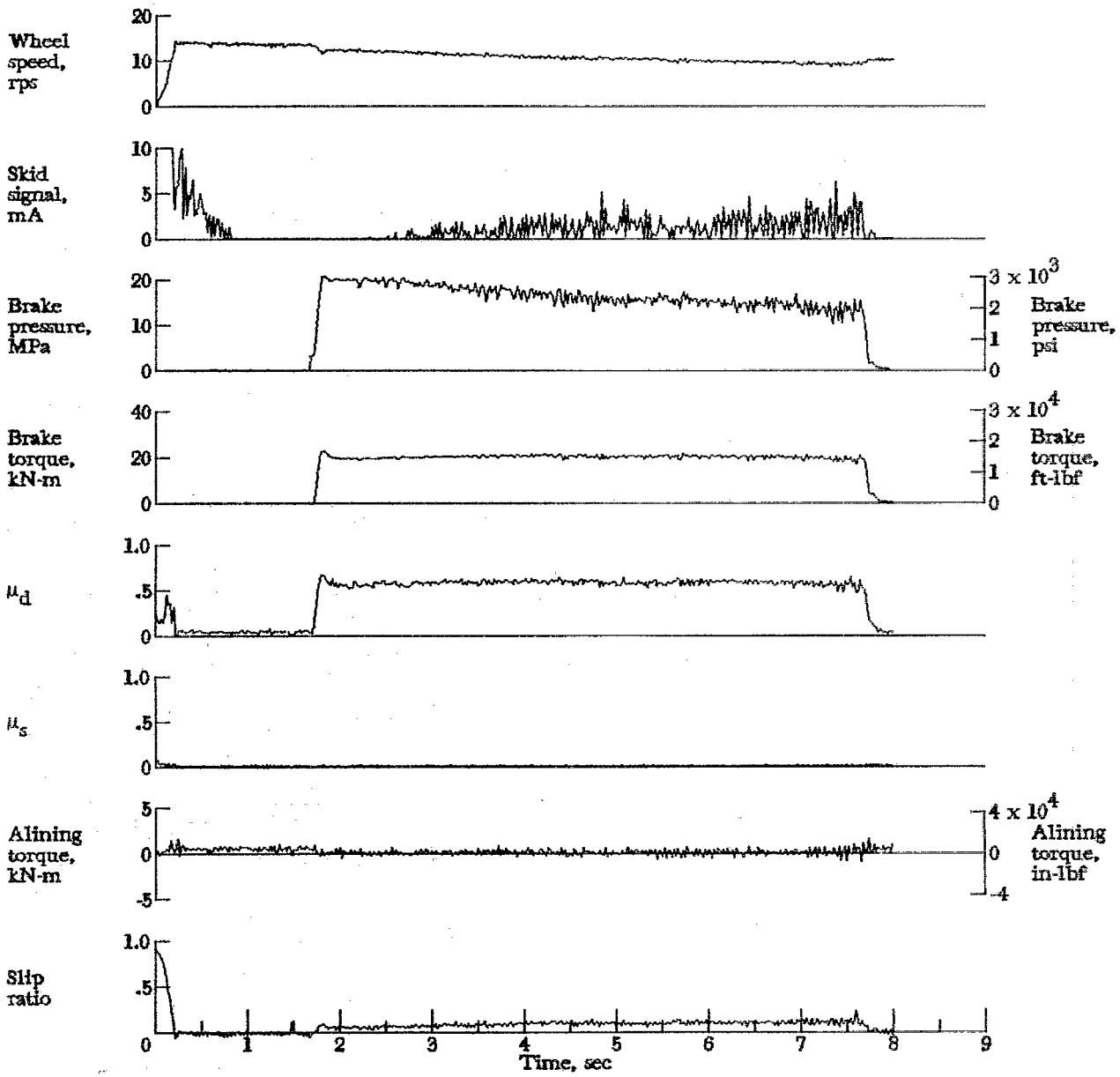

Figure A3.- Time histories for run 3. Nominal carriage speed, 68 knots; vertical load, 80.1 kN (18 000 lbf); yaw angle, 0°; brake pressure, 21 MPa (3000 psi); tire condition, new; surface condition, dry.

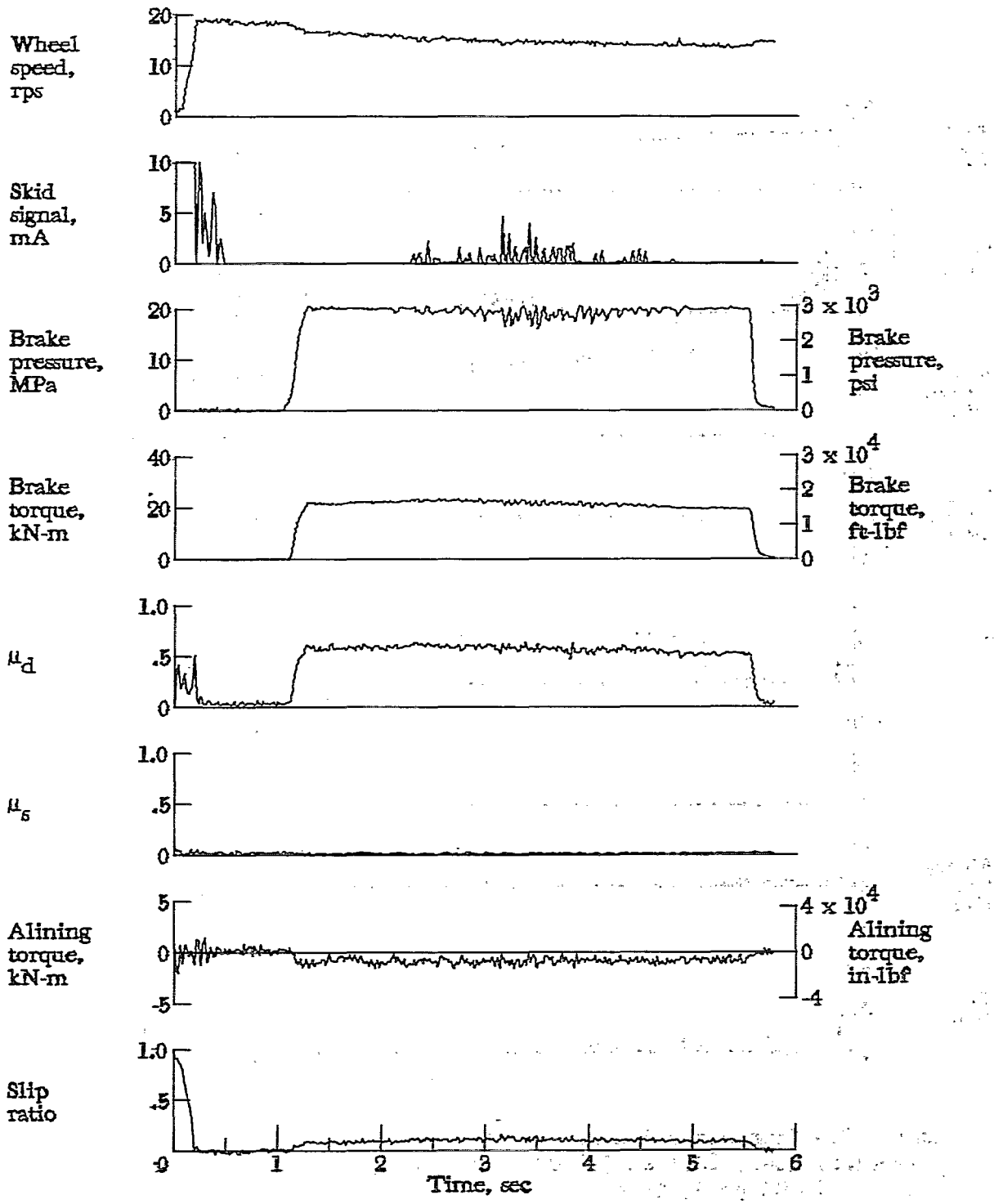

Figure A4.- Time histories for run 4. Nominal carriage speed, 95 knots; vertical load, 81.8 kN (18 400 lbf); yaw angle, 0°; brake pressure, 20 MPa (2890 psi); tire condition, new; surface condition, dry.

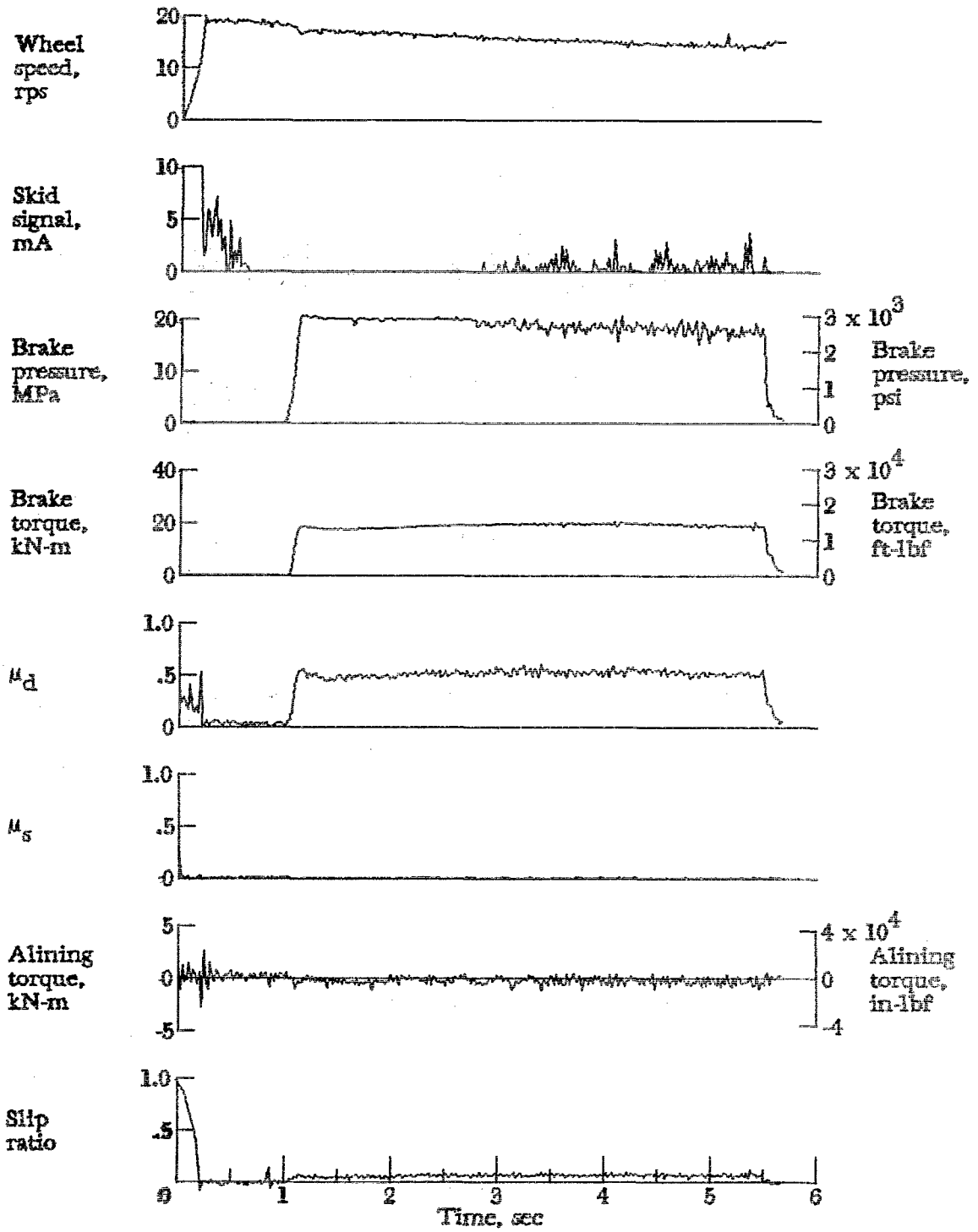

Figure A5.- Time histories for run 5. Nominal carriage speed, 98 knots; vertical load, 81.4 kN (18 300 lbf); yaw angle, 0°; brake pressure, 20 MPa (2940 psi); tire condition, new; surface condition, dry.

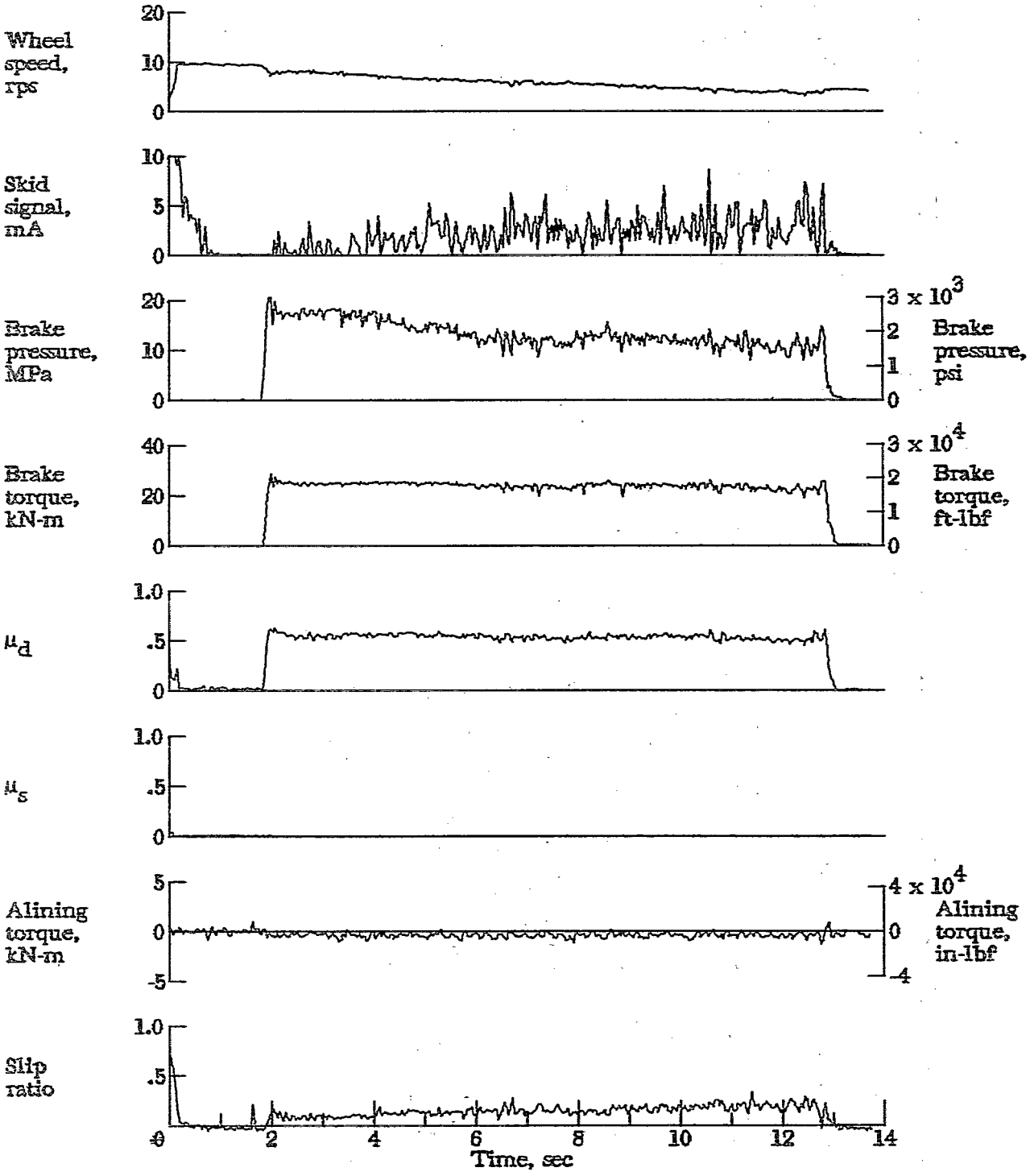

Figure A6.- Time histories for run 6. Nominal carriage speed, 39 knots; vertical load, 98.3 kN (22 100 lbf); yaw angle, 0°; brake pressure, 21 MPa (3000 psi); tire condition, new; surface condition, dry.

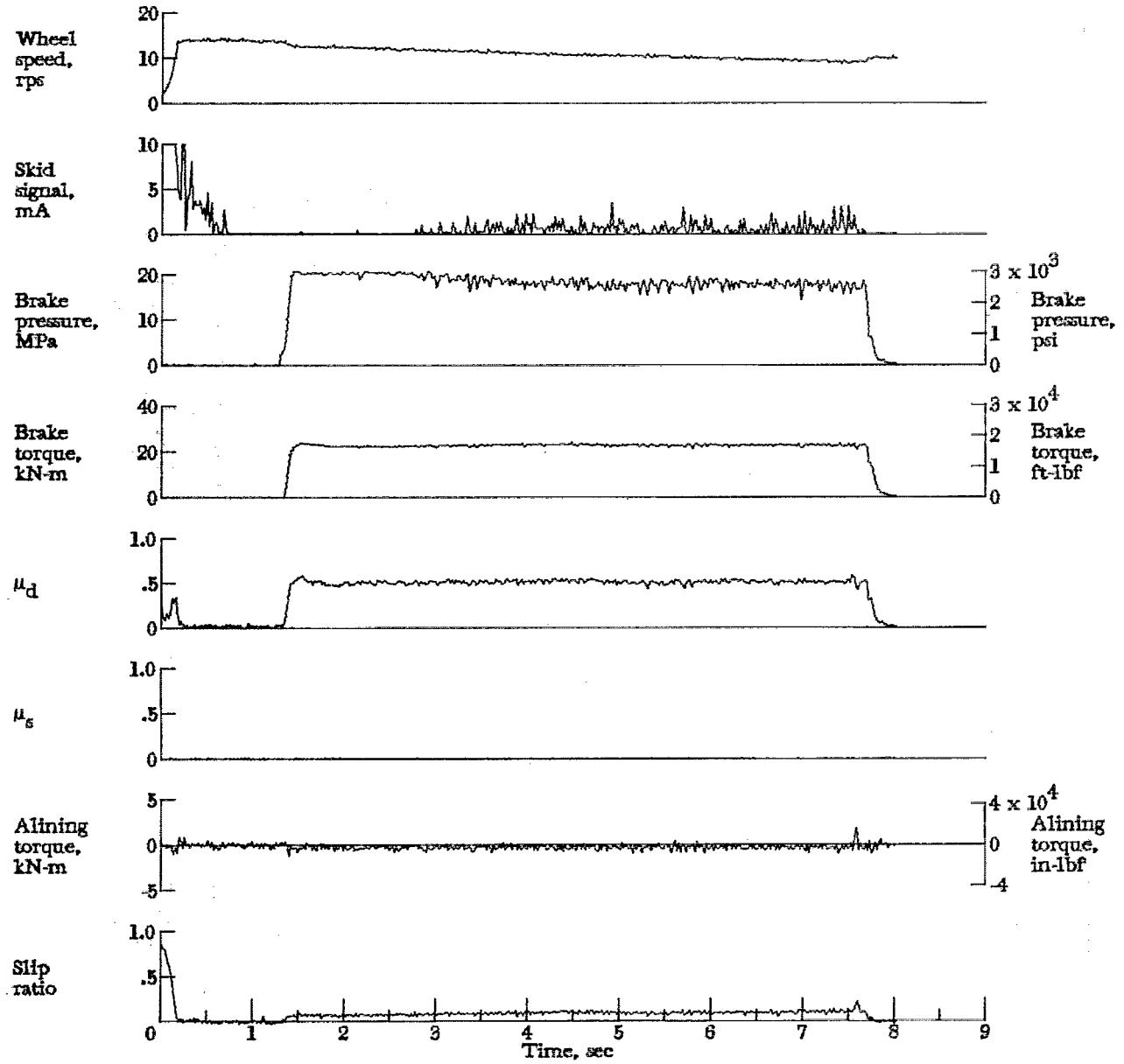

Figure A7.- Time histories for run 7. Nominal carriage speed, 68 knots; vertical load, 98.3 kN (22 100 lbf); yaw angle, 0°; brake pressure, 21 MPa (2950 psi); tire condition, new; surface condition, dry.

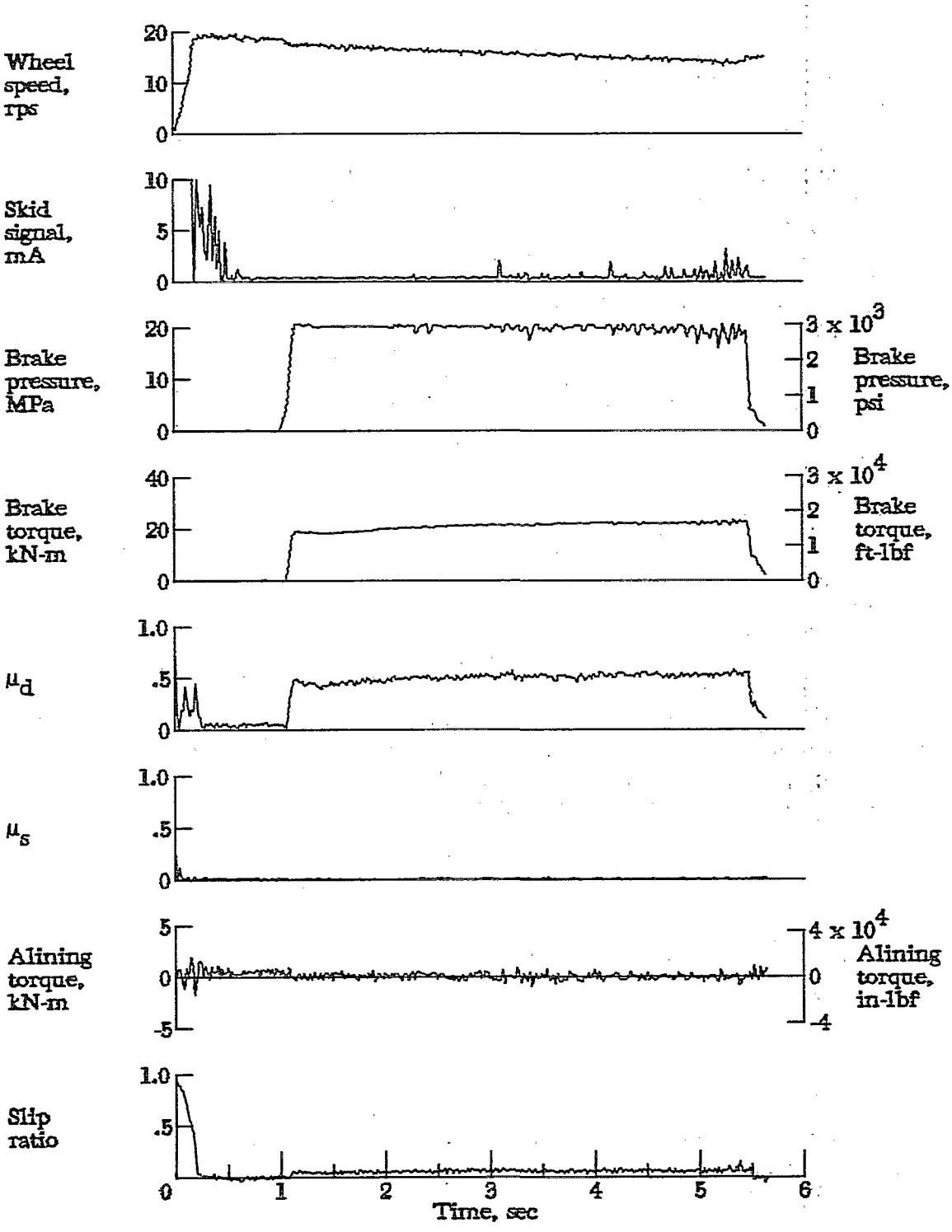

Figure A8.- Time histories for run 8. Nominal carriage speed, 98 knots; vertical load, 97.4 kN (21 900 lbf); yaw angle, 0°; brake pressure, 21 MPa (2950 psi); tire condition, new; surface condition, dry.

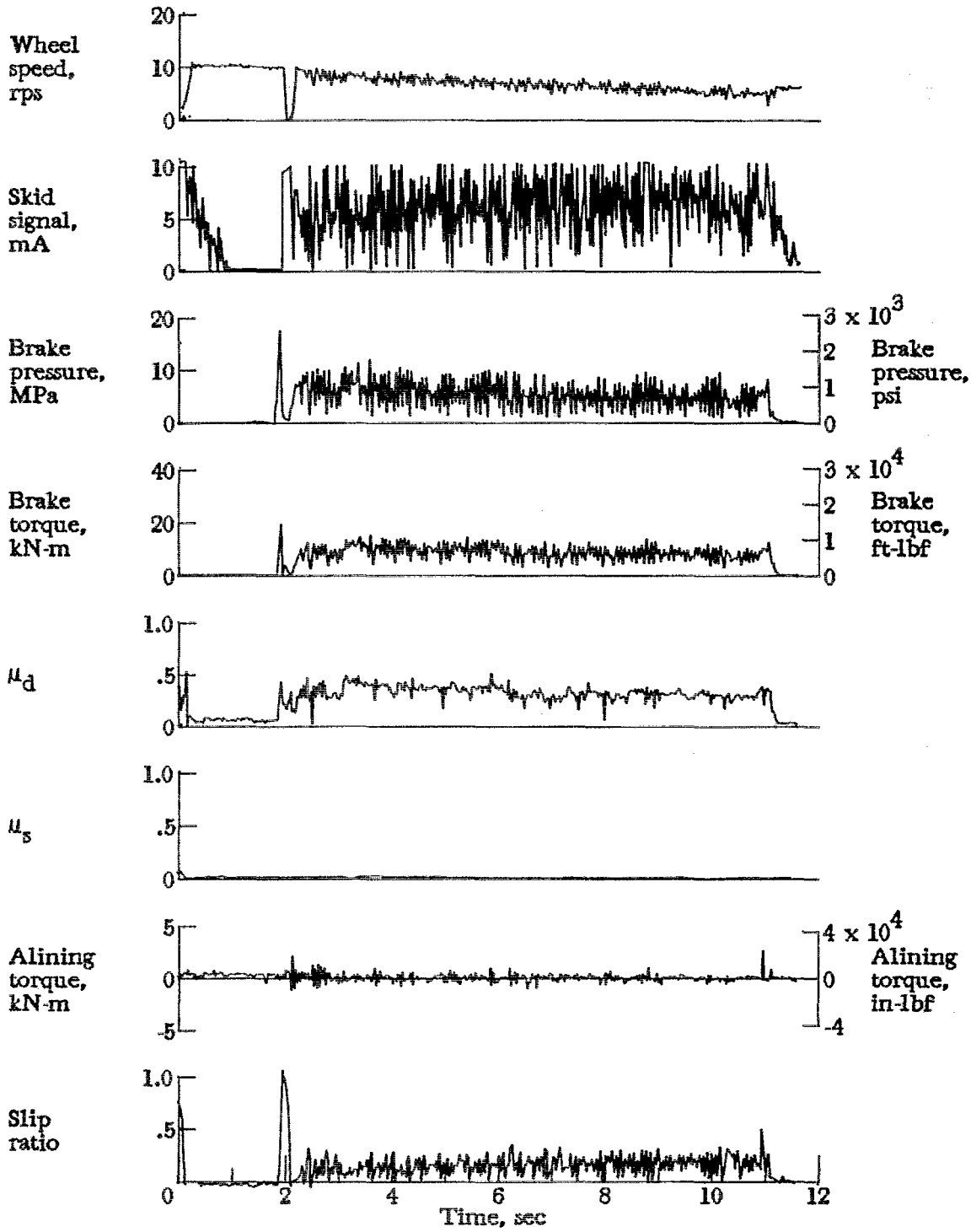

Figure A9.- Time histories for run 9. Nominal carriage speed, 47 knots; vertical load, 62.3 kN (14 000 lbf); yaw angle, 0°; brake pressure, 21 MPa (3000 psi); tire condition, new; surface condition, damp.

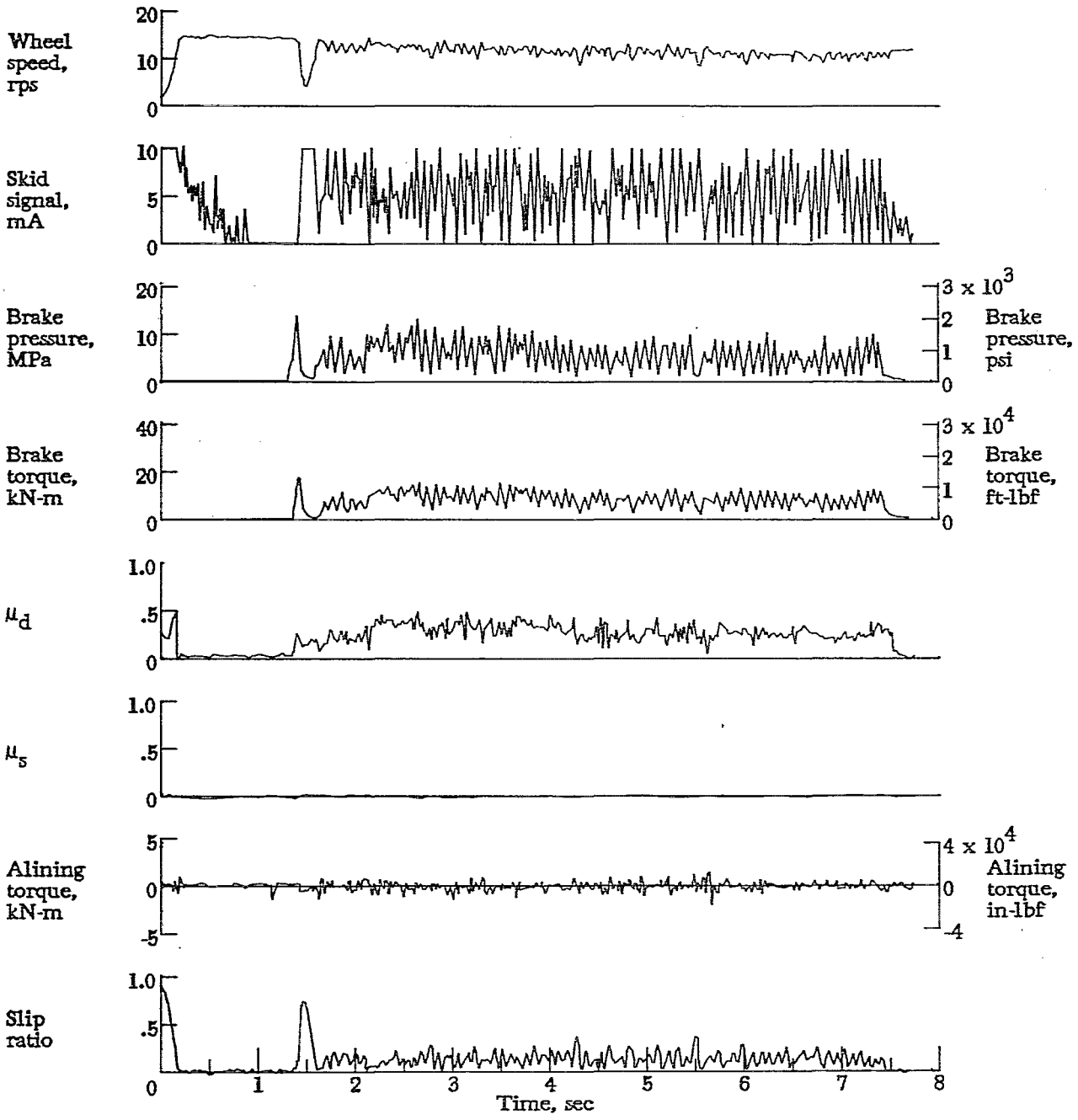

Figure A10.- Time histories for run 10. Nominal carriage speed, 71 knots; vertical load, 63.2 kN (14 200 lbf); yaw angle, 0°; brake pressure, 21 MPa (3000 psi); tire condition, new; surface condition, damp.

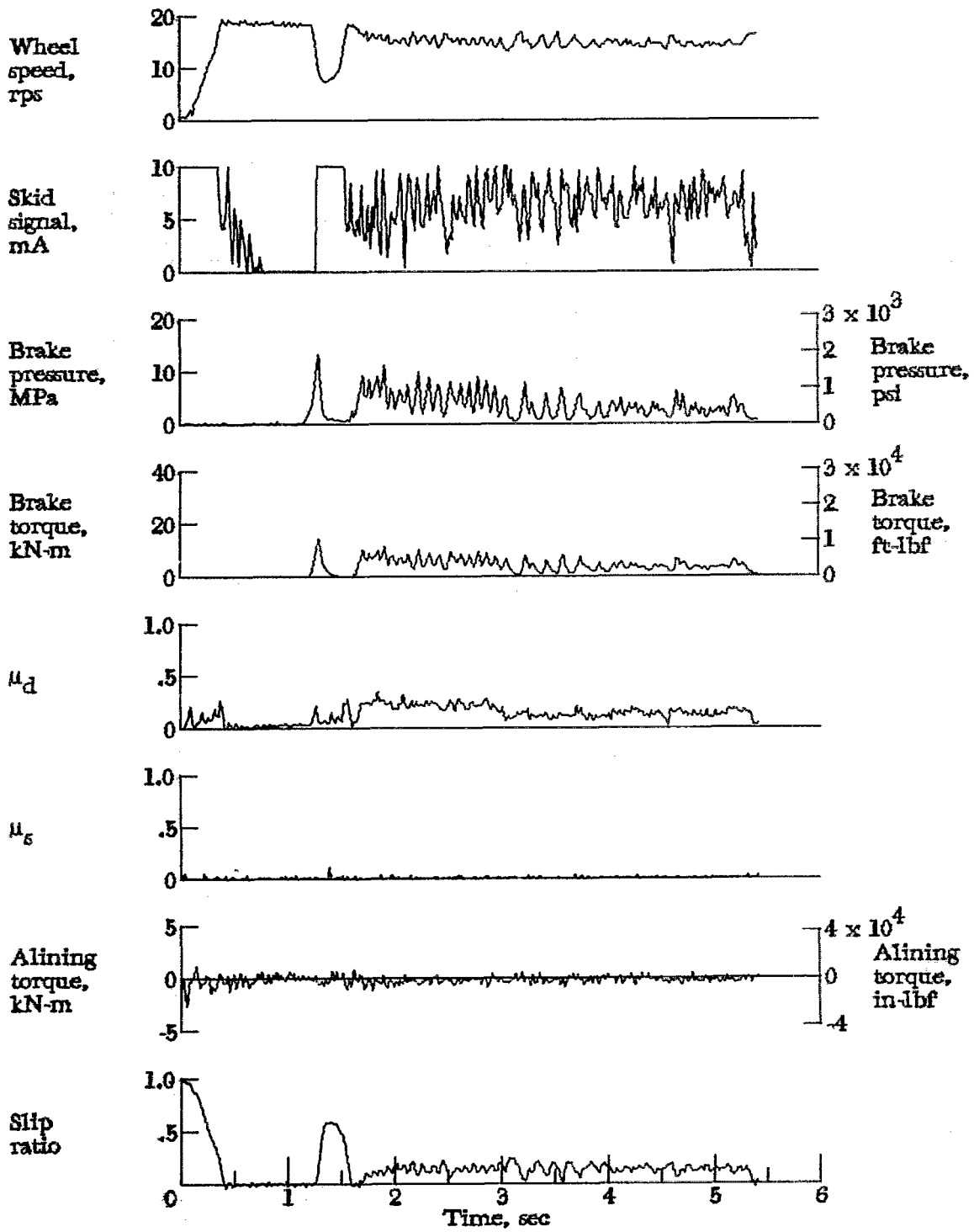

Figure A11.- Time histories for run 11. Nominal carriage speed, 103 knots; vertical load, 61.8 kN (13 900 lbf); yaw angle, 0°; brake pressure, 21 MPa (3000 psi); tire condition, new; surface condition, damp.

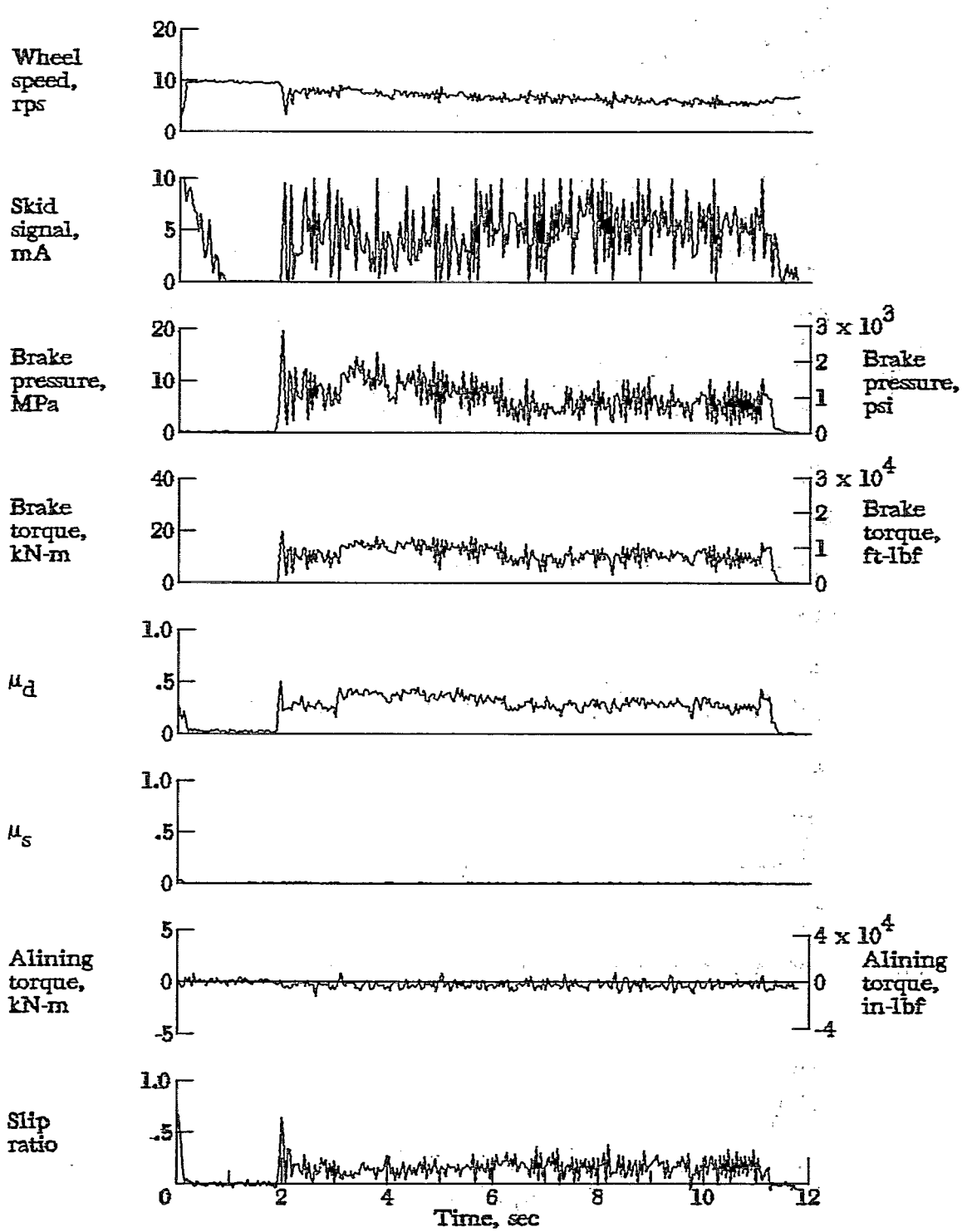

Figure A12.- Time histories for run 12. Nominal carriage speed, 46 knots; vertical load, 81.0 kN (18 200 lbf); yaw angle, 0°; brake pressure, 21 MPa (3000 psi); tire condition, new; surface condition, damp.

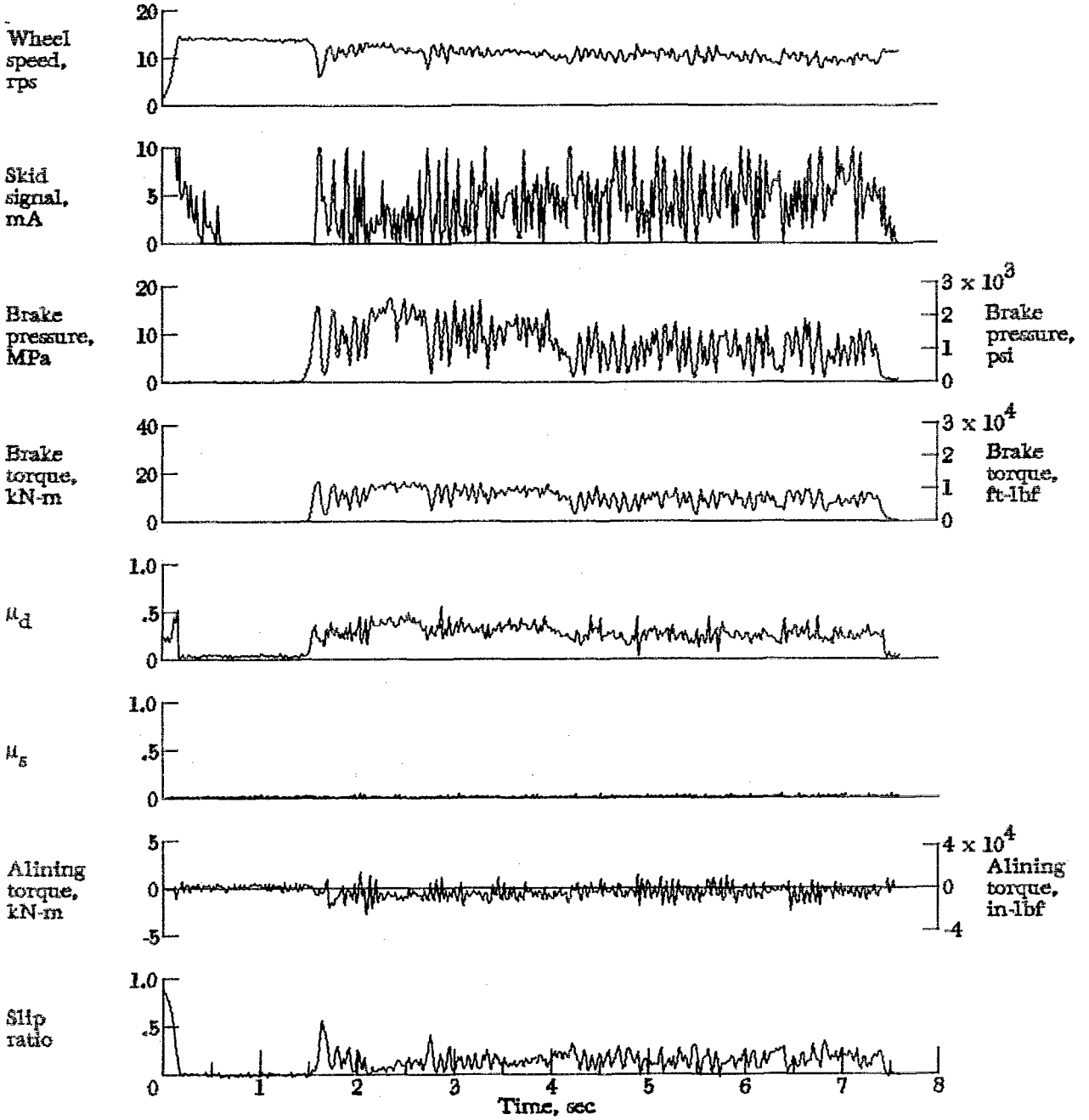

Figure A13.- Time histories for run 13. Nominal carriage speed, 73 knots; vertical load, 80.5 kN (18 100 lbf); yaw angle, 0°; brake pressure, 21 MPa (3000 psi); tire condition, new; surface condition, damp.

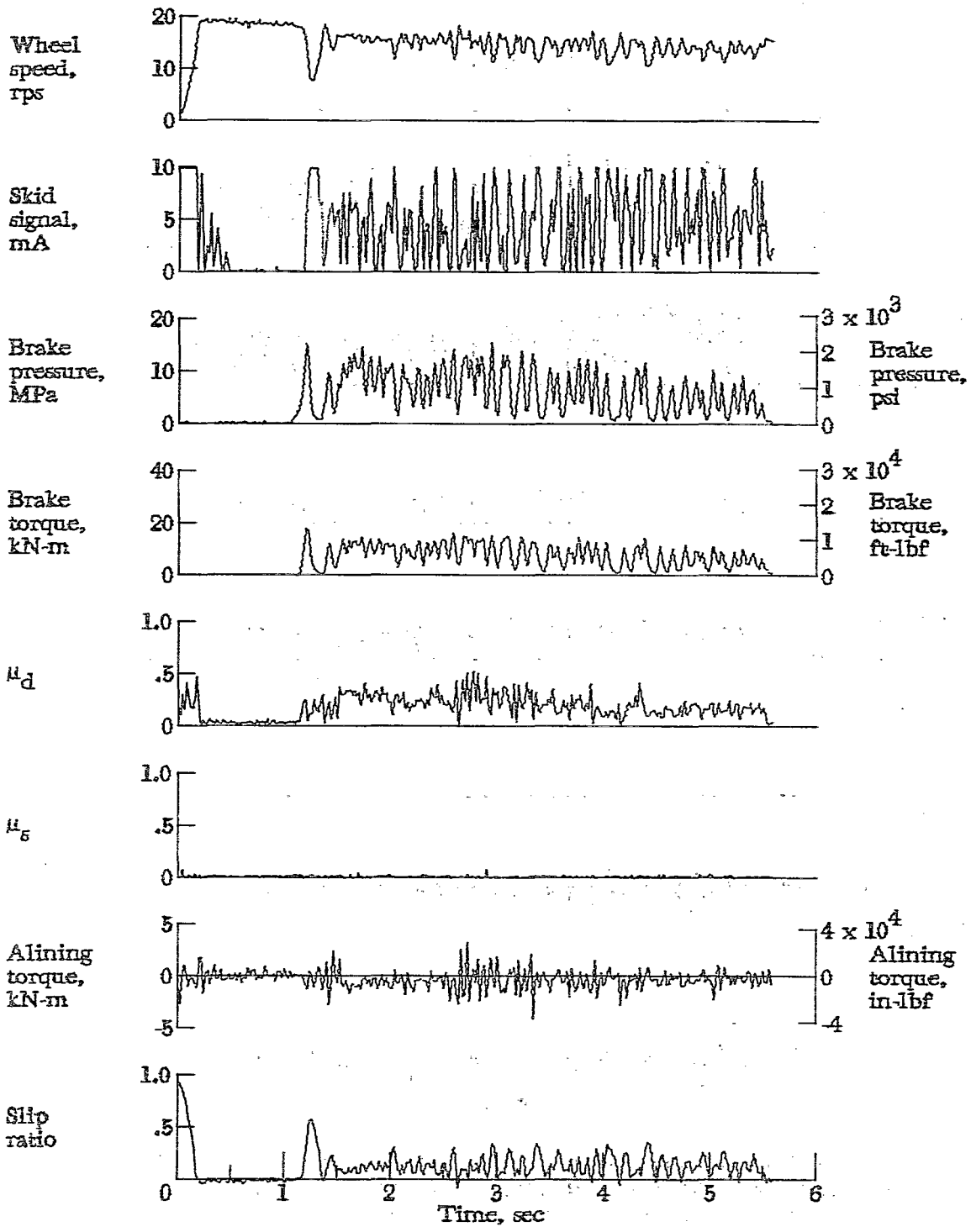

Figure A14.- Time histories for run 14. Nominal carriage speed, 99 knots; vertical load, 81.0 kN (18 200 lbf); yaw angle, 0°; brake pressure, 21 MPa (3000 psi); tire condition, new; surface condition, damp.

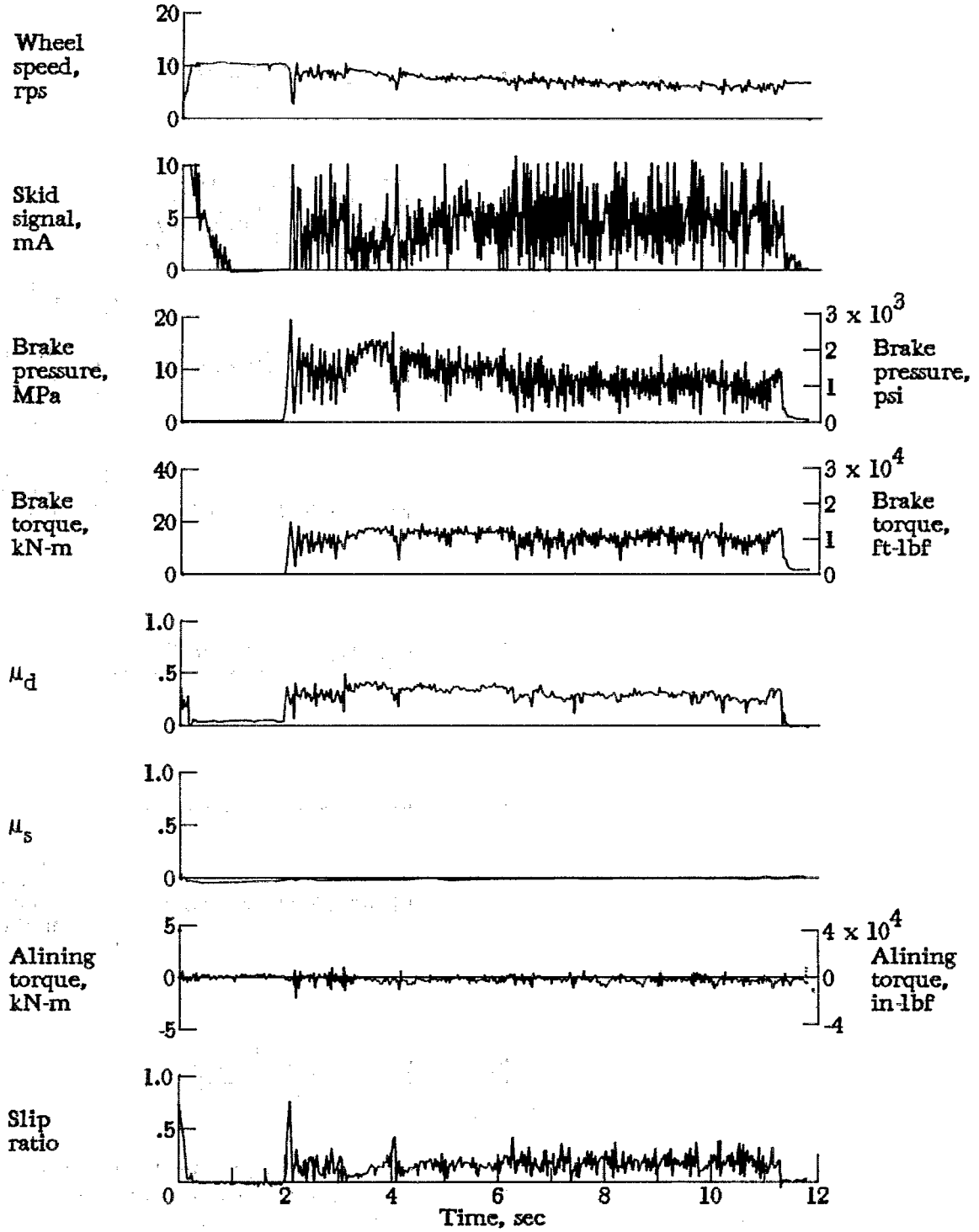

Figure A15.- Time histories for run 15. Nominal carriage speed, 46 knots; vertical load, 97.9 kN (22 000 lbf); yaw angle, 0°; brake pressure, 21 MPa (3000 psi); tire condition, new; surface condition, damp.

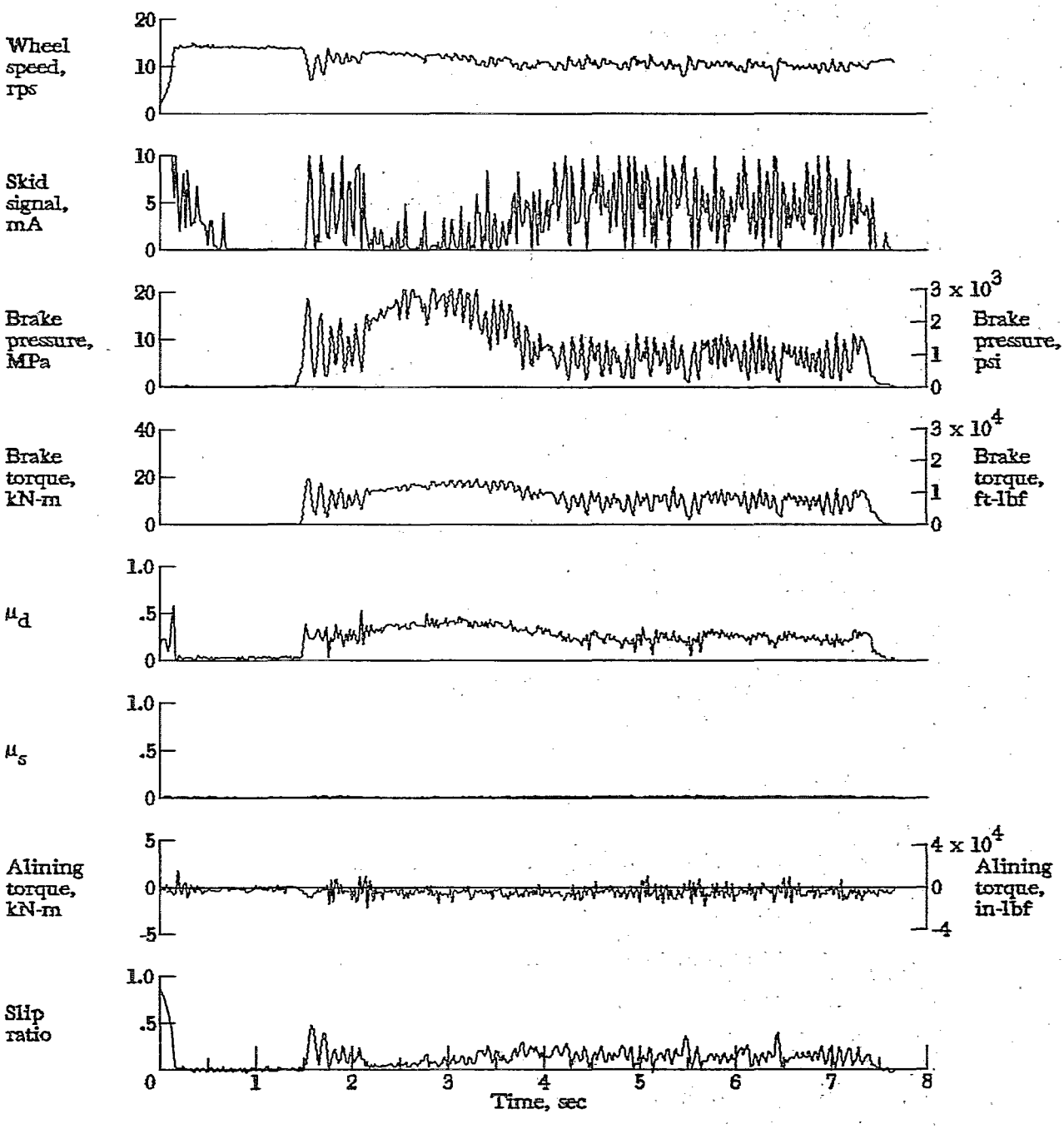

Figure A16.- Time histories for run 16. Nominal carriage speed, 72 knots; vertical load, 97.4 kN (21 900 lbf); yaw angle, 0°; brake pressure, 21 MPa (3000 psi); tire condition, new; surface condition, damp.

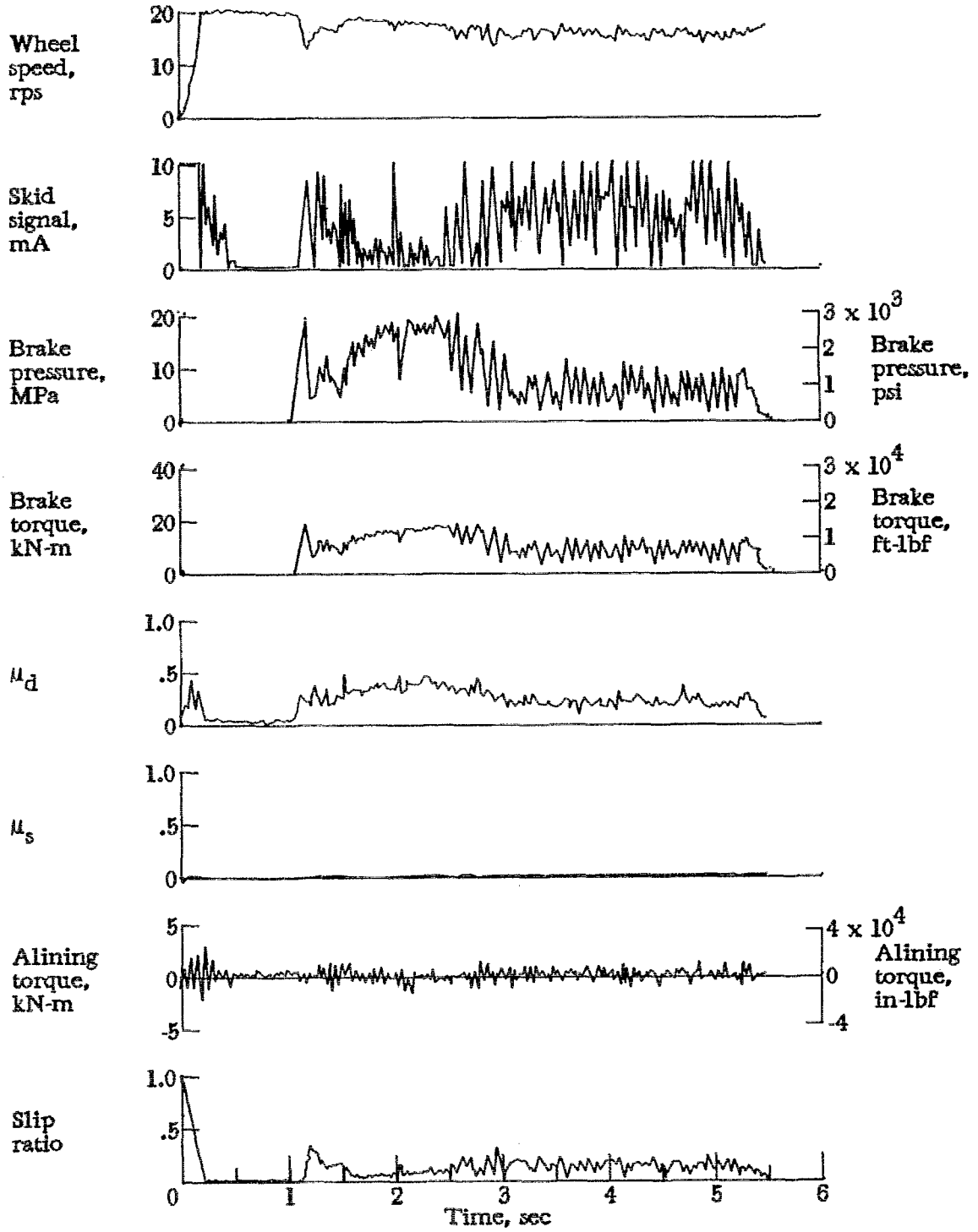

Figure A17.- Time histories for run 17. Nominal carriage speed, 101 knots; vertical load, 97.4 kN (21 900 lbf); yaw angle, 0°; brake pressure, 21 MPa (3000 psi); tire condition, new; surface condition, damp.

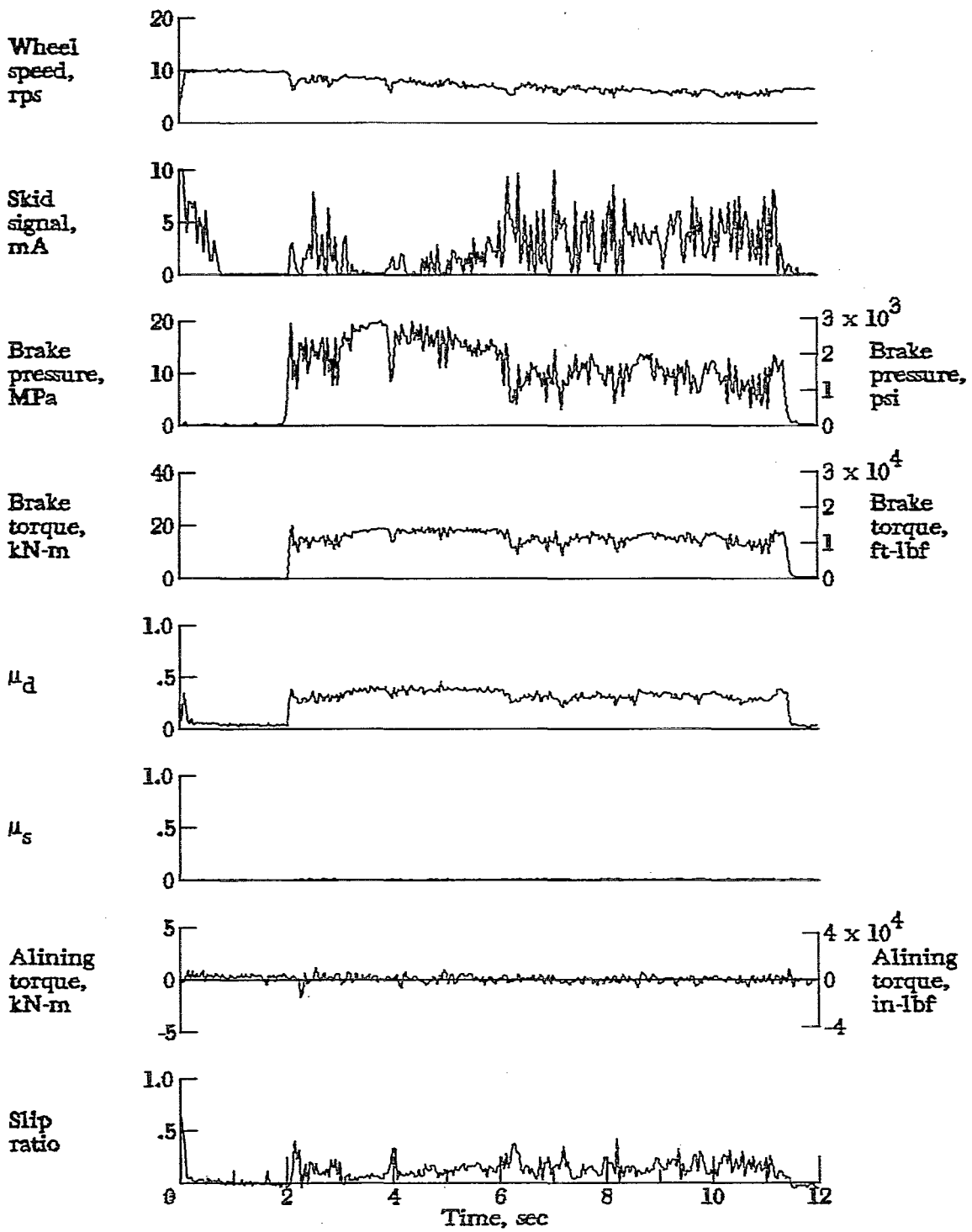

Figure A18.- Time histories for run 18. Nominal carriage speed, 45 knots; vertical load, 117.9 kN (26 500 lbf); yaw angle, 0°; brake pressure, 21 MPa (3000 psi); tire condition, new; surface condition, damp.

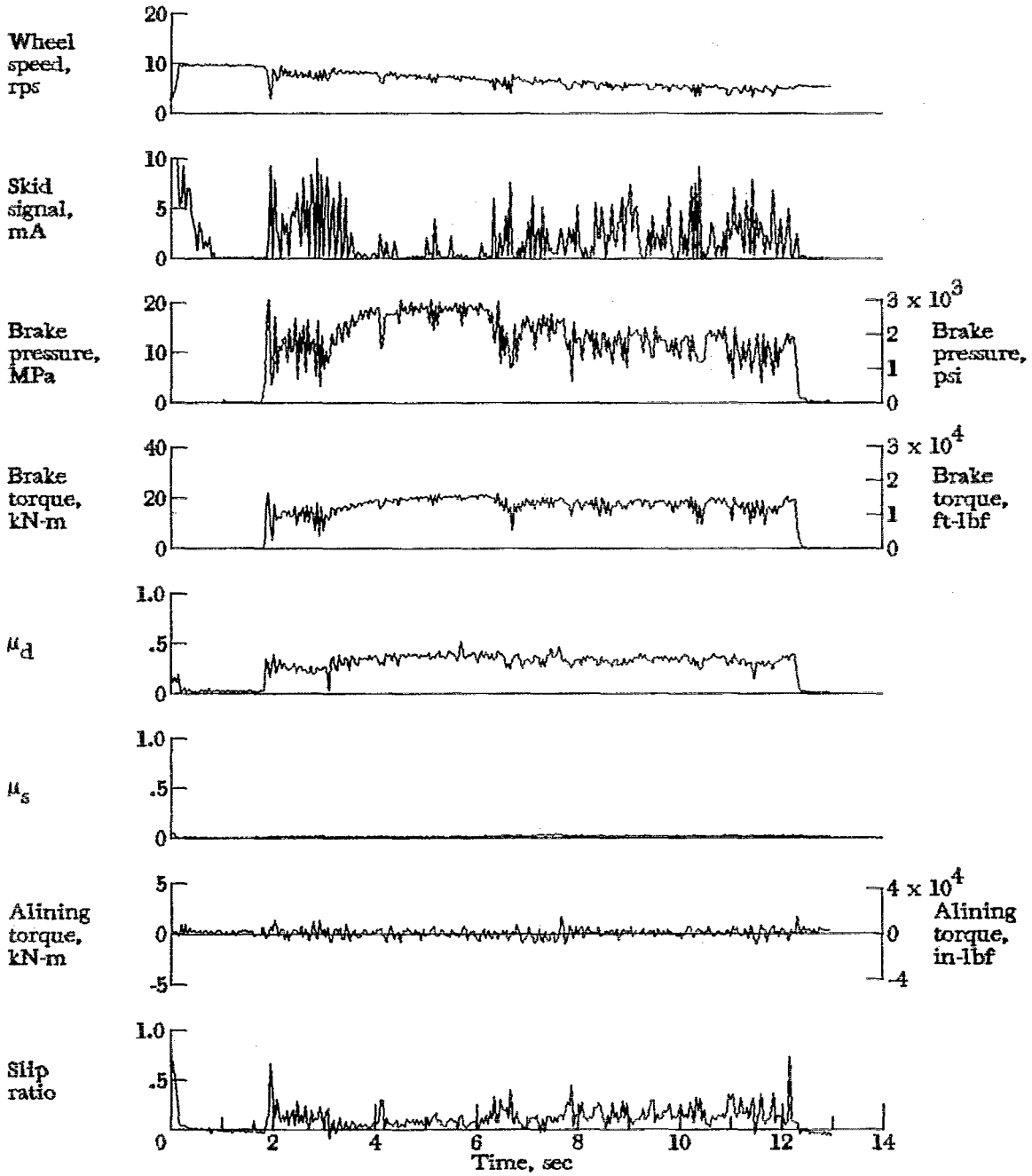

Figure A19.- Time histories for run 19. Nominal carriage speed, 41 knots; vertical load, 118.3 kN (26 600 lbf); yaw angle, 0°; brake pressure, 21 MPa (3000 psi); tire condition, new; surface condition, damp.

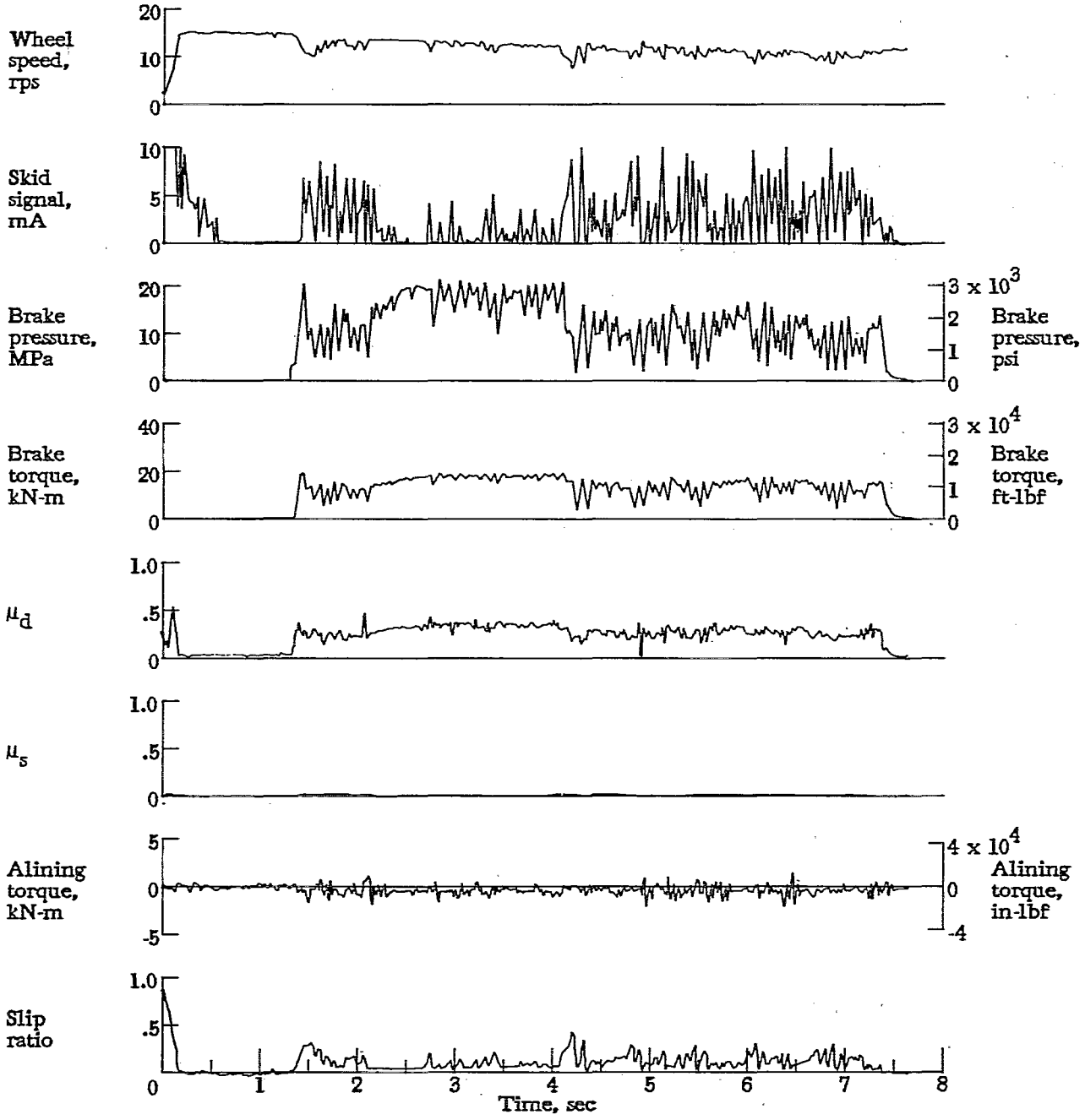

Figure A20.- Time histories for run 20. Nominal carriage speed, 72 knots; vertical load, 118.3 kN (26 600 lbf); yaw angle, 0°; brake pressure, 20 MPa (2900 psi); tire condition, new; surface condition, damp.

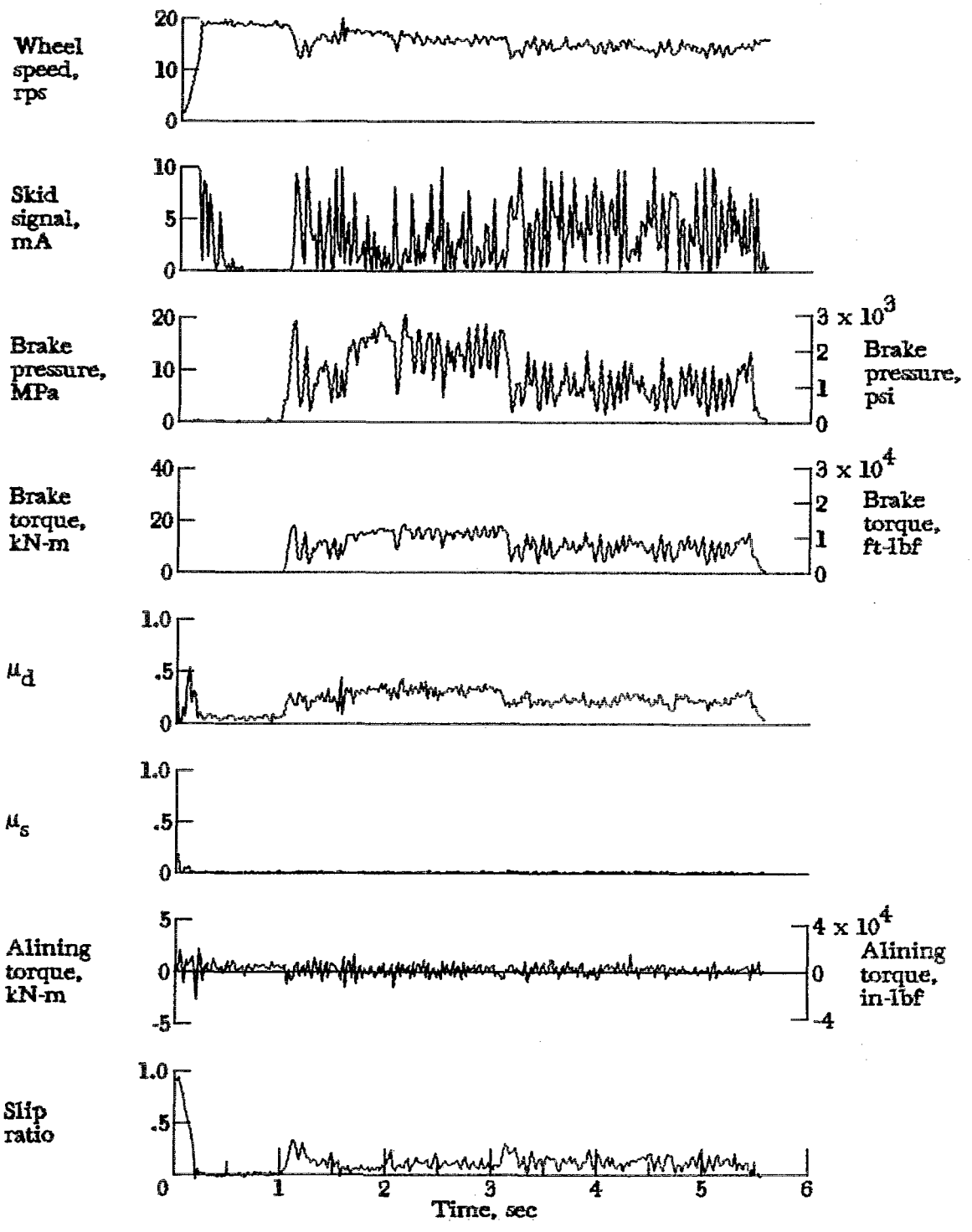

Figure A21.- Time histories for run 21. Nominal carriage speed, 99 knots; vertical load, 118.8 kN (26 700 lbf); yaw angle, 0°; brake pressure, 21 MPa (3000 psi); tire condition, new; surface condition, damp.

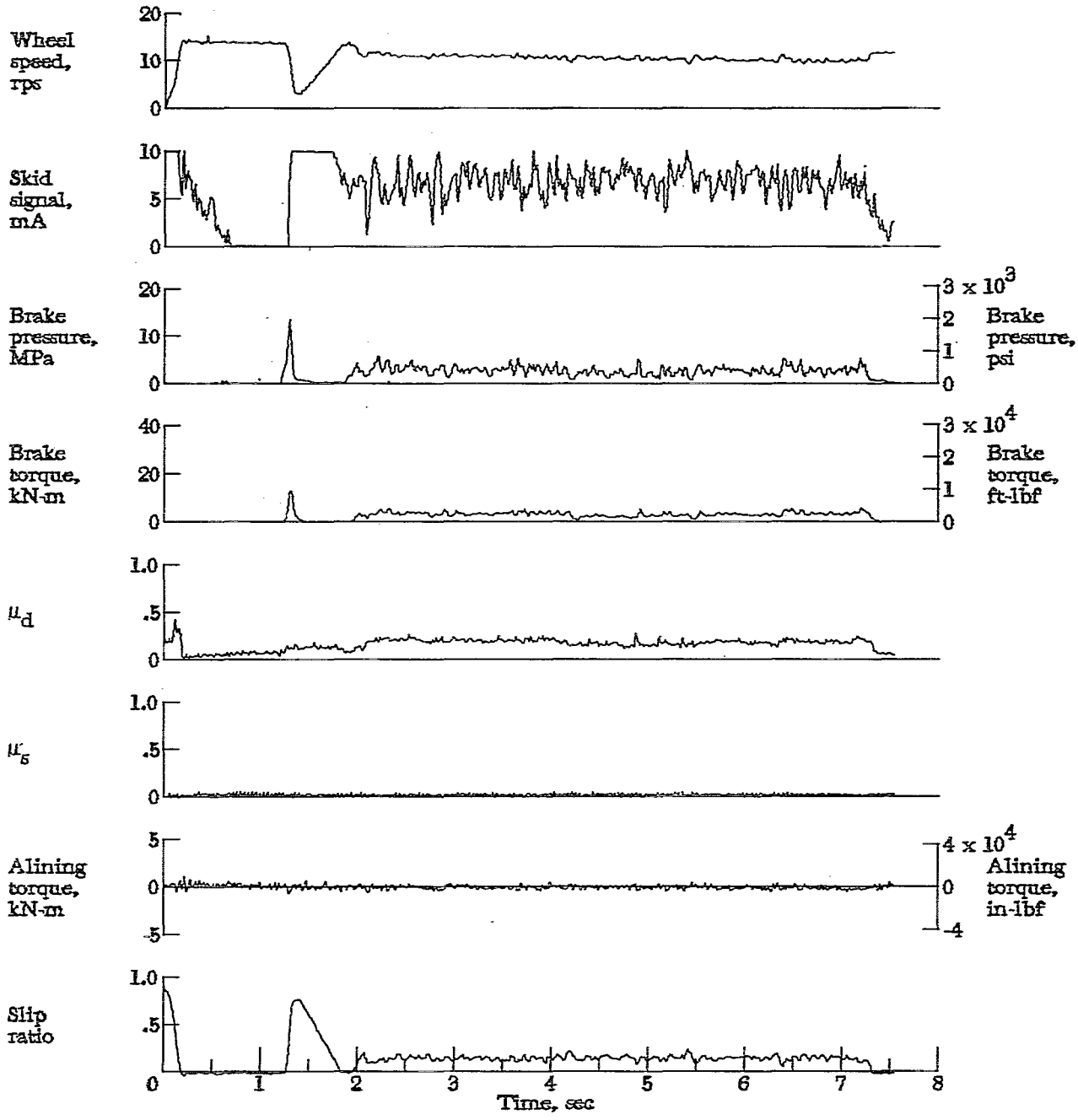

Figure A22.- Time histories for run 22. Nominal carriage speed, 74 knots; vertical load, 61.8 kN (13 900 lbf); yaw angle, 0°; brake pressure, 21 MPa (3000 psi); tire condition, new; surface condition, flooded.

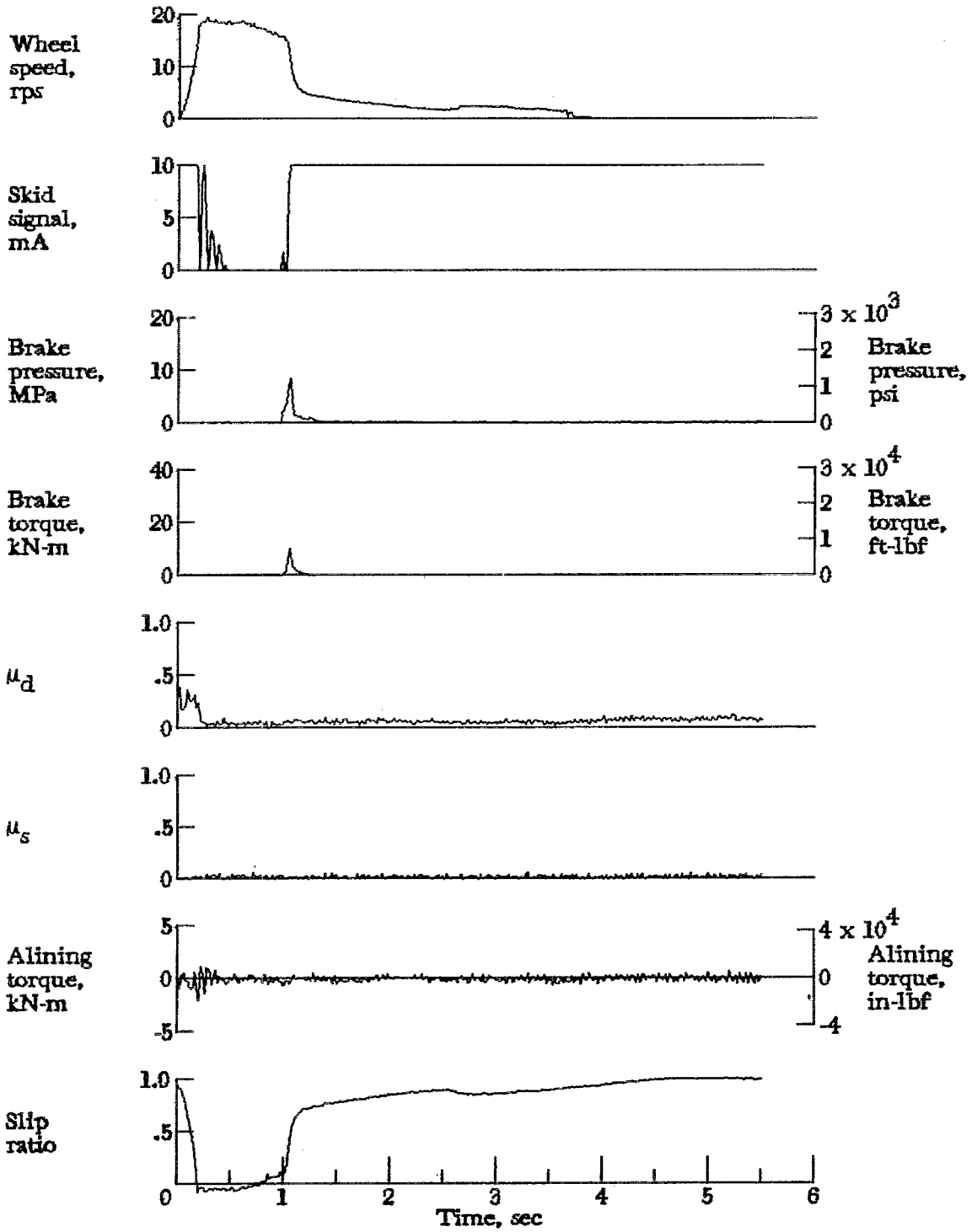

Figure A23.- Time histories for run 23. Nominal carriage speed, 101 knots; vertical load, 61.8 kN (13 900 lbf); yaw angle, 0°; brake pressure, 20 MPa (2930 psi); tire condition, new; surface condition, flooded.

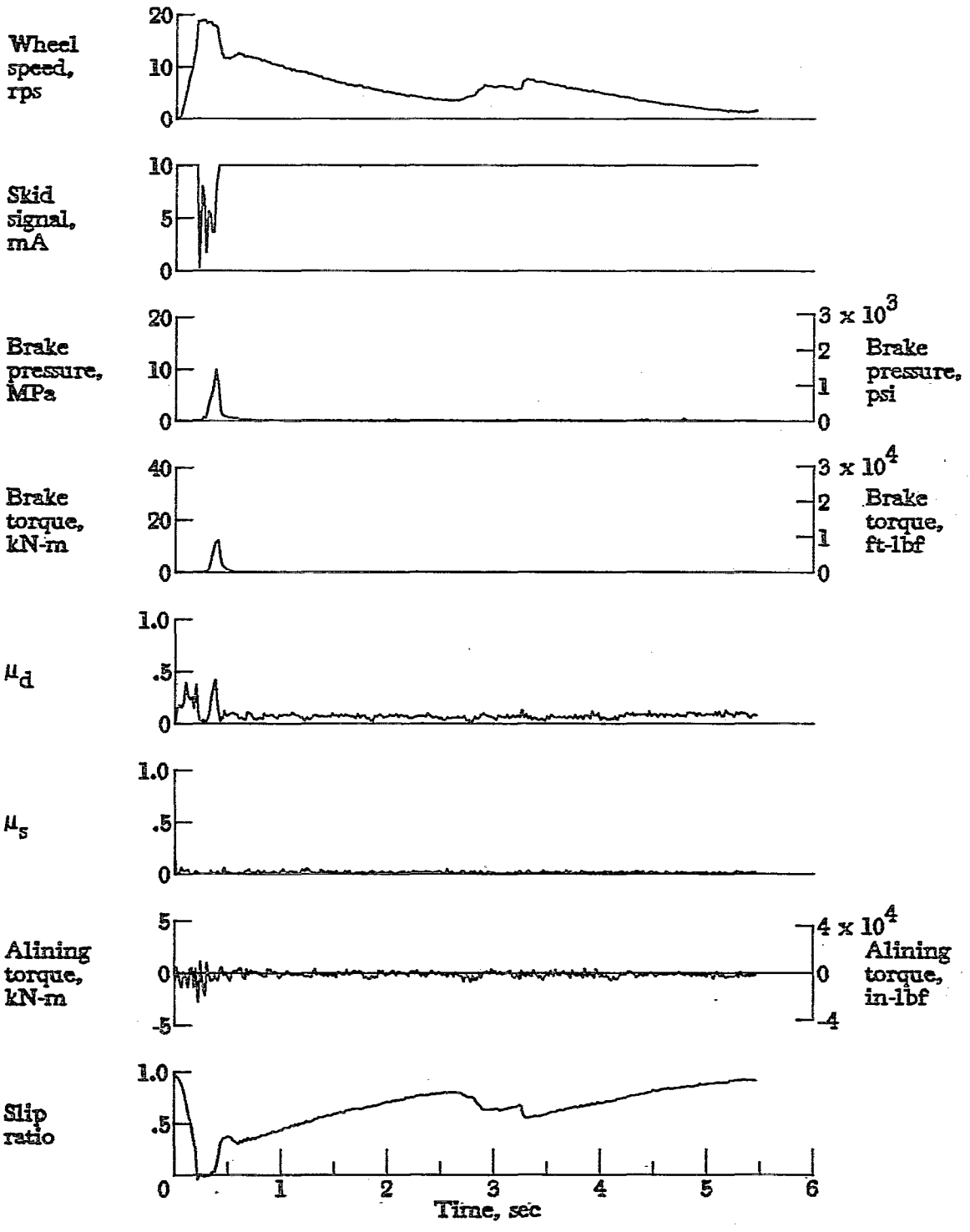

Figure A24.- Time histories for run 24. Nominal carriage speed, 102 knots; vertical load, 61.4 kN (13 800 lbf); yaw angle, 0°; brake pressure, 20 MPa (2880 psi); tire condition, new; surface condition, flooded.

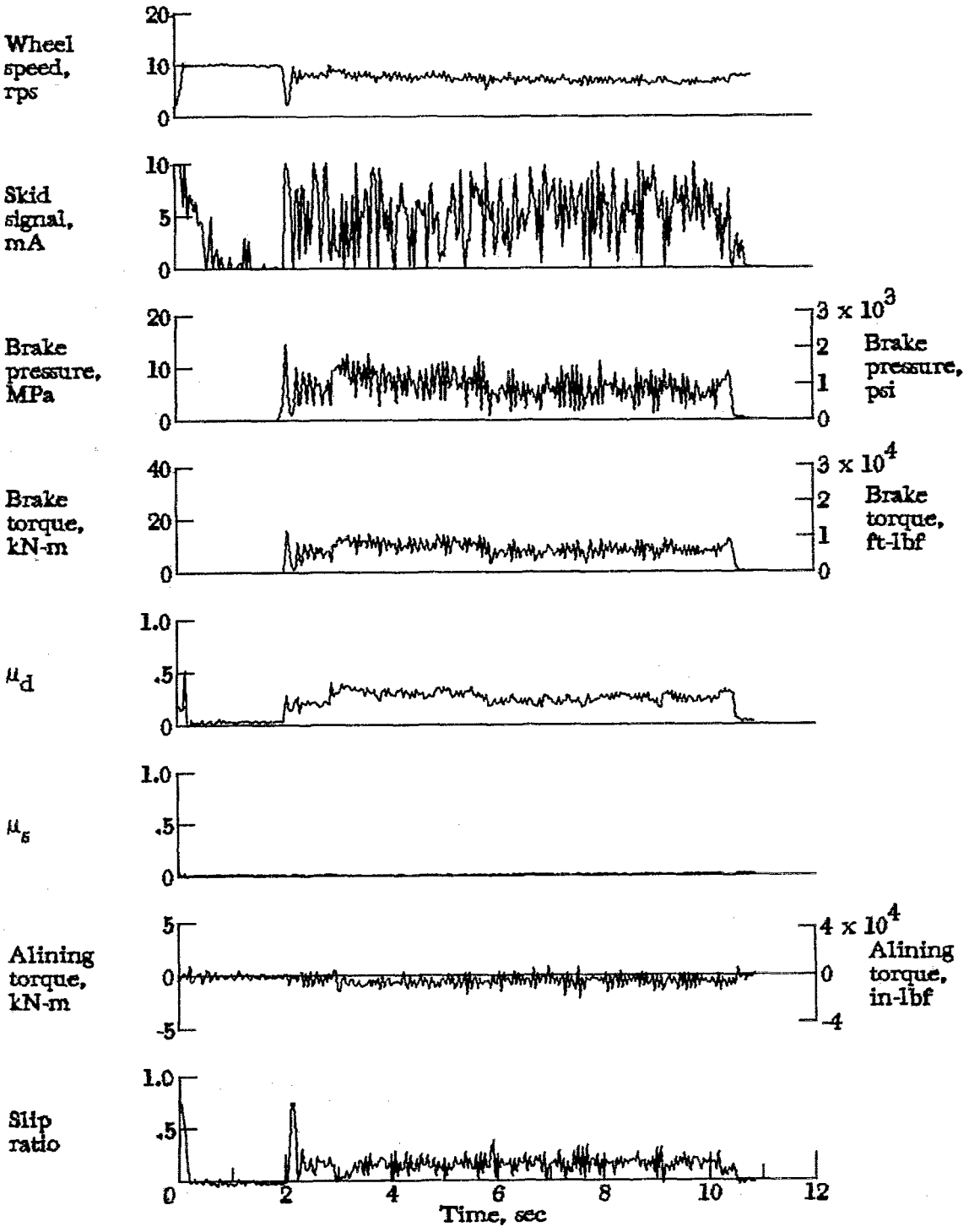

Figure A25.- Time histories for run 25. Nominal carriage speed, 50 knots; vertical load, 81.4 kN (18 300 lbf); yaw angle, 0°; brake pressure, 21 MPa (3000 psi); tire condition, new; surface condition, flooded.

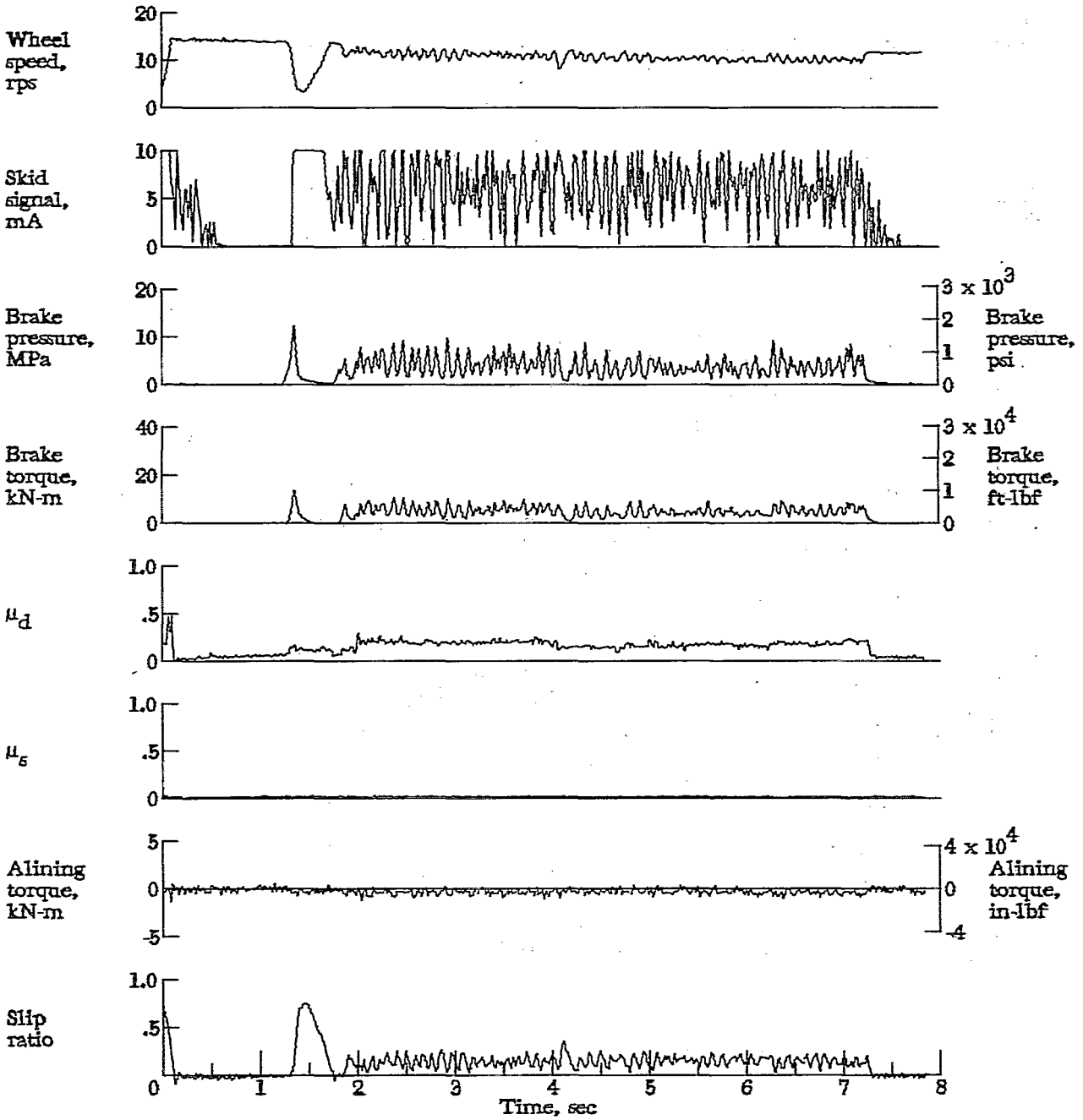

Figure A26.- Time histories for run 26. Nominal carriage speed, 74 knots; vertical load, 81.0 kN (18 200 lbf); yaw angle, 0°; brake pressure, 21 MPa (3000 psi); tire condition, new; surface condition, flooded.

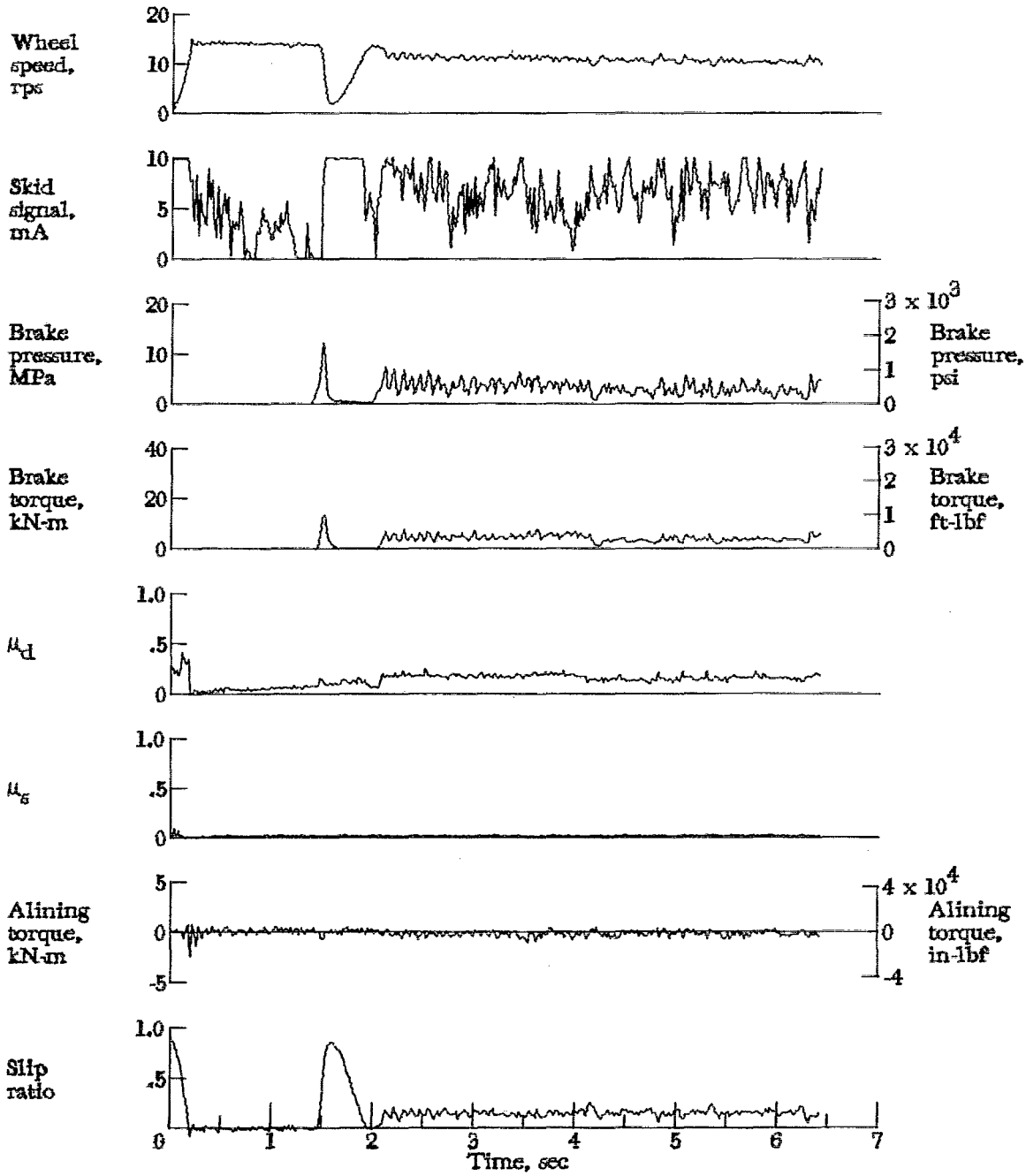

Figure A27.- Time histories for run 27. Nominal carriage speed, 75 knots; vertical load, 80.5 kN (18 100 lbf); yaw angle, 0°; brake pressure, 20 MPa (2900 psi); tire condition, new; surface condition, flooded.

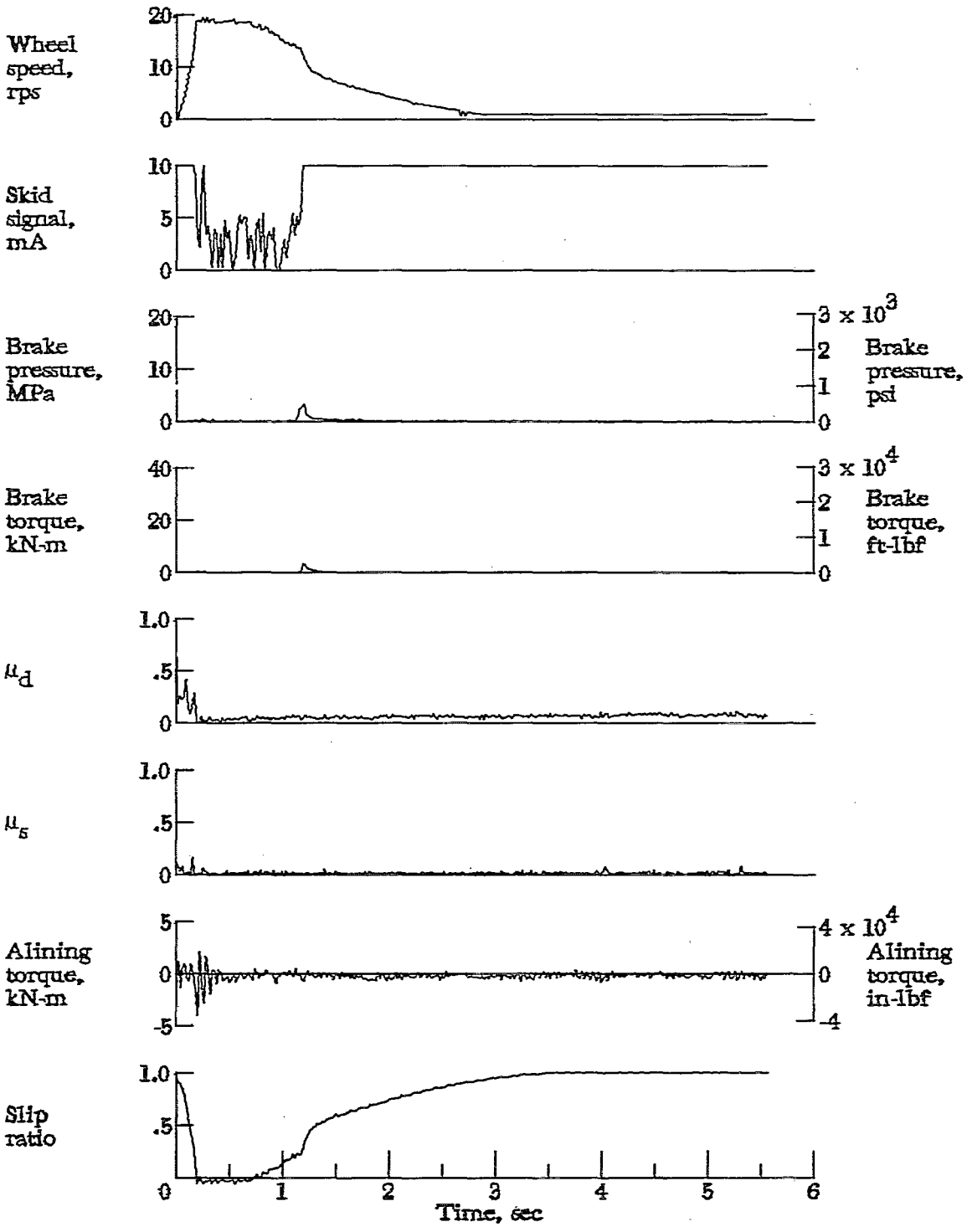

Figure A28.- Time histories for run 28. Nominal carriage speed, 100 knots; vertical load, 80.1 kN (18 000 lbf); yaw angle, 0°; brake pressure, 20 MPa (2910 psi); tire condition, new; surface condition, flooded.

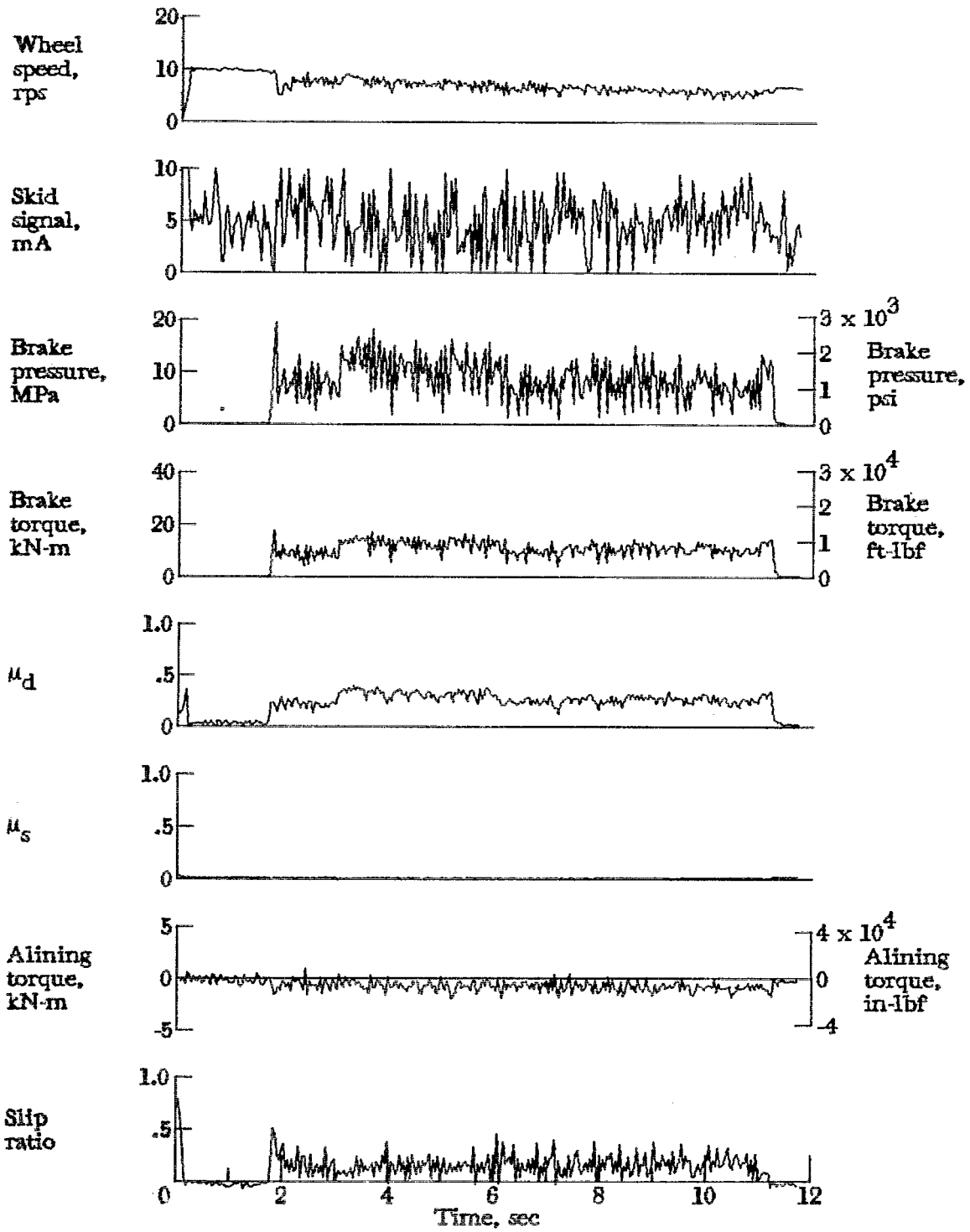

Figure A29.- Time histories for run 29. Nominal carriage speed, 46 knots; vertical load, 97.9 kN (22 000 lbf); yaw angle, 0°; brake pressure, 21 MPa (3000 psi); tire condition, new; surface condition, flooded.

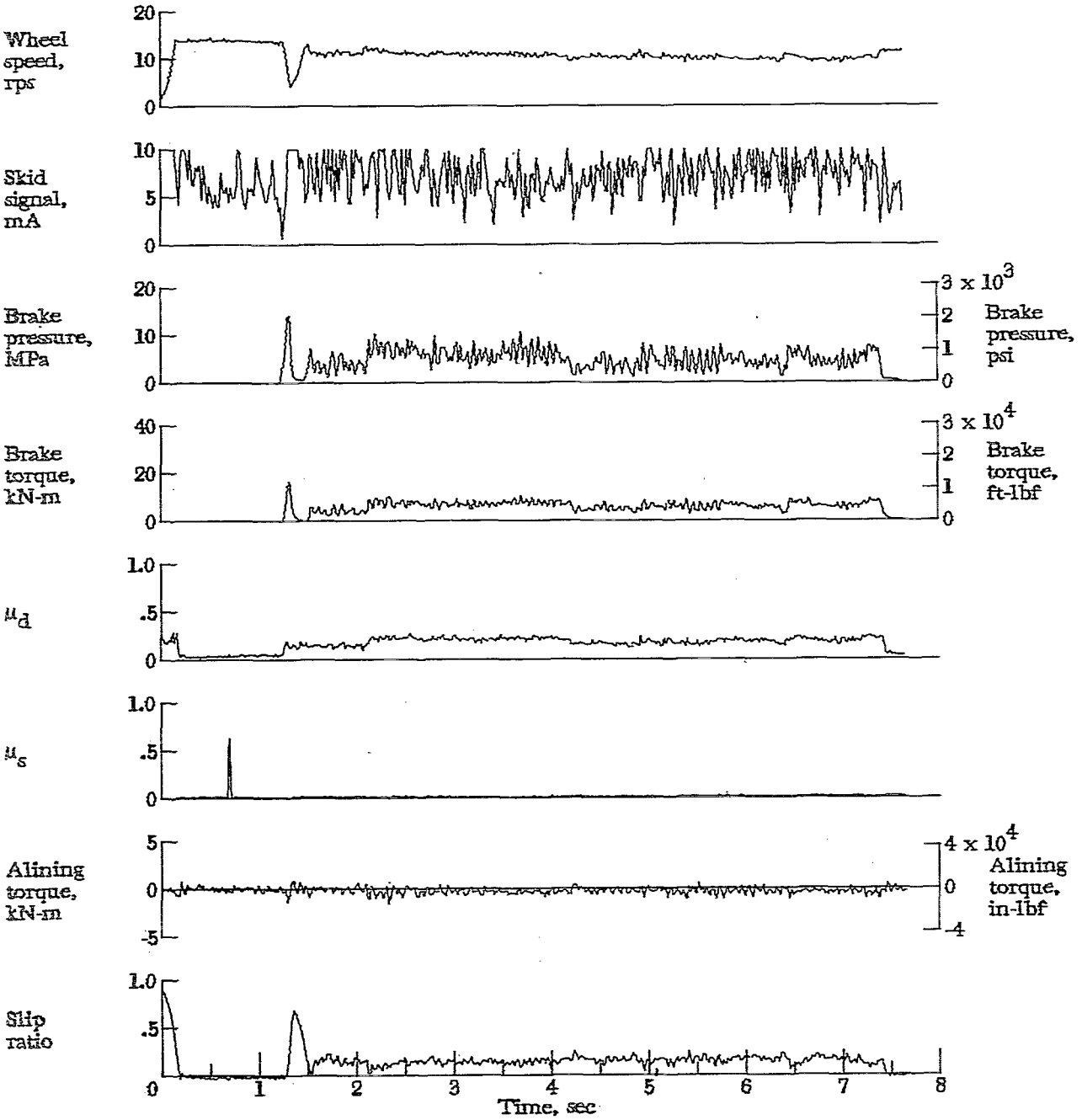

Figure A30.- Time histories for run 30. Nominal carriage speed, 72 knots; vertical load, 97.0 kN (21 800 lbf); yaw angle, 0°; brake pressure, 21 MPa (3000 psi); tire condition, new; surface condition, flooded.

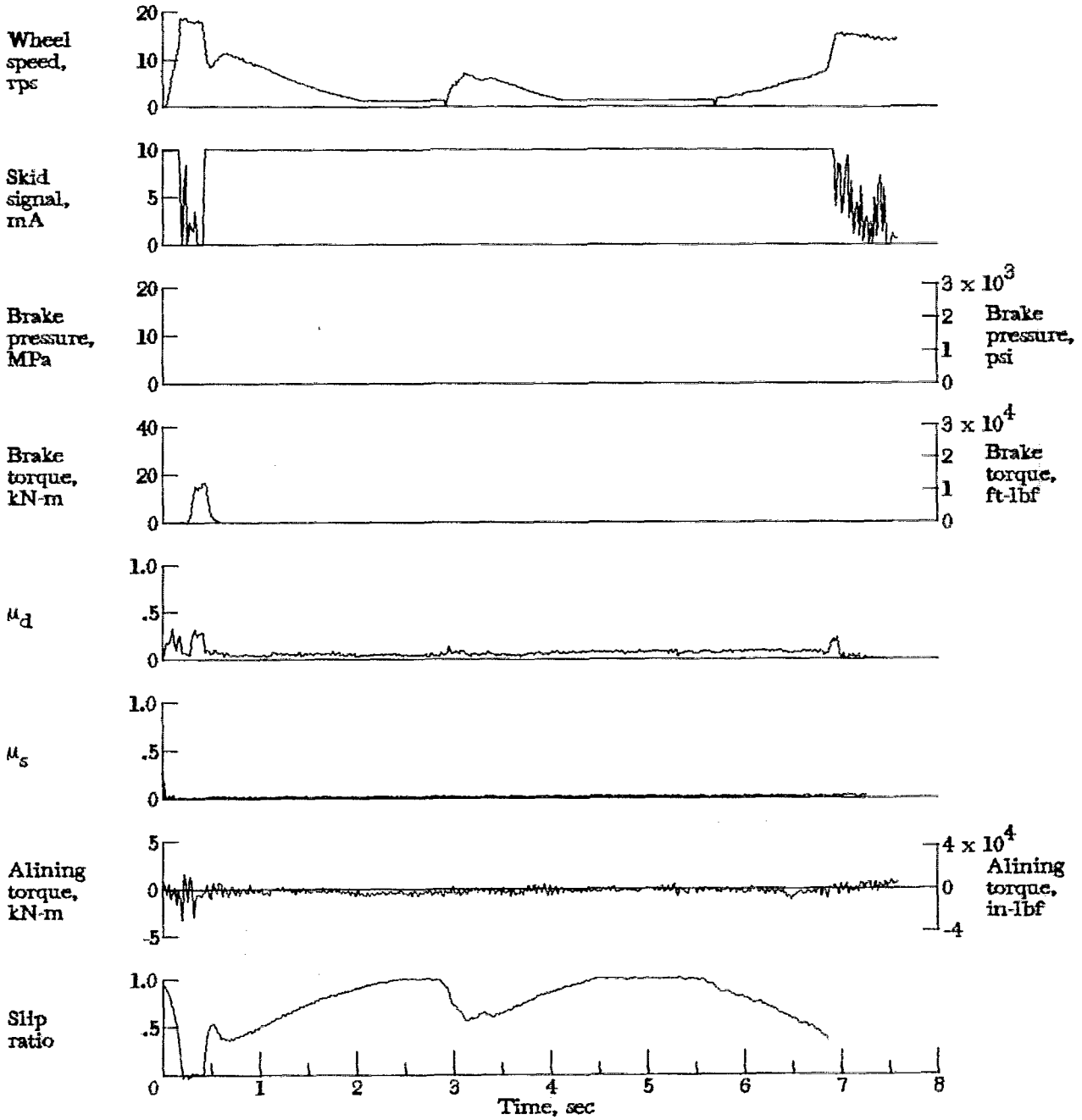

Figure A31.- Time histories for run 31. Nominal carriage speed, 100 knots; vertical load, 98.8 kN (22 200 lbf); yaw angle, 0°; brake pressure, 21 MPa (3000 psi); tire condition, new; surface condition, flooded.

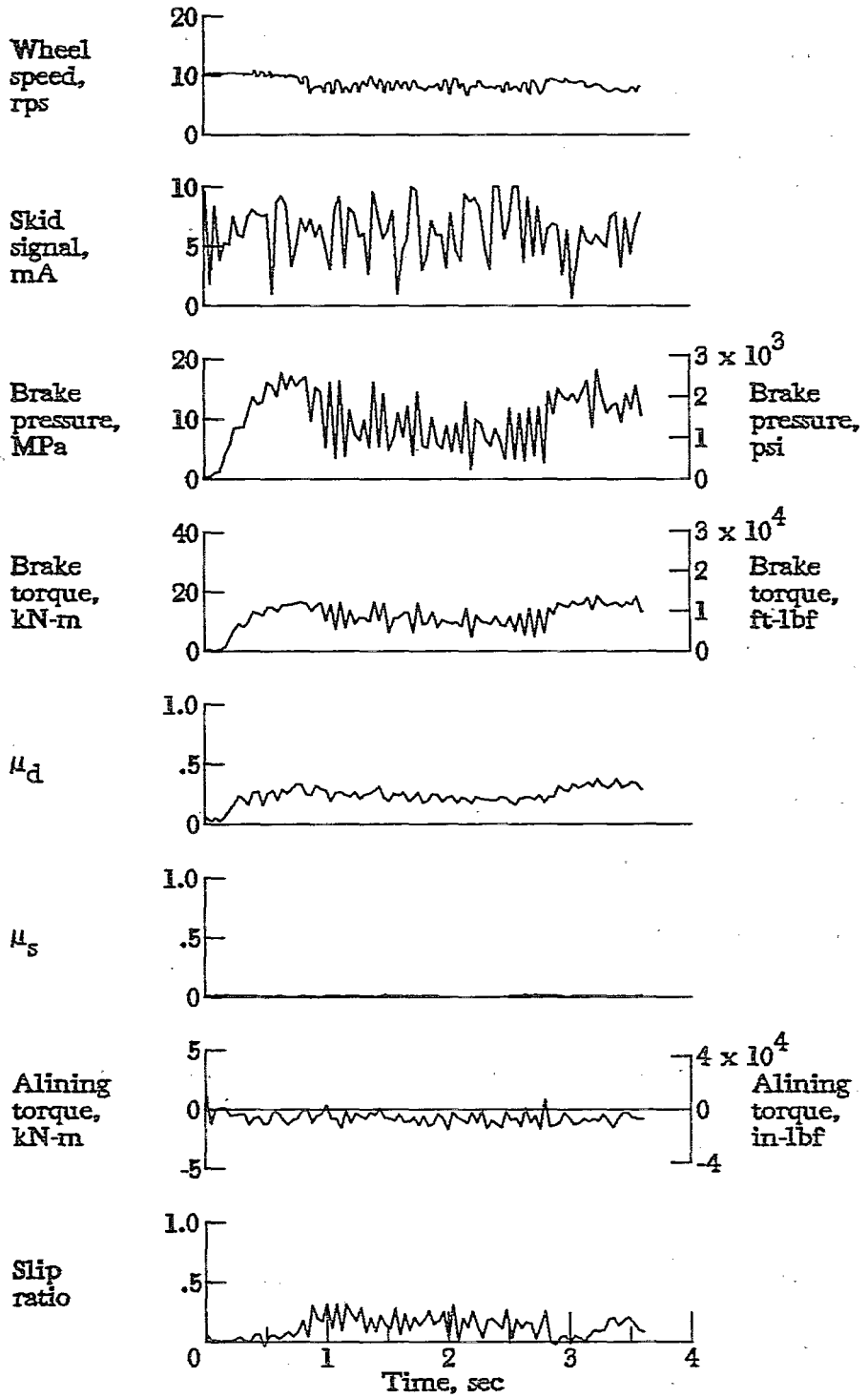

Figure A32.- Time histories for run 32. Nominal carriage speed, 46 knots; vertical load, 122.3 kN (27 500 lbf); yaw angle, 0°; brake pressure, 19 MPa (2820 psi); tire condition, new; surface condition, flooded.

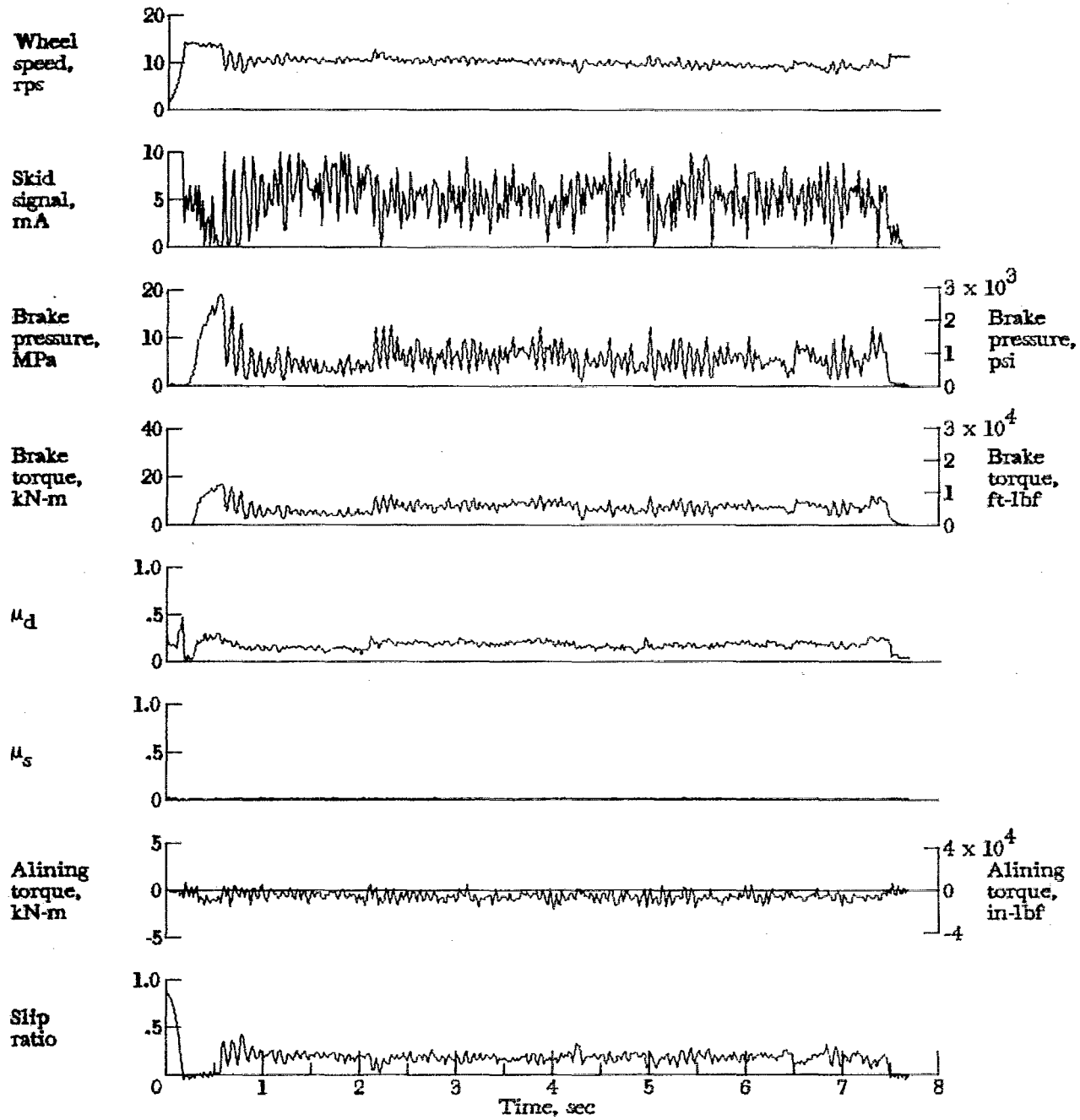

Figure A33.- Time histories for run 33. Nominal carriage speed, 72 knots; vertical load, 118.8 kN (26 700 lbf); yaw angle, 0°; brake pressure, 18 MPa (2640 psi); tire condition, new; surface condition, flooded.

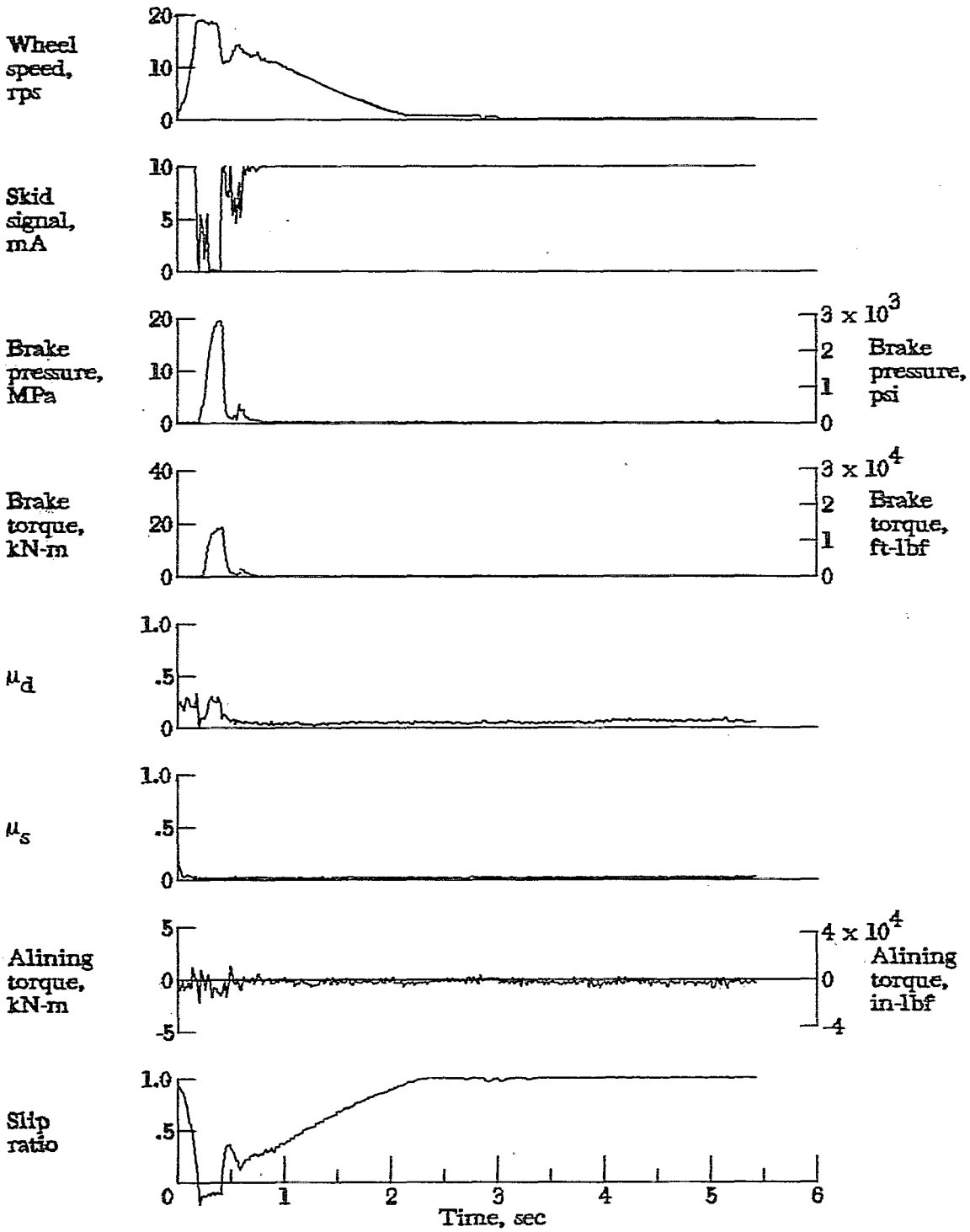

Figure A34.- Time histories for run 34. Nominal carriage speed, 103 knots; vertical load, 117.9 kN (26 500 lbf); yaw angle, 0°; brake pressure, 19 MPa (2770 psi); tire condition, new; surface condition, flooded.

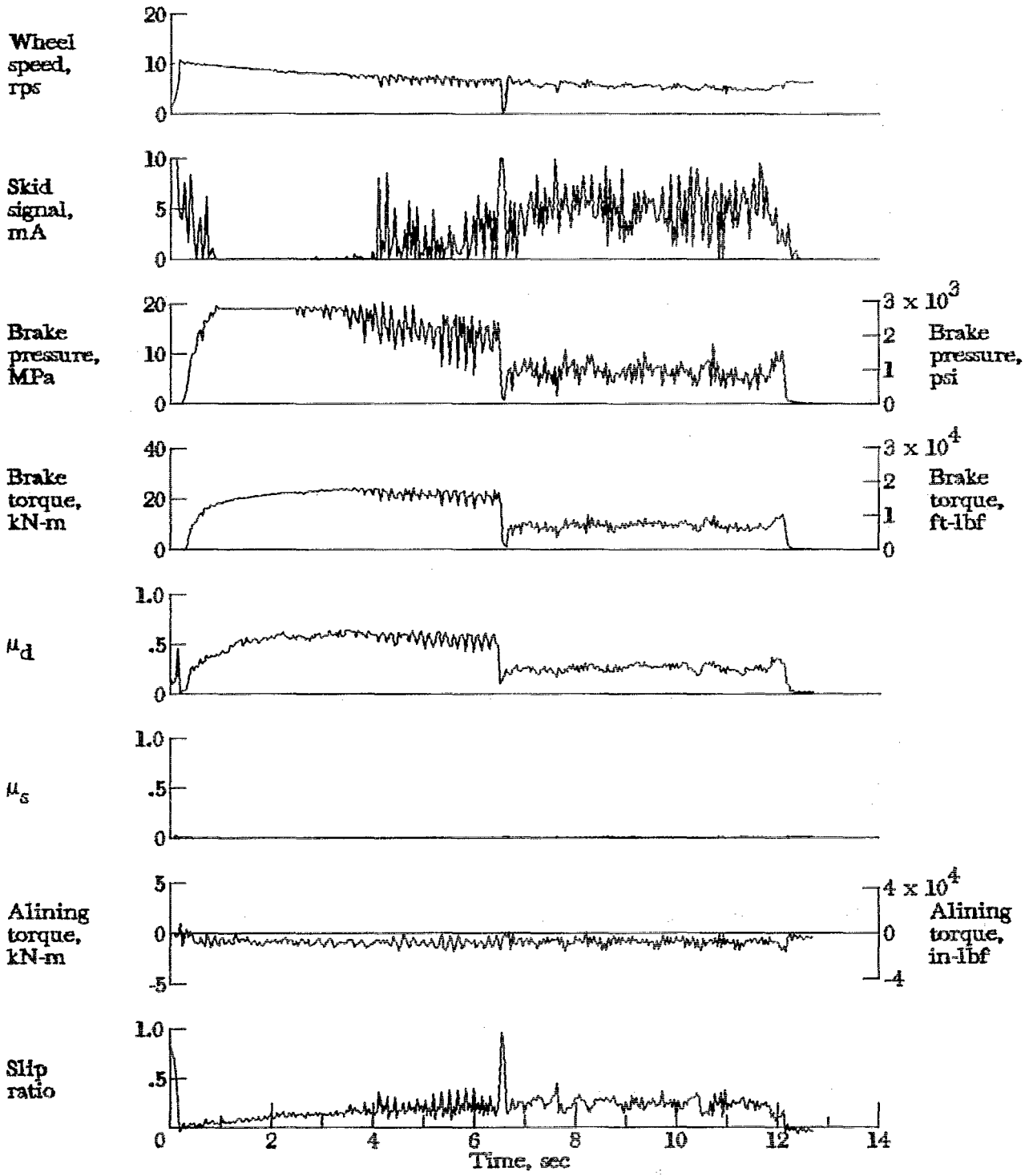

Figure A35.- Time histories for run 35. Nominal carriage speed, 41 knots; vertical load, 83.2 kN (18 700 lbf); yaw angle, 0°; brake pressure, 19 MPa (2760 psi); tire condition, new; surface condition, dry to flooded.

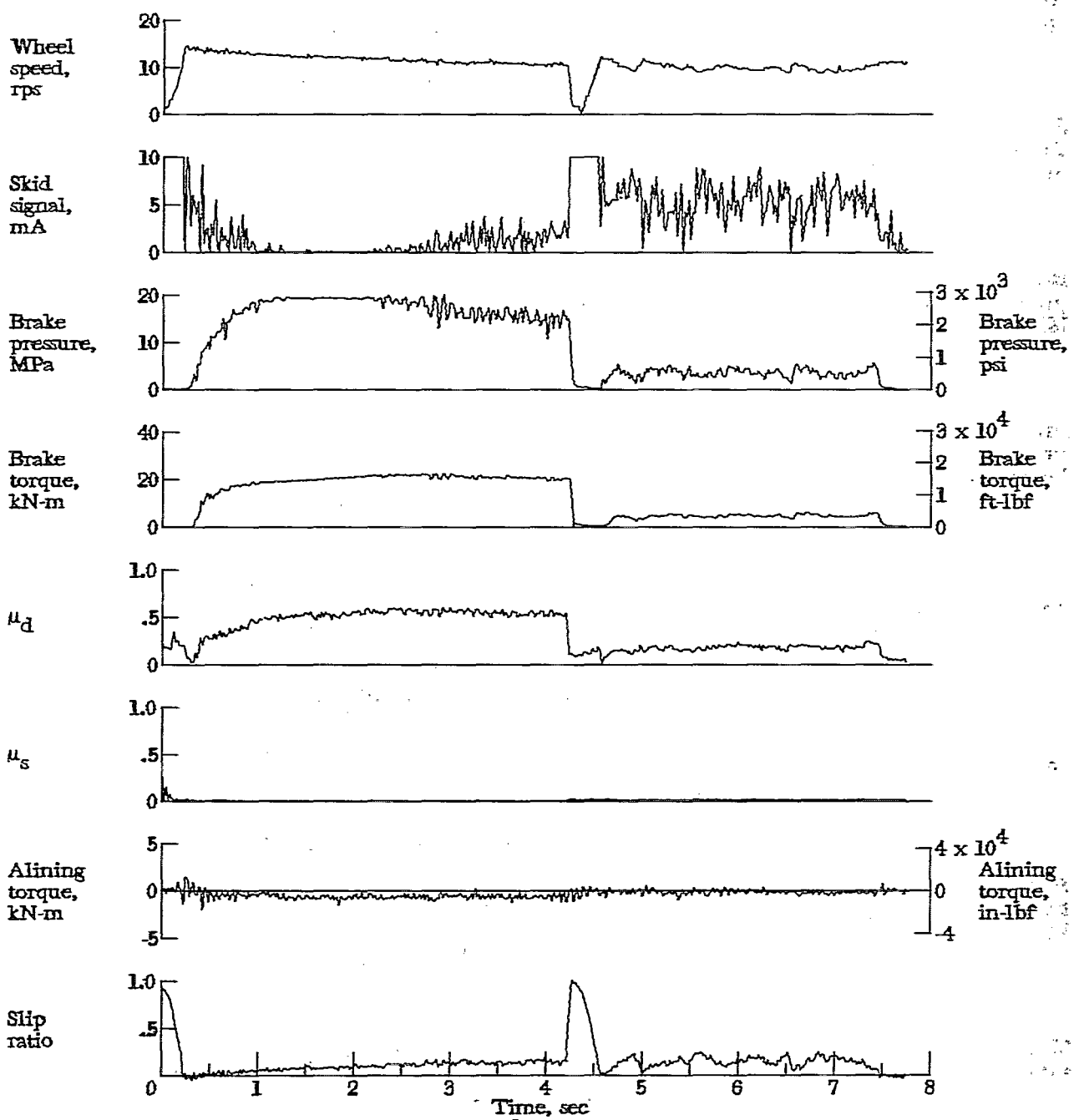

Figure A36.- Time histories for run 36. Nominal carriage speed, 70 knots; vertical load, 84.1 kN (18 900 lbf); yaw angle, 0°; brake pressure, 19 MPa (2780 psi); tire condition, new; surface condition, dry to flooded.

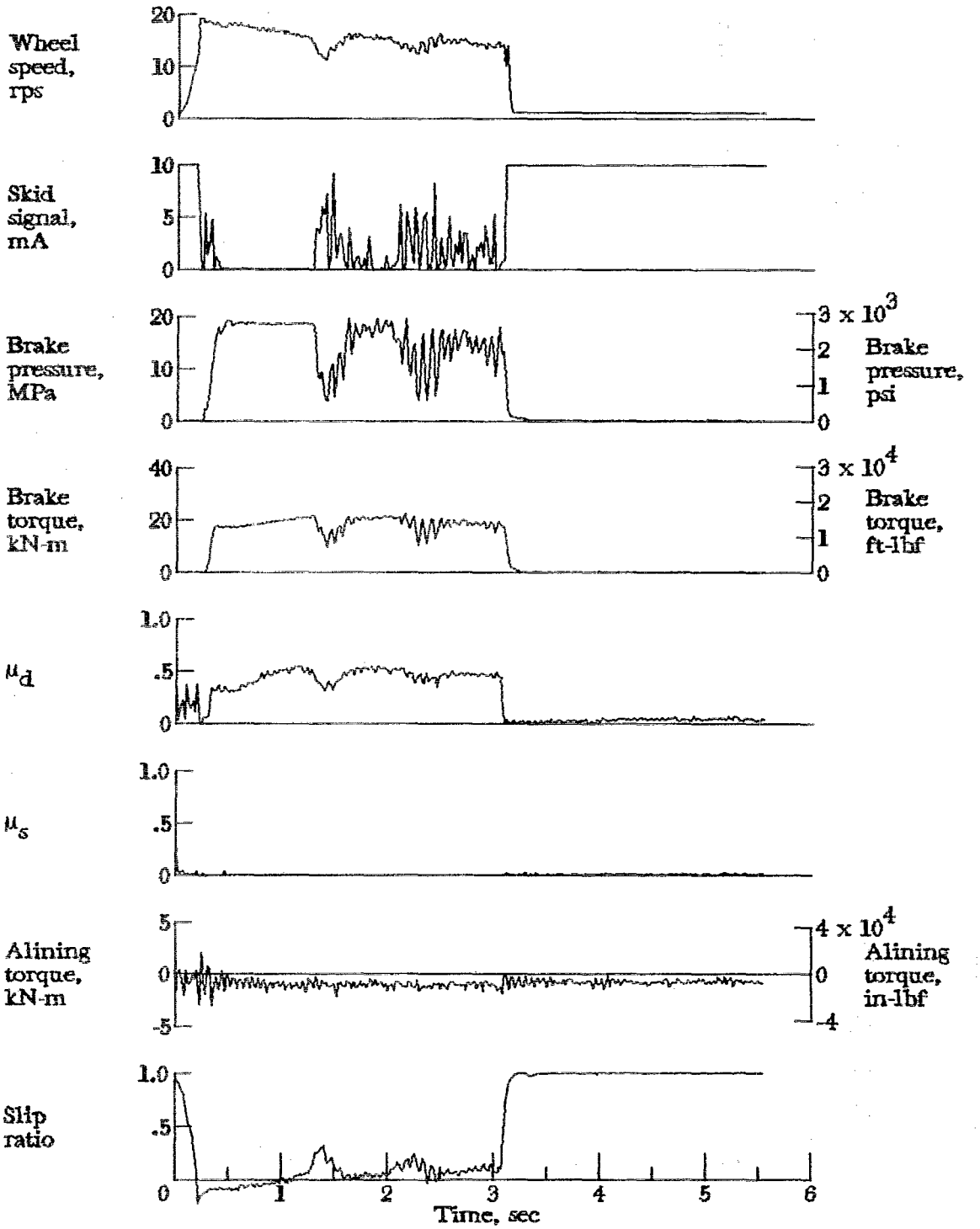

Figure A37.- Time histories for run 37. Nominal carriage speed, 100 knots; vertical load, 85.0 kN (19 100 lbf); yaw angle, 0°; brake pressure, 19 MPa (2820 psi); tire condition, new; surface condition, dry to flooded.

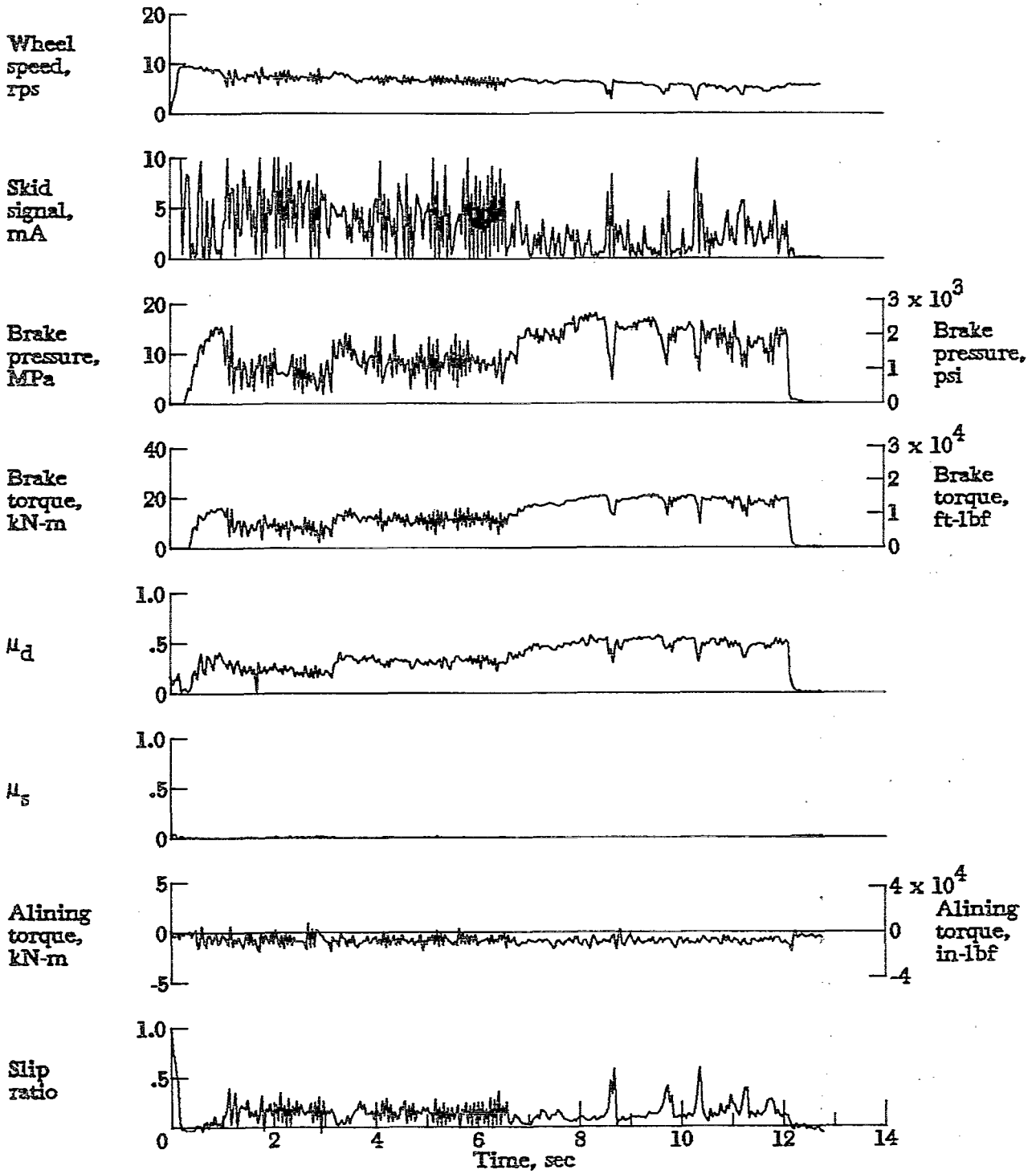

Figure A38.- Time histories for run 38. Nominal carriage speed, 43 knots; vertical load, 83.2 kN (18 700 lbf); yaw angle, 0°; brake pressure, 19 MPa (2800 psi); tire condition, new; surface condition, flooded to dry.

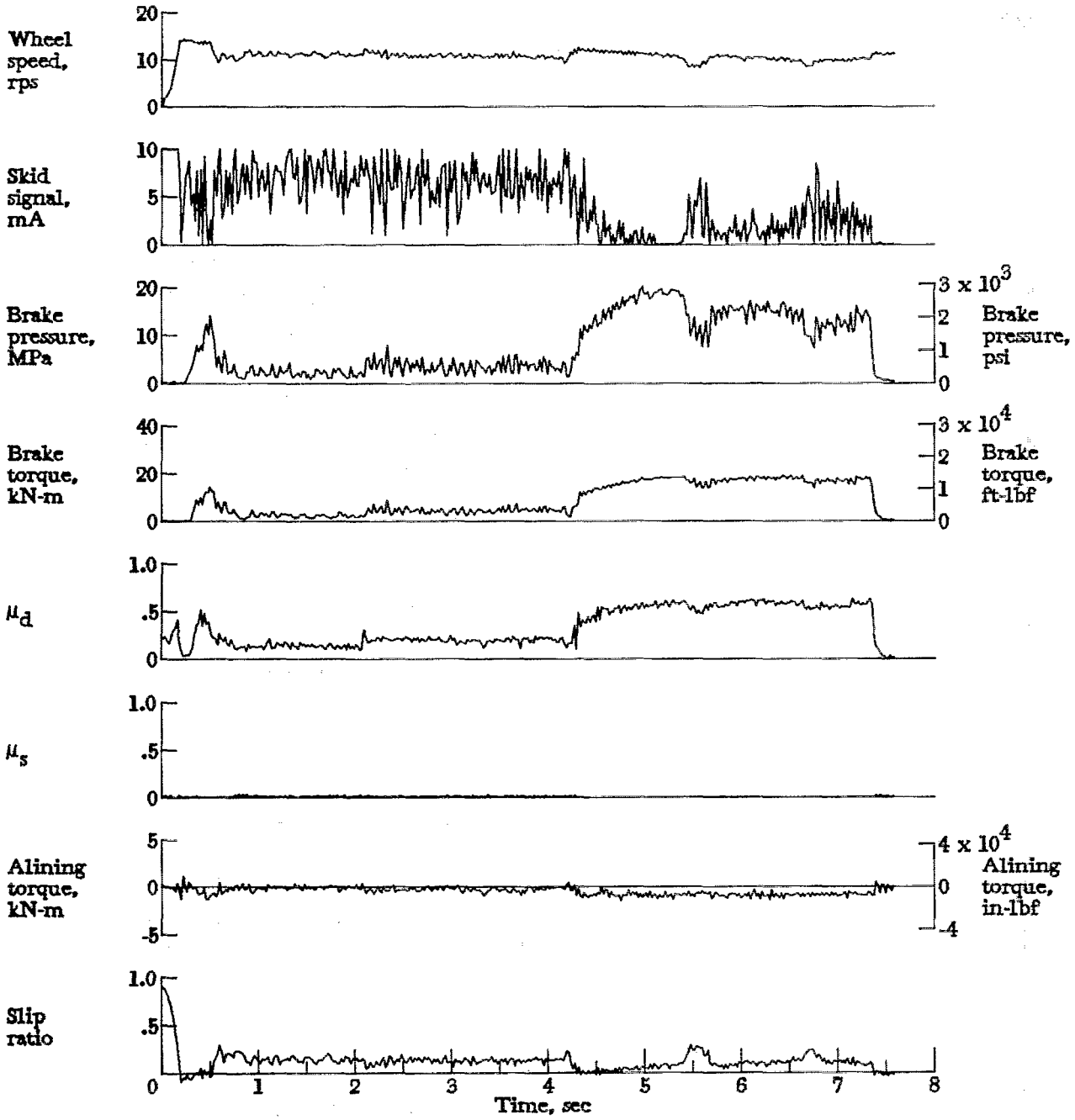

Figure A39.- Time histories for run 39. Nominal carriage speed, 73 knots; vertical load, 63.6 kN (14 300 lbf); yaw angle, 0°; brake pressure, 19 MPa (2840 psi); tire condition, new; surface condition, flooded to dry.

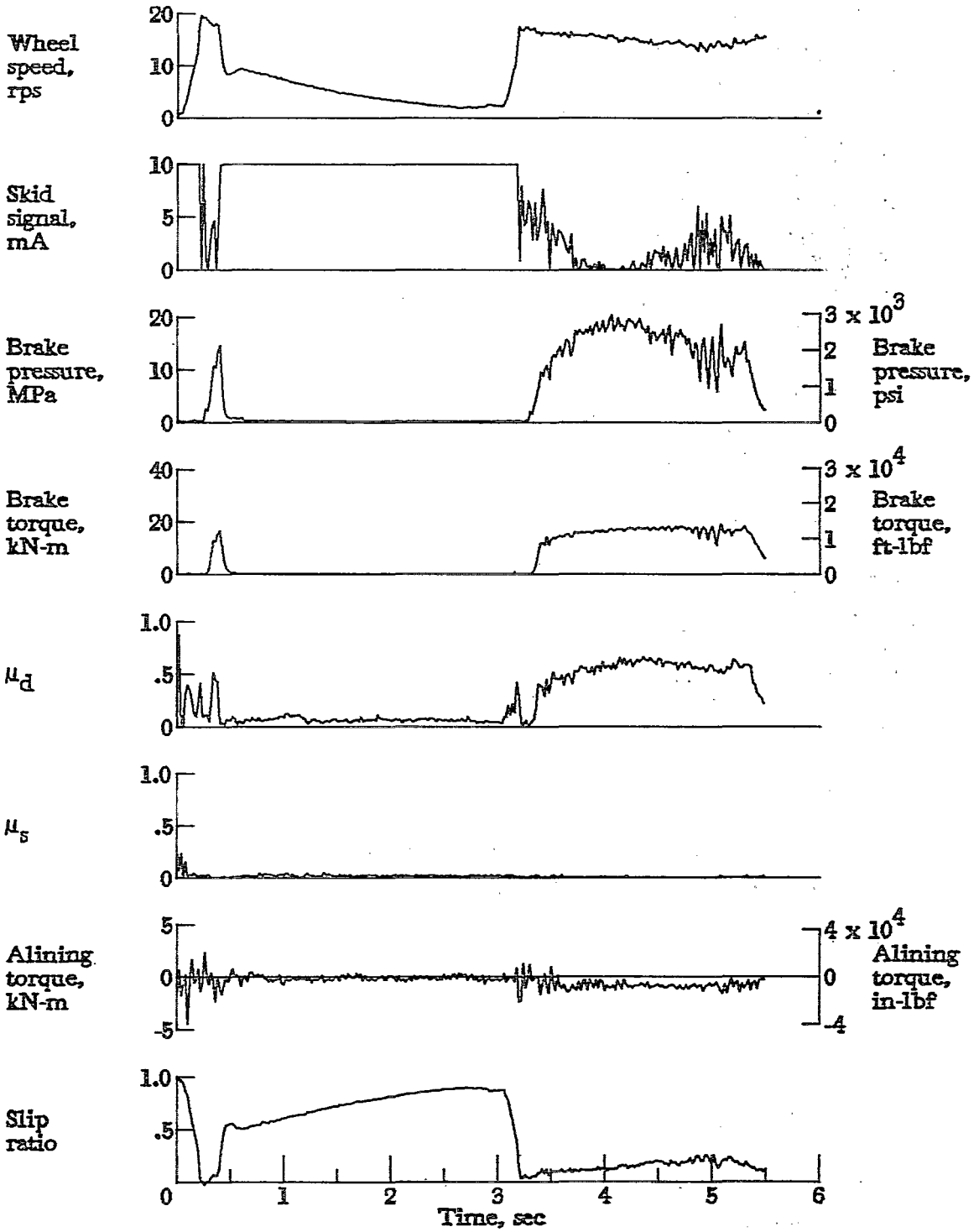

Figure A40.- Time histories for run 40. Nominal carriage speed, 102 knots; vertical load, 64.5 kN (14 500 lbf); yaw angle, 0°; brake pressure, 20 MPa (2870 psi); tire condition, new; surface condition, flooded to dry.

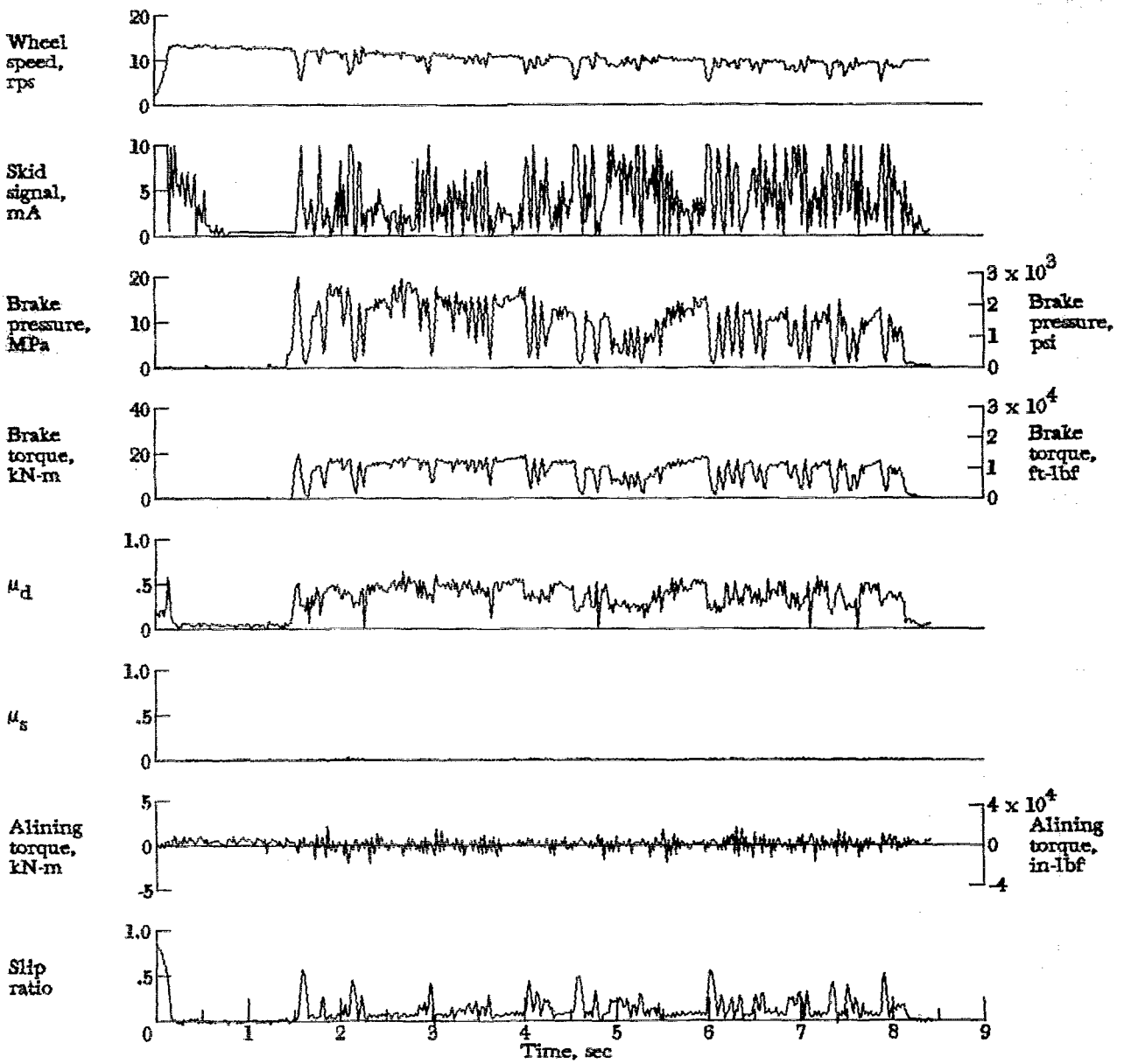

Figure A41.- Time histories for run 41. Nominal carriage speed, 65 knots; vertical load, 79.6 kN (17 900 lbf); yaw angle, 0°; brake pressure, 21 MPa (3000 psi); tire condition, new; surface condition, random dry/damp.

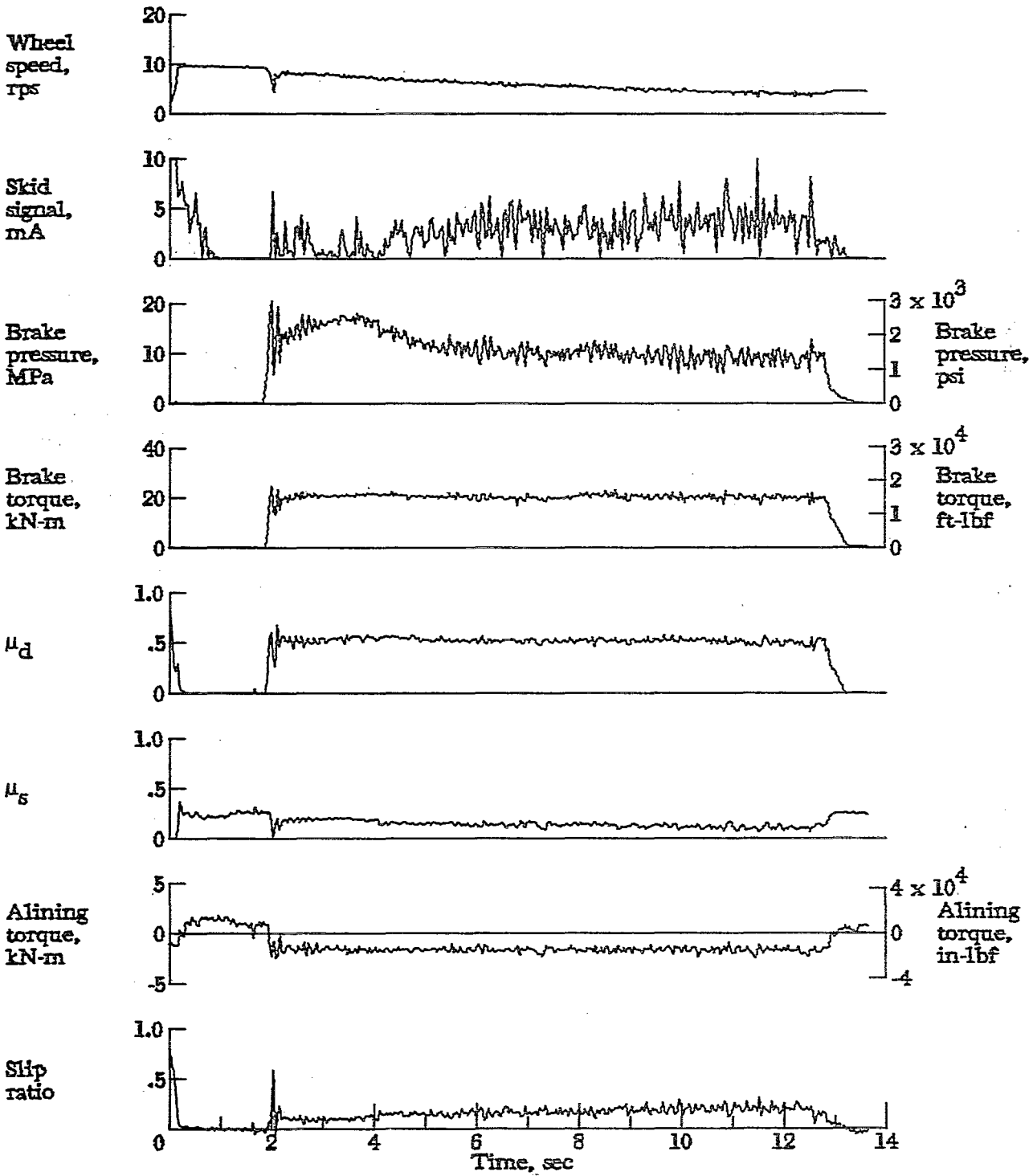

Figure A42.- Time histories for run 42. Nominal carriage speed, 39 knots; vertical load, 80.5 kN (18 100 lbf); yaw angle, 3°; brake pressure, 21 MPa (3000 psi); tire condition, new; surface condition, dry.

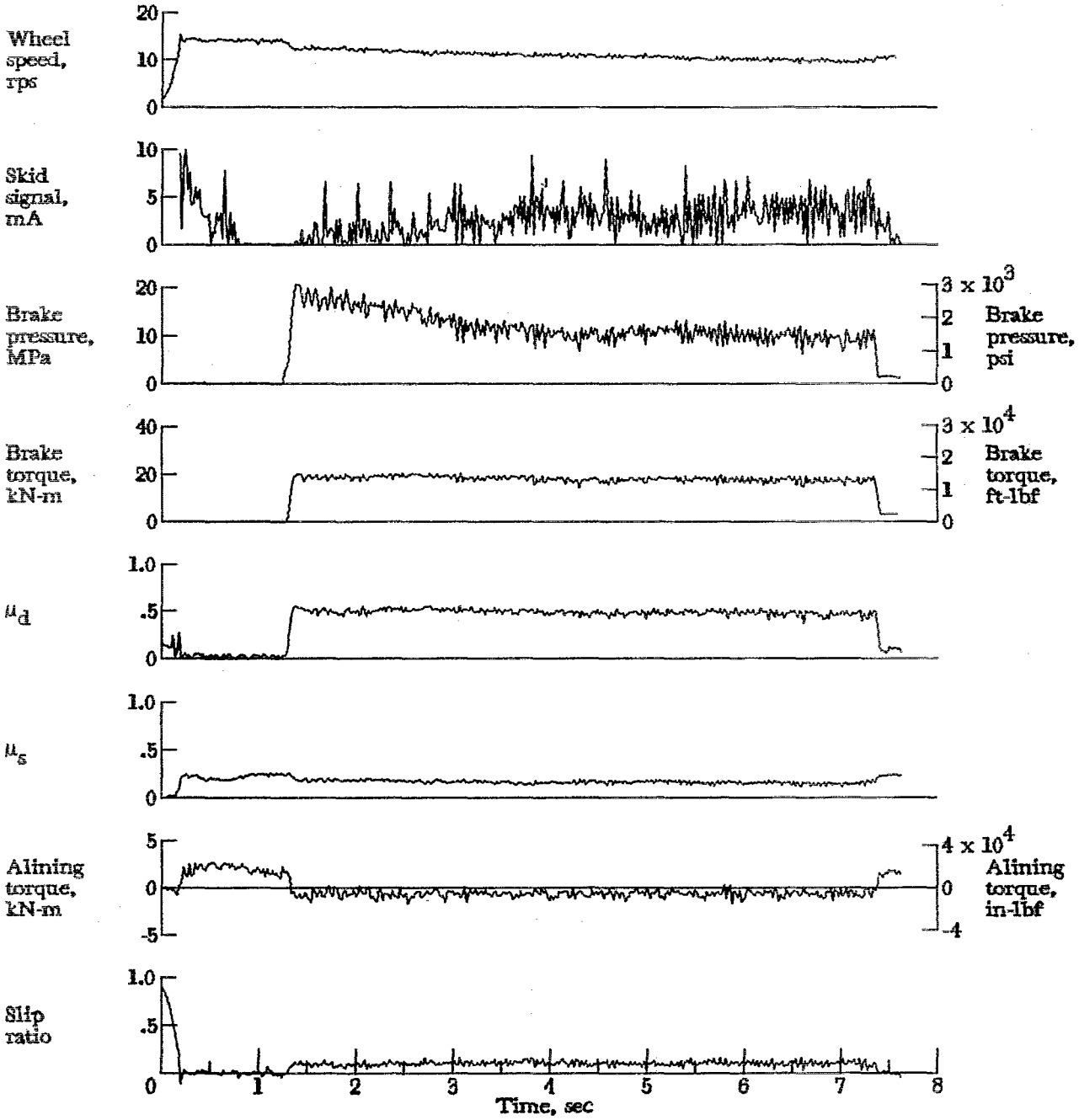

Figure A43.- Time histories for run 43. Nominal carriage speed, 72 knots; vertical load, 81.8 kN (18 400 lbf); yaw angle, 3°; brake pressure, 21 MPa (3000 psi); tire condition, new; surface condition, dry.

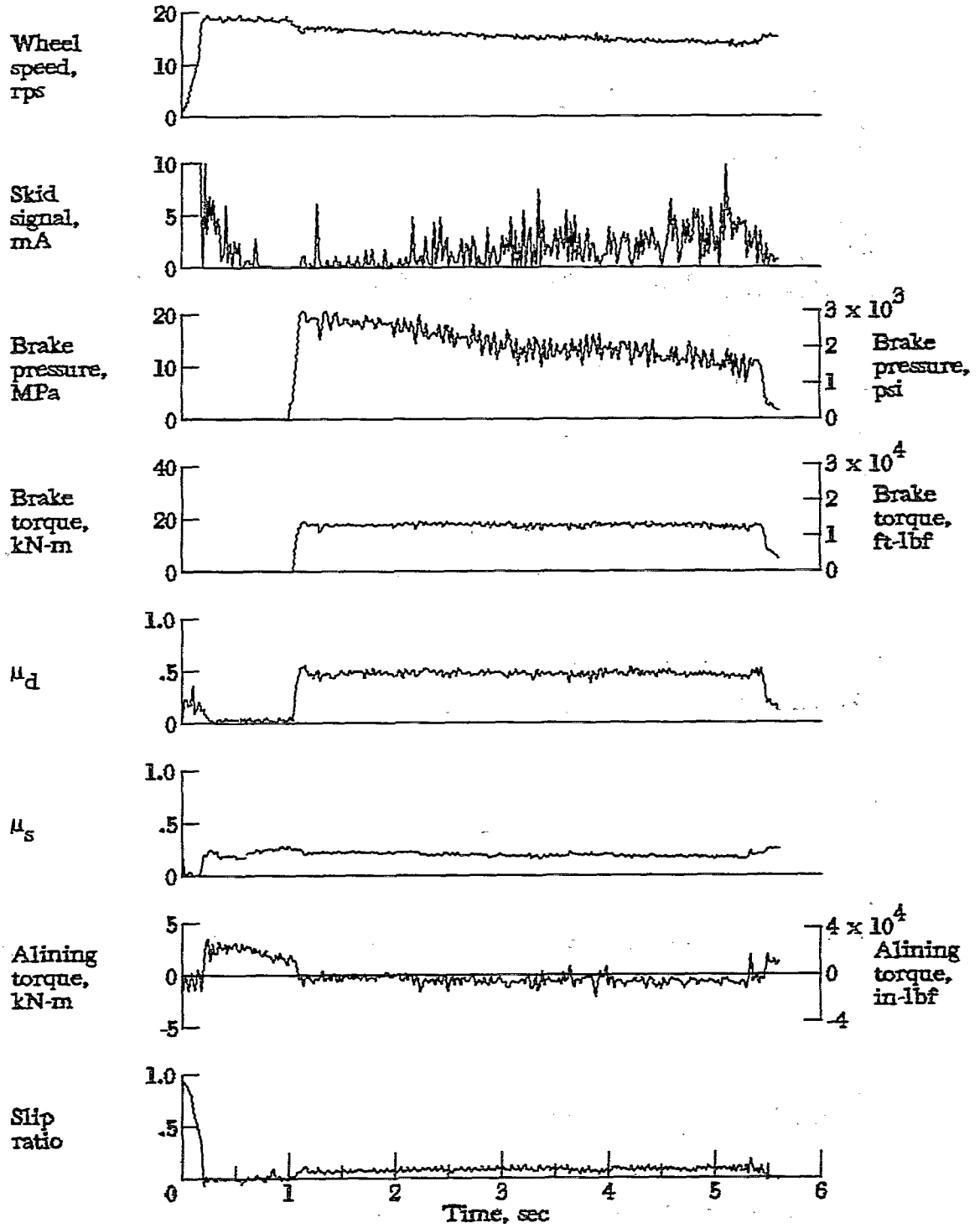

Figure A44.- Time histories for run 44. Nominal carriage speed, 99 knots; vertical load, 82.3 kN (18 500 lbf); yaw angle, 3°; brake pressure, 21 MPa (3000 psi); tire condition, new; surface condition, dry.

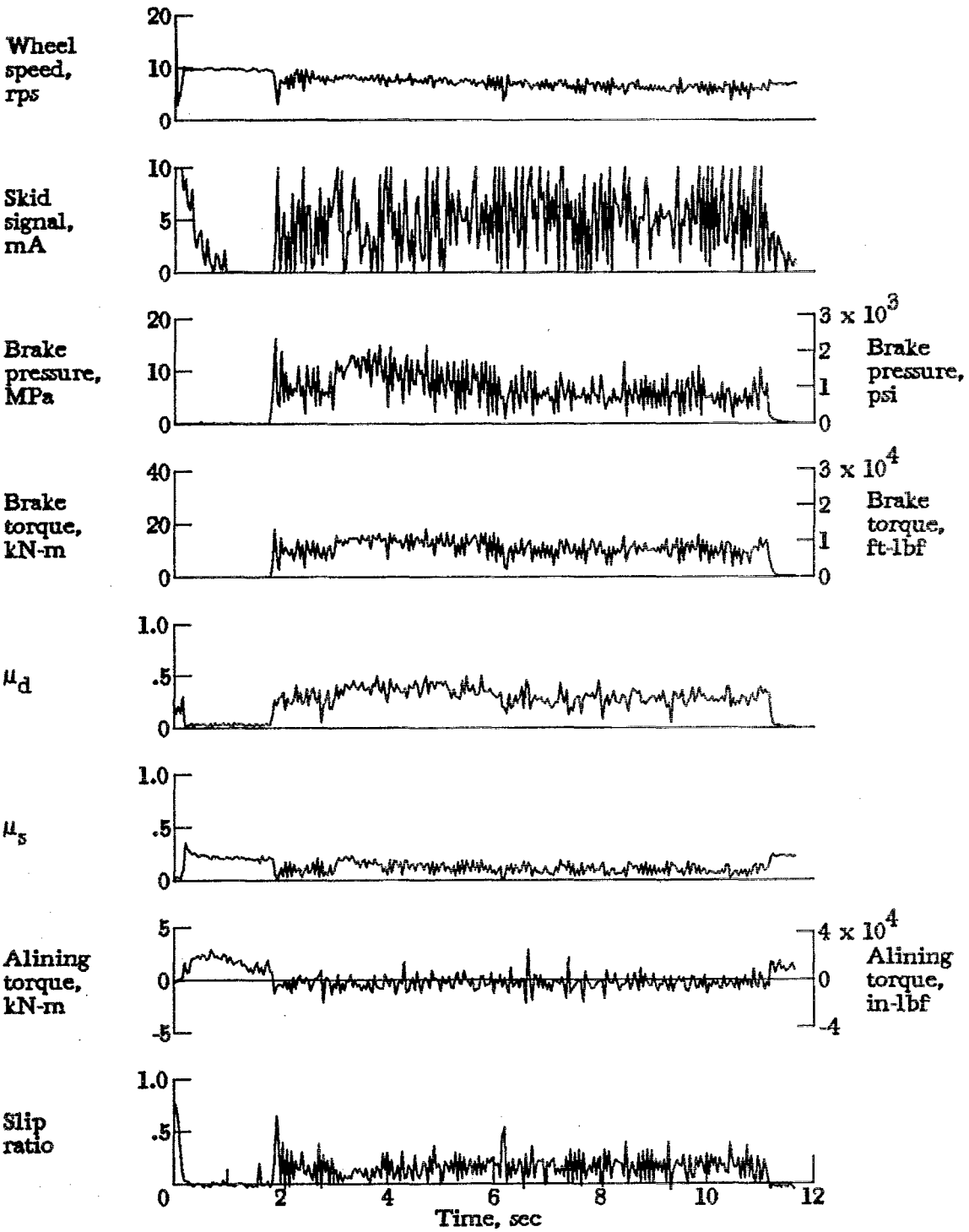

Figure A45.- Time histories for run 45. Nominal carriage speed, 46 knots; vertical load, 81.0 kN (18 200 lbf); yaw angle, 3°; brake pressure, 21 MPa (3000 psi); tire condition, new; surface condition, damp.

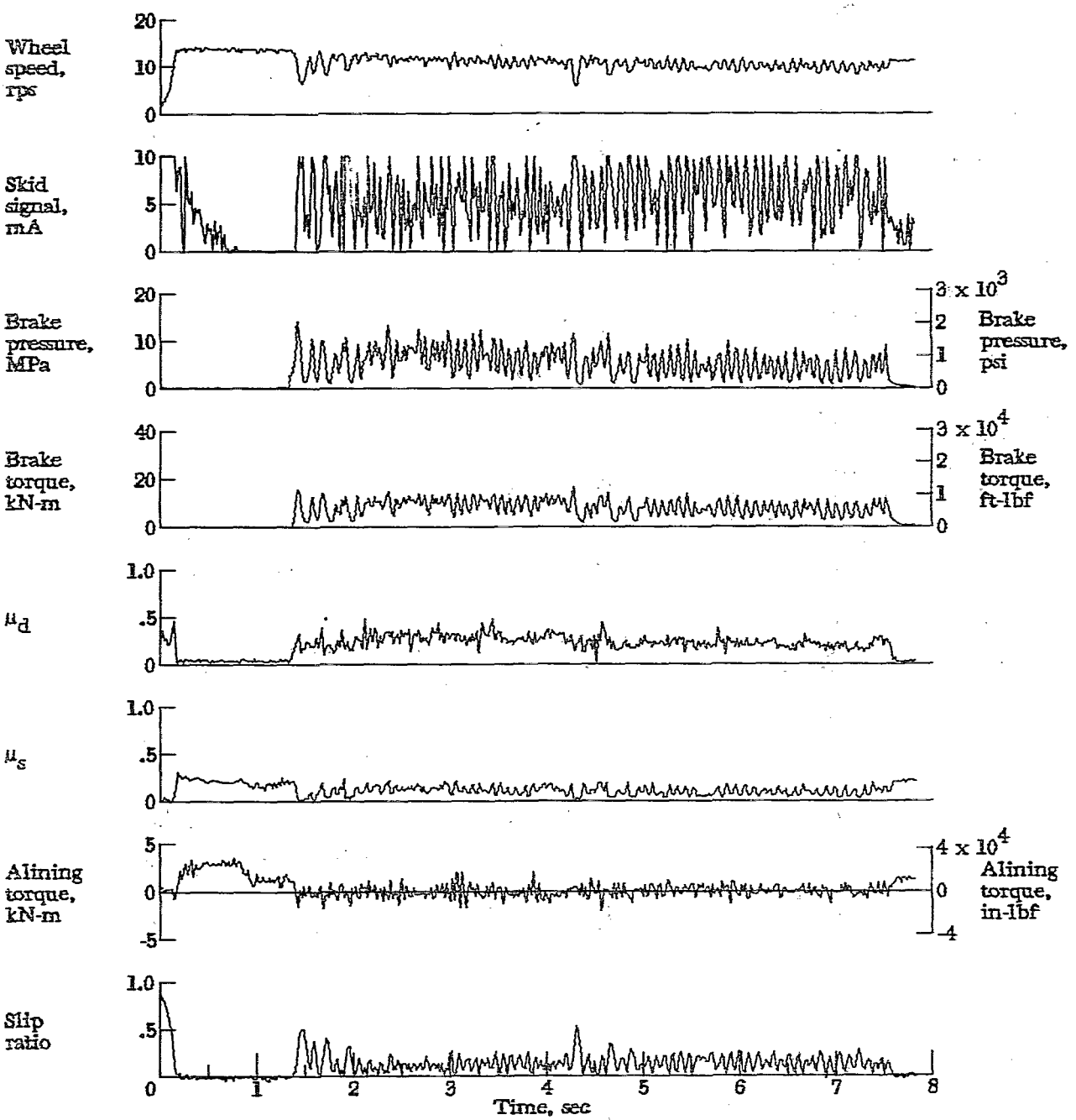

Figure A46.- Time histories for run 46. Nominal carriage speed, 70 knots; vertical load, 81.0 kN (18 200 lbf); yaw angle, 3°; brake pressure, 21 MPa (3000 psi); tire condition, new; surface condition, damp.

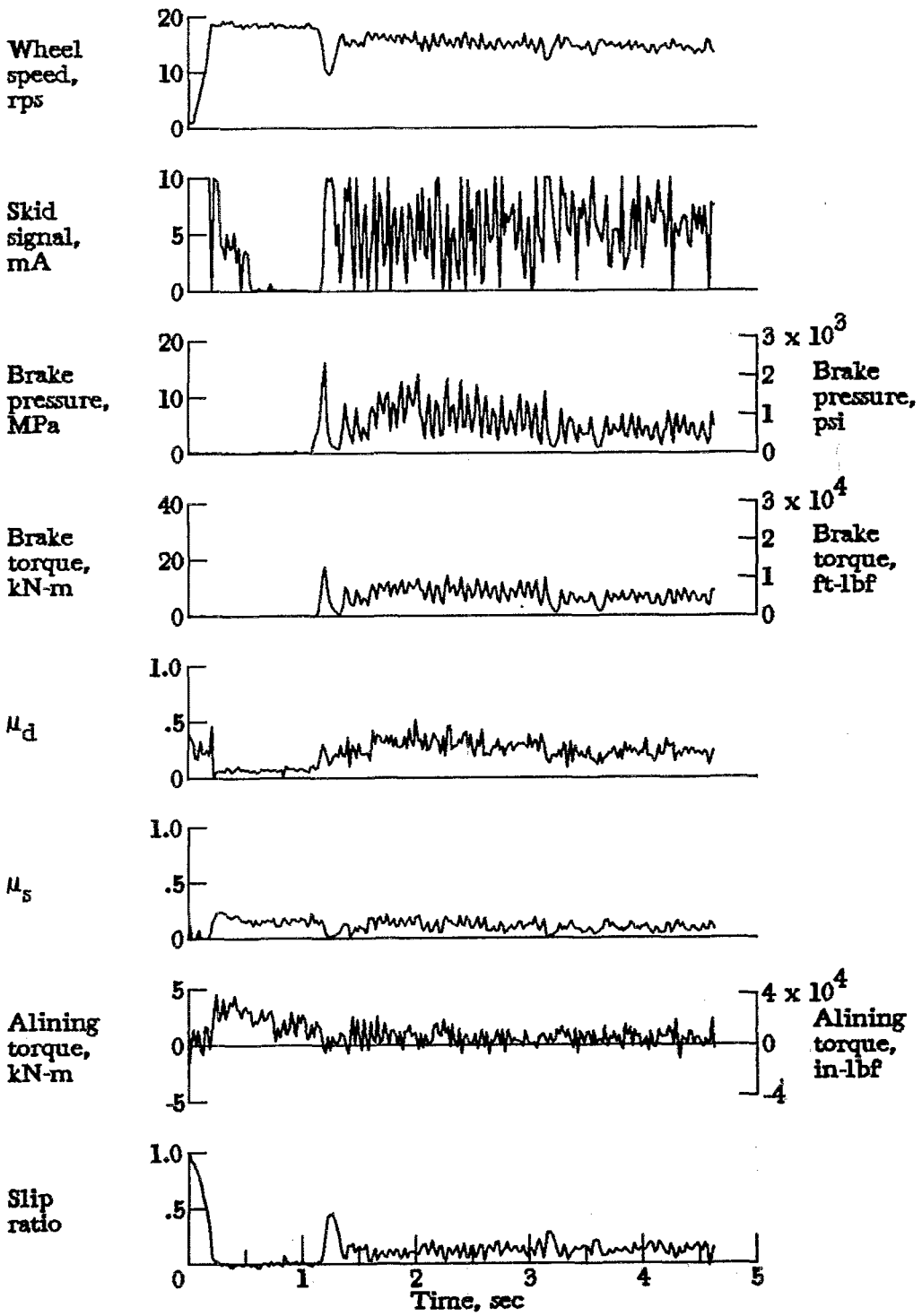

Figure A47.- Time histories for run 47. Nominal carriage speed, 98 knots; vertical load, 80.1 kN (18 000 lbf); yaw angle, 3°; brake pressure, 21 MPa (3000 psi); tire condition, new; surface condition, damp.

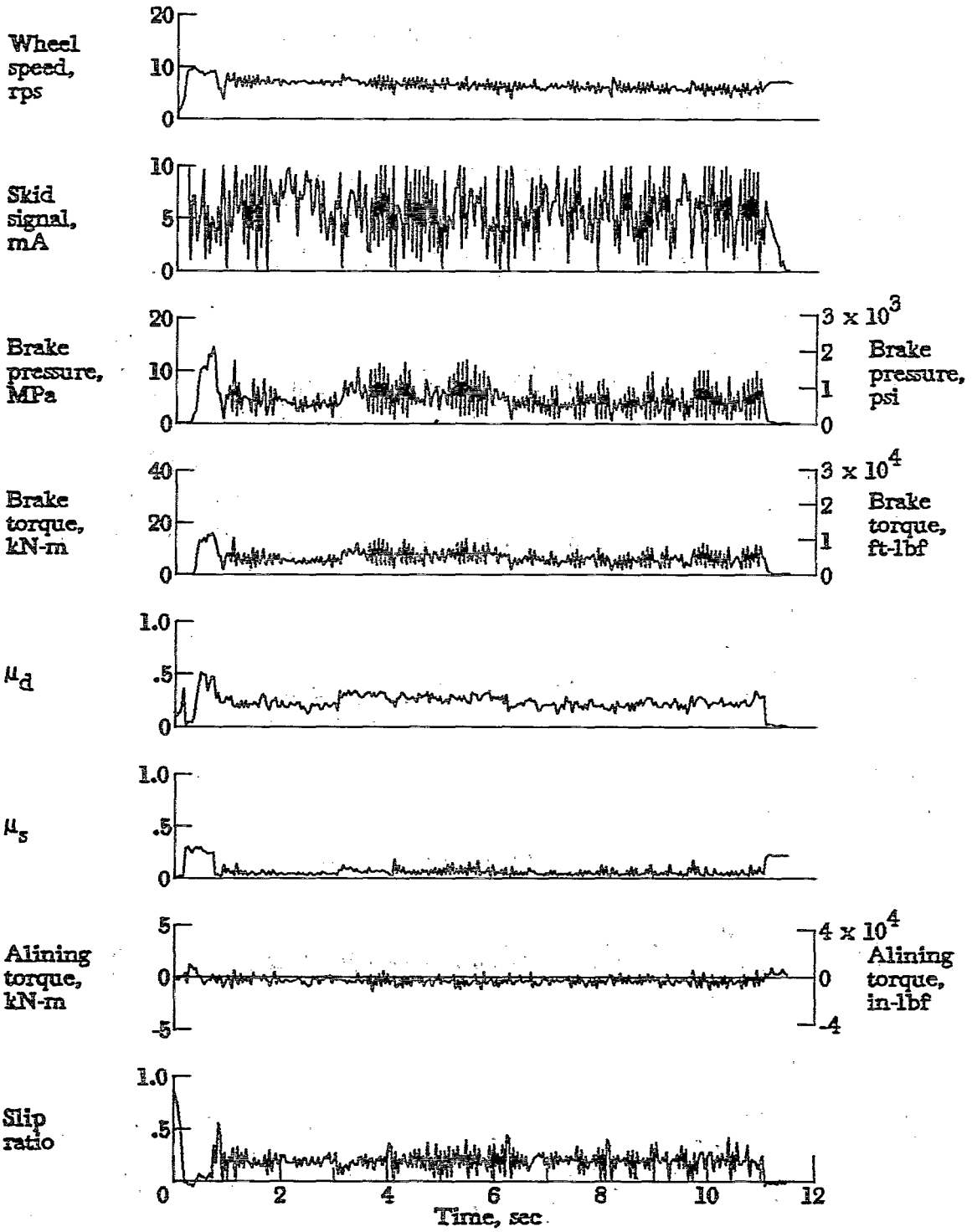

Figure A48.- Time histories for run 48. Nominal carriage speed, 48 knots; vertical load, 64.5 kN (14 500 lbf); yaw angle, 3°; brake pressure, 19 MPa (2800 psi); tire condition, new; surface condition, flooded.

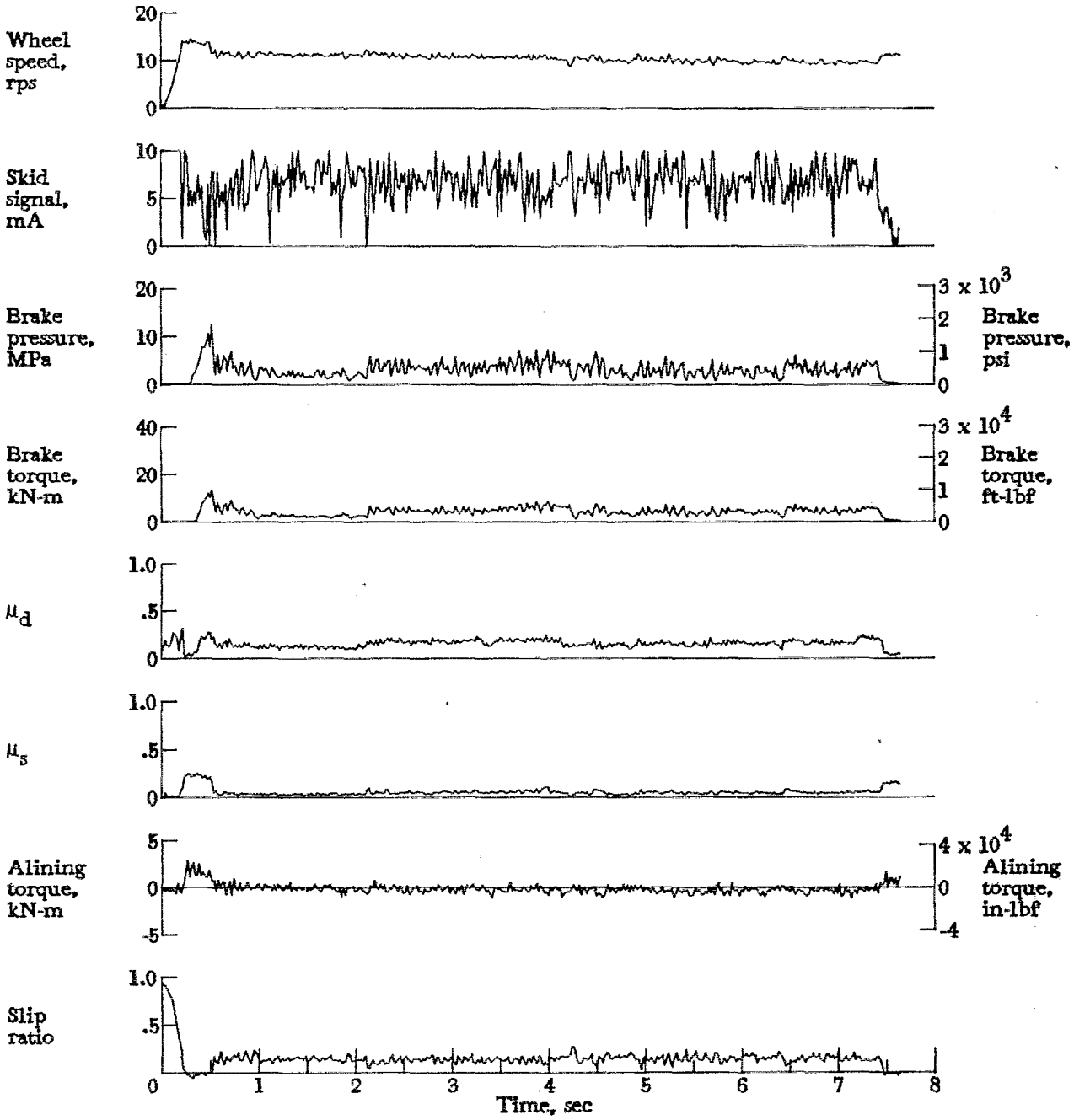

Figure A49.- Time histories for run 49. Nominal carriage speed, 72 knots; vertical load, 82.3 kN (18 500 lbf); yaw angle, 3°; brake pressure, 19 MPa (2820 psi); tire condition, new; surface condition, flooded.

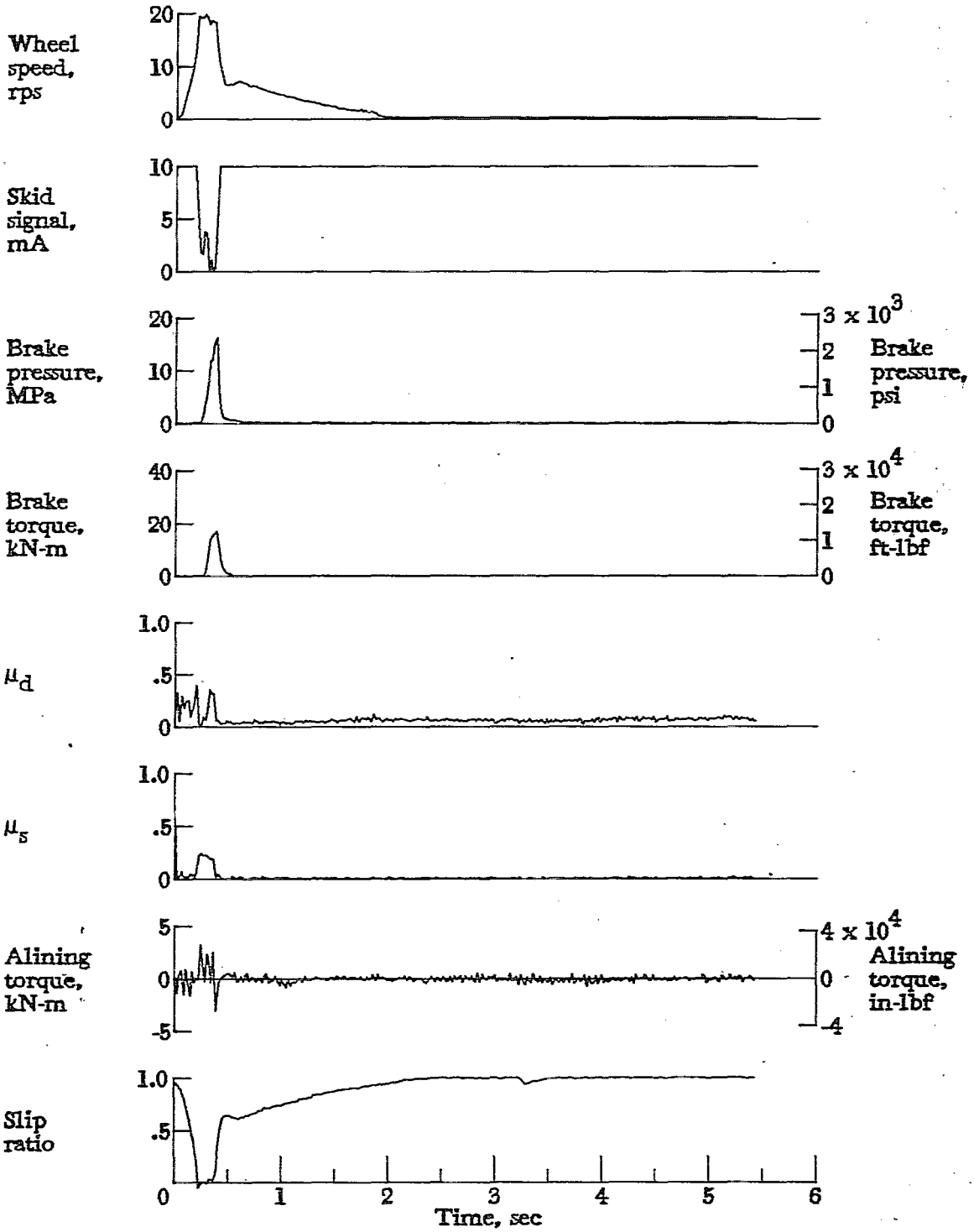

Figure A50.- Time histories for run 50. Nominal carriage speed, 102 knots; vertical load, 83.2 kN (18 700 lbf); yaw angle, 3°; brake pressure, 20 MPa (2860 psi); tire condition, new; surface condition, flooded.

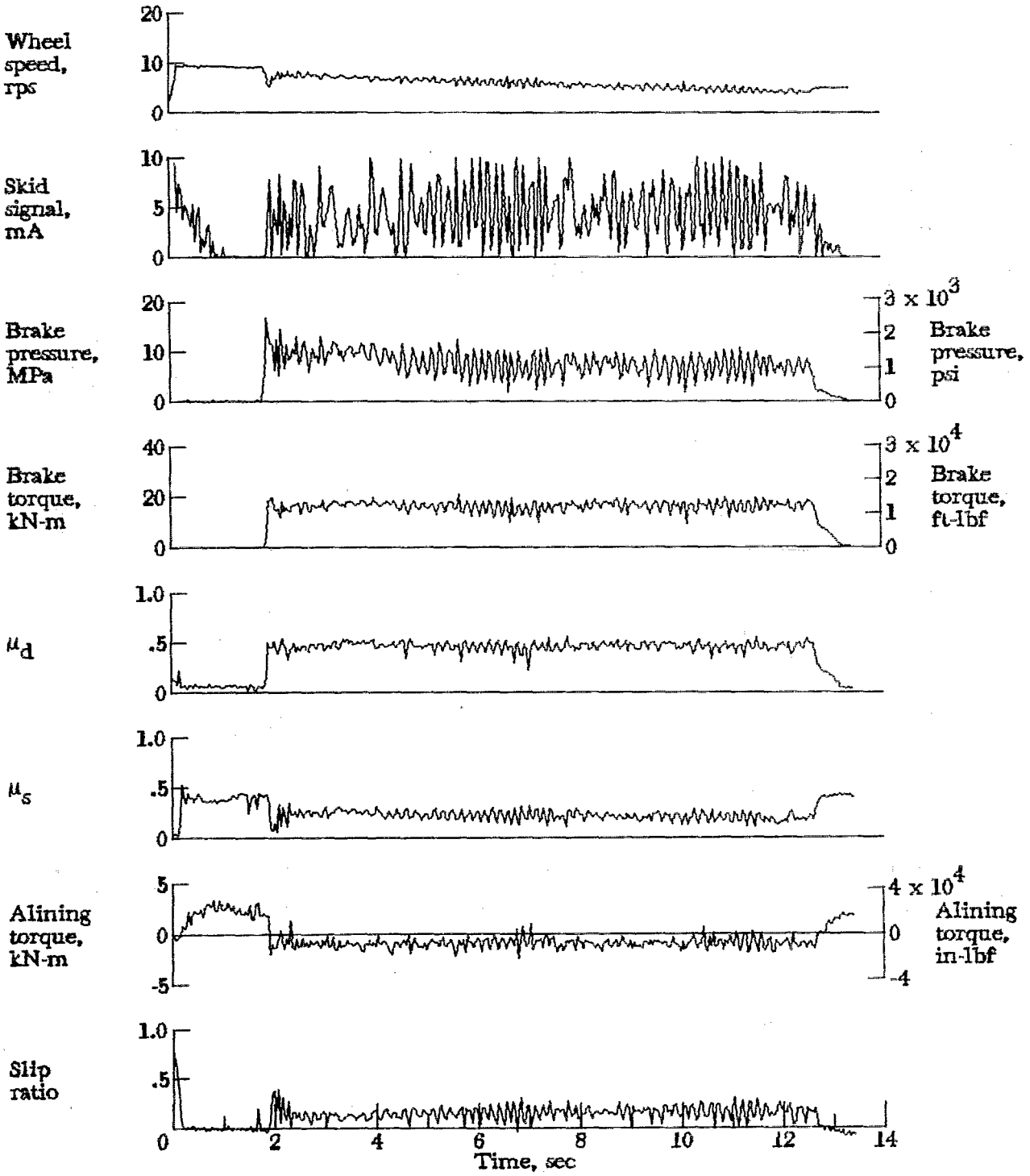

Figure A51.- Time histories for run 51. Nominal carriage speed, 40 knots; vertical load, 81.4 kN (18 300 lbf); yaw angle, 6°; brake pressure, 21 MPa (3000 psi); tire condition, new; surface condition, dry.

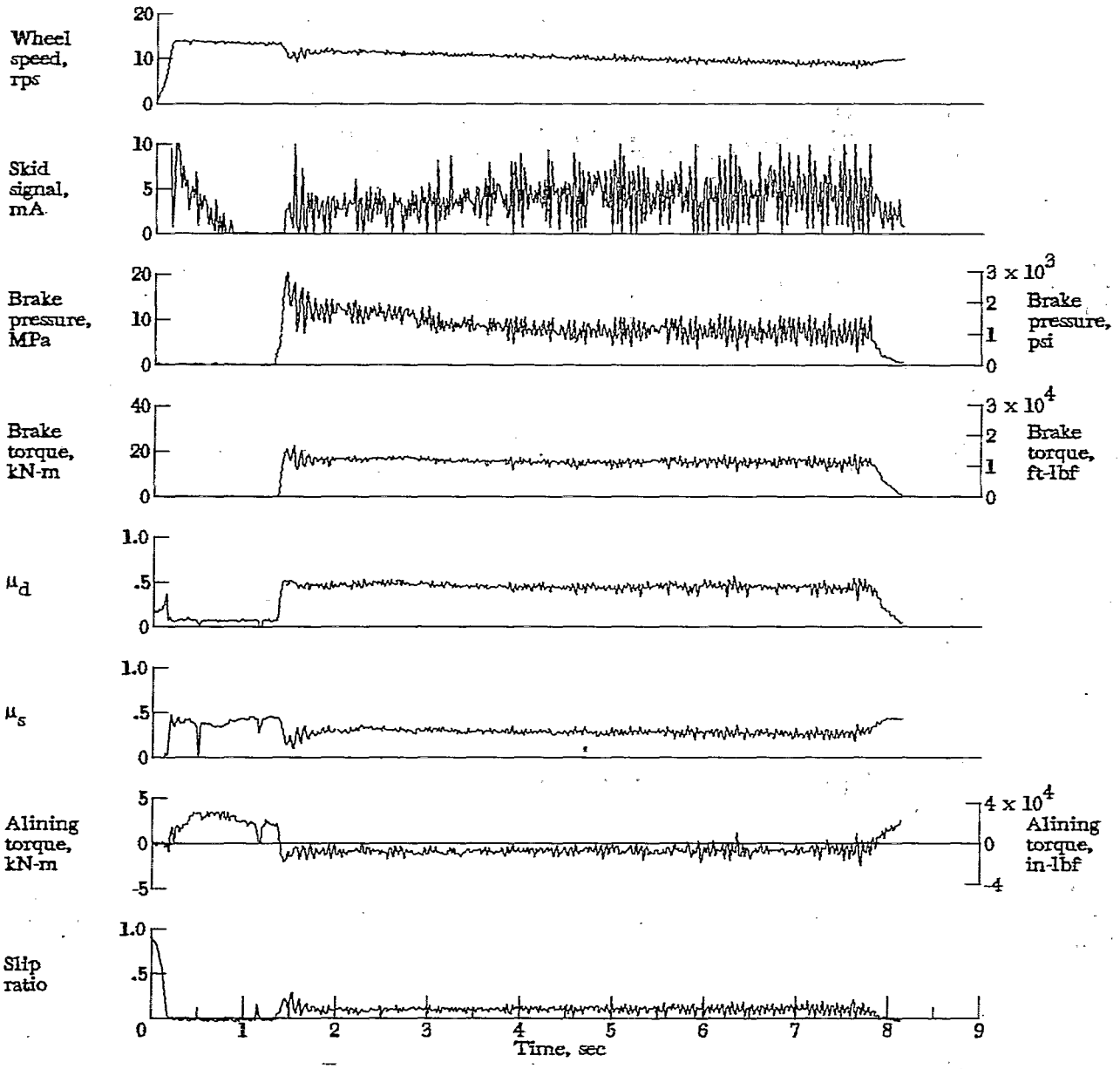

Figure A52.- Time histories for run 52. Nominal carriage speed, 67 knots; vertical load, 81.4 kN (18 300 lbf); yaw angle, 6°; brake pressure, 21 MPa (3000 psi); tire condition, new; surface condition, dry.

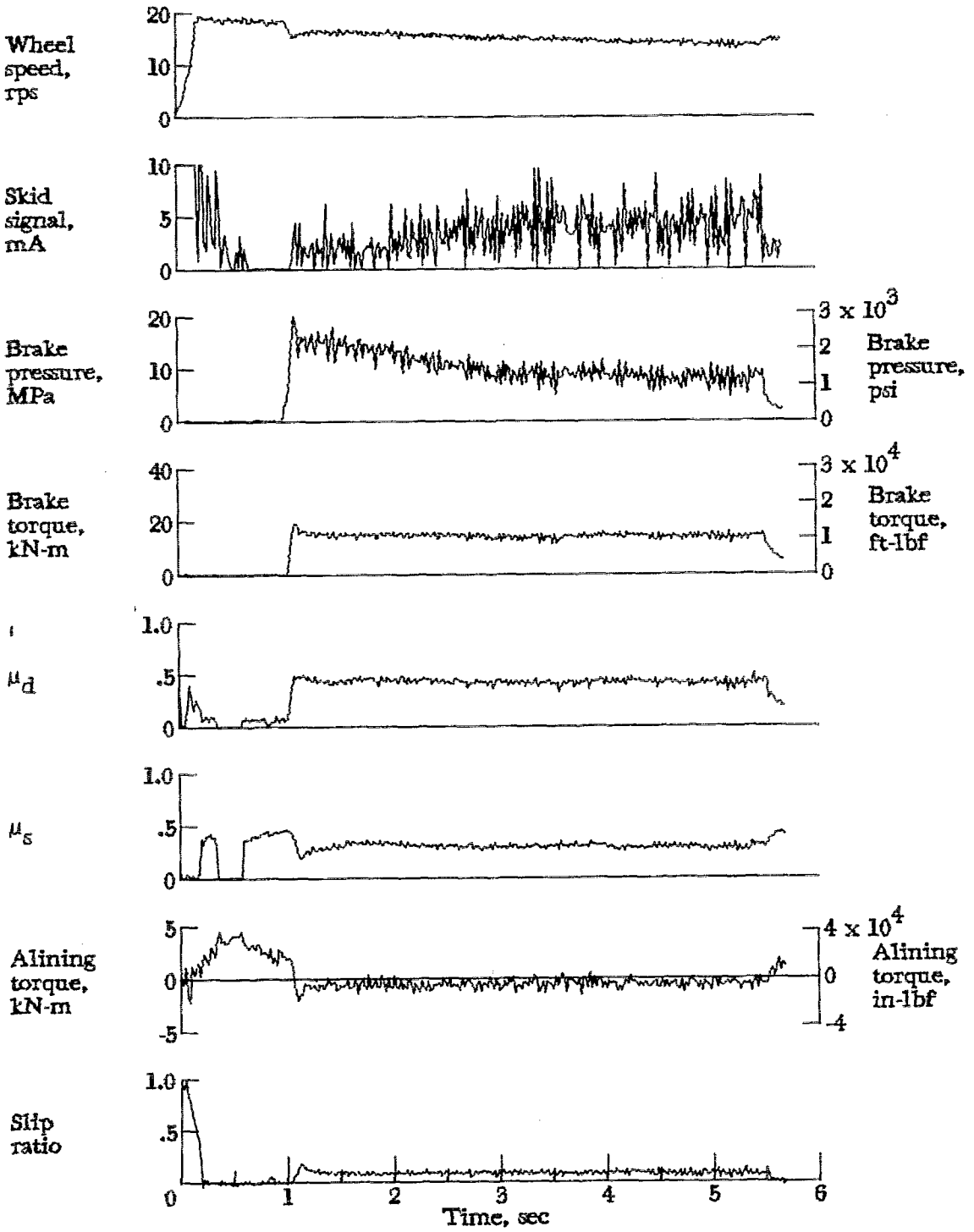

Figure A53.- Time histories for run 53. Nominal carriage speed, 97 knots; vertical load, 82.3 kN (18 500 lbf); yaw angle, 6°; brake pressure, 21 MPa (3000 psi); tire condition, new; surface condition, dry.

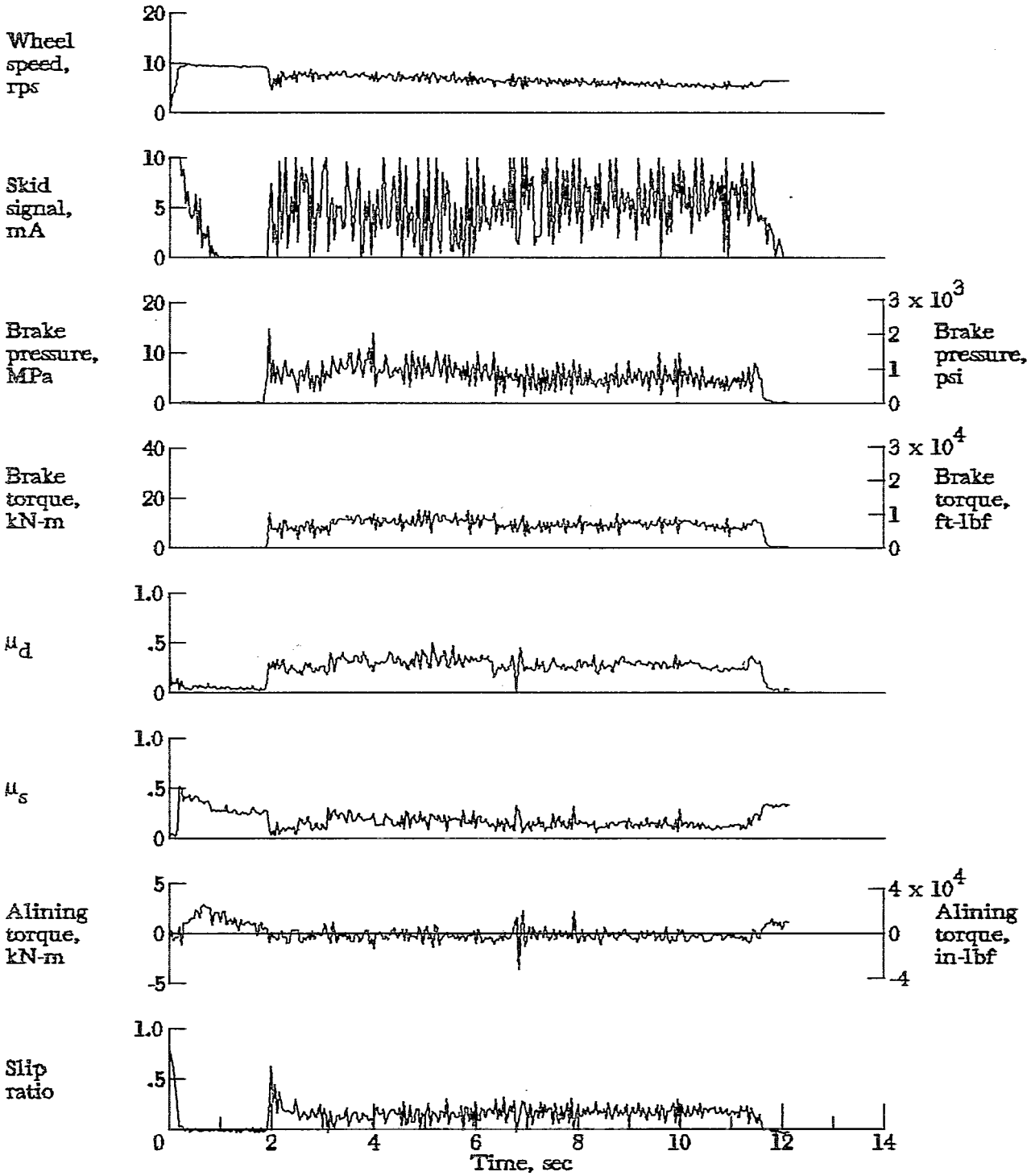

Figure A54.- Time histories for run 54. Nominal carriage speed, 44 knots; vertical load, 81.0 kN (18 200 lbf); yaw angle, 6°; brake pressure, 21 MPa (3000 psi); tire condition, new; surface condition, damp.

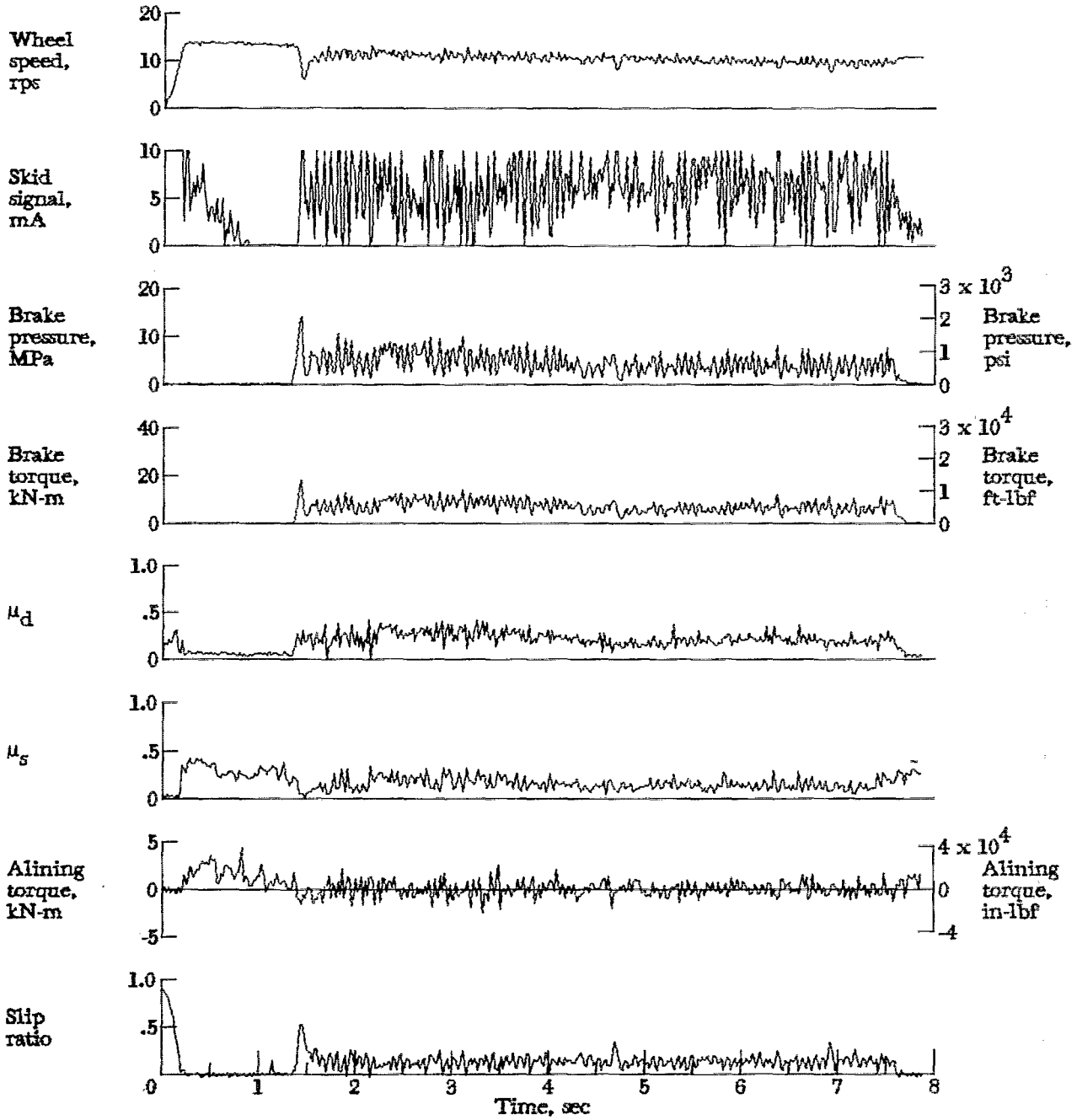

Figure A55.- Time histories for run 55. Nominal carriage speed, 70 knots; vertical load, 81.0 kN (18 200 lbf); yaw angle, 6°; brake pressure, 21 MPa (3000 psi); tire condition, new; surface condition, damp.

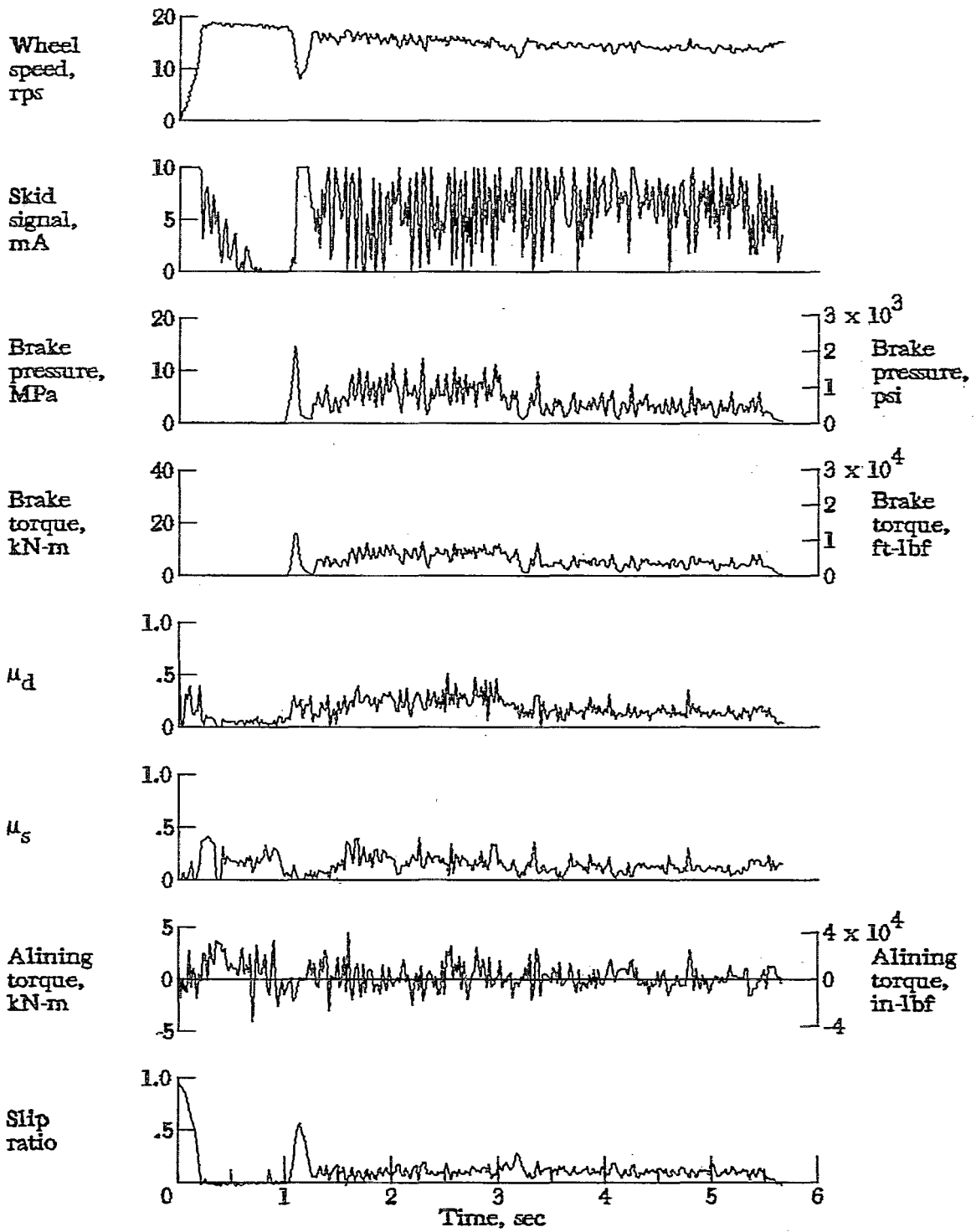

Figure A56.- Time histories for run 56. Nominal carriage speed, 98 knots; vertical load, 81.0 kN (18 200 lbf); yaw angle, 6°; brake pressure, 21 MPa (3000 psi); tire condition, new; surface condition, damp.

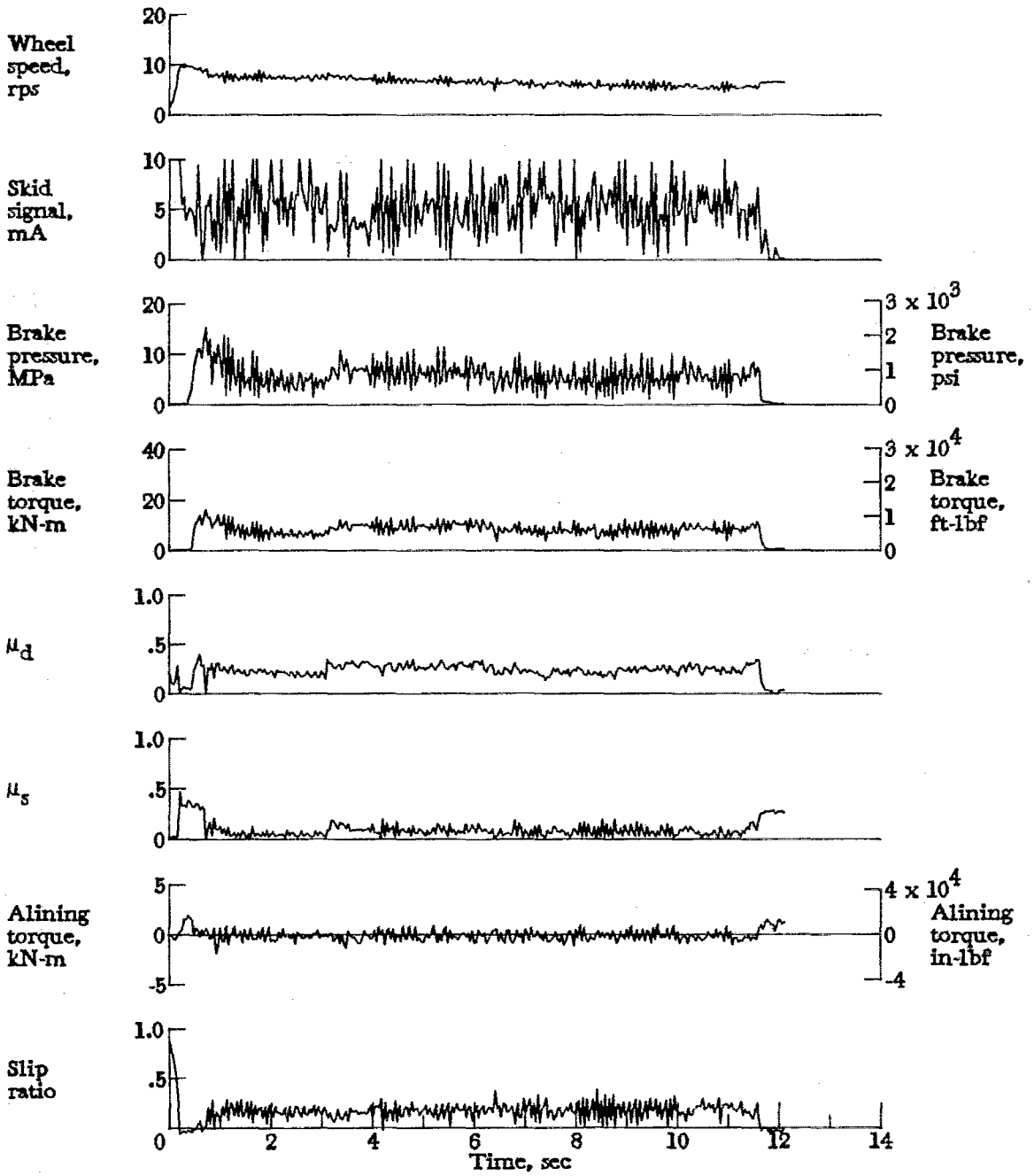

Figure A57.- Time histories for run 57. Nominal carriage speed, 45 knots; vertical load, 84.1 kN (18 900 lbf); yaw angle, 6°; brake pressure, 19 MPa (2840 psi); tire condition, new; surface condition, flooded.

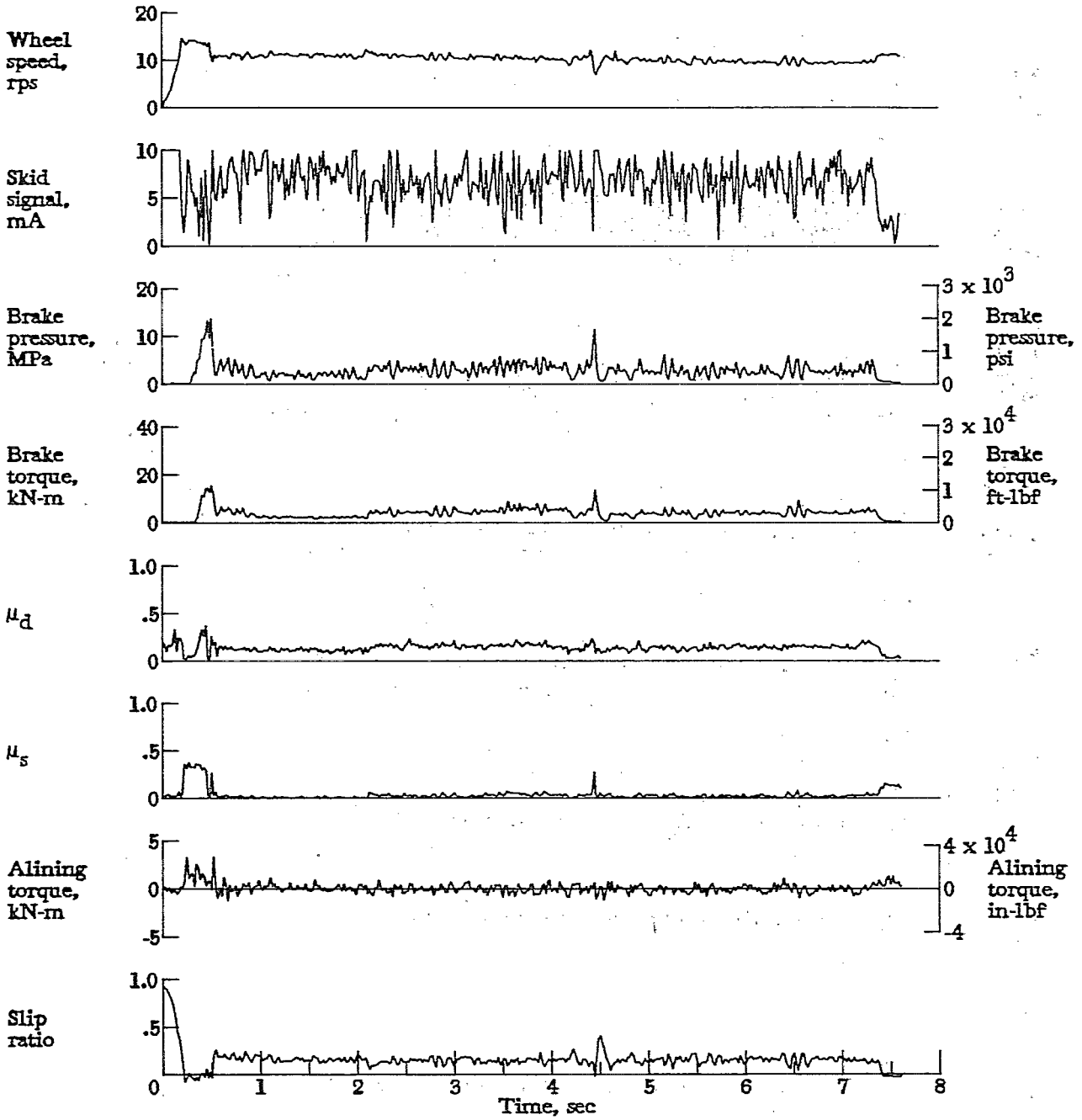

Figure A58.- Time histories for run 58. Nominal carriage speed, 72 knots; vertical load, 84.1 kN (18 900 lbf); yaw angle, 6°; brake pressure, 19 MPa (2740 psi); tire condition, new; surface condition, flooded.

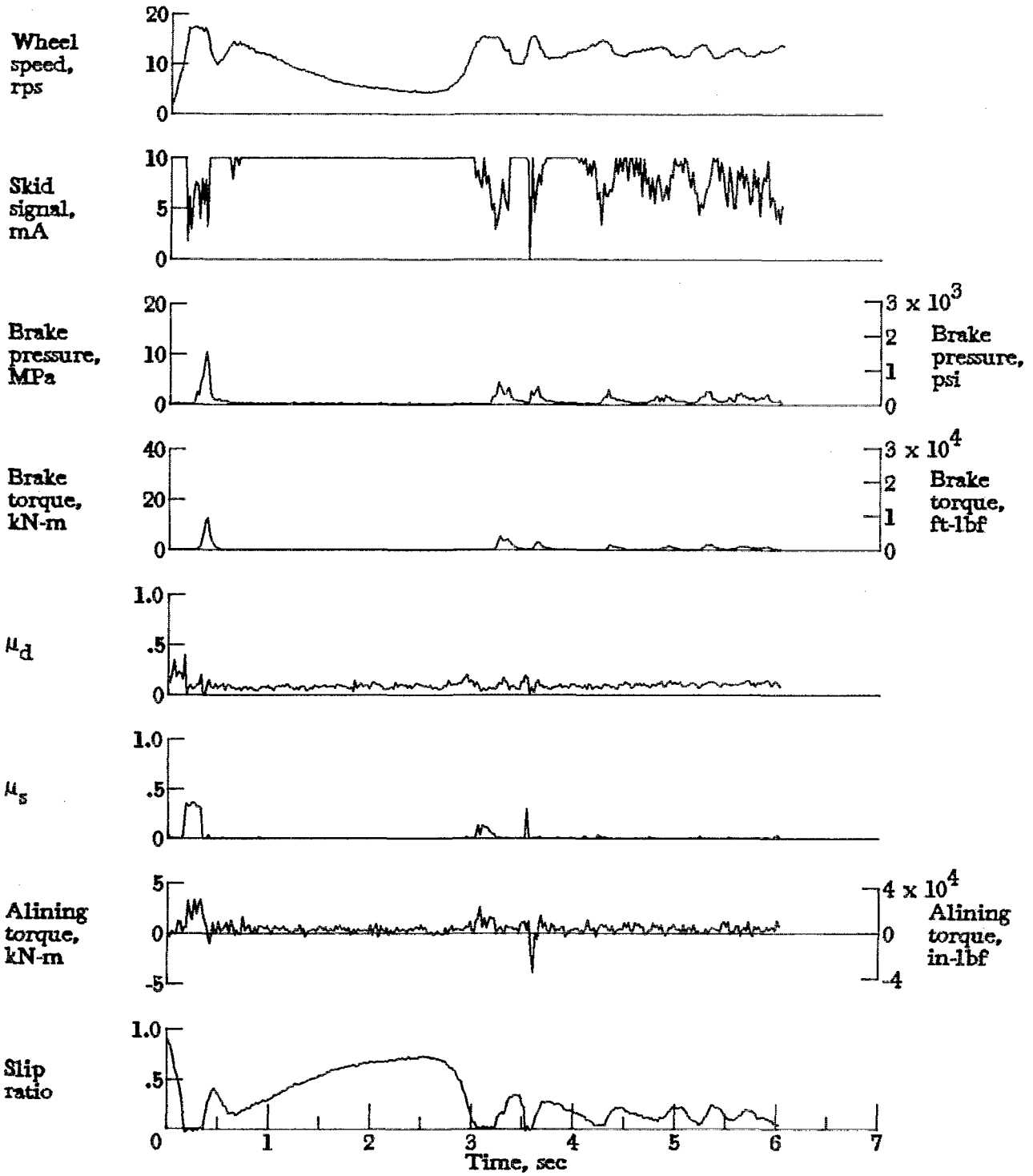

Figure A59.- Time histories for run 59. Nominal carriage speed, 92 knots; vertical load, 83.6 kN (18 800 lbf); yaw angle, 6°; brake pressure, 20 MPa (2870 psi); tire condition, new; surface condition, flooded.

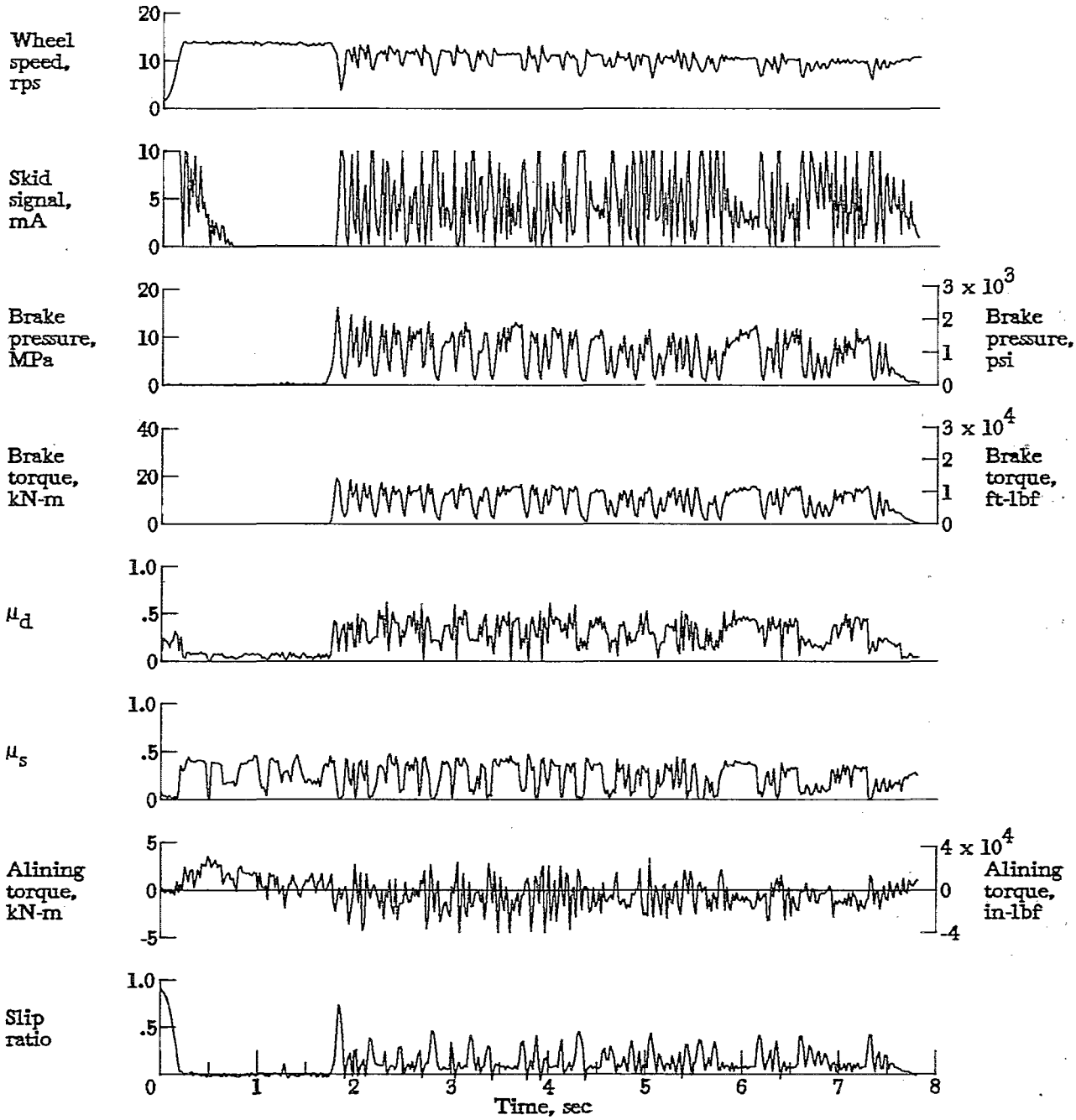

Figure A60.- Time histories for run 60. Nominal carriage speed, 70 knots; vertical load, 80.1 kN (18 000 lbf); yaw angle, 6°; brake pressure, 21 MPa (3000 psi); tire condition, new; surface condition, random dry/damp.

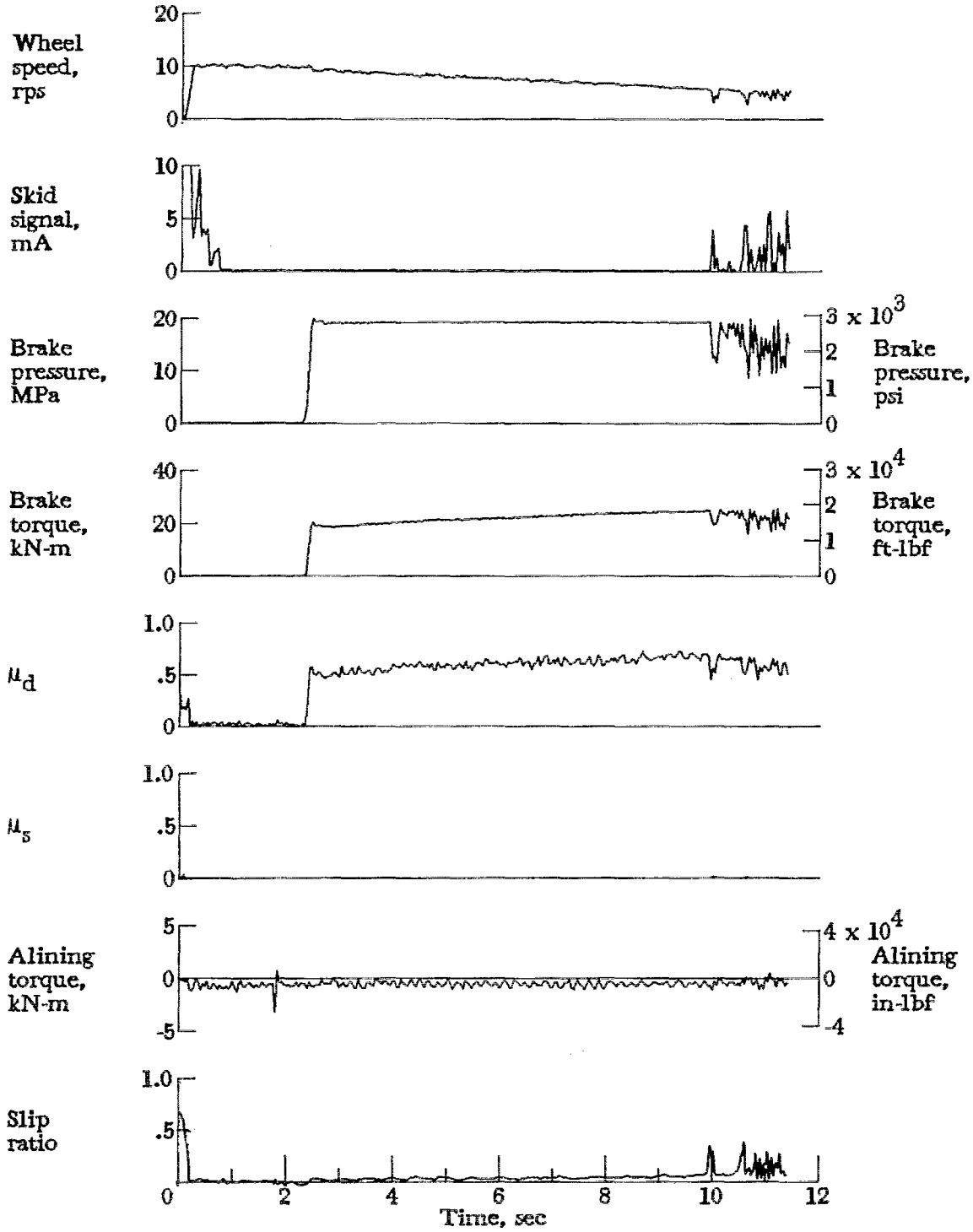

Figure A61.- Time histories for run 61. Nominal carriage speed, 42 knots; vertical load, 79.6 kN (17 900 lbf); yaw angle, 0°; brake pressure, 20 MPa (2880 psi); tire condition, worn; surface condition, dry.

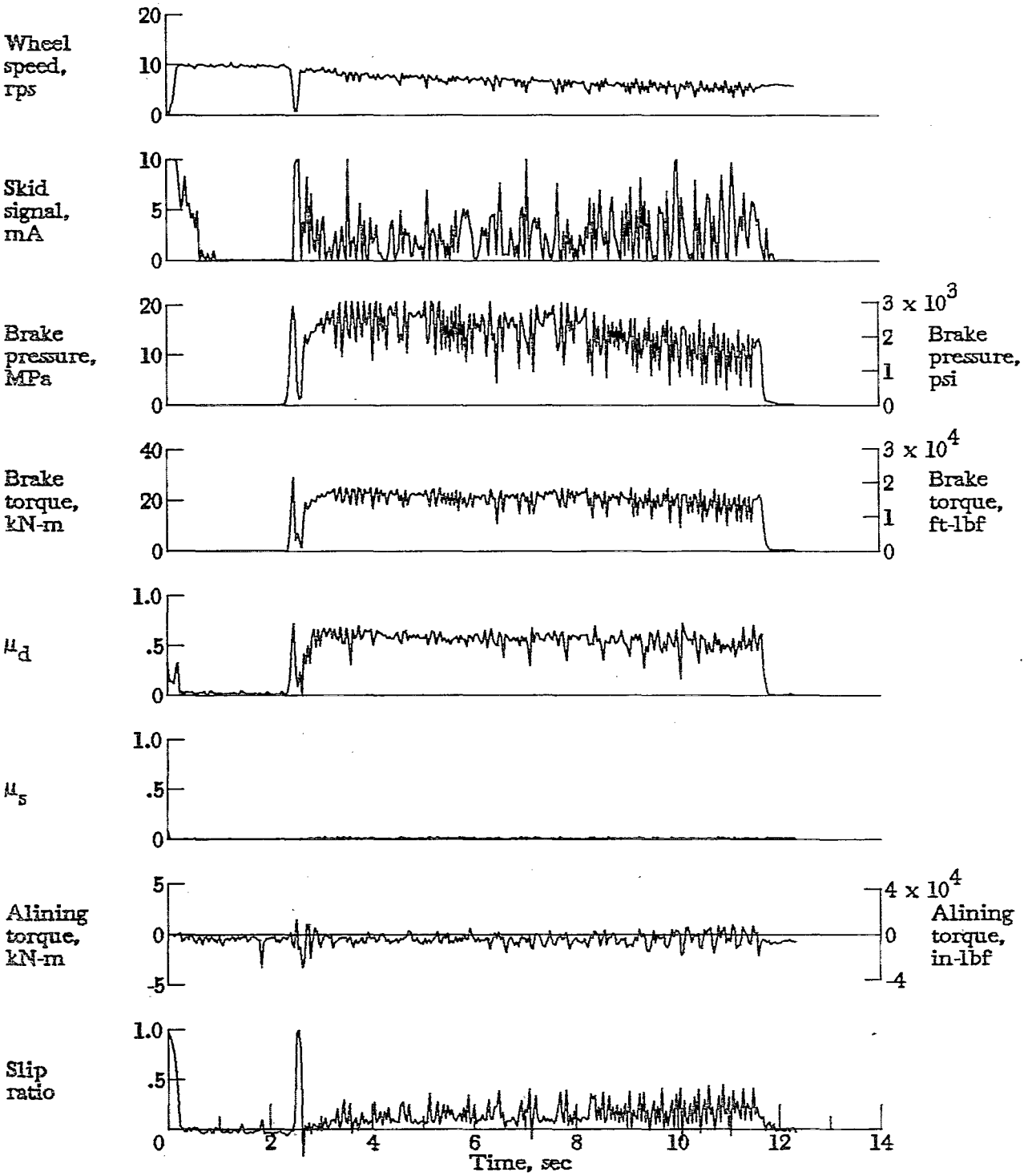

Figure A62.- Time histories for run 62. Nominal carriage speed, 43 knots; vertical load, 80.5 kN (18 100 lbf); yaw angle, 0°; brake pressure, 21 MPa (3000 psi); tire condition, worn; surface condition, dry.

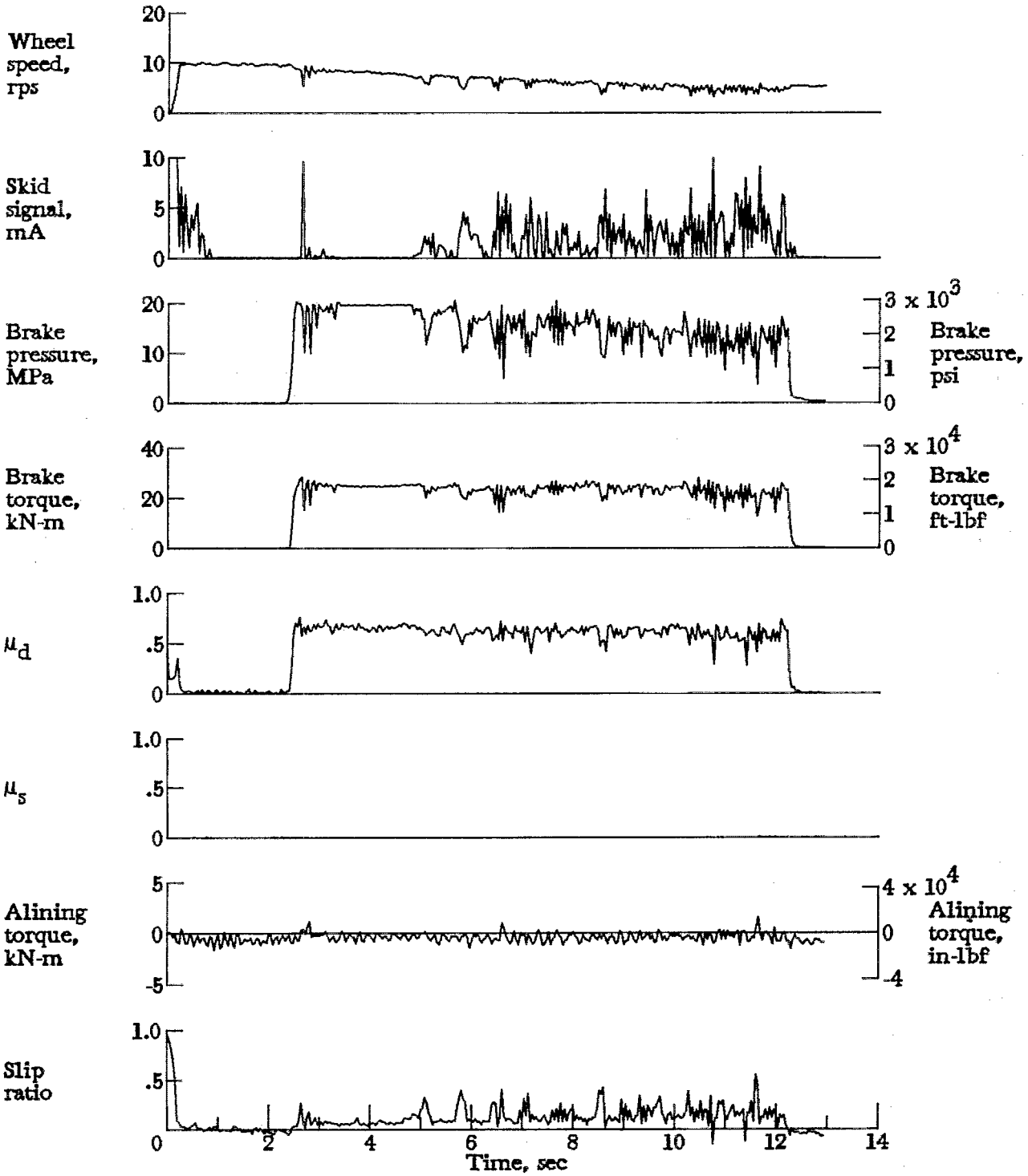

Figure A63.- Time histories for run 63. Nominal carriage speed, 40 knots; vertical load, 81.4 kN (18 300 lbf); yaw angle, 0°; brake pressure, 20 MPa (2920 psi); tire condition, worn; surface condition, dry.

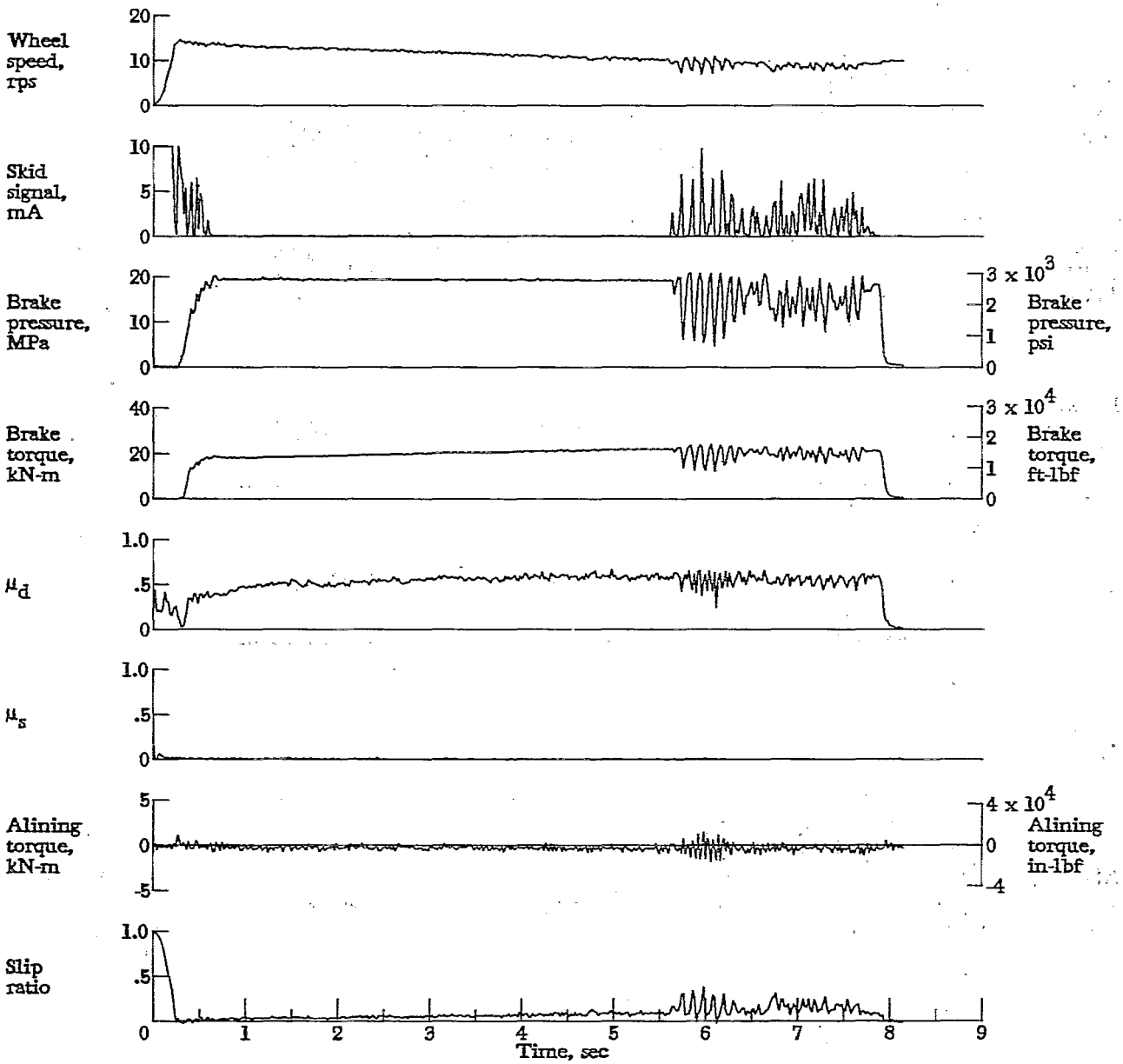

Figure A64.- Time histories for run 64. Nominal carriage speed, 66 knots; vertical load, 84.1 kN (18 900 lbf); yaw angle, 0°; brake pressure, 20 MPa (2860 psi); tire condition, worn; surface condition, dry.

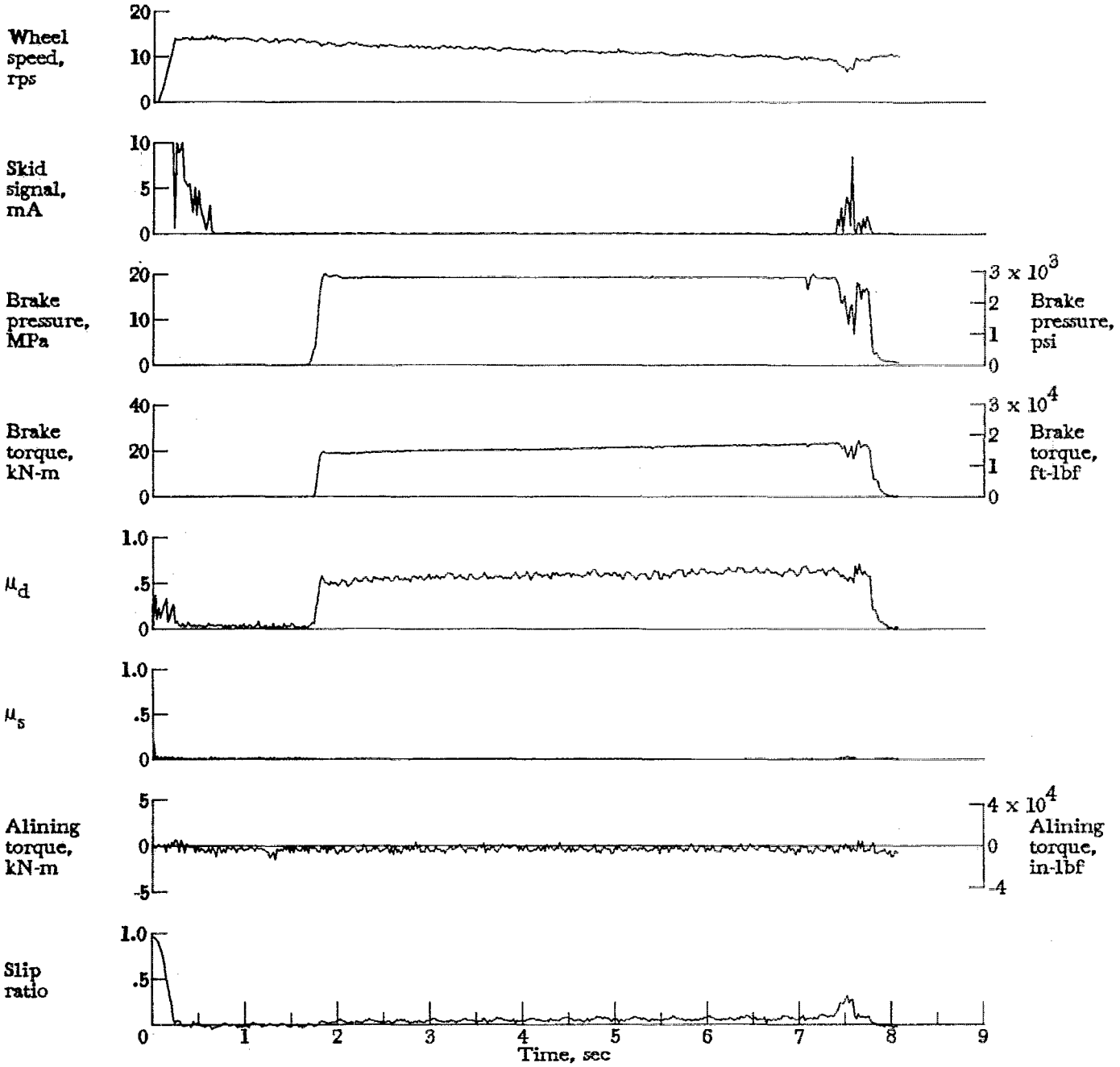

Figure A65.- Time histories for run 65. Nominal carriage speed, 67 knots; vertical load, 81.0 kN (18 200 lbf); yaw angle, 0°; brake pressure, 20 MPa (2910 psi); tire condition, worn; surface condition, dry.

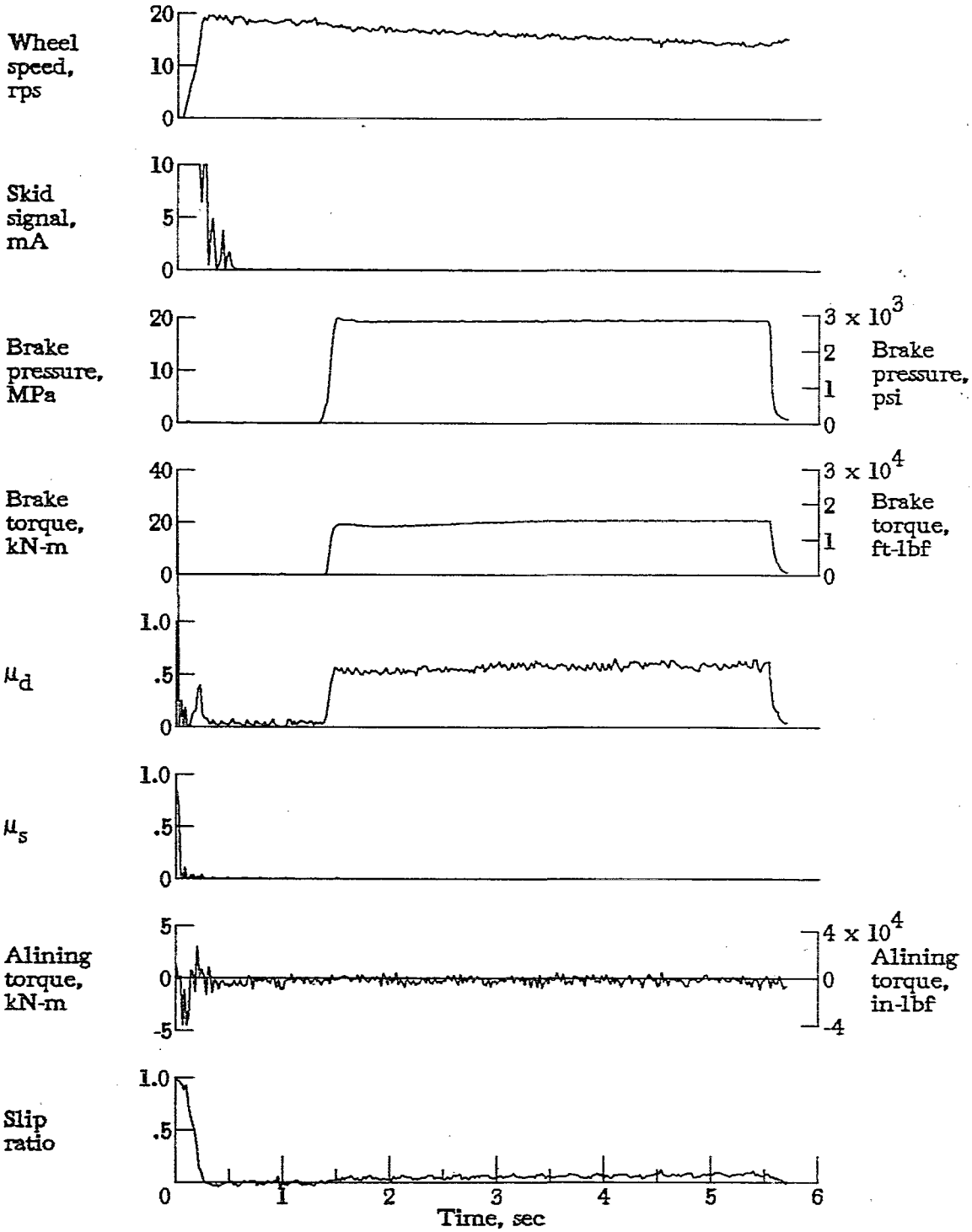

Figure A66.- Time histories for run 66. Nominal carriage speed, 100 knots; vertical load, 81.0 kN (18 200 lbf); yaw angle, 0°; brake pressure, 20 MPa (2910 psi); tire condition, worn; surface condition, dry.

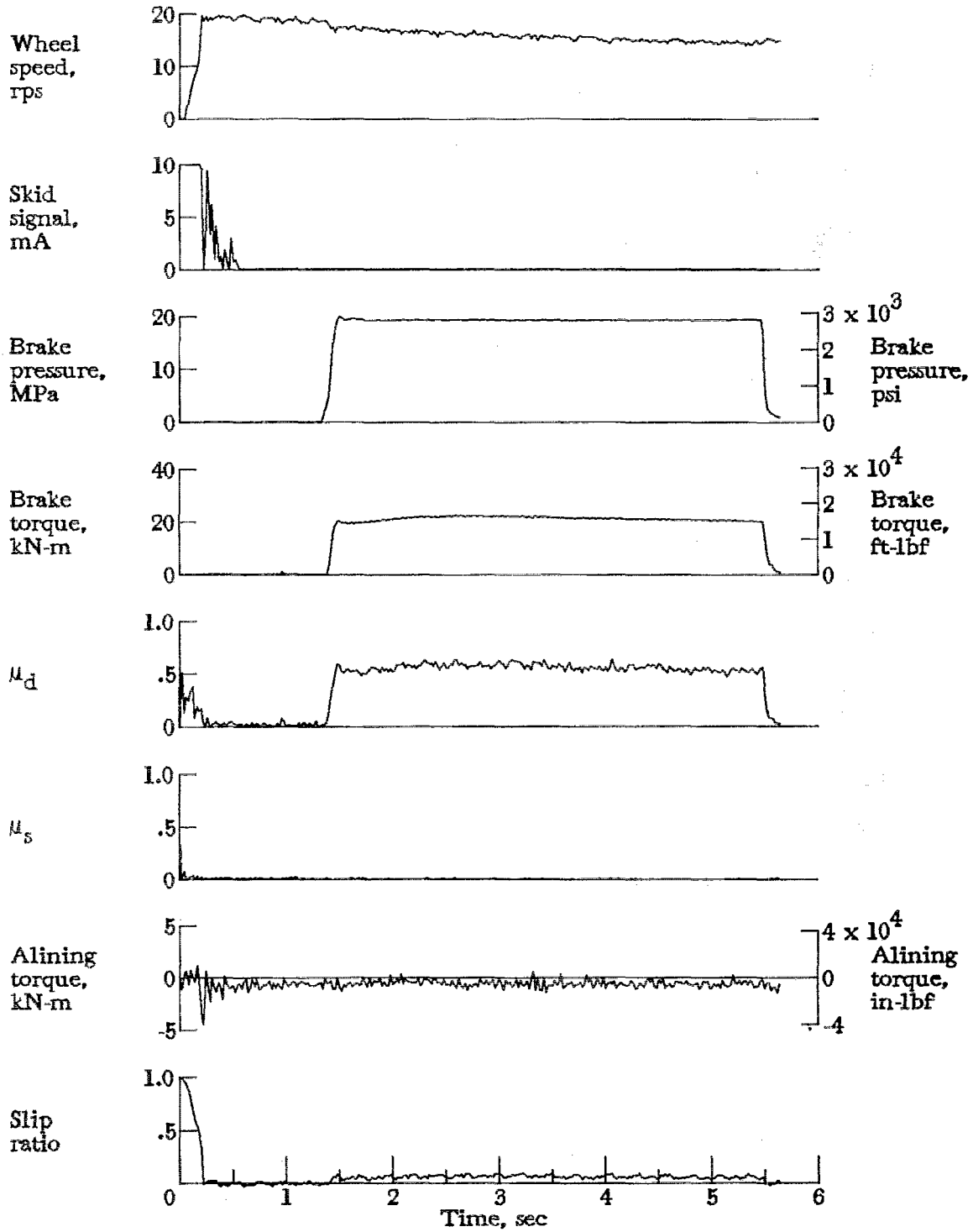

Figure A67.- Time histories for run 67. Nominal carriage speed, 97 knots; vertical load, 81.4 kN (18 300 lbf); yaw angle, 0°; brake pressure, 20 MPa (2880 psi); tire condition, worn; surface condition, dry.

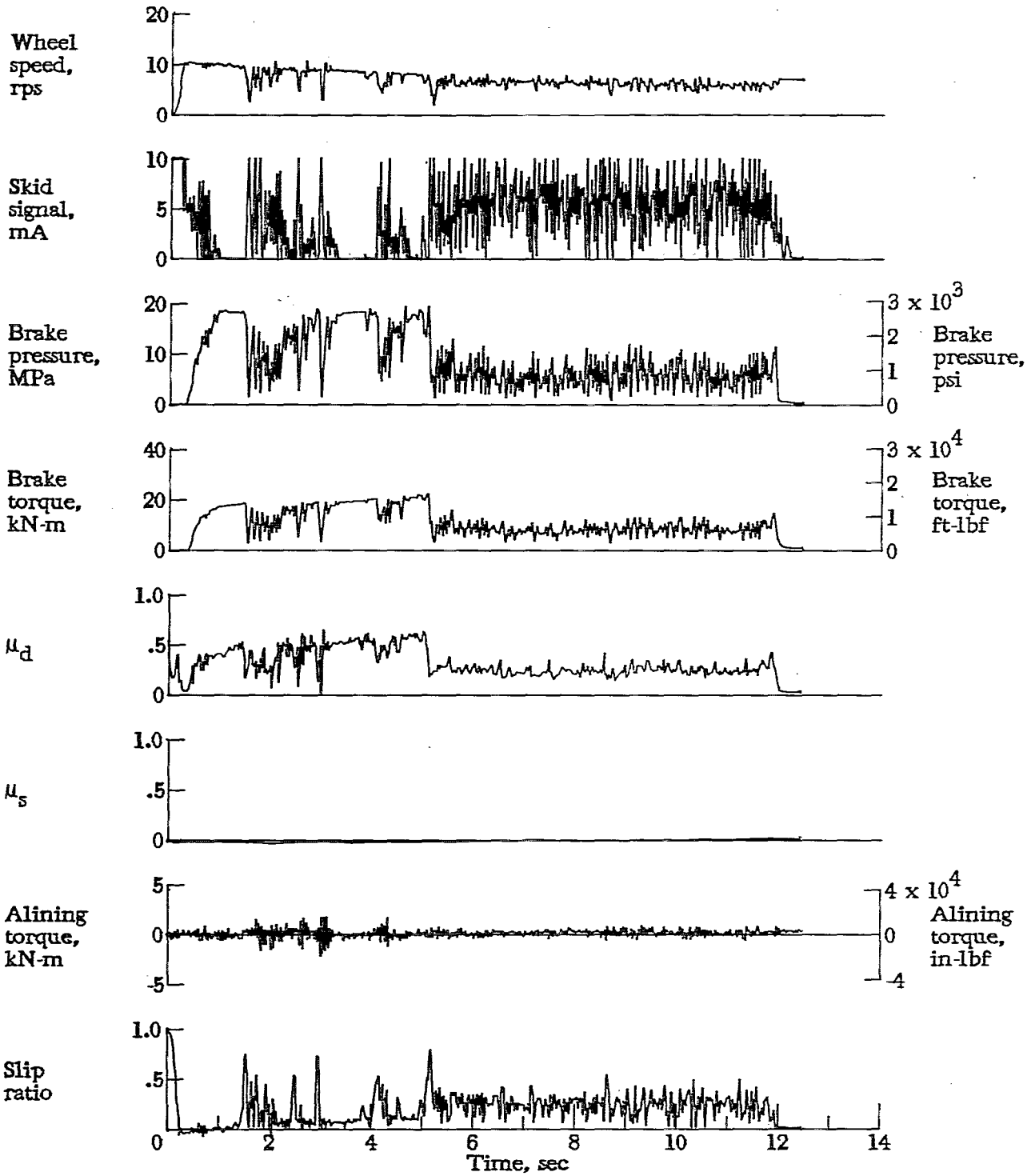

Figure A68.- Time histories for run 68. Nominal carriage speed, 43 knots; vertical load, 83.6 kN (18 800 lbf); yaw angle, 0°; brake pressure, 18 MPa (2640 psi); tire condition, worn; surface condition, damp.

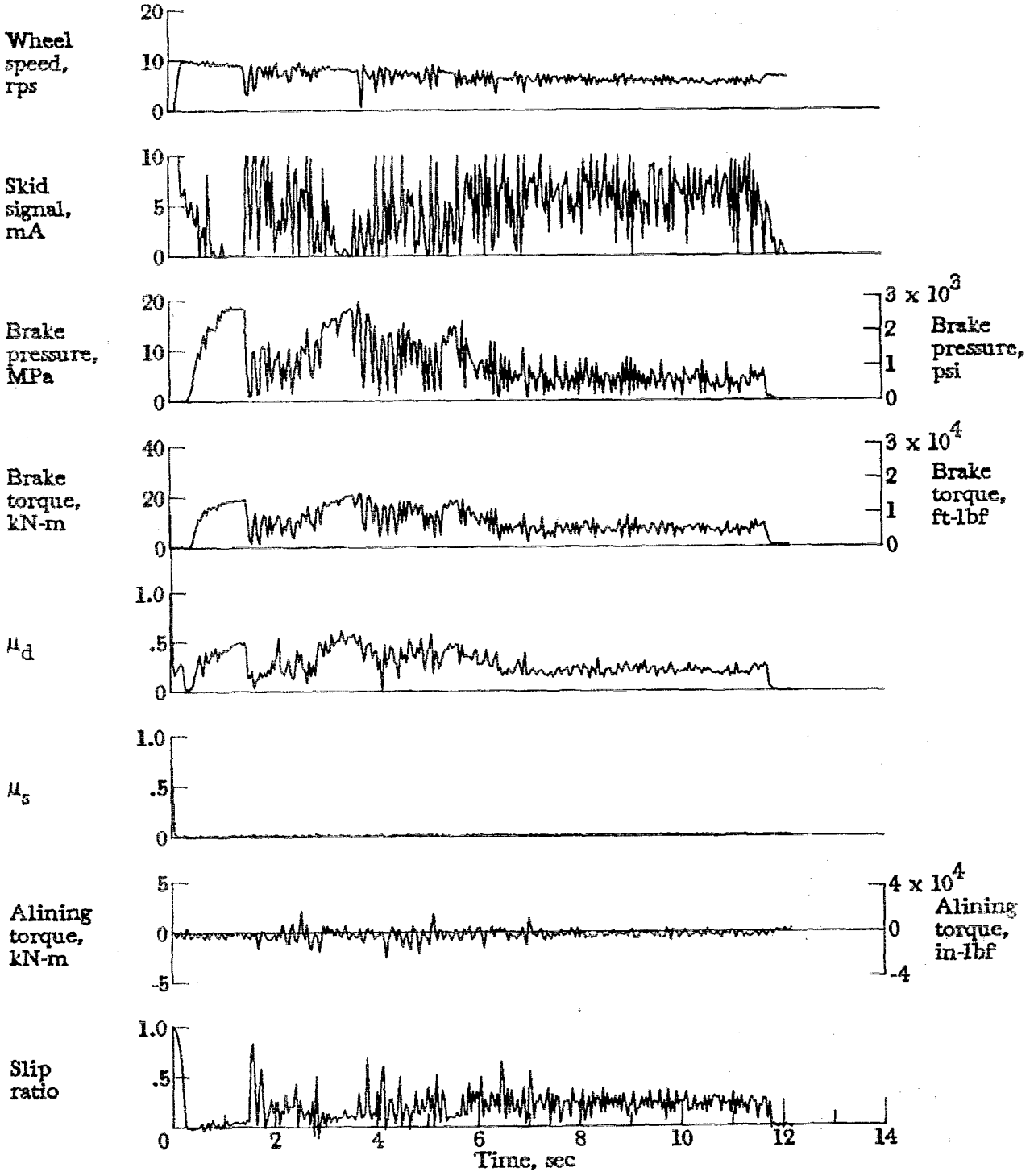

Figure A69.- Time histories for run 69. Nominal carriage speed, 44 knots; vertical load, 83.6 kN (18 800 lbf); yaw angle, 0°; brake pressure, 18 MPa (2640 psi); tire condition, worn; surface condition, damp.

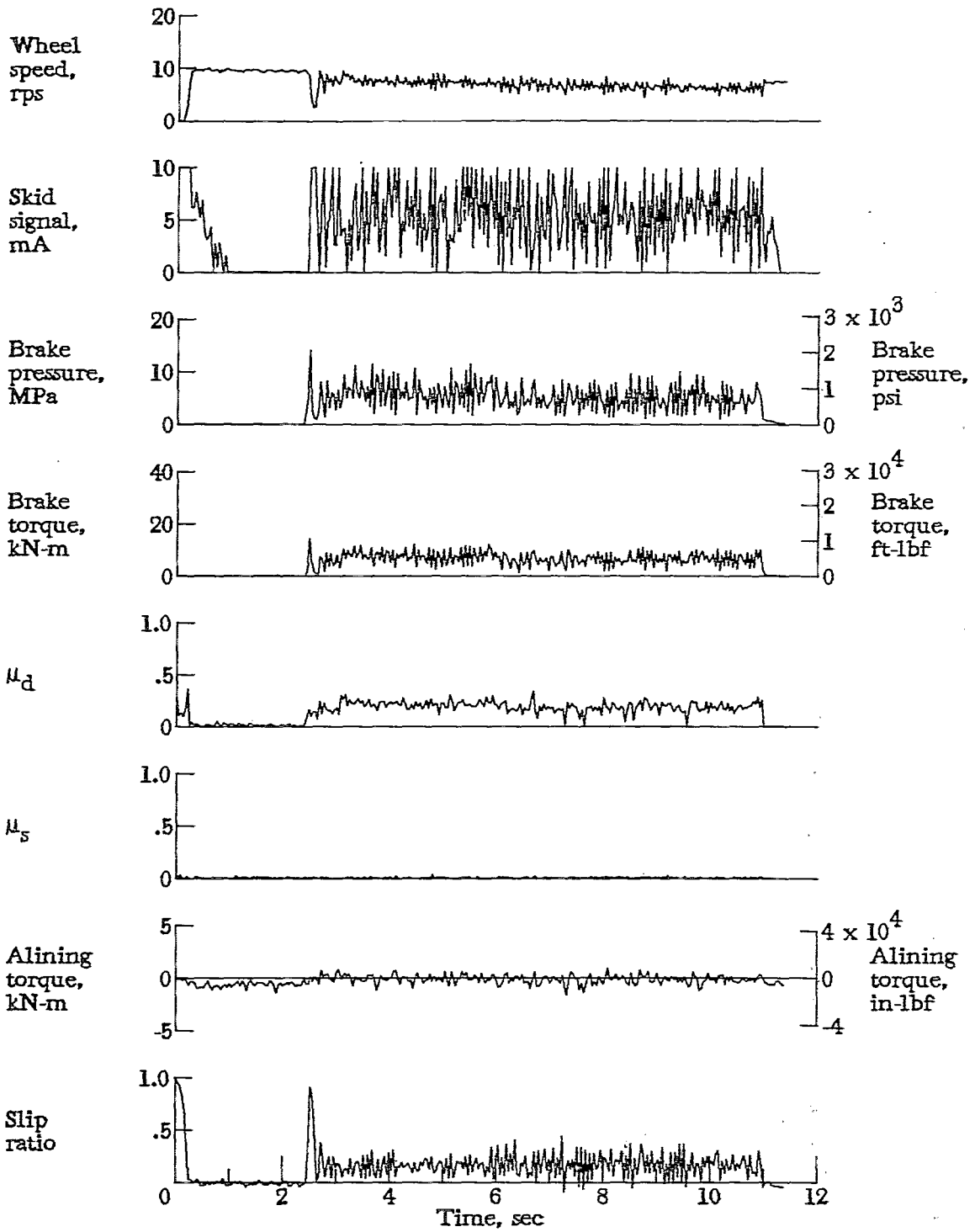

Figure A70.- Time histories for run 70. Nominal carriage speed, 48 knots; vertical load, 79.2 kN (17 800 lbf); yaw angle, 0°; brake pressure, 21 MPa (3000 psi); tire condition, worn; surface condition, damp.

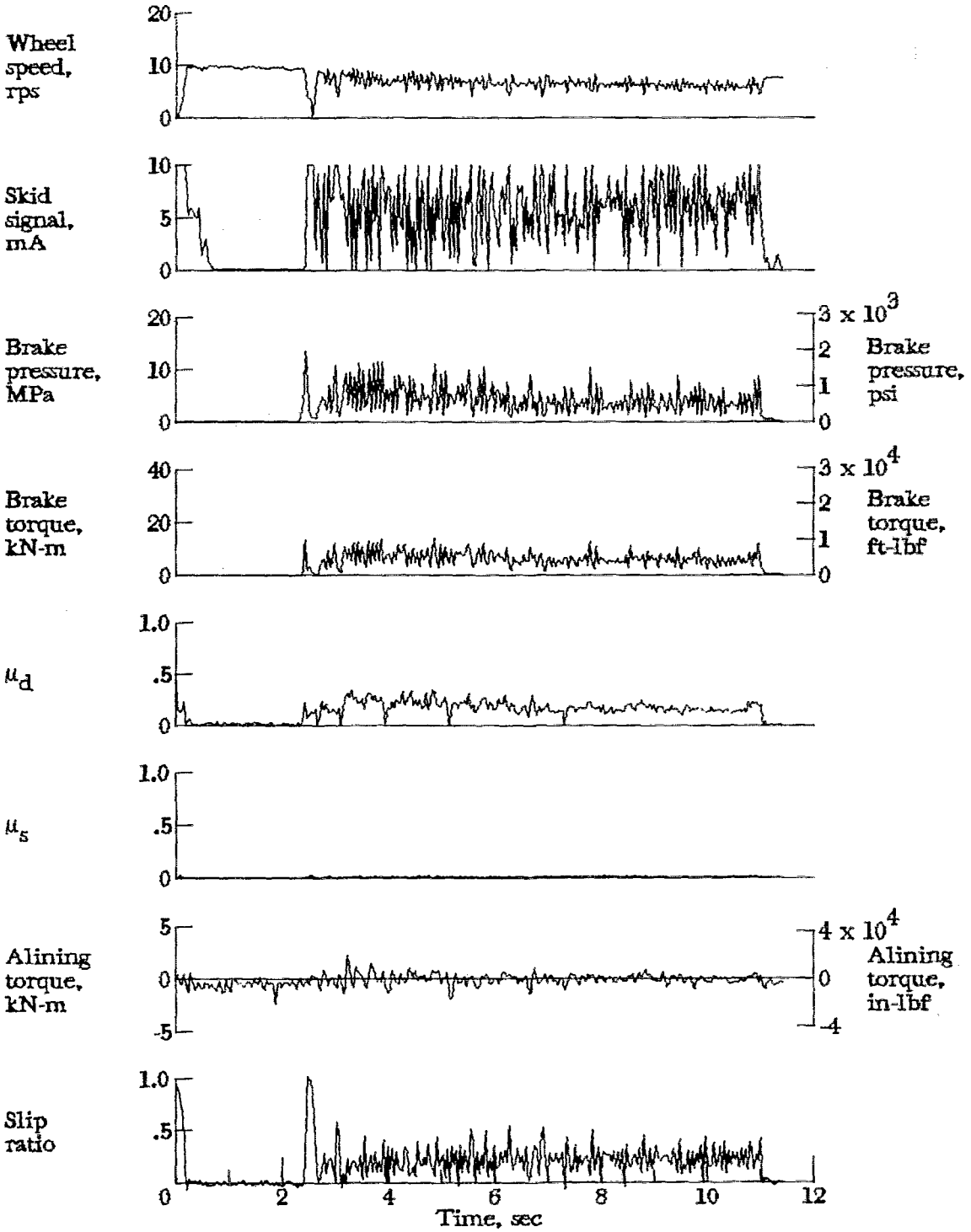

Figure A71.- Time histories for run 71. Nominal carriage speed, 48 knots; vertical load, 79.6 kN (17 900 lbf); yaw angle, 0°; brake pressure, 21 MPa (3000 psi); tire condition, worn; surface condition, damp.

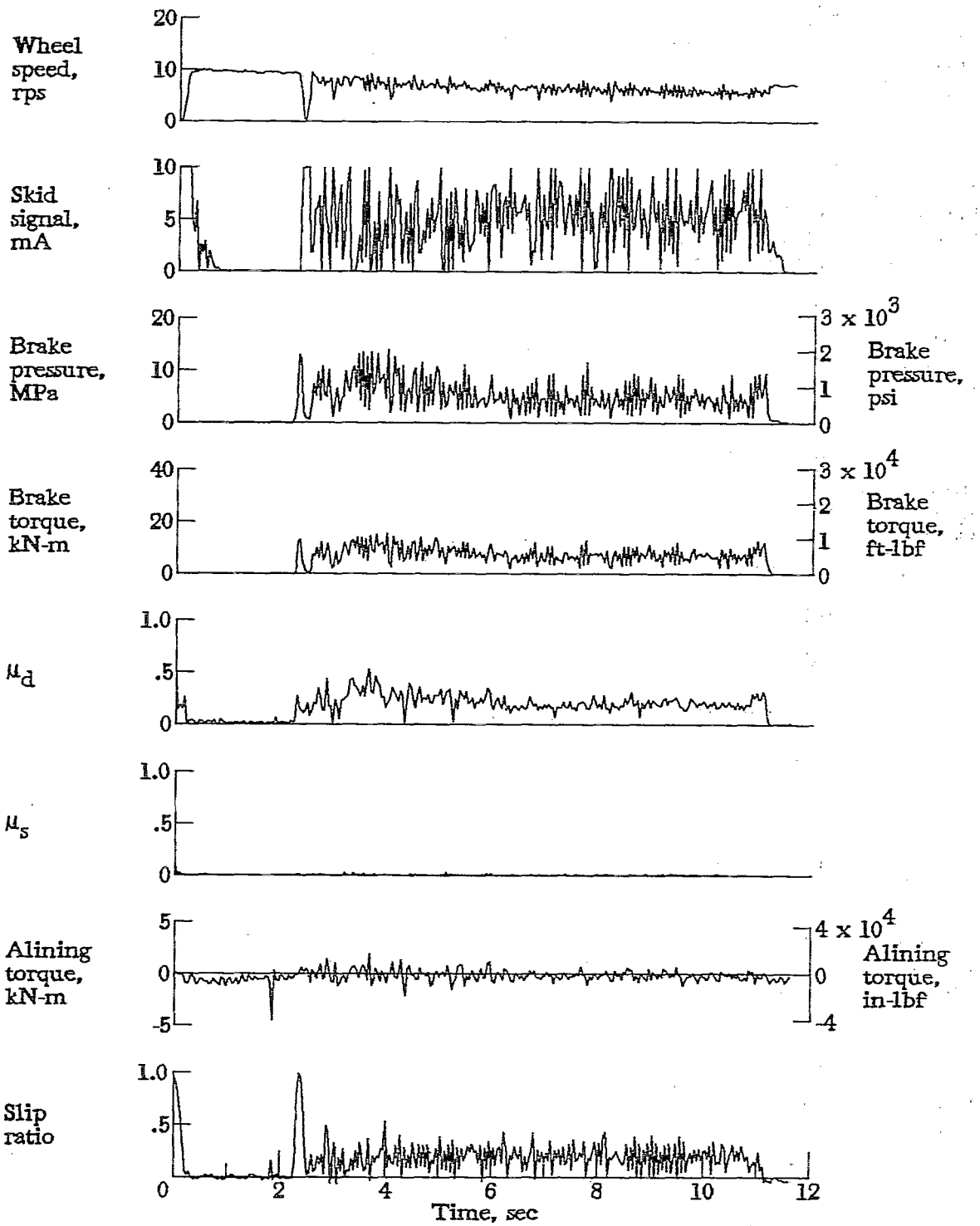

Figure A72.- Time histories for run 72. Nominal carriage speed, 47 knots; vertical load, 79.2 kN (17 800 lbf); yaw angle, 0°; brake pressure, 21 MPa (3000 psi); tire condition, worn; surface condition, damp.

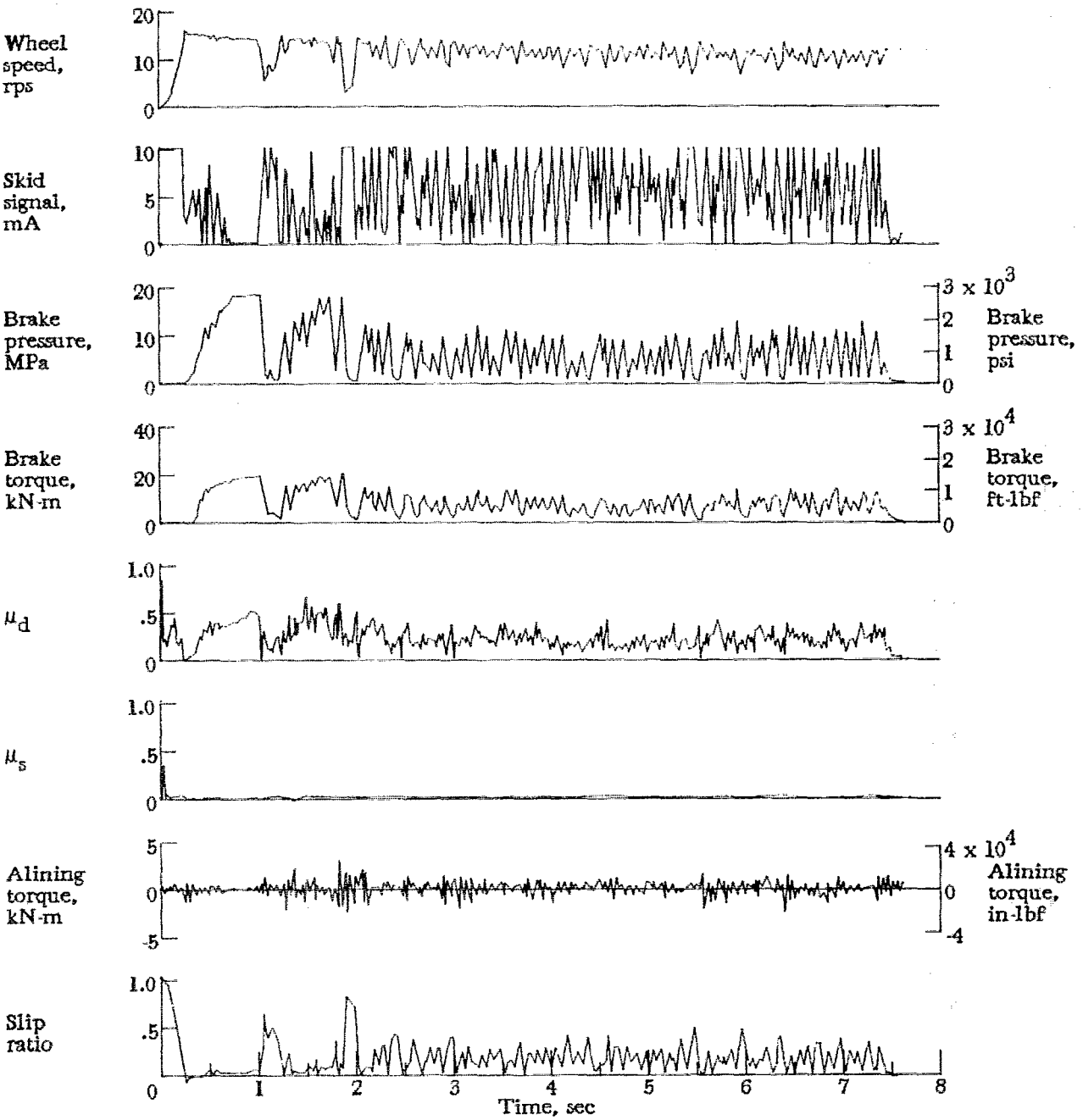

Figure A73.- Time histories for run 73. Nominal carriage speed, 72 knots; vertical load, 83.2 kN (18 700 lbf); yaw angle, 0°; brake pressure, 18 MPa (2600 psi); tire condition, worn; surface condition, damp.

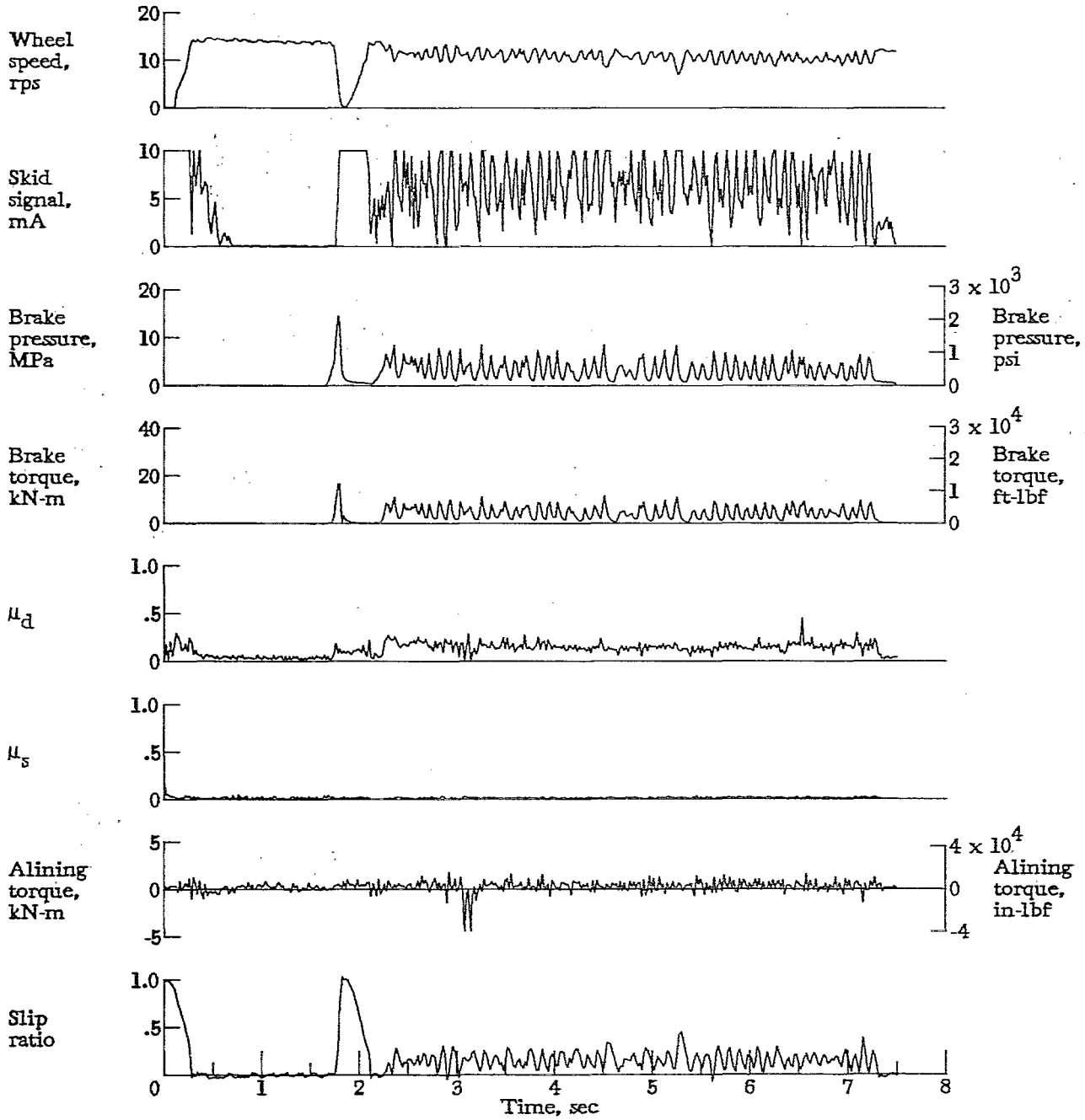

Figure A74.- Time histories for run 74. Nominal carriage speed, 74 knots; vertical load, 79.2 kN (17 800 lbf); yaw angle, 0°; brake pressure, 21 MPa (3000 psi); tire condition, worn; surface condition, damp.

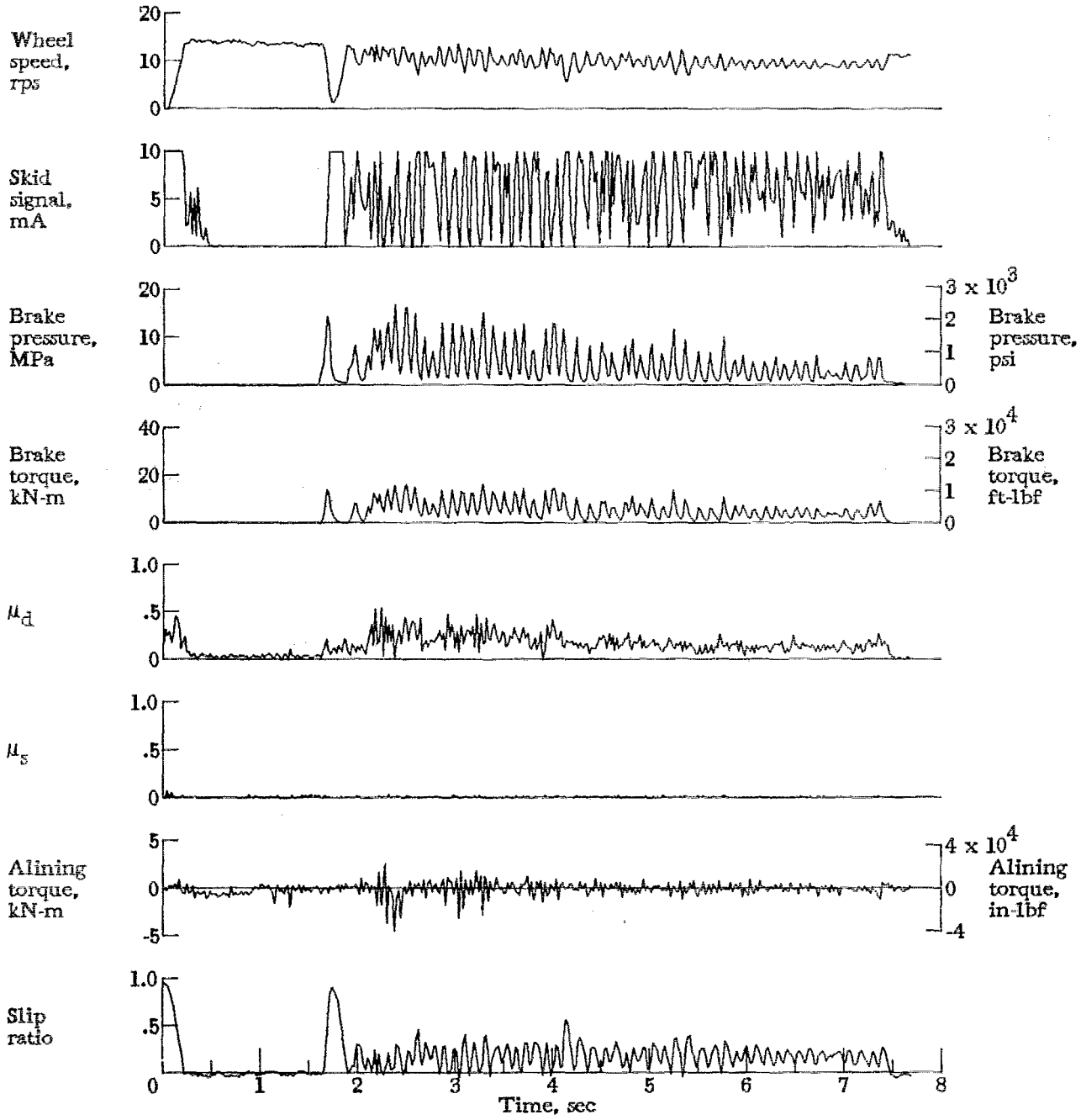

Figure A75.- Time histories for run 75. Nominal carriage speed, 72 knots; vertical load, 79.2 kN (17 800 lbf); yaw angle, 0°; brake pressure, 21 MPa (3000 psi); tire condition, worn; surface condition, damp.

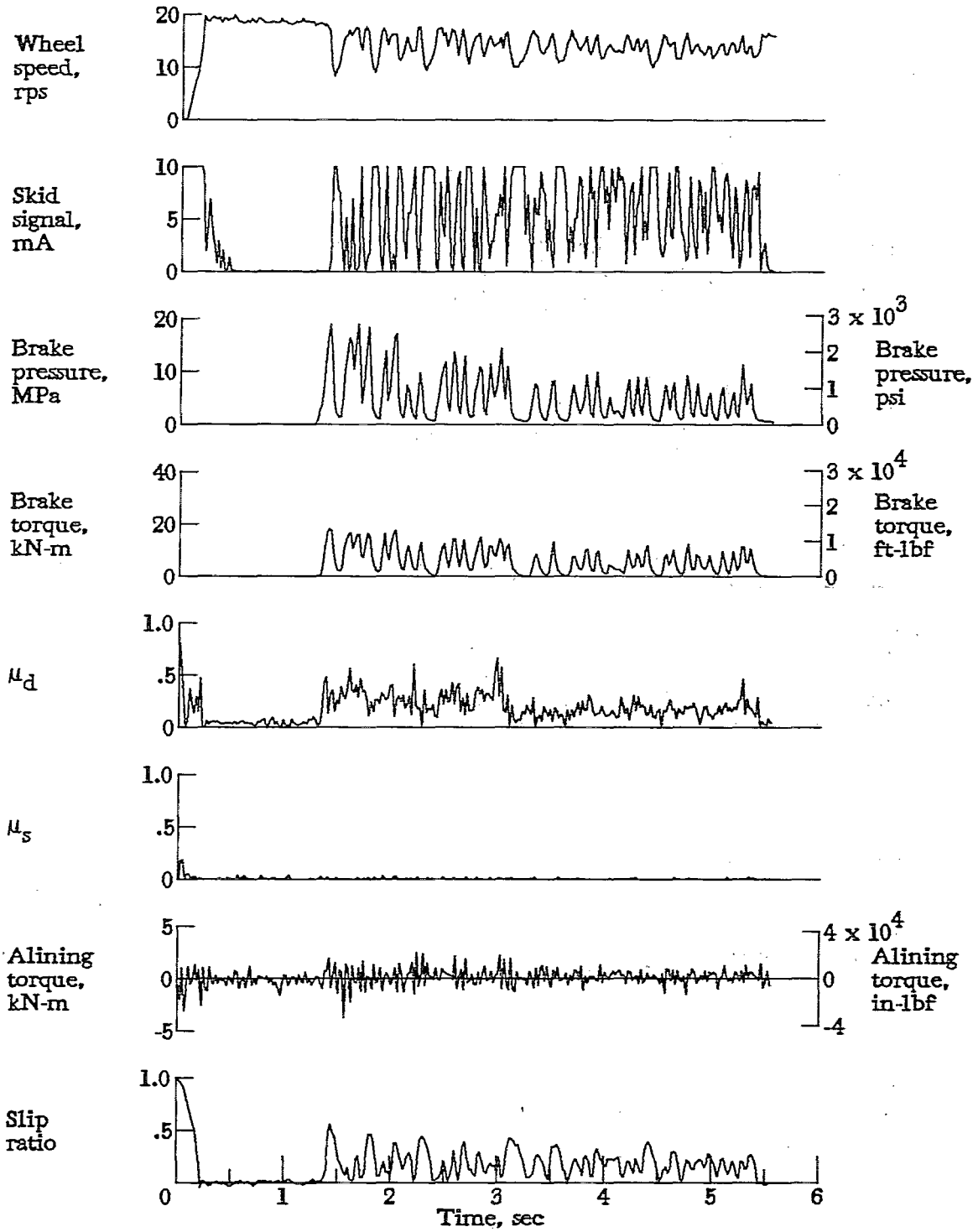

Figure A76.- Time histories for run 76. Nominal carriage speed, 100 knots; vertical load, 80.1 kN (18 000 lbf); yaw angle, 0°; brake pressure, 21 MPa (3000 psi); tire condition, worn; surface condition, damp.

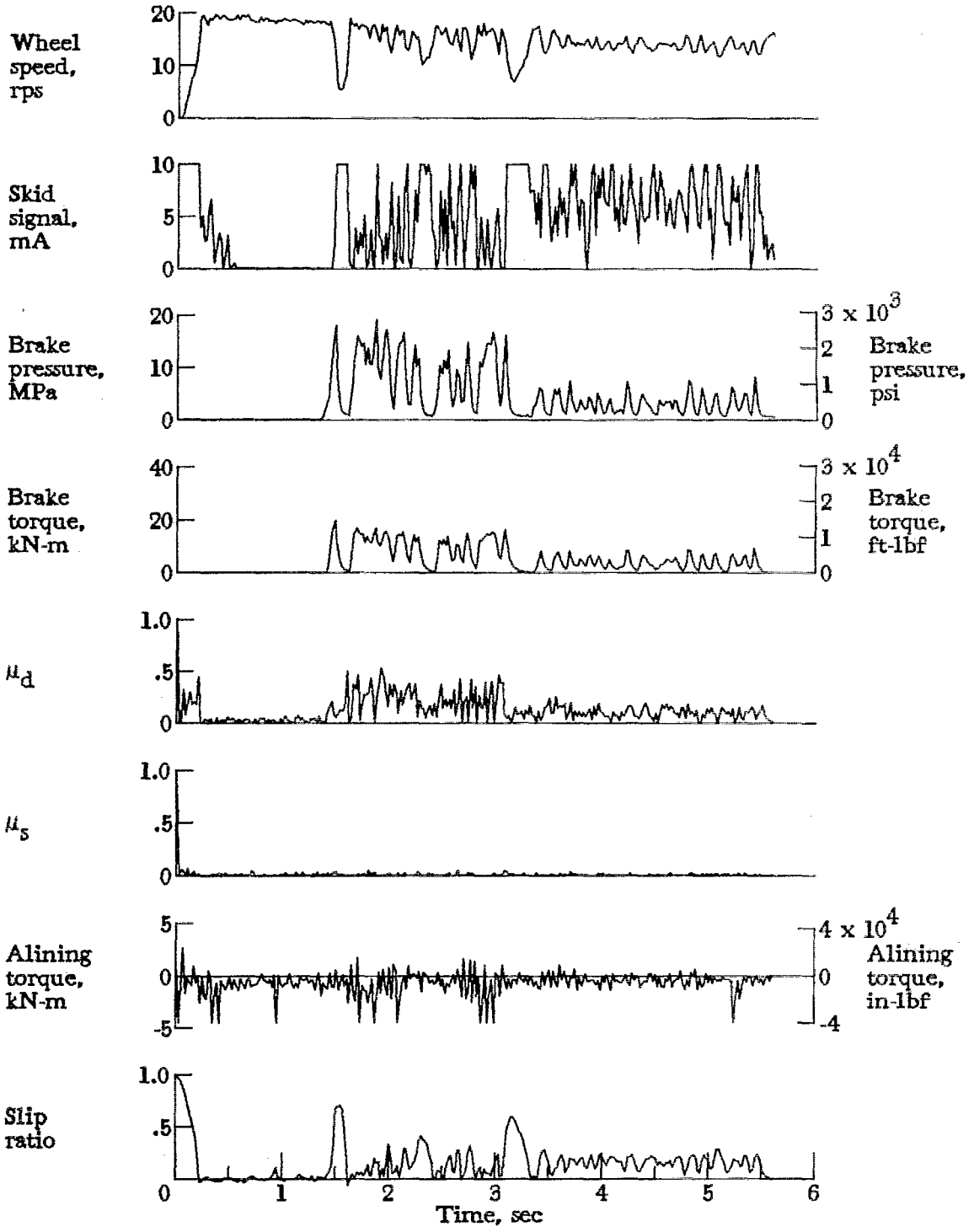

Figure A77.- Time histories for run 77. Nominal carriage speed, 99 knots; vertical load, 80.5 kN (18 100 lbf); yaw angle, 0°; brake pressure, 21 MPa (3000 psi); tire condition, worn; surface condition, damp.

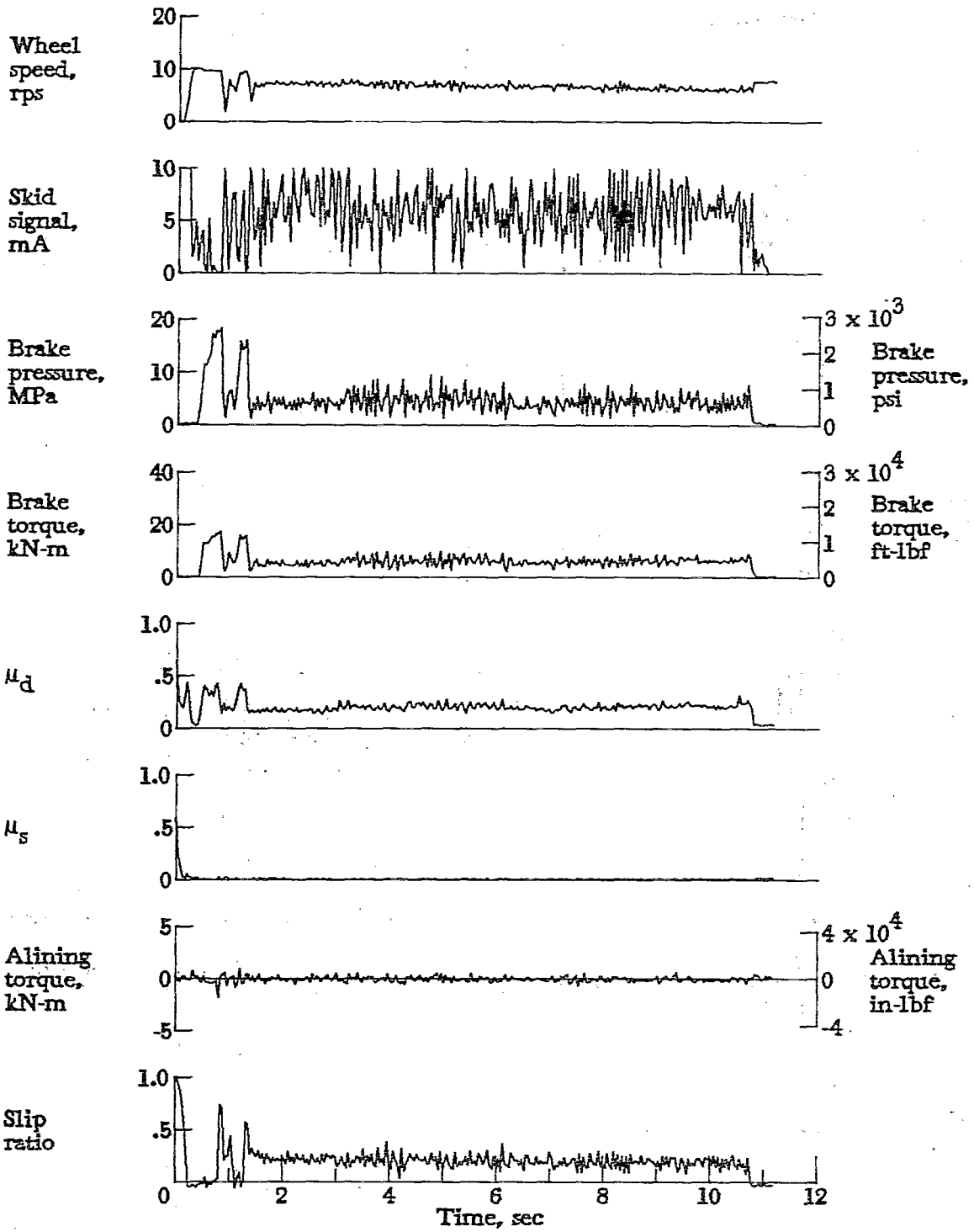

Figure A78.- Time histories for run 78. Nominal carriage speed, 49 knots; vertical load, 84.1 kN (18 900 lbf); yaw angle, 0°; brake pressure, 18 MPa (2620 psi); tire condition, worn; surface condition, flooded.

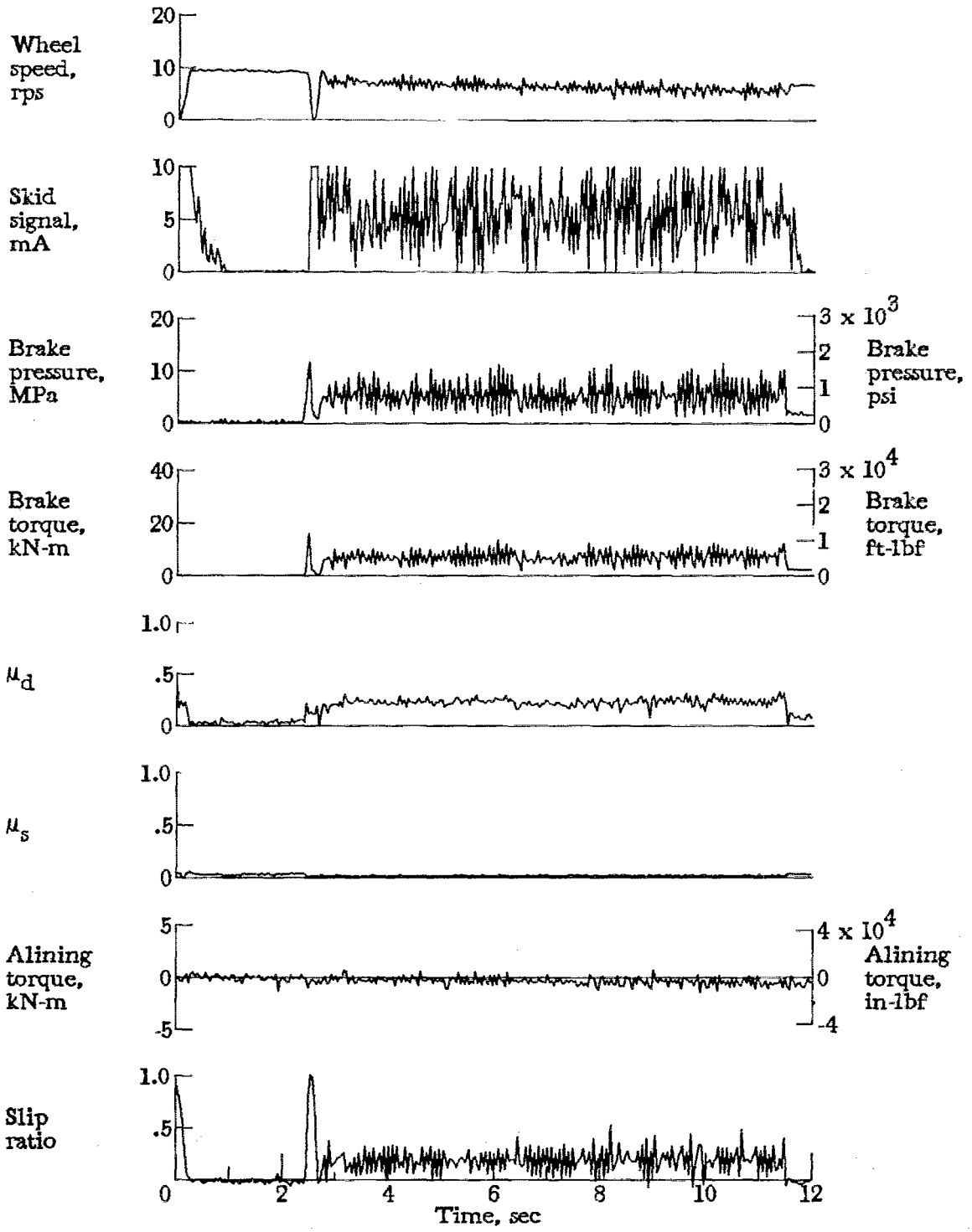

Figure A79.- Time histories for run 79. Nominal carriage speed, 45 knots; vertical load, 78.3 kN (17 600 lbf); yaw angle, 0°; brake pressure, 21 MPa (3000 psi); tire condition, worn; surface condition, flooded.

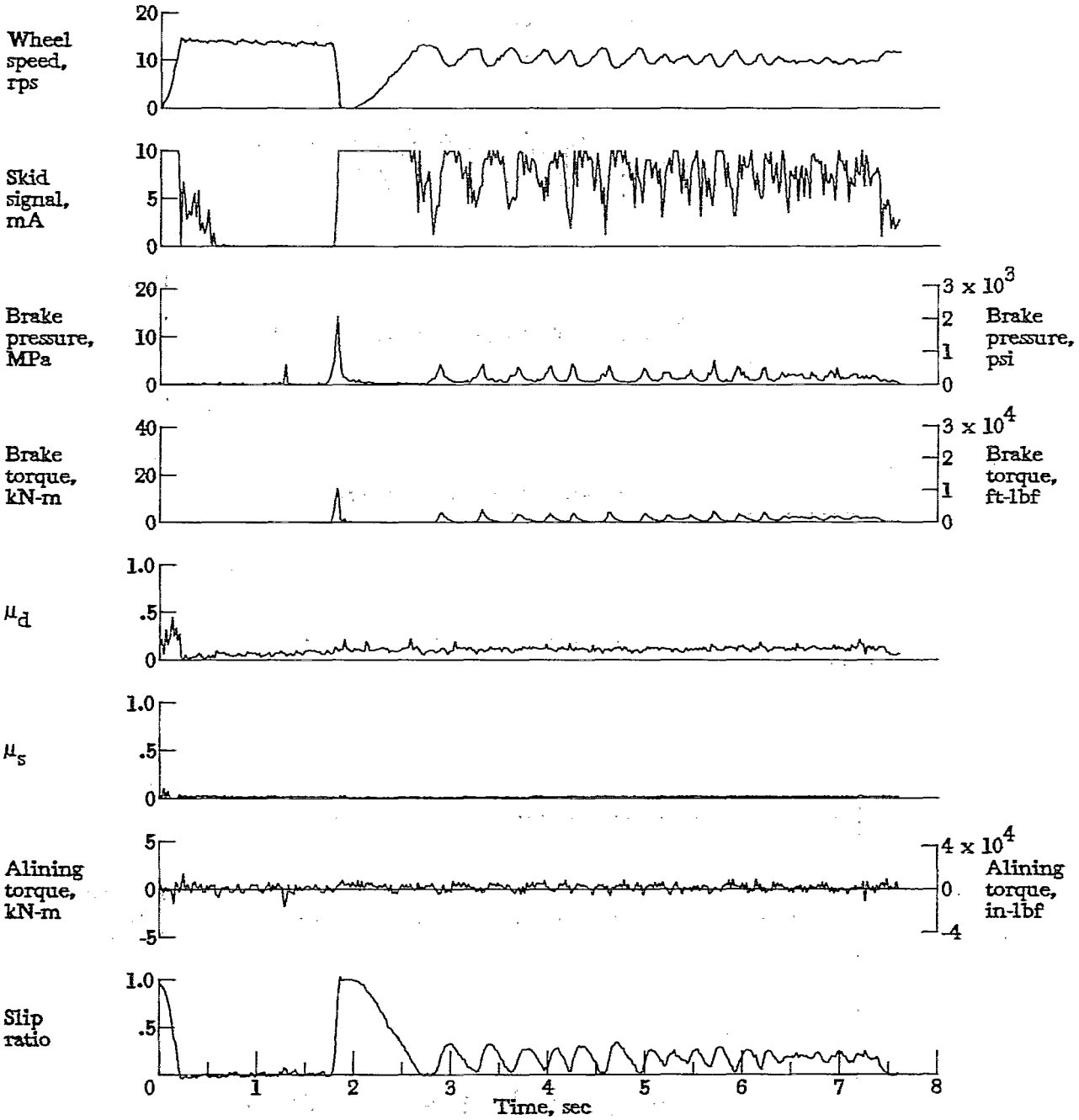

Figure A80.- Time histories for run 80. Nominal carriage speed, 73 knots; vertical load, 78.3 kN (17 600 lbf); yaw angle, 0°; brake pressure, 21 MPa (3000 psi); tire condition, worn; surface condition, flooded.

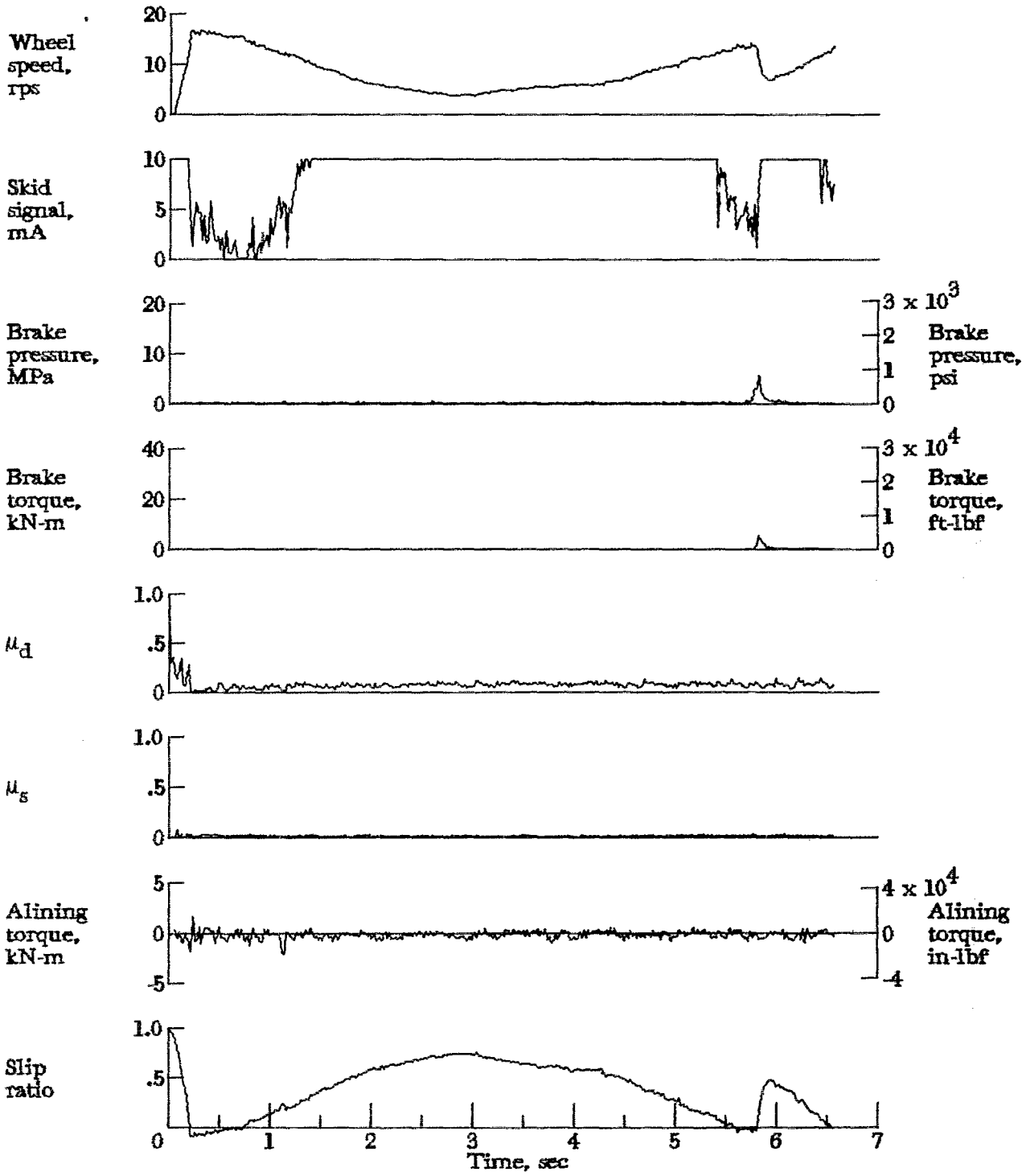

Figure A81.- Time histories for run 81. Nominal carriage speed, 100 knots; vertical load, 78.7 kN (17 700 lbf); yaw angle, 0°; brake pressure, 20 MPa (2930 psi); tire condition, worn; surface condition, flooded.

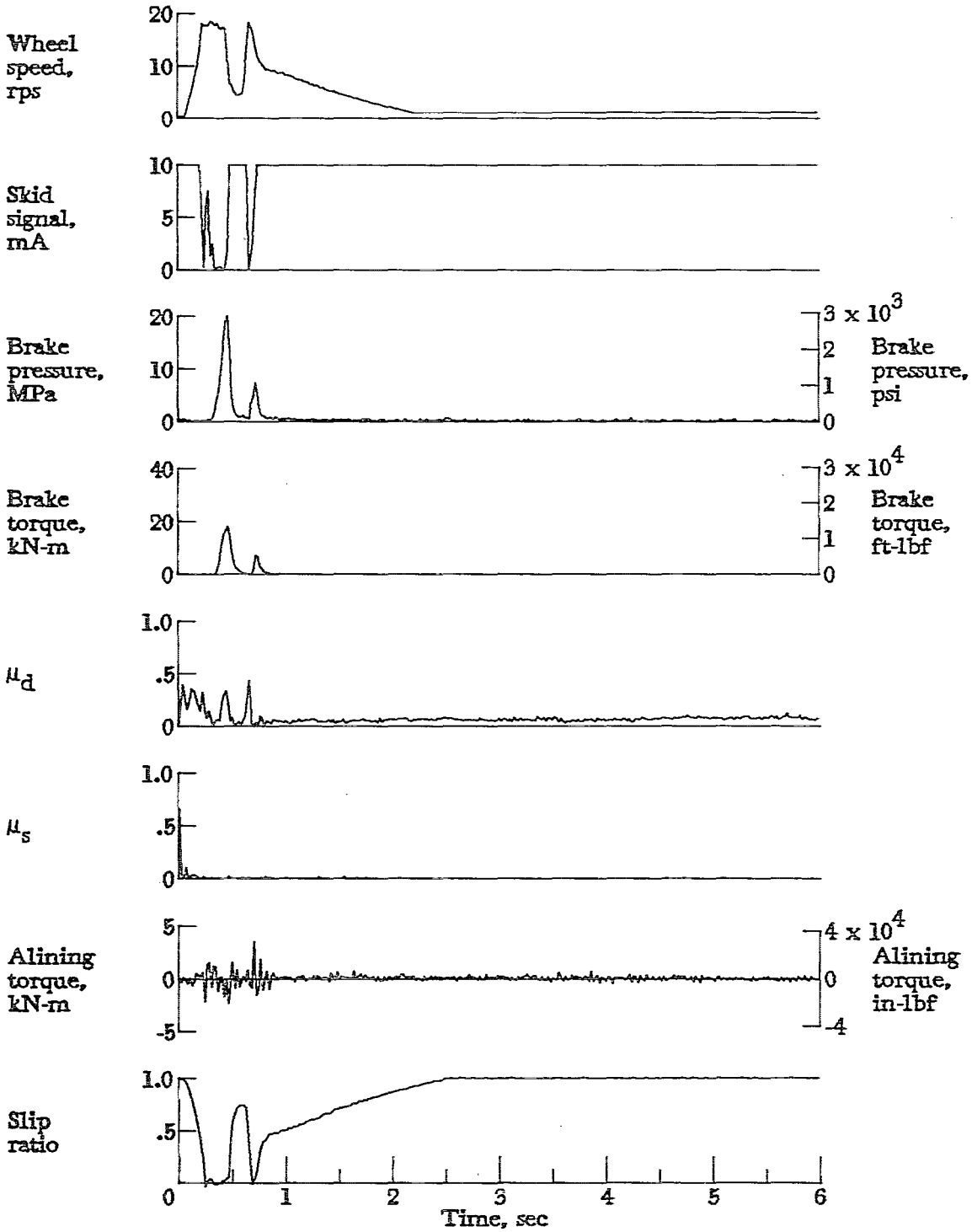

Figure A82.- Time histories for run 82. Nominal carriage speed, 93 knots; vertical load, 81.4 kN (18 300 lbf); yaw angle, 0°; brake pressure, 19 MPa (2830 psi); tire condition, worn; surface condition, flooded.

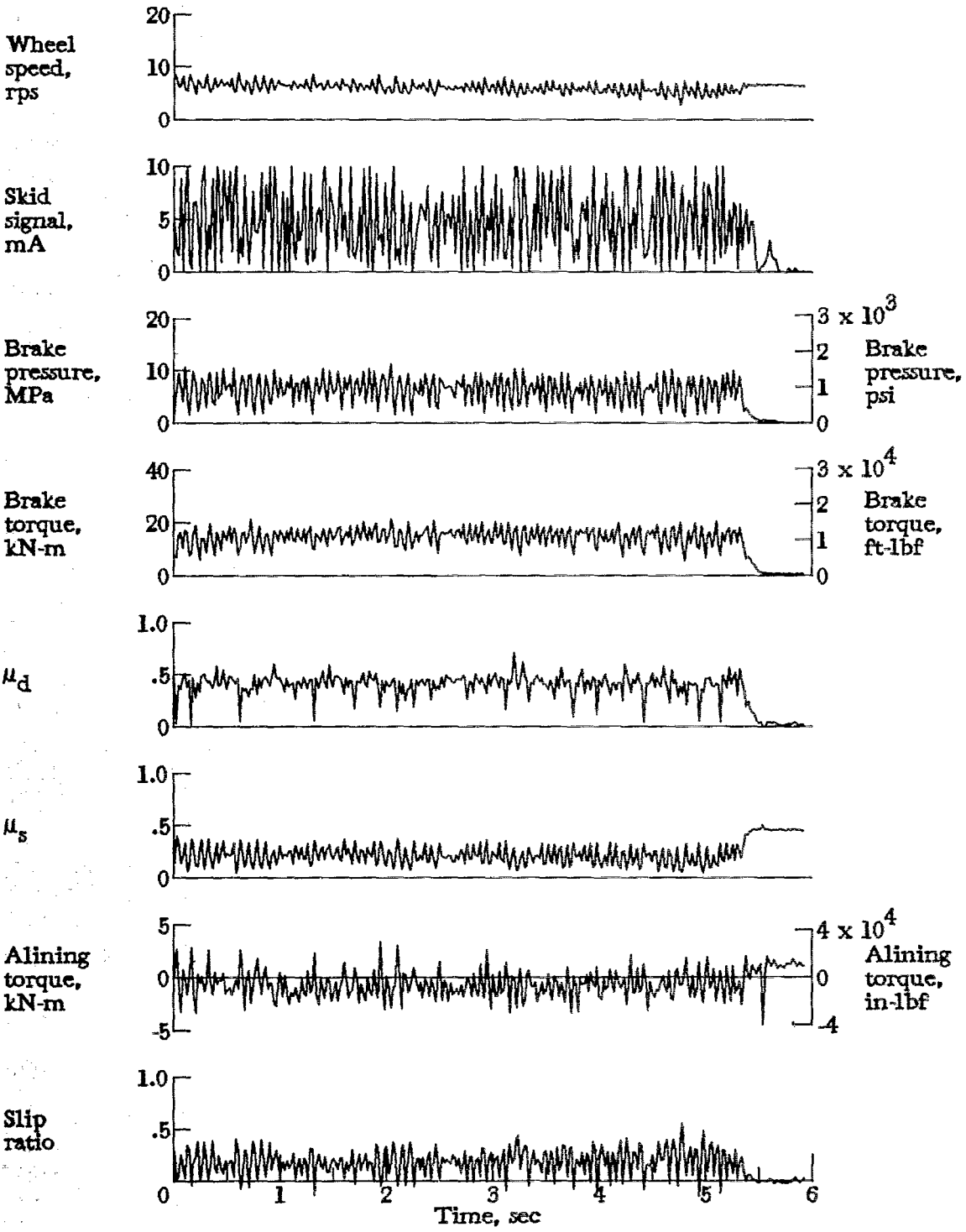

Figure A83.- Time histories for run 83. Nominal carriage speed, 45 knots; vertical load, 81.4 kN (18 300 lbf); yaw angle, 6°; brake pressure, 21 MPa (3000 psi); tire condition, worn; surface condition, dry.

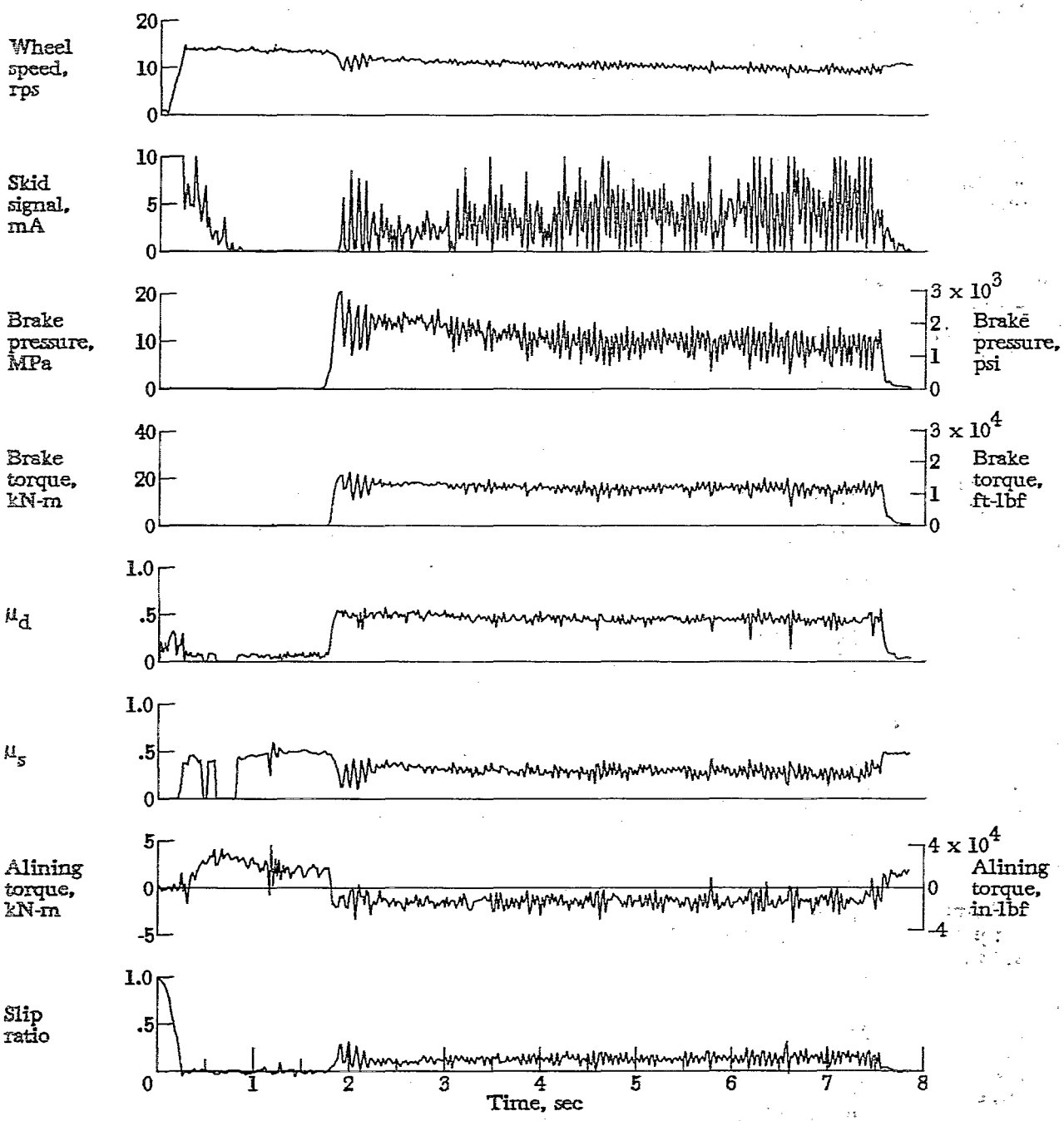

Figure A84.- Time histories for run 84. Nominal carriage speed, 70 knots; vertical load, 83.2 kN (18 700 lbf); yaw angle, 6°; brake pressure, 21 MPa (3000 psi); tire condition, worn; surface condition, dry.

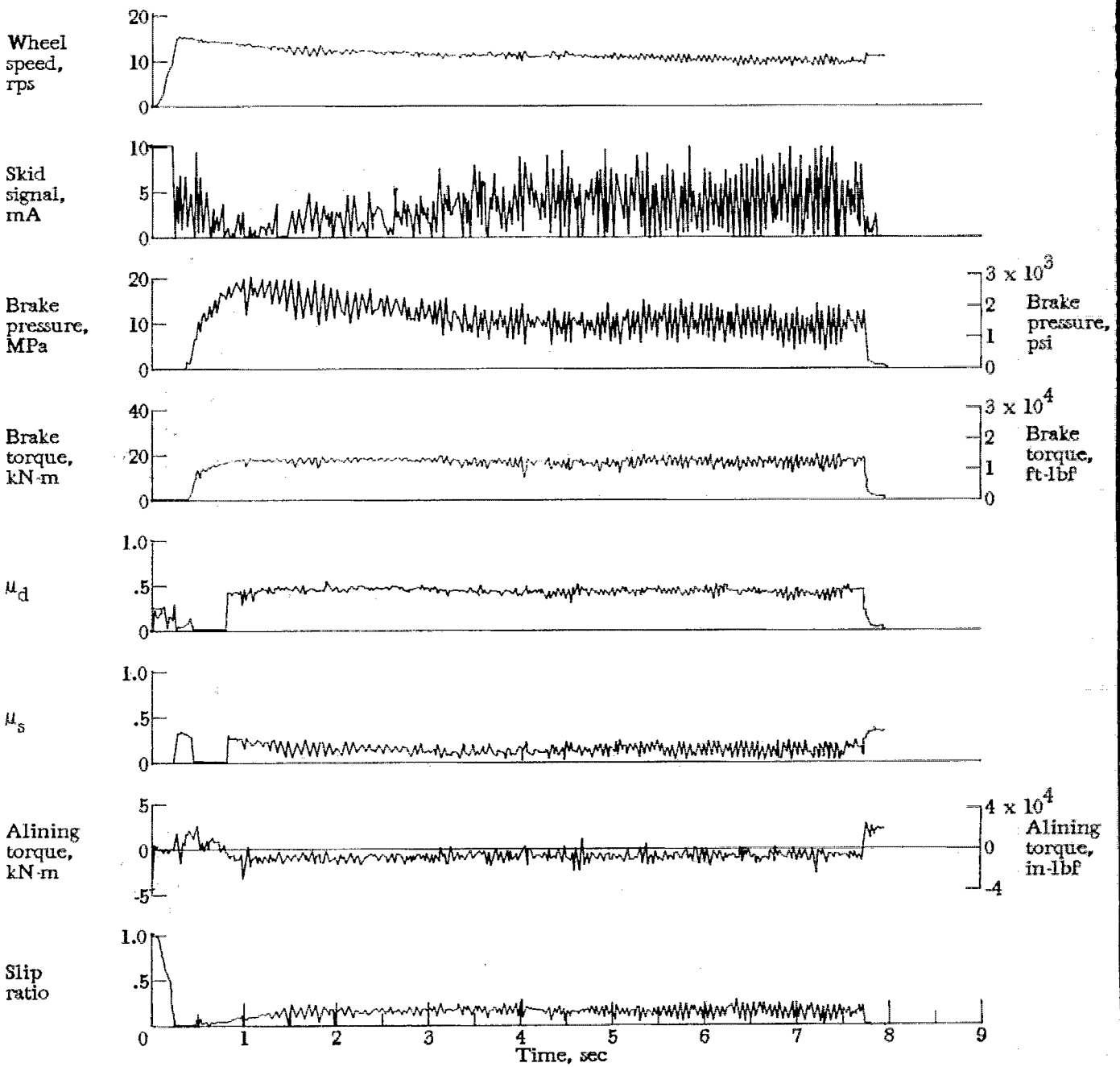

Figure A85.- Time histories for run 85. Nominal carriage speed, 68 knots; vertical load, 86.7 kN (19 500 lbf); yaw angle, 6°; brake pressure, 19 MPa (2690 psi); tire condition, worn; surface condition, dry.

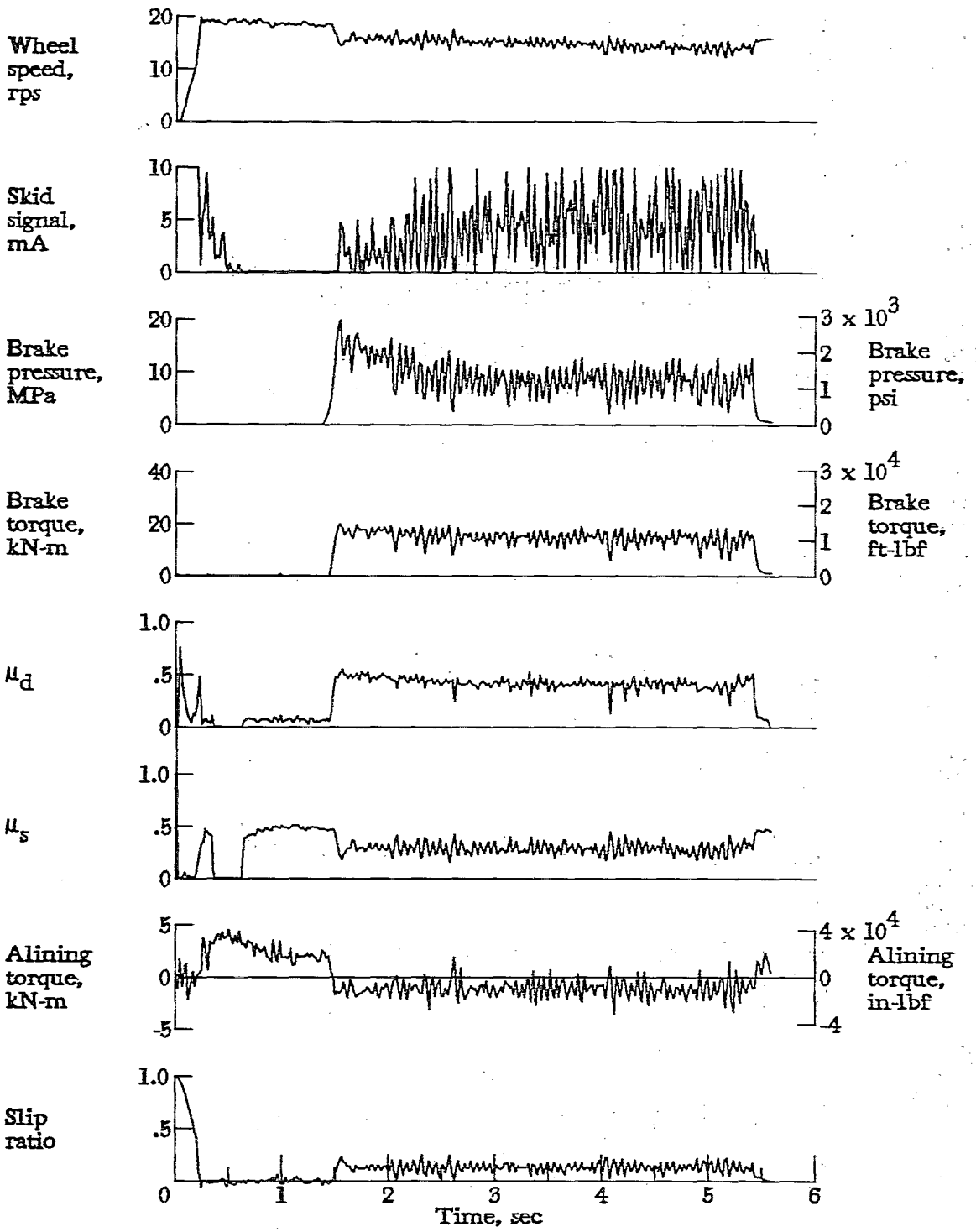

Figure A86.- Time histories for run 86. Nominal carriage speed, 99 knots; vertical load, 82.7 kN (18 600 lbf); yaw angle, 6°; brake pressure, 21 MPa (3000 psi); tire condition, worn; surface condition, dry.

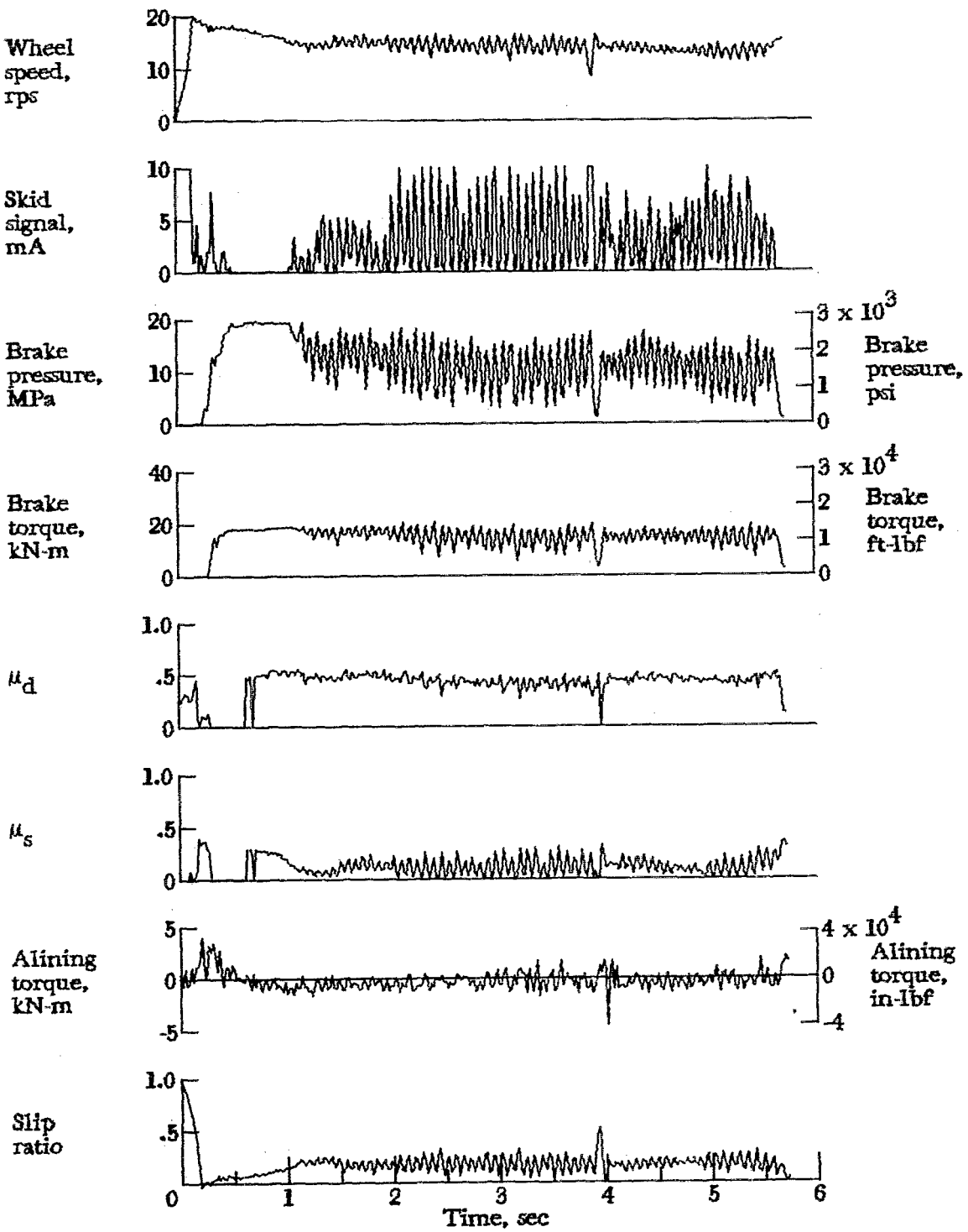

Figure A87.- Time histories for run 87. Nominal carriage speed, 95 knots; vertical load, 87.2 kN (19 600 lbf); yaw angle, 6°; brake pressure, 19 MPa (2750 psi); tire condition, worn; surface condition, dry.

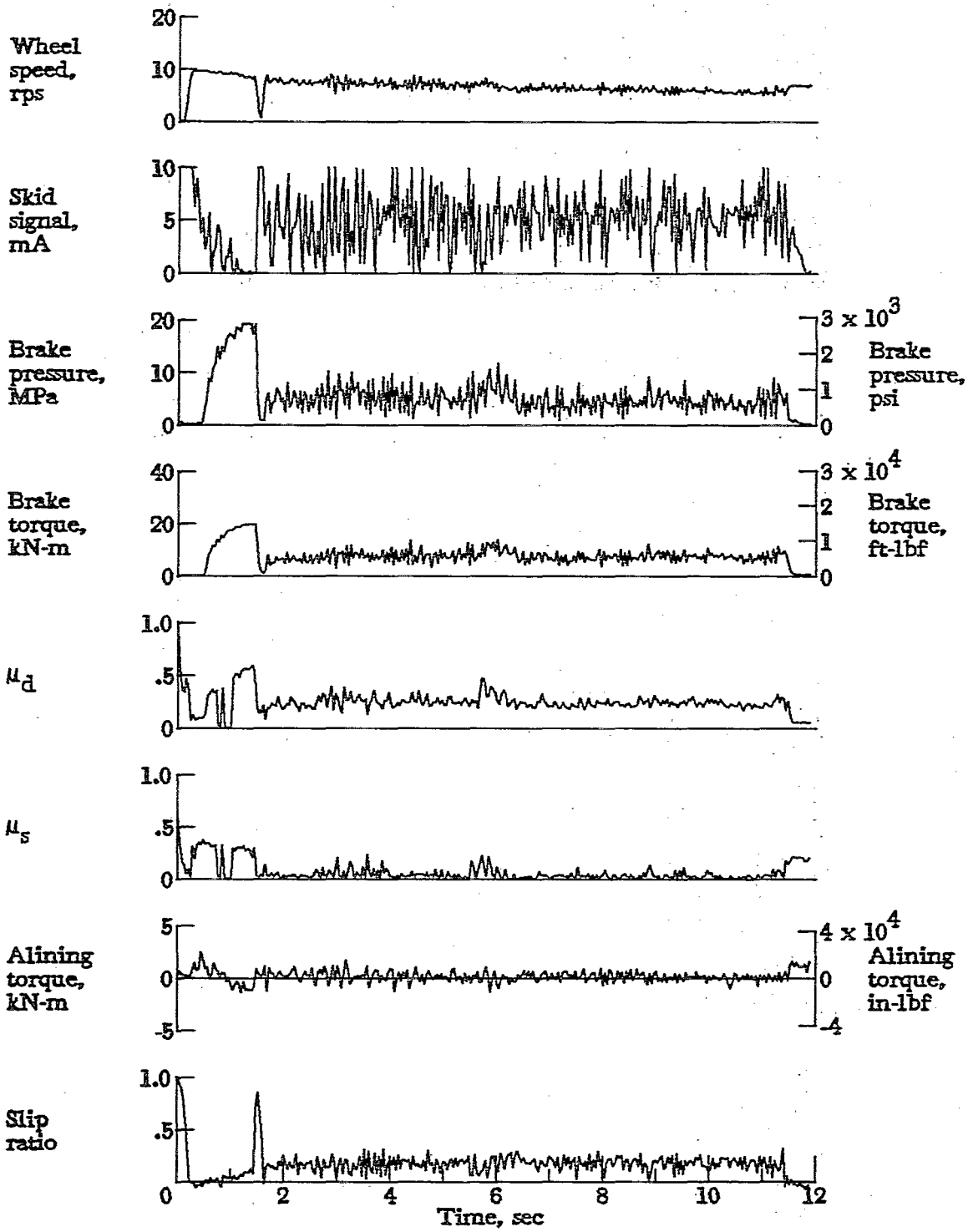

Figure A88.- Time histories for run 88. Nominal carriage speed, 46 knots; vertical load, 84.5 kN (19 000 lbf); yaw angle, 6°; brake pressure, 19 MPa (2750 psi); tire condition, worn; surface condition, damp.

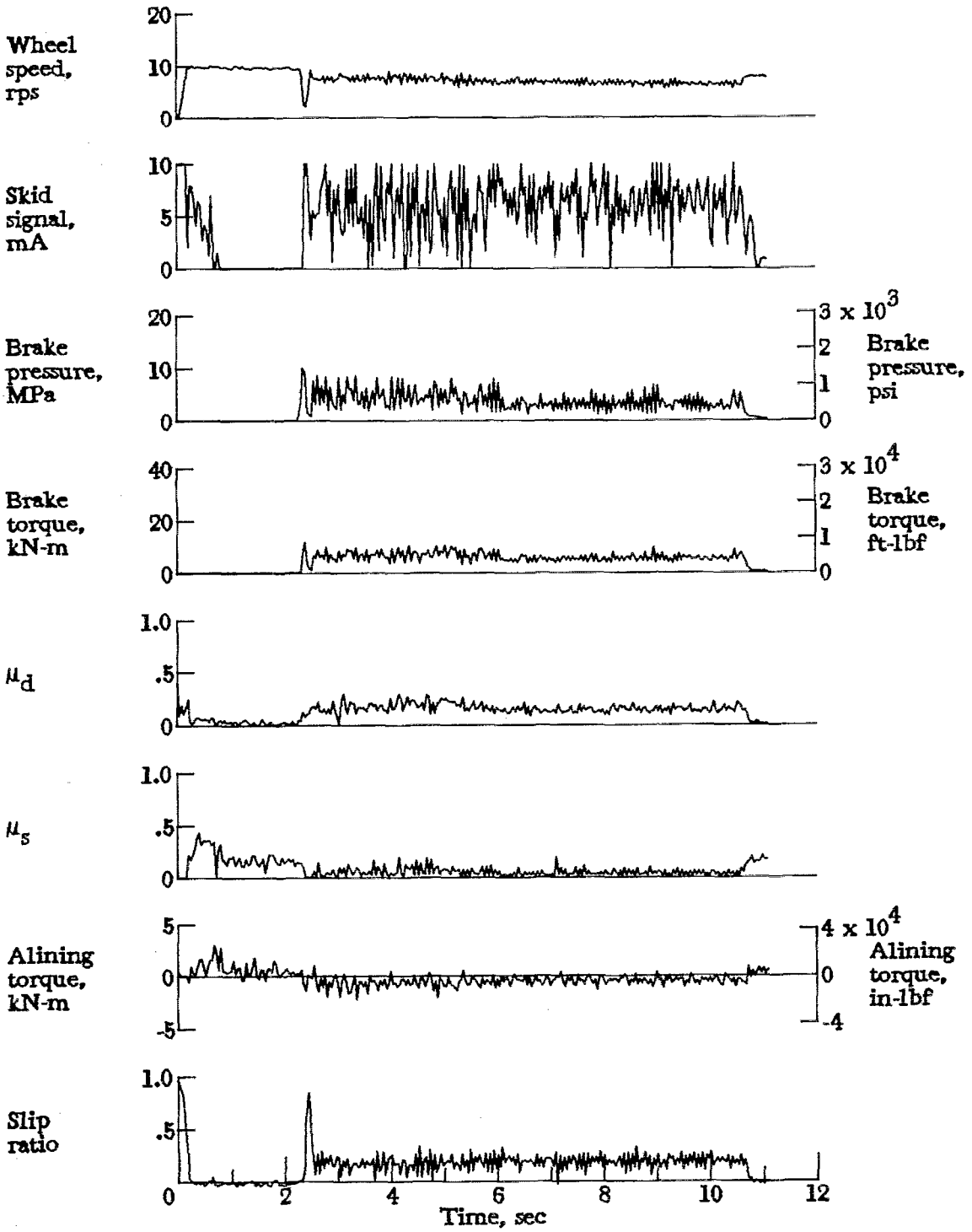

Figure A89.- Time histories for run 89. Nominal carriage speed, 50 knots; vertical load, 80.5 kN (18 100 lbf); yaw angle, 6°; brake pressure, 21 MPa (3000 psi); tire condition, worn; surface condition, damp.

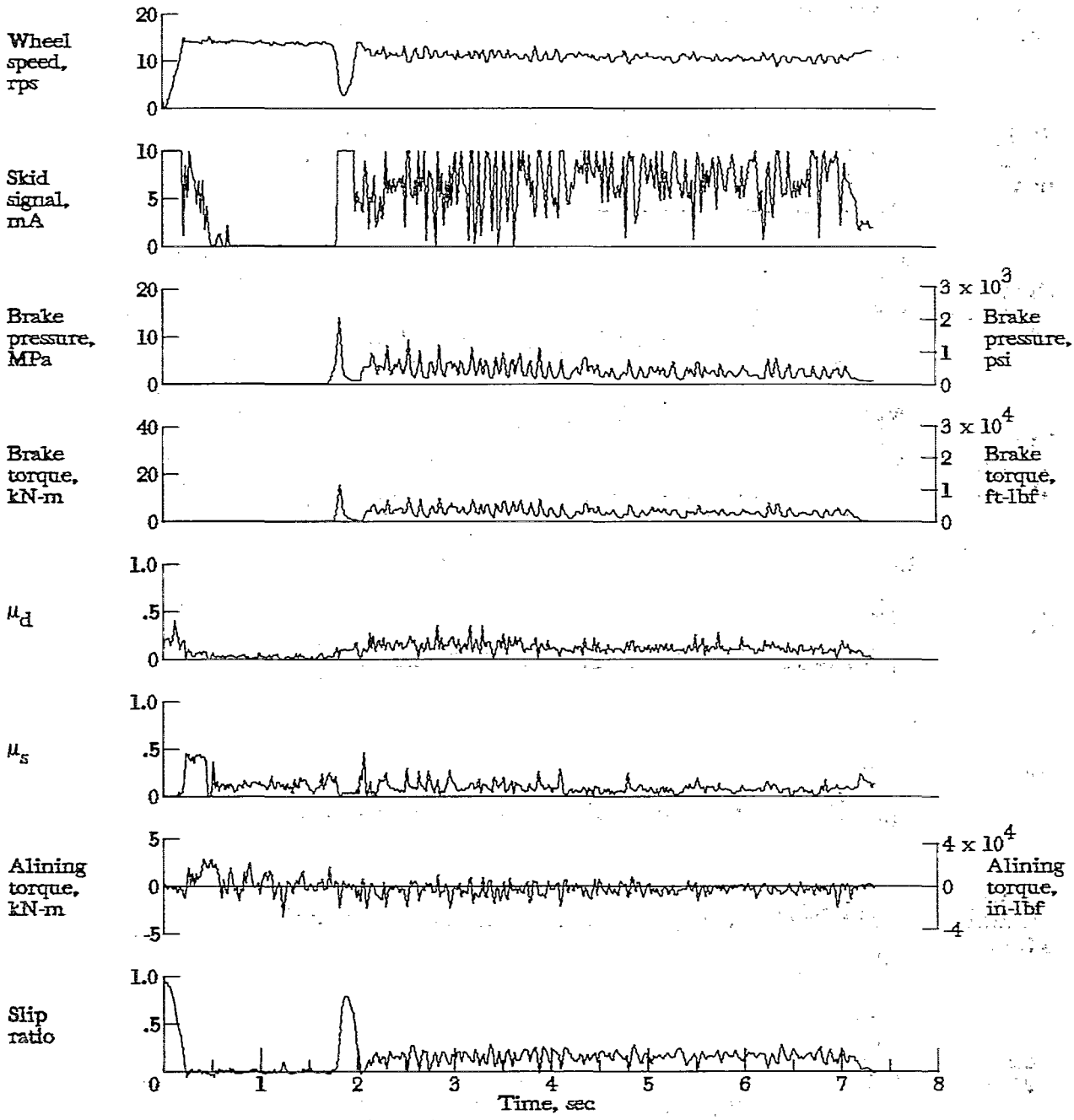

Figure A90.- Time histories for run 90. Nominal carriage speed, 76 knots; vertical load, 79.6 kN (17 900 lbf); yaw angle, 6°; brake pressure, 21 MPa (3000 psi); tire condition, worn; surface condition, damp.

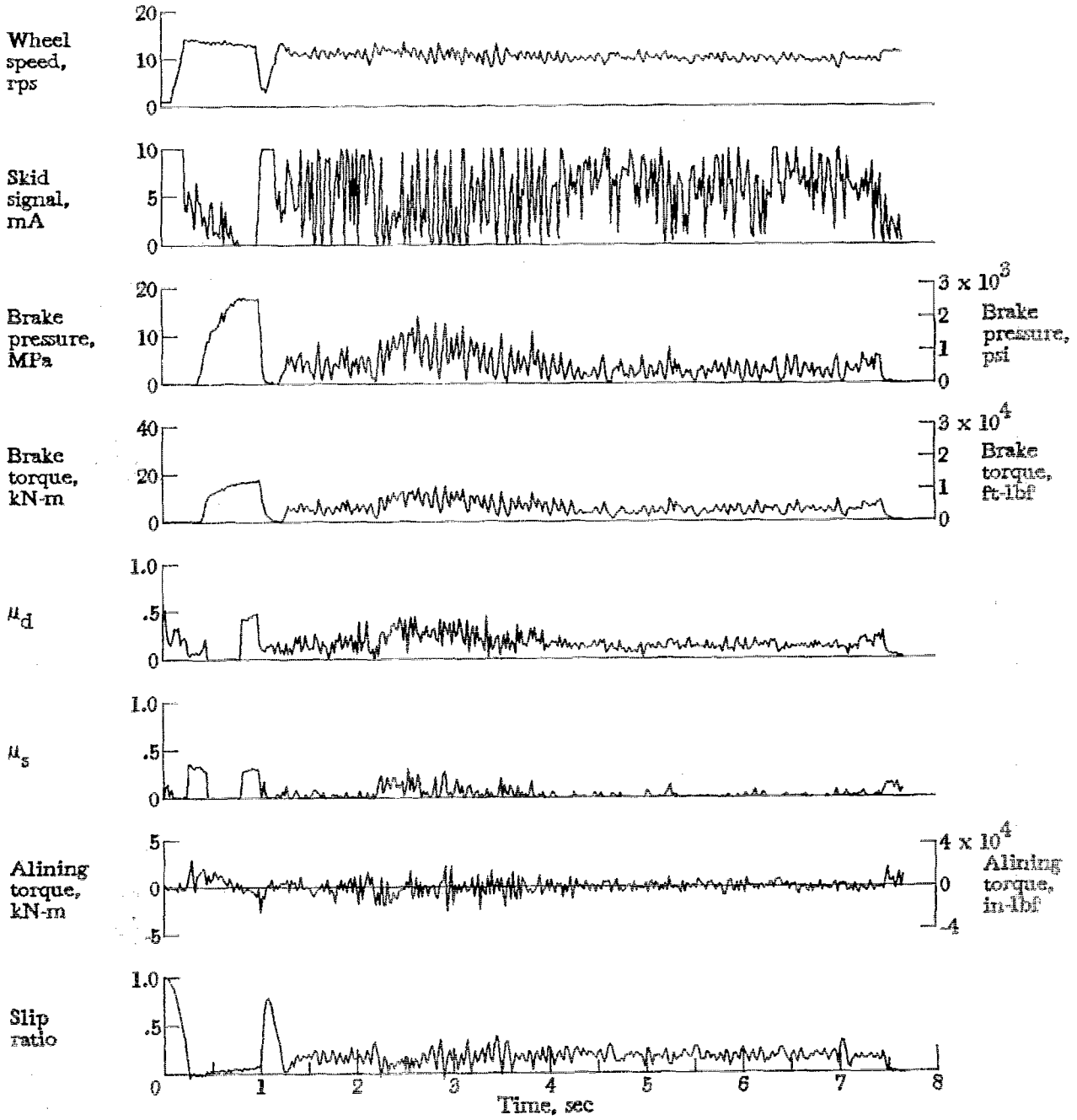

Figure A91.- Time histories for run 91. Nominal carriage speed, 72 knots; vertical load, 85.0 kN (19 100 lbf); yaw angle, 6°; brake pressure, 18 MPa (2620 psi); tire condition, worn; surface condition, damp.

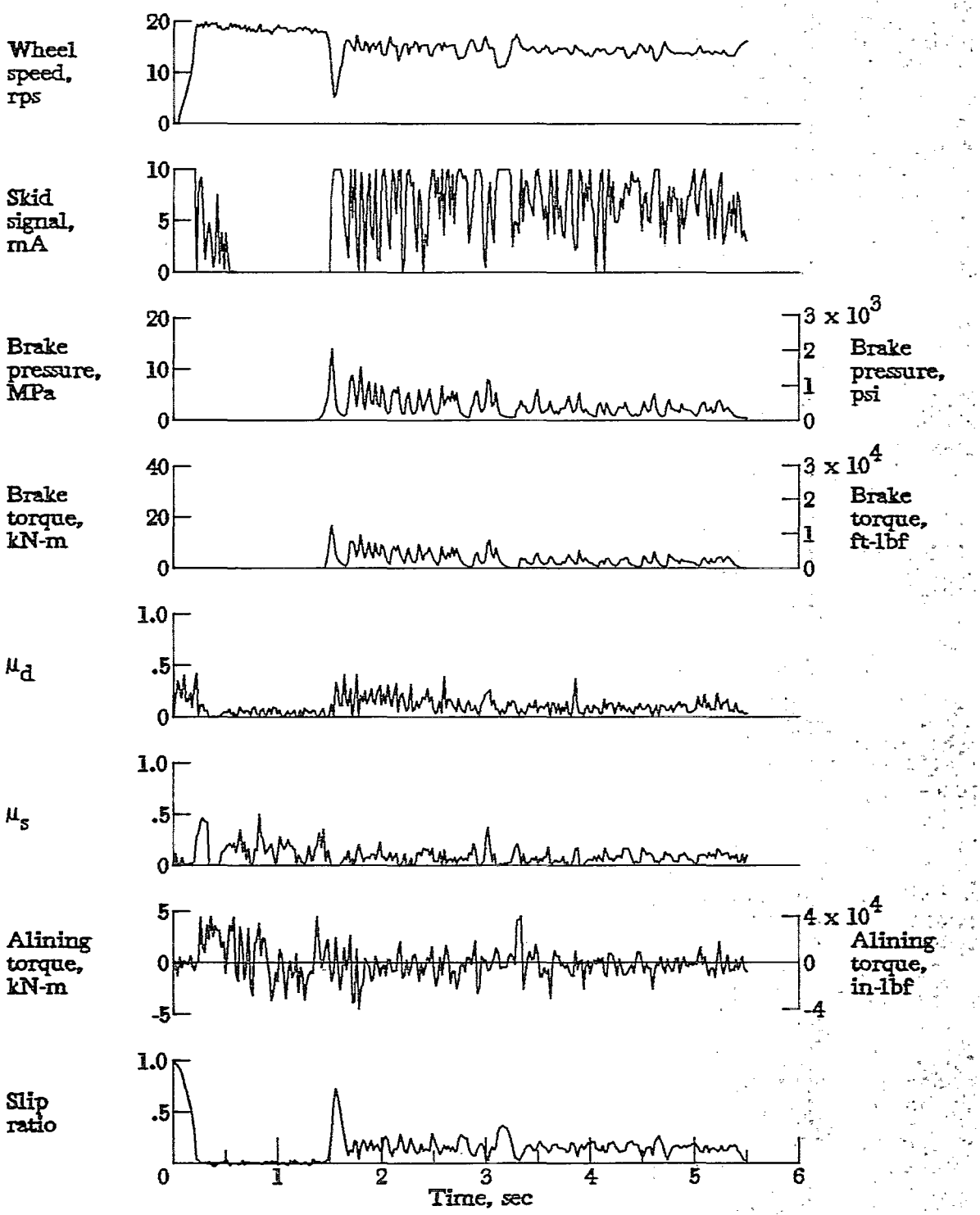

Figure A92.- Time histories for run 92. Nominal carriage speed, 101 knots; vertical load, 80.5 kN (18 100 lbf); yaw angle, 6°; brake pressure, 21 MPa (3000 psi); tire condition, worn; surface condition, damp.

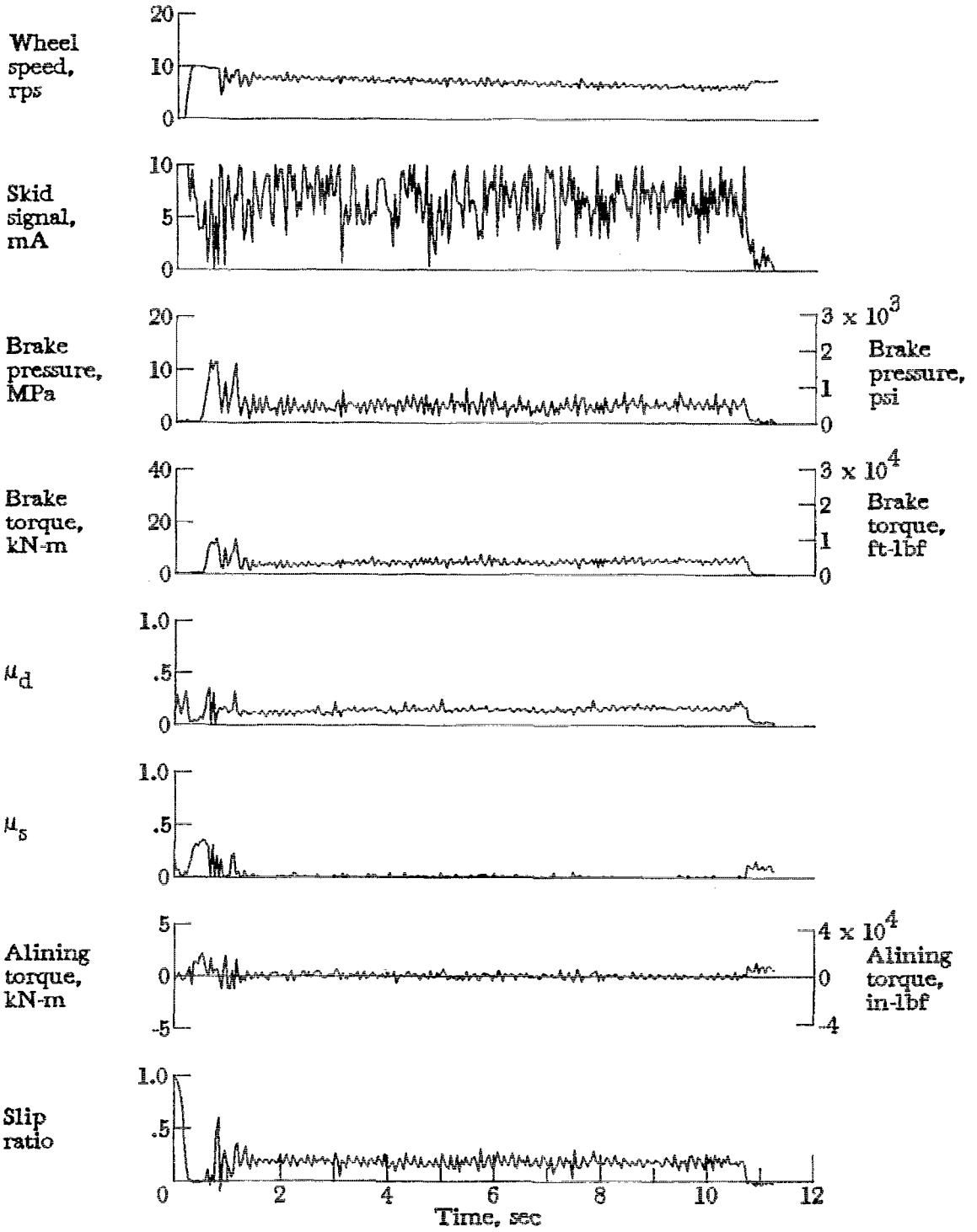

Figure A93.- Time histories for run 93. Nominal carriage speed, 49 knots; vertical load, 85.0 kN (19 100 lbf); yaw angle, 6°; brake pressure, 17 MPa (2470 psi); tire condition, worn; surface condition, flooded.

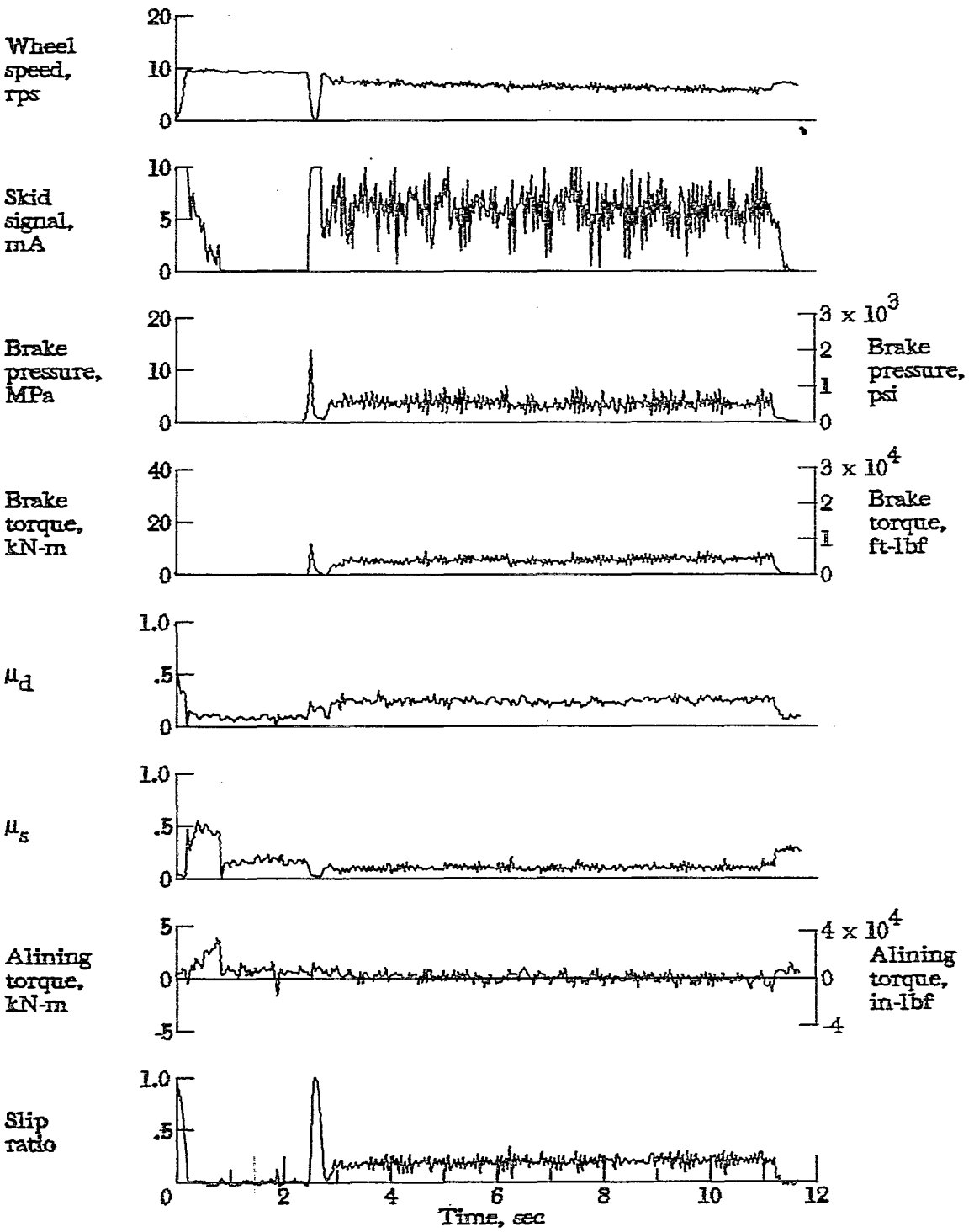

Figure A94.- Time histories for run 94. Nominal carriage speed, 46 knots; vertical load, 77.0 kN (17 300 lbf); yaw angle, 6°; brake pressure, 21 MPa (3000 psi); tire condition, worn; surface condition, flooded.

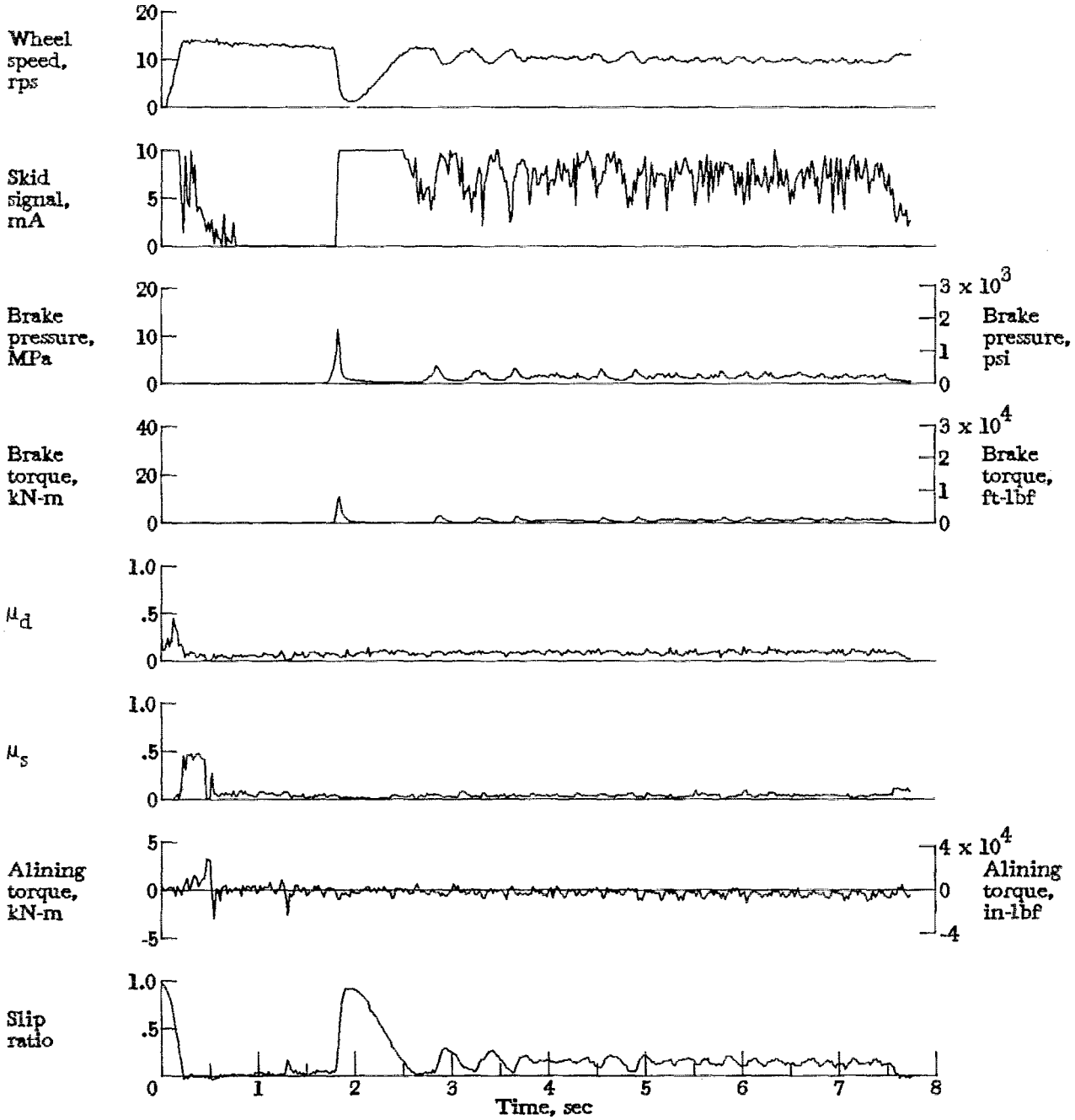

Figure A95.- Time histories for run 95. Nominal carriage speed, 72 knots; vertical load, 79.2 kN (17 800 lbf); yaw angle, 6°; brake pressure, 21 MPa (3000 psi); tire condition, worn; surface condition, flooded.

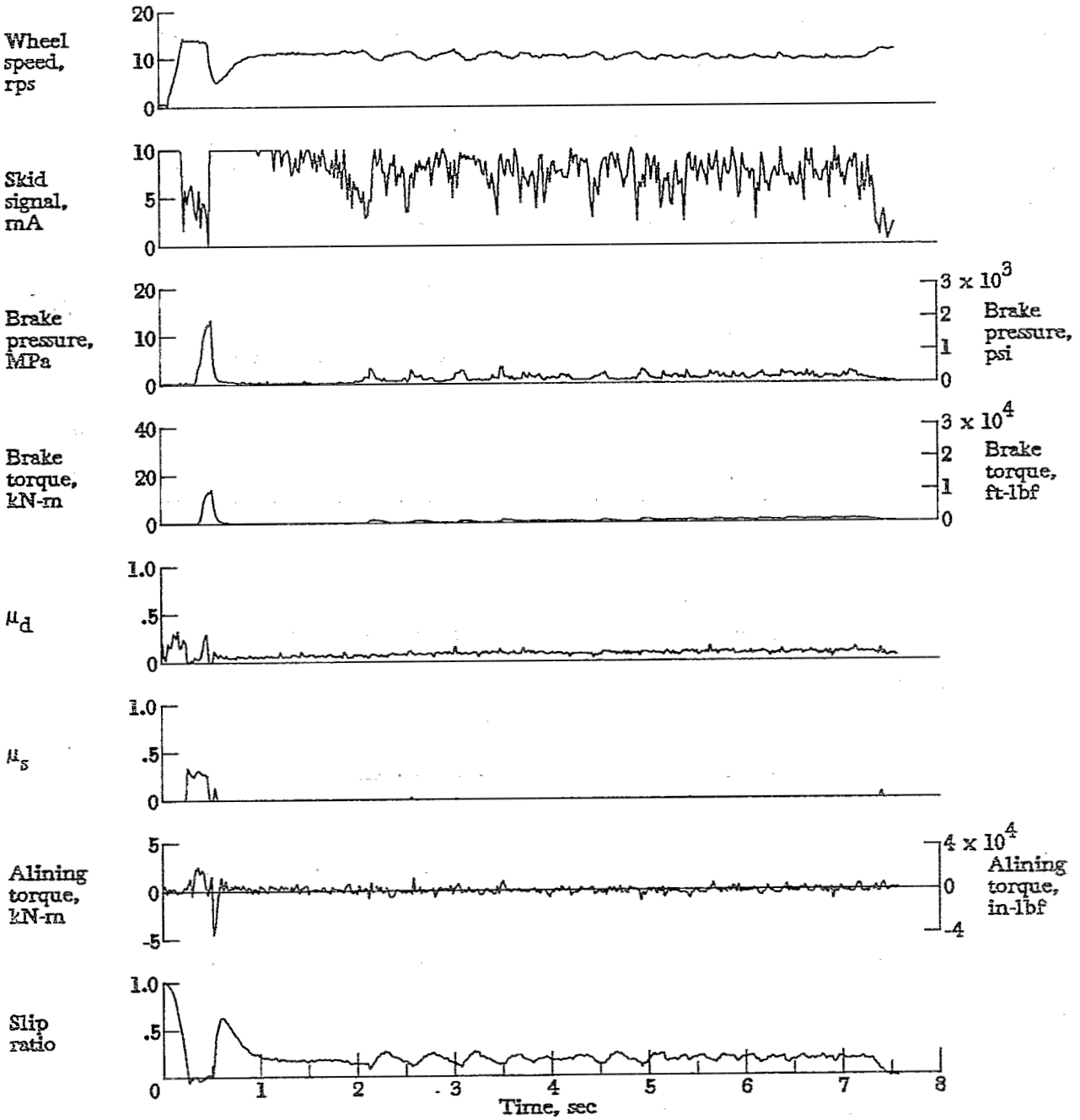

Figure A96.- Time histories for run 96. Nominal carriage speed, 73 knots; vertical load, 83.6 kN (18 800 lbf); yaw angle, 6°; brake pressure, 19 MPa (2660 psi); tire condition, worn; surface condition, flooded.

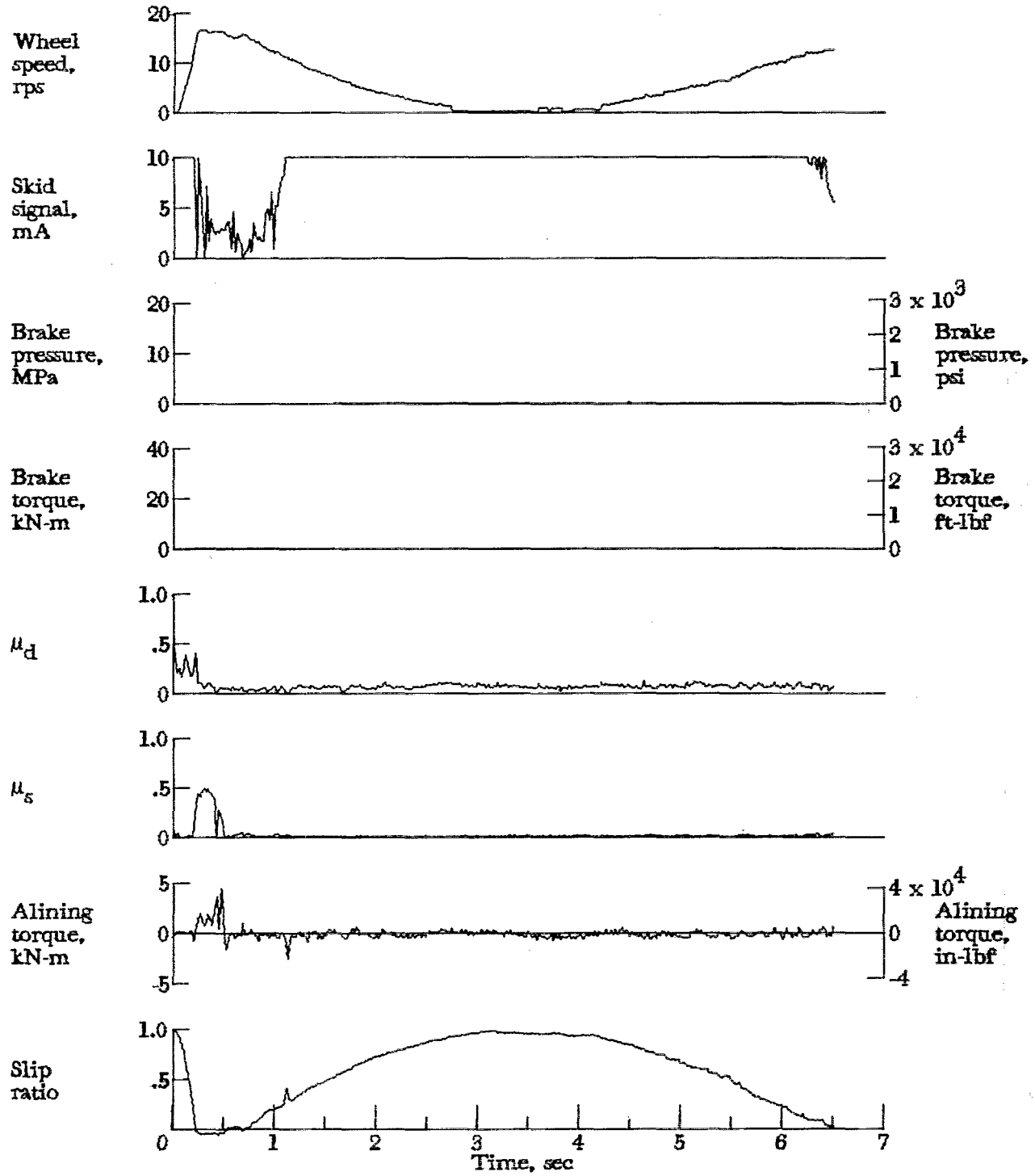

Figure A97.- Time histories for run 97. Nominal carriage speed, 85 knots; vertical load, 78.3 kN (17 600 lbf); yaw angle, 6°; brake pressure, 20 MPa (2900 psi); tire condition, worn; surface condition, flooded.

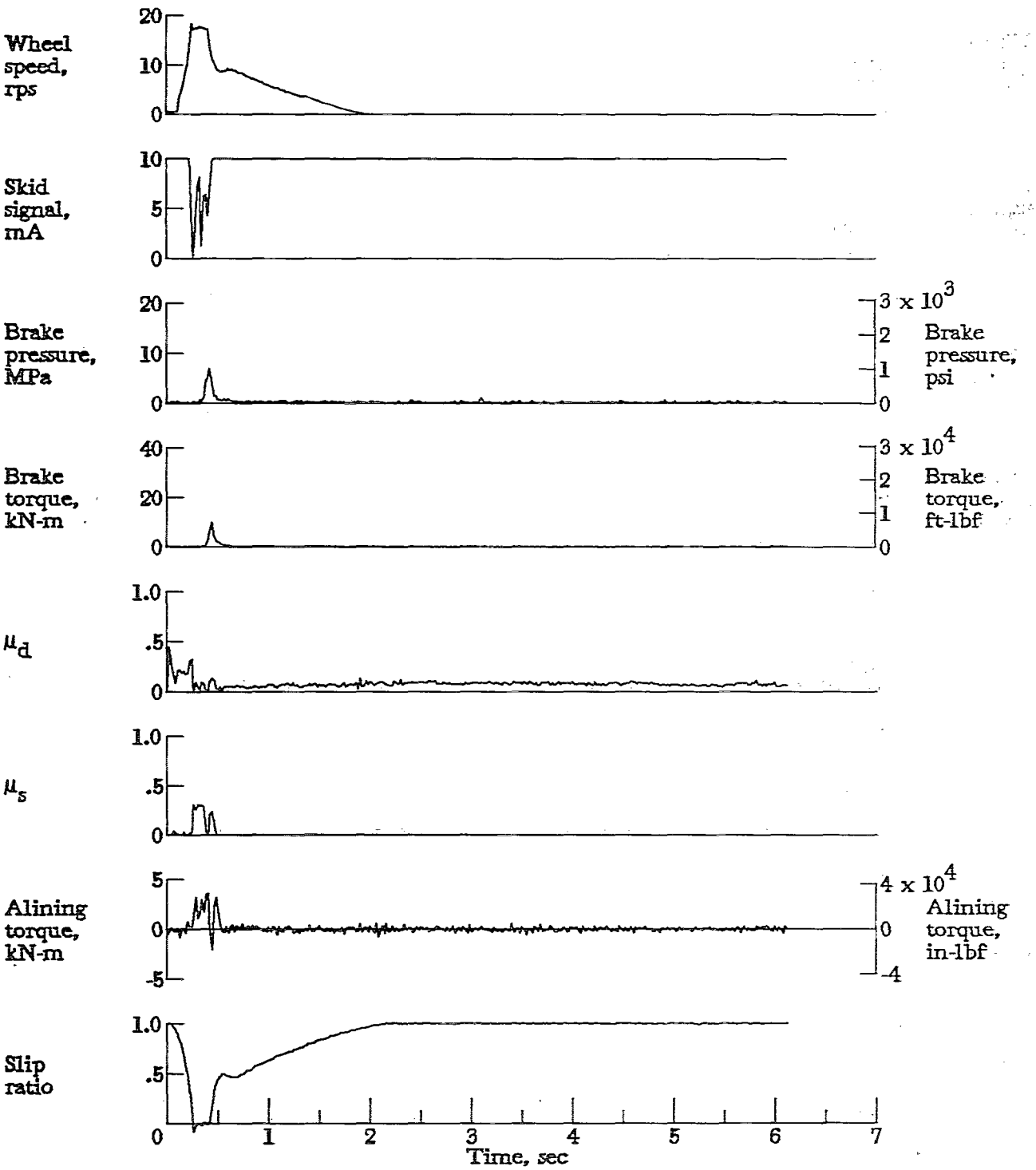

Figure A98.- Time histories for run 98. Nominal carriage speed, 91 knots; vertical load, 82.7 kN (18 600 lbf); yaw angle, 6°; brake pressure, 19 MPa (2690 psi); tire condition, worn; surface condition, flooded.

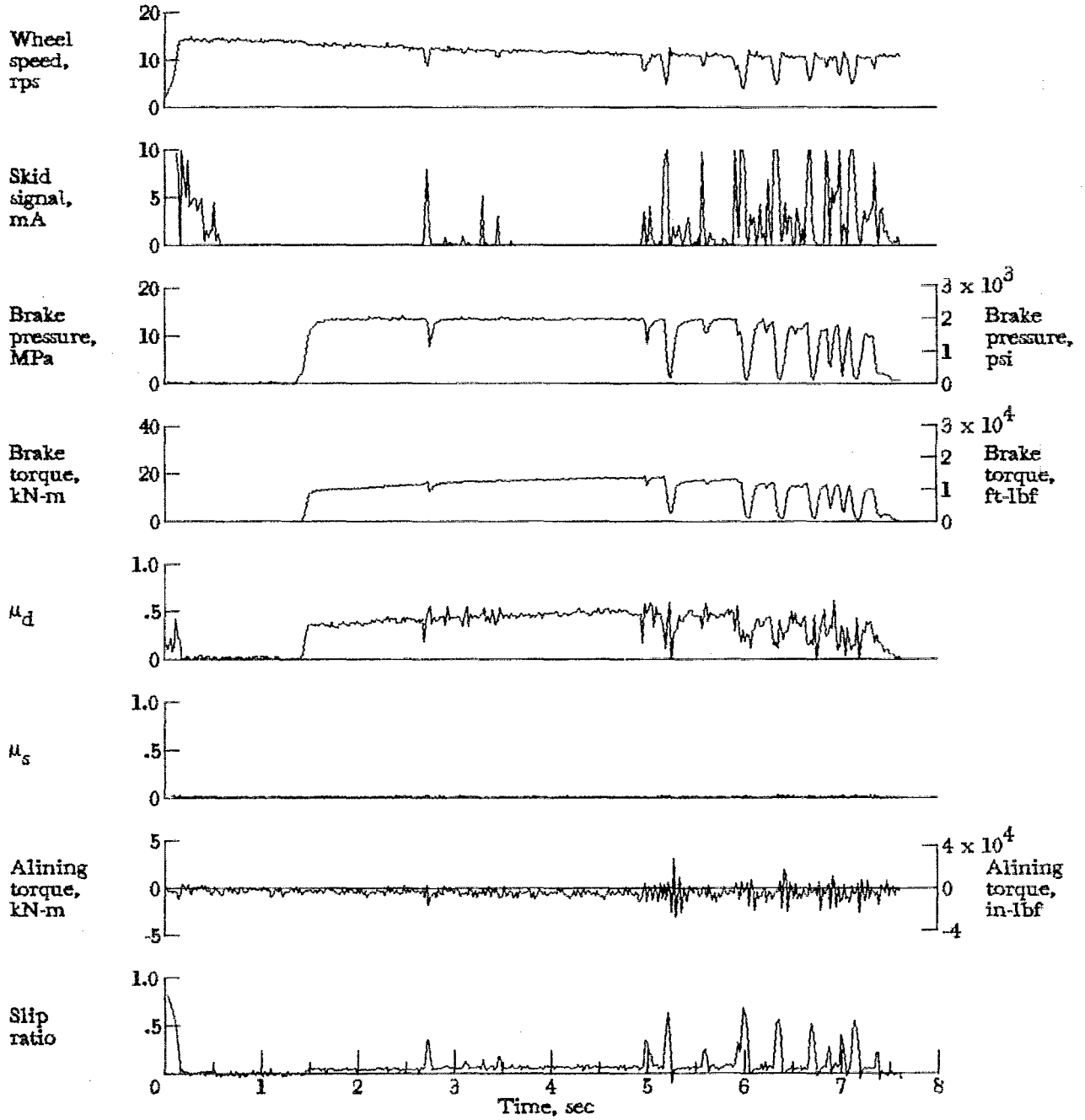

Figure A99.- Time histories for run 99. Nominal carriage speed, 72 knots; vertical load, 80.5 kN (18 100 lbf); yaw angle, 0°; brake pressure, 14 MPa (2000 psi); tire condition, new; surface condition, random dry/damp (natural rain).

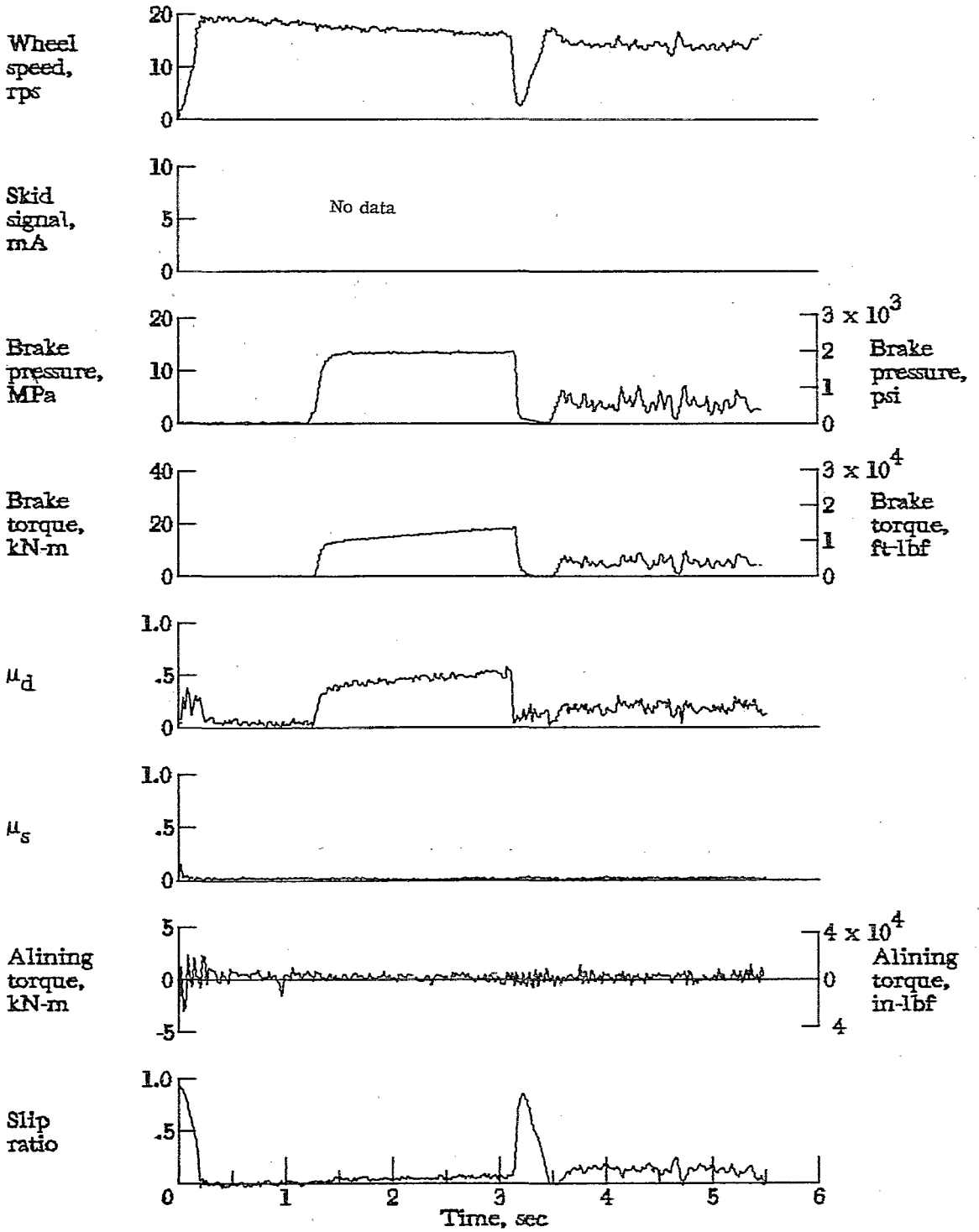

Figure A100.- Time histories for run 100. Nominal carriage speed, 100 knots; vertical load, 79.2 kN (17 800 lbf); yaw angle, 0°; brake pressure, 14 MPa (2000 psi); tire condition, new; surface condition, dry to wet.

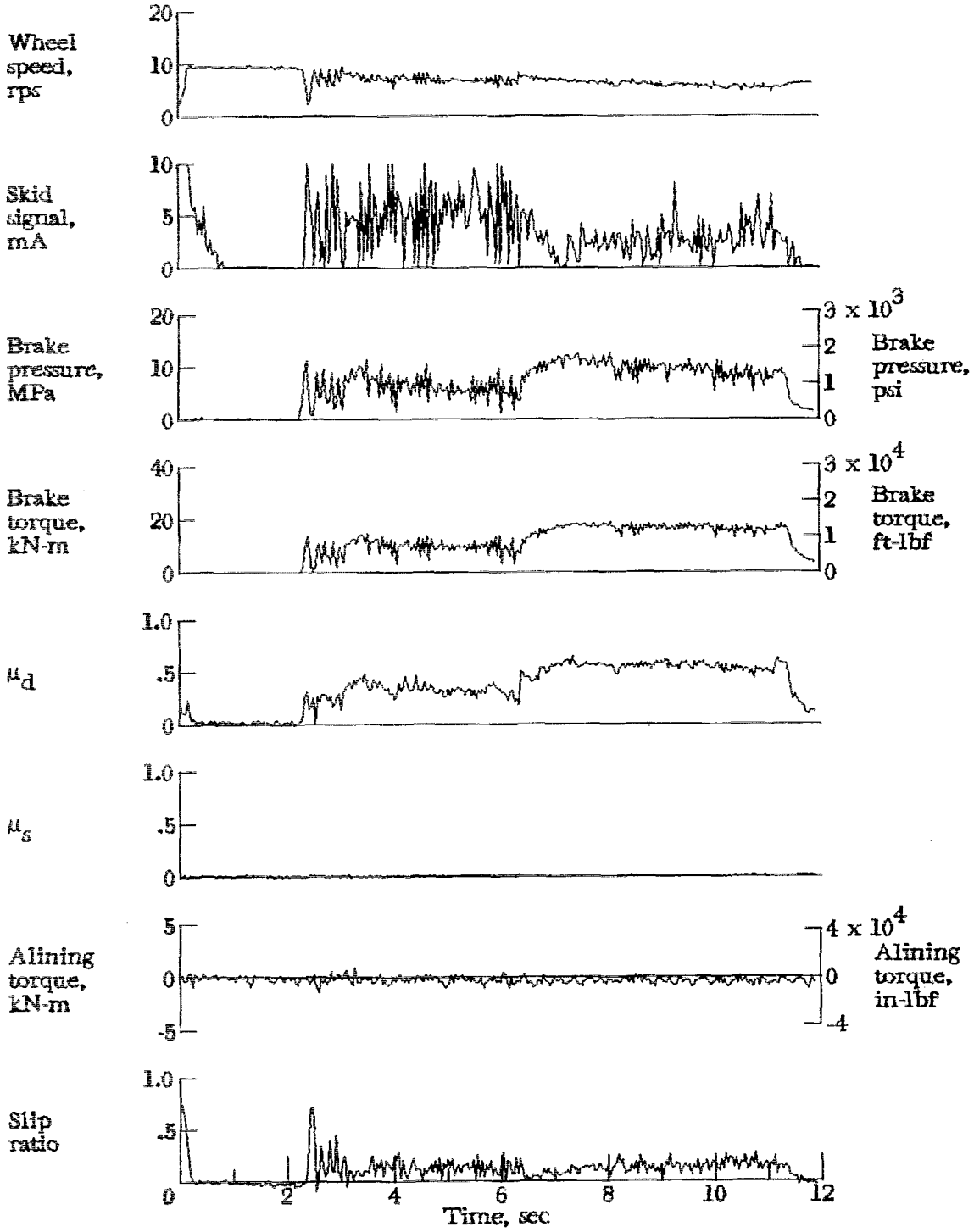

Figure A101.- Time histories for run 101. Nominal carriage speed, 45 knots; vertical load, 63.6 kN (14 300 lbf); yaw angle, 0°; brake pressure, 14 MPa (2000 psi); tire condition, new; surface condition, wet to dry.

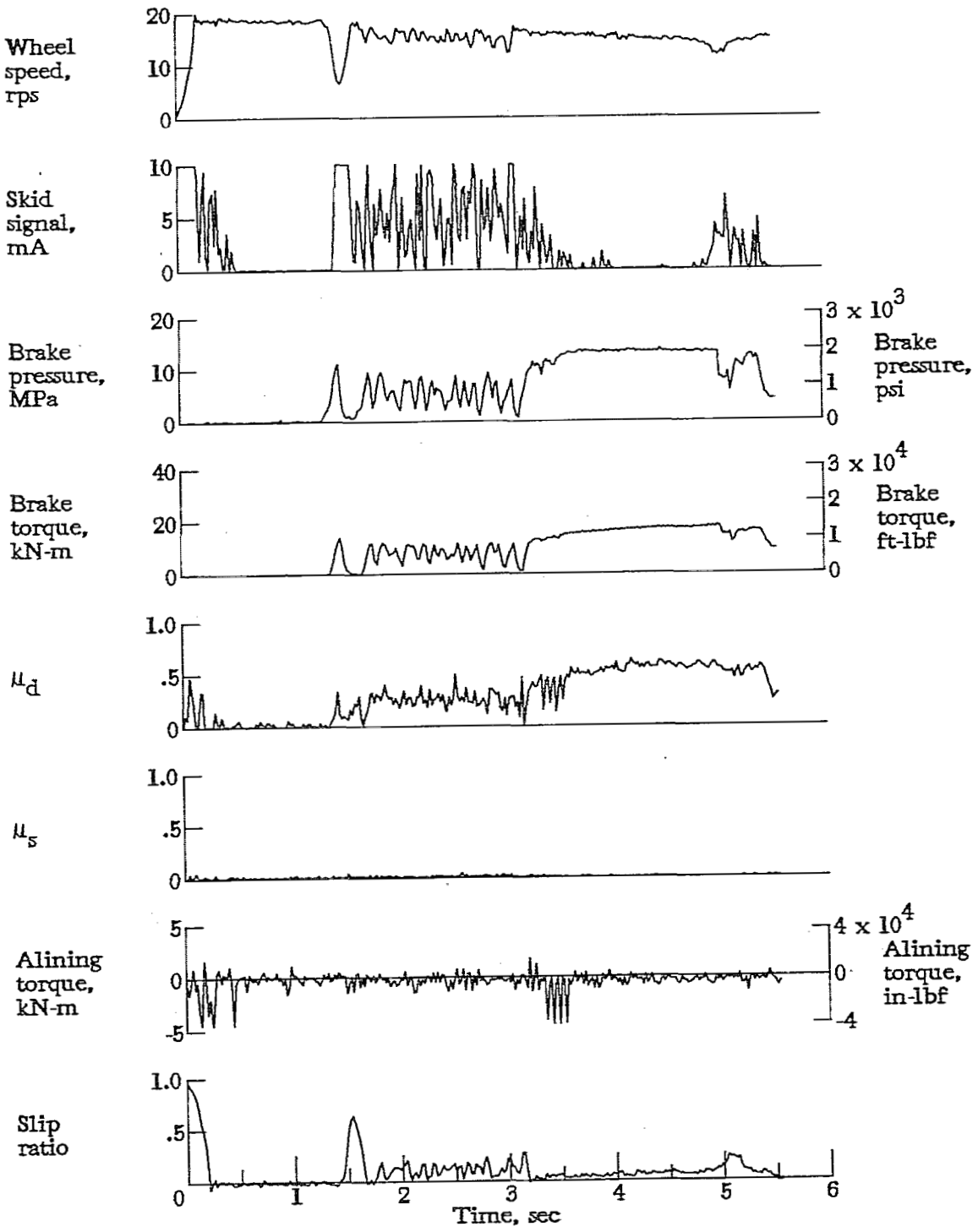

Figure A102.- Time histories for run 102. Nominal carriage speed, 100 knots; vertical load, 63.6 kN (14 300 lbf); yaw angle, 0°; brake pressure, 13 MPa (1940 psi); tire condition, new; surface condition, wet to dry.

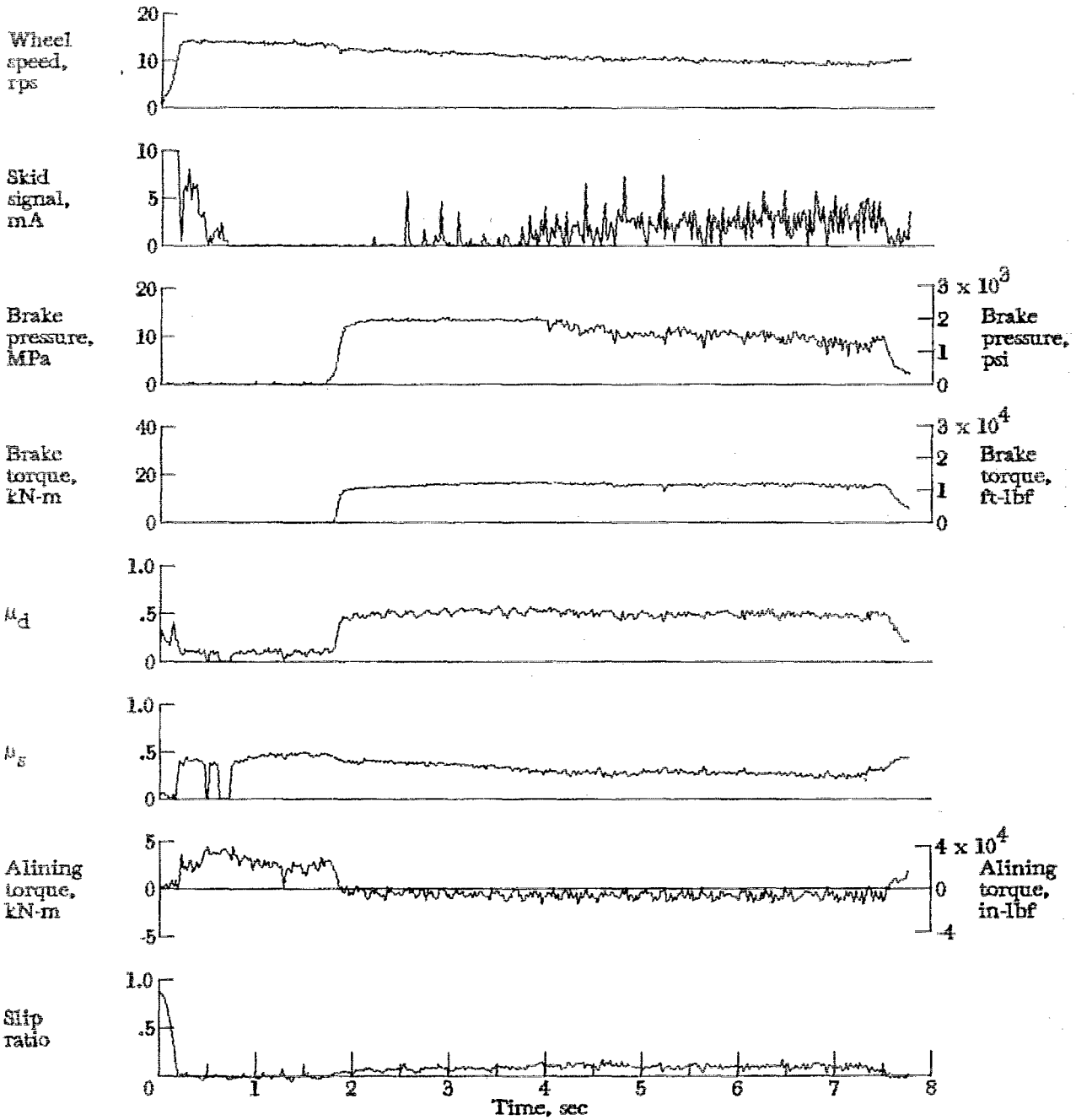

Figure A103.- Time histories for run 103. Nominal carriage speed, 70 knots; vertical load, 81.0 kN (18 200 lbf); yaw angle, 6°; brake pressure, 13 MPa (1940 psi); tire condition, new; surface condition, dry.

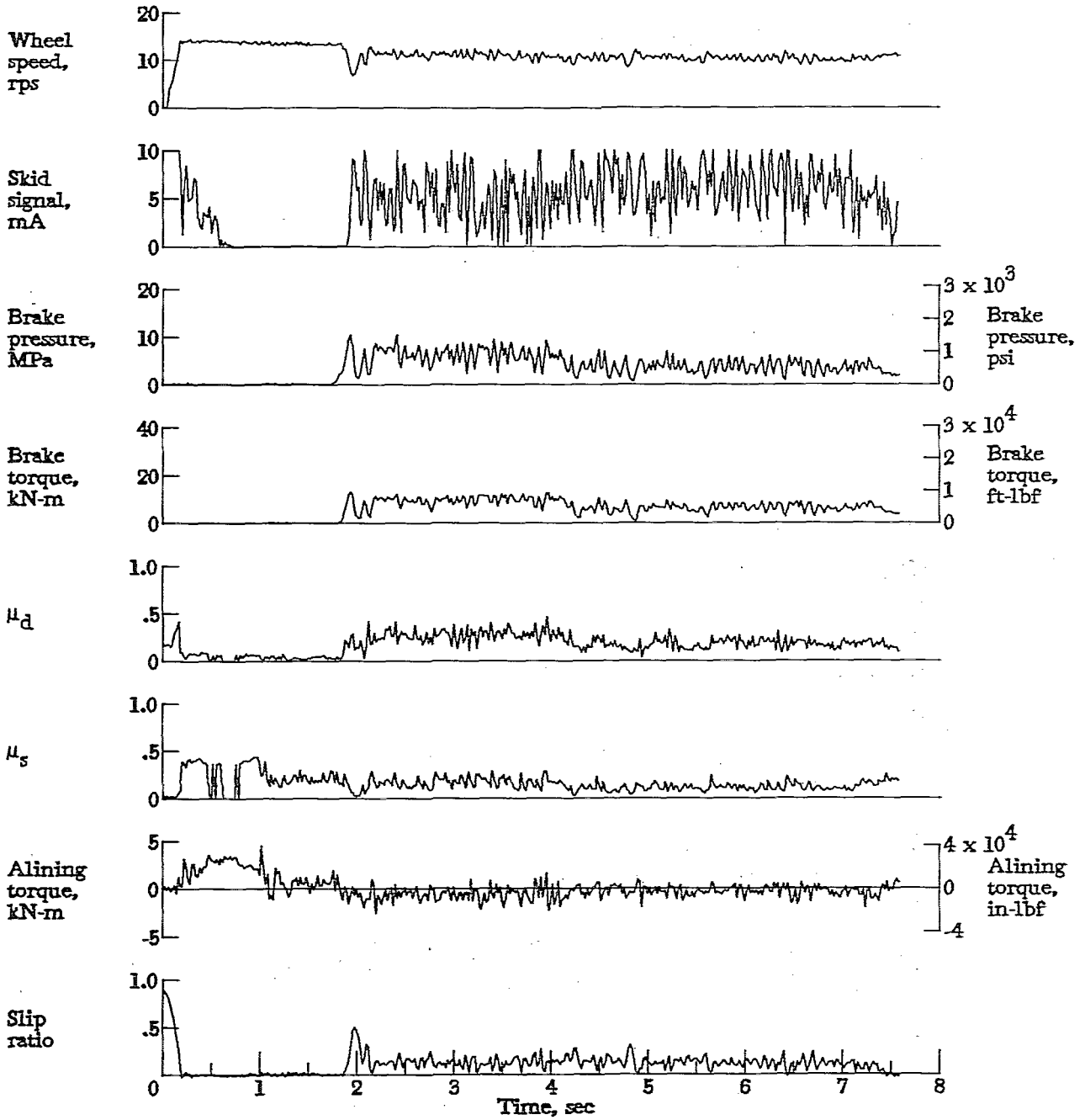

Figure A104.- Time histories for run 104. Nominal carriage speed, 75 knots; vertical load, 80.5 kN (18 100 lbf); yaw angle, 6°; brake pressure, 14 MPa (2000 psi); tire condition, new; surface condition, damp.

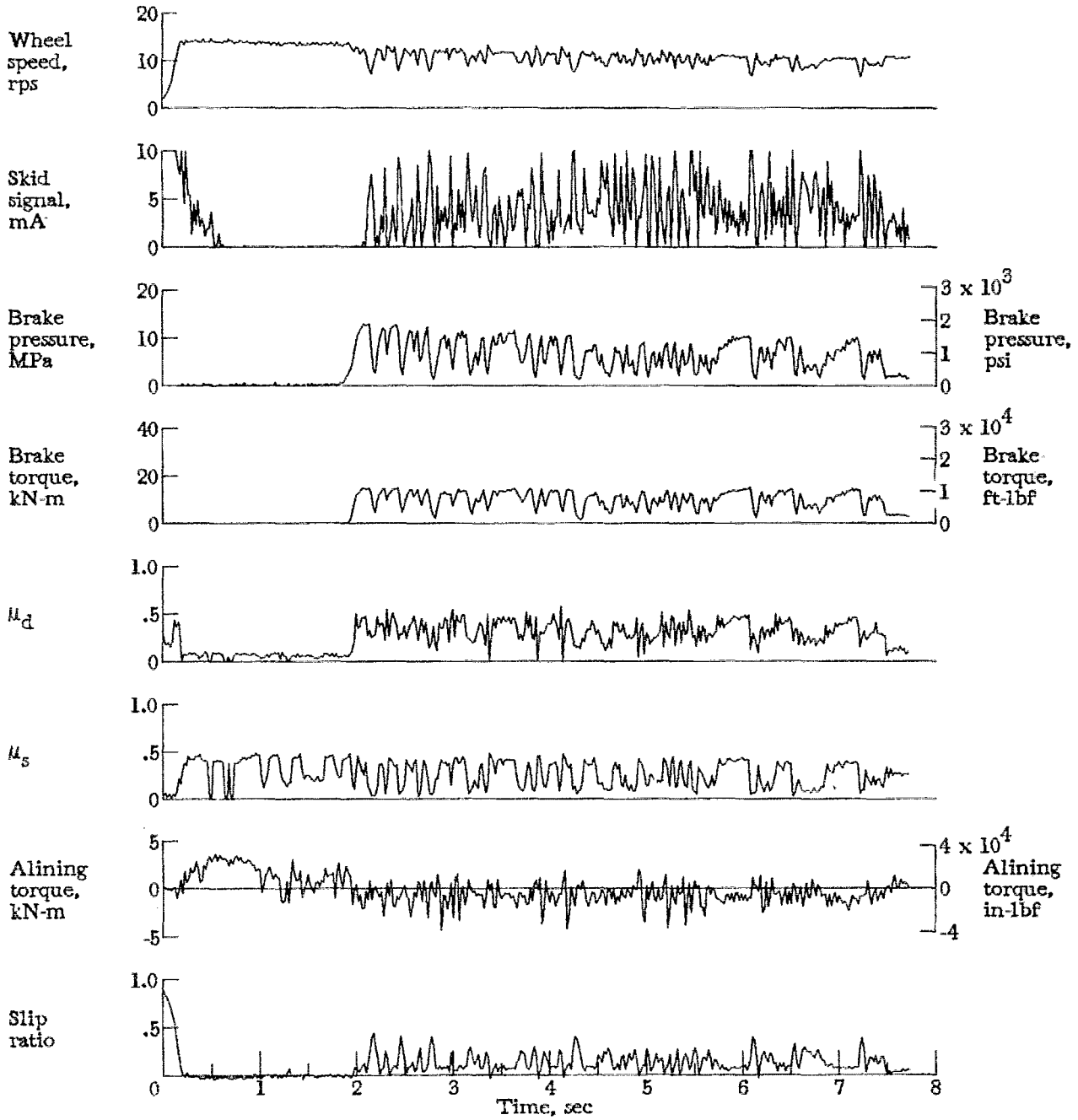

Figure A105.- Time histories for run 105. Nominal carriage speed, 71 knots; vertical load, 78.7 kN (17 700 lbf); yaw angle, 6°; brake pressure, 14 MPa (2000 psi); tire condition, new; surface condition, random dry/damp.

*U.S. GOVERNMENT PRINTING OFFICE: 1977 - 735-004/36

578 001 C1 U A 770819 S00903DS
DEPT OF THE AIR FORCE
AF WEAPONS LABORATORY
ATTN: TECHNICAL LIBRARY (SUL)
KIRTLAND AFB NM 87117